Utilisation of Bone China Ceramic Waste as Fine Aggregate in Sustainable Concrete

Submitted in

fulfillment of the requirements for the degree of

Doctor of Philosophy

by

SALMAN SIDDIQUE
(2014RCE9551)

Under the Supervision of

Dr. Sandeep Shrivastava
and
Prof. Sandeep Chaudhary

DEPARTMENT OF CIVIL ENGINEERING

MALAVIYA NATIONAL INSTITUTE OF TECHNOLOGY JAIPUR

JAIPUR

November, 2018

MALAVIYA NATIONAL INSTITUTE OF TECHNOLOGY JAIPUR,
JAIPUR

DECLARATION

I, **Salman Siddique**, declare that this thesis titled, "**Utilisation of Bone China Ceramic Waste as Fine Aggregate in Sustainable Concrete**" and the work presented in it, are my own. I confirm that:

- This work was done wholly or mainly while in candidature for a research degree at this university.
- Where any part of this thesis has previously been submitted for a degree or any other qualification at this university or any other institution, this has been clearly stated.
- Where I have consulted the published work of others, this is always clearly attributed.
- Where I have quoted from the work of others, the source is always given. With the exception of such quotations, this thesis is entirely my own work.
- I have acknowledged all main sources of help.
- Where the thesis is based on work done by myself, jointly with others, I have made clear exactly what was done by others and what I have contributed myself.

Date: 01-11-2018

Salman Siddique
(2014RCE9551)

MALAVIYA NATIONAL INSTITUTE OF TECHNOLOGY JAIPUR,
JAIPUR

CERTIFICATE

This is to certify that the thesis report entitled, "**Utilisation of Bone China Ceramic Waste as Fine Aggregate in Sustainable Concrete**" being submitted by **Salman Siddique, (2014RCE9551)** is a bonafide research work carried out under our supervision and guidance in fulfillment of the requirement for the award of the degree of **Doctor of Philosophy** in the Department of Civil Engineering in the Malaviya National Institute of Technology, Jaipur, India. The matter embodied in this thesis is original and has not been submitted to any other University or Institute for the award of any other degree.

Place: Jaipur
Date: 01-11-2018

(Prof. Sandeep Chaudhary)
External Supervisor
Professor
Discipline of Civil Engineering
IIT Indore-453552 (India)

(Dr. Sandeep Shrivastava)
Supervisor
Assistant Professor
Department of Civil Engineering
MNIT Jaipur-302017 (India)

ACKNOWLEDGEMENT

First of all, Praise is due to almighty ALLAH who taught humankind everything they knew not and giving me the opportunity to step in the excellent world of technology. I am fully indebted to the strength and countless blessings received from almighty, the good wishes and never-ending support from each of my teachers, friends, colleagues and members of the family. The favors received from each of them in completing this work are immense and immeasurable.

I take this opportunity to extend my most sincere gratitude and thanks to my supervisors, Dr. Sandeep Shrivastava, MNIT Jaipur and Prof. Sandeep Chaudhary, IIT Indore. This work would have been impossible without their guidance and would have never been completed without their perception to put things in to right perspective.

I also wish to thank the DREC members Prof. Ravindra Nagar, Prof. A.K. Vyas, and Dr. Rajesh Gupta, and other eminent faculty members of MNIT Jaipur for their valuable support and comments which helped in refining the work at different stages. I am grateful for the unceasing help provided Prof. Mahesh Kumar Jat, Head, Department of Civil Engineering, MNIT Jaipur during the study.

I would like to thank Dr. Trilok Gupta, Dr. Kashyap Patel, Dr. Pankaj Chaudhary, Hemant Jain, Ankit Bharadwaj, Syed Ahmed Kabeer K.I, Kunal, Nishant Rai, Sapan Gaur, Ramswaroop Mandolia and all other colleagues and friends for their constant support. A special thanks also to the technical and support staff of Department of Civil Engineering at MNIT Jaipur and CTAE, Udaipur for their support throughout this study.

I would like to thank my family members for being and bearing with me ever always. I also wish to thank with all sincerity, family members of Prof. Sandeep Chaudhary for their cooperative behavior and considering me as their family member.

Date: 01 November, 2018 (Salman Siddique)
Jaipur

ABSTRACT

Due to the ongoing awareness to the environmental issues and the ever growing concern of efficient waste management, efforts are being put into different areas of knowledge, in order to determine, adapt and channelize solutions for a sustainable future. Among these challenges, there are the ones that are related to concrete production in construction sector. These are generally related to the utilisation of natural resources and the manufacture of cement, two of the most important components. As of past decade, one of the most candid and creative solution is recycling of various industrial waste and by products for the production of concrete making aggregates. This is so for not the best solution as, albeit the mining and dredging of natural resources is reduced and consequently the conservation of natural resources takes place, more quantities of cement are needed to achieve the properties which are comparable to natural aggregate concrete. Cement being a major contributor to global warming negates the positive impacts associated to the lower mining frequency.

Consequently, use of ceramic waste as aggregate in concrete design, so called ceramic concrete was aimed on solving the aforementioned issues by basing its principals on the idea of producing a concrete that achieved similar properties to those of natural aggregate concrete with no needs for compensatory cement quantities. The essence of this effort encourages to study, investigate and understand more about the possibilities associated with the huge ceramic industry and consider their waste products as aggregate for concrete, for which the present doctoral thesis is proposed.

On an initial stage, the fine bone china table ware ceramic industry is identified and its production techniques and products are studied to understand and produce the specific type of ceramic waste/by products aggregate. This is achieved by investigating the chemical, physical, microstructural and thermal properties of ceramic aggregate. From the work carried out, it is concluded that the this type of ceramic aggregate is suitable as fine aggregate and can represent a feasible and environmental friendly solution while being thoroughly adaptable to concrete design methodologies.

The next stage consists on the investigation and analysis of some of the fresh state, mechanical, microstructural, chemical and durability properties of different concrete mixes. This was achieved by

elaborating different and extensive experimental campaigns of different concrete mixes with varying percentage of ceramic aggregate as fine aggregate. The findings of these campaigns show that the concrete designed with ceramic aggregate achieve, in the majority of the studied properties, comparable or superior results to those of natural aggregate concrete.

In the following stage, the select few properties of optimum replaced ceramic aggregate concrete are studied. This was done to provide a broad and comprehensive outlook on some of the special applications properties of concrete. It was observed that the concrete designed with ceramic aggregate can provide encouraging characteristics to those of the natural aggregate concrete.

The final stage summarised the assessments of various designs of ceramic aggregate concrete with specific applicability areas. The future recommendation provides an exciting scope of study to reduce the global warming footprint of cement on the planet.

LIST OF CONTENTS

LIST OF FIGURES

LIST OF TABLES

CHAPTER 1

INTRODUCTION

1.1 INTRODUCTION

The indicator for any developed society has always been an improved life style along with the presence of better elemental and infrastructural facilities providing and fulfilling ever growing needs of the world. Construction industry is one of the main productive division of any thriving society. Modern day construction techniques are the legacy of fast and refined processes and consumption of by-materials originated from the industrial revolution. In India, construction sector contributes more than 8% of the gross domestic product and is the second largest employer of the citizens (Make in India, 2015).

The sustainable development idea of ensuring the needs of the present without compromising the ability of future generation (World commission on environment and development, 1987) is gaining exciting pace.

Sustainable construction an offshoot of sustainable development is steadily progressing and has several fields of interest. Industrial waste recycling is one of the fields that focuses on the effective utilisation of solid waste generated from the manufacturing sector into the construction sector. This step towards new ideas, results in formulation of procedure, introduction of new materials, improvement of existing techniques and the bigger objective of environmentally friendly product in focus.

In India, for example, specific guidelines and rules have been created to contain the ever increasing industrial waste. Such progress and headways are always a great steps towards an integrated sustainable development, but there is still much vacuum in this area. In the case of ceramic industries, India accounts for nearly 2.5% of the total global production and ranks 8th

in the list of highest ceramic producing countries (Ceramics industries in India, CII 2009). It provides employment to nearly 550,000 individual citizens. The ceramic industry consists of sanitary ware, electrical insulators, tile production (collectively called as technical ceramics), tableware ceramics and glass. Concrete is a well-known, used and popular material in construction sector. The production of concrete is environmentally exhaustive, its constituent materials are the major source of environmental imbalance. The fact that concrete production requires natural aggregates (coarse and fine) and it results in abundant consumption of natural resources is raising serious concerns. These are some causes on which concrete industry is focusing on the production of alternative/recycled aggregates to produce new concrete.

1.2 CERAMIC INDUSTRY CURRENT SCENARIO

The importance on environmental issues worldwide has resulted in high research interest in using ceramic industrial waste in concrete production and several initiatives are being taken by researchers worldwide. Recycled ceramic aggregates is one of these initiative, as it relaxes the environmental burden introduced by both the sectors.

In Spain, the share of ceramic sanitary ware production is nearly 26% within the European Union. The annual production rate for year 2008 was nearly 7 million ceramic units. Such high production results in approximately 24 tons of ceramic waste which is simply dumped (Medina et al., 2012).

The ceramic industry in china represents 35% share of the global market making it one of the largest producers of ceramic products. The ceramic sanitary ware industry has seen an annual growth of 28% in the year 2012. The annual output of the ceramic waste has exceeded 4 million tons and its management has become top priority for the industries.

India is the second highest manufacturer of bone china tableware just below china (AIGMF 2011). The total production of table ware bone china from both organised and small scale sector

is nearly 3, 43,000 tonnes per annum (Department of Industrial Policy and Promotion, DIPP, 2010). The manufacturing defects generated in biscuit fired products range from 15% to 20% of overall production (CGCRI, 2012). Considering the lower value of 15% for the estimation of waste generated, the figure achieved is nearly 51,450 tonnes per annum.

1.2.1 Ceramics sector in Rajasthan

Currently around 500 ceramic units covering glass and mineral grinding units are operating successfully in Rajasthan. Bikaner contributes nearly 80% of Rajasthan annual ceramic production. The state of Rajasthan accounts for more than 70% of India's bone china tableware production. One of the largest bone china ceramic producing industry unit is located in Jaipur. The daily production of the major industrial units is nearly 10 Tonnes. The waste generated from a single unit is 400-500 kg daily. Presently RIICO (Rajasthan State Industrial Development and Investment Corporation) has provided dumping yards for the industries to dispose of the waste.

1.3 PROBLEM STATEMENT

As of today, various studies are being conducted by taking into account the difference between the properties of natural aggregates and recycled ceramic aggregates, as their water absorption, micro structure and unit weight presents variations.

It is worth noting that the ceramic production and methods for various units vary greatly globally. Even the properties of the raw materials and the mix proportions are found to be divergent for respective countries. The firing temperature and finishing processes contribute further to physical and microstructural properties of the final product.

Such details imply that, even when recycled ceramic aggregate helps in conserving the natural resources and reducing transportation emissions, its impact on the properties of concrete should

be assessed by specifically considering the table ware ceramic waste of the local industries and then comparing it with globally available results.

1.4 MOTIVATION

The obstructions usually faced towards the waste utilisation activities are economical, technical, lack of understanding and management among others. The small rate of utilisation of waste material in concrete production is an example of aforementioned restraints that can be countered and improved (As evident by recently upgraded BIS 383:2016).

The technical aspect of waste materials along with their influence on properties of concrete are the decisive factors to approach between one and another alternative. The accomplishment of a ceramic fine aggregate that fulfils the existing technical boundaries, that reaches near similar behaviour as that of conventional concrete and making it more environment friendly as well as economical, along with representing an innovative and comprehensive idea are reasons enough for the study of such alternative fine aggregate.

1.5 OBJECTIVES

The objectives of this investigation is to examine, study, analyse and provide novel solutions and data about the use of recycled fine bone china aggregates (RFBCA) in concrete.

The specific objectives are listed below.

- To study the physical, chemical, microstructural and pozzolanic properties of the fine bone china ceramic aggregate.
- To analyse some of the fresh state, mechanical and durability properties of concrete mixes designed with different mix proportioning quantities and the use of natural and/or fine bone china ceramic aggregate.

- To observe the microstructural and chemical properties of concrete in terms of micro/nano structure and intensity, bond, chain length and phase of hydration products.
- To obtain the durability of fine bone china ceramic concrete mixes under various adverse conditions such as water, chloride, corrosion, acid and sulphate attack.
- To obtain the impact and fire performance of the optimum concrete mixes containing fine bone china ceramic aggregate.
- To evaluate the economical and photocatalytic aspect of the optimum concrete mixes containing fine bone china ceramic aggregate.

1.5 STRUCTURE OF THE THESIS

This thesis has been divided in eleven chapters. The document chapters are summarised below.

In Chapter 1, the main aspects regarding this investigation are mentioned, by presenting a brief introduction to the study subject, the current scenarios, the problem statement and the motivation. Finally, the main objectives of the investigations are declared and the methodology followed to present the investigation in the current form of the document is presented.

Chapter 2 presents a comprehensive study of the current and most relevant characteristics of ceramic concrete carried out in various investigations.

Chapter 3 presents the description of different materials used to make concrete mixes and the three experimental programme for the said constituent of concrete mixes.

Chapter 4 presents the fresh state and hardened state mechanical properties results of the concrete experimental programme.

Chapter 5 presents the microstructural and chemical characteristics of the selected concrete mixes.

Chapter 6, 7 and 8 present the durability properties of the concrete mixes under various conditions and external agents.

Chapter 9 presents the properties investigated for optimum replacement concrete mixes.

The conclusions of different chapters and recommendations for future investigations are finally presented in Chapter 10 and 11.

CHAPTER 2

STATE OF THE ART

2.1 INTRODUCTION

The most relevant characteristics of the ceramic aggregate concrete will be presented in this chapter, the materials used, production methods, material properties, application and innovation. The applicable studies and investigations are reviewed, focusing on the latest ones in order to properly describe the path followed until now, and also the studies which are of fundamental character.

2.2 CERAMIC CONCRETE MAKING MATERIALS

The materials used in the production of ceramic concrete are mainly the same used in natural aggregate concrete. The only difference is the presence of ceramic aggregates (CA) or ceramic powder (CP), which are responsible for the name of above mentioned concrete. The properties and quantities of these materials are the one that create major difference between these two types of concretes.

The main composition of CAC are cement, natural aggregates (NA), CA and admixtures as per requirements. The inclusion of CA is the one material that require conditioning, whether of type or quantity, such issues will be reviewed in the sections of this chapter.

The ceramic industry is a vast enterprise covering everything from stoneware to glass. Many divisions and classifications exist to simplify the ceramic industry. For this study the division of red ceramics and white ceramics will be considered. The colour of the ceramic product is dependent on the raw materials and production specifications.

In this review the CA compromise only of aggregates produced from white ceramics such as sanitary ware, electrical insulators, tiles and tableware etc. are focused and reviewed. However,

Table 2.1 provides a brief summary of red ceramic waste used as aggregate in various studies highlighting the source of ceramic waste, replacement percentage and its influence on compressive strength.

Table 2.1 Red ceramic waste used in different studies

Authors	**Source of red ceramic waste**	**Replacement**	**Influence on the compressive strength of concrete**
Torgal and Jalali (2010)	Ceramic brick	100% fine aggregate	Slight increase at 28 days curing period
Alves et al. (2014)	Ceramic brick	20%, 50% and 100% fine aggregate	Slight decrease at all curing ages and replacement levels
Etxeberria and Vegas (2015)	Construction and demolition waste containing 70% ceramic brick	10%, 20%, 35% and 50% fine aggregate	Increase in compressive strength at all curing ages and replacement levels
Vieira et al. (2016)	Ceramic brick	20%, 50% and 100% fine aggregate	Slight decrease at all curing ages and replacement levels
Gonzalez et al. (2017)	Ceramic brick and tile	20%, 35%, 50%, 70% and 100% fine and coarse aggregate	Maximum decrease of 28% at 100% replacement level
Adamson et al. (2015)	Ceramic brick	25% and 50% coarse aggregate	Slight increase at all replacement levels.

Cachim (2009)	Ceramic brick	15% and 30% coarse aggregate	Minor decrease at 30% replcement

2.3 WHITE CERAMIC WASTE

White ceramics generally consists of products that attain white to yellowish white colour upon firing. The chemical composition of white ceramics vary depending upon the type of raw aggregates to manufacturing processes. Table 2.2 highlights the chemical composition of various white ceramic waste used in concrete.

Table 2.2 Chemical composition of different types of white ceramic waste

Authors	**Type of ceramic waste**	**SiO_2**	**Al_2O_3**	**CaO**	**P_2O_5**	**Fe_2O_3**	**MgO**	**K_2O**
Torgal and Jalali (2010)	Sanitary ware	65.80%	22.20%	0.1%	-	0.6%	0.1%	3.50%
Halicka et al. (2013)	Sanitary ware	67.63%	24.05%	-	-	0.55%	0.36%	3.00%
Higashiyama et al. (2014)	Electrical Insulator	70.90%	21.0%	0.76%	-	0.81%	0.24%	3.57%

2.3.1 Ceramic waste as cement replacement

This subsection reviews the studies which considered white ceramic waste as cement replacement or as supplementary cementations material and its influence on various properties of concrete.

2.3.1.1 Workability

Kannan et al. (2017) observed that on utilisation of crushed sanitary ware powder the slump values are decreased. Although the slump retention values doubled on replacing upto 20% of cement with ceramic waste powder. The loss in workability was attributed to high surface area of ceramic waste powder. Subasi et al. (2017) reported that use of ceramic waste powder as filler in self-compacting concrete resulted in lower flow values than control concrete.

2.3.1.2 Fresh density

Subasi et al. (2017) observed lower values of fresh density of ceramic waste powder concrete than control concrete. The formation of air pockets on utilisation of ceramic waste powder was considered a prime factor for low fresh density.

2.3.1.3 Compressive strength

Kannan et al. (2017) observed lower compressive strength on replacing cement by 20%-40% sanitary ware ceramic waste powder. On examination of pozzolanic activity of ceramic waste, they reported presence of slight pozzolanic potential upto 40% ceramic waste powder. The lower compressive strength values were attributed to lower slump values and the corresponding improper compaction. Subasi et al. (2017) reported lower compressive strength values on utilising upto 20% waste ceramic powder as filler in concrete. The imbalance between C_3S and C_2S was identified as a probable cause for such effect.

2.3.1.4 Density

Subasi et al. (2017) reported that lower specific gravity of ceramic powder and the formation of air voids in concrete resulted in lower density of hardened concrete.

2.3.1.5 Split tensile strength

Subasi et al. (2017) observed a decrease in split tensile strength values with increase in ceramic waste powder ratio in concrete.

2.3.1.6 Microstructural

Kannan et al. (2017) observed that use of sanitary ware ceramic powder as cement replacement resulted in higher degree of hydration along with higher amount of free silica in concrete matrix.

2.3.1.7 Permeability

Kannan et al. (2017) reported lower values of chloride ion permeability in concrete containing sanitary ware ceramic waste powder. The reduction in permeable pores and densification of concrete matrix due to particle packing were found to be the effective causes for lower ingress of chloride ions.

2.3.2 Ceramic waste as aggregate

This subsection reviews the studies which considered white ceramic waste as coarse or fine aggregate and its influence on various properties of concrete.

2.3.2.1 Workability

Medina et al. (2012) found that with the increase in the replacement level of natural aggregates with coarse ceramic aggregates the workability decreased. The reduction in workability was linearly correlated with a coefficient of 0.9878 when the substitution was increased from 0% to 25%.

Halicka et al. (2013) examined that the workability of concrete mixes with 100 % fine and coarse ceramic recycled aggregate as a natural aggregate replacement. Sanitary ware based

recycled aggregates used in this investigation were diversified into two types of particles (passing No. 4 sieve) and coarse particle (passing No. 8 sieve and retained on No.4). They observed that the mixes containing recycled ceramic aggregates had lower workability as compared to the control mixture keeping a constant amount of water.

Alves et al. (2014) examined the effects of recycled ceramic aggregates as fine aggregates on the workability property of concrete. They found that for the fixed workability, the water-cement ratio required in the case of 100% fine recycled ceramic aggregate concrete mix, was higher as compared to the control concrete mix. For a concrete mix containing 50% fine recycled ceramic aggregates, water requirement reduced significantly.

Rashid et al. (2017) found that introduction of sanitary ware coarse aggregate results in reduced workability. High water absorption of ceramic waste was the leading cause of lowered amount of water causing lower slump values. The angularity and texture of ceramic aggregate also resulted in increased interparticle friction.

However, some studies do not show the results of reduced workability while utilising recycled ceramic aggregates in concrete. The published literature that show increased concrete workability on the use of recycled ceramic aggregates are presented below:

Senthamarai and Manoharan (2005) investigated the effect of ceramic electrical insulator based coarse recycled aggregates as natural coarse aggregates replacement on fresh properties of structural concrete mixtures. Six different water-cement ratios were used. The water content was kept constant. The slump increased with increase in coarse recycled ceramic aggregate content. Corominas and Etxeberria (2014) found that on increasing the replacement ratio of fine recycled ceramic aggregate the slump values of fresh concrete were increased. They observed that the smoother texture and low water absorption of the ceramic aggregates resulted in better workability.

2.3.2.2 Compressive strength

Correia et al. (2006) reported that the compressive strength of ceramic aggregate concrete was lower than that of control concrete sample. At the age of 28 days, the concrete mix incorporating 100% recycled ceramic aggregate recorded an approximate decrease of 44%.

Senthamarai and Manoharan (2005) studied the compressive strength at the age of 28 days of 100% recycled coarse ceramic aggregate in concrete on with six different water-cement ratios. They reported that the compressive strength of ceramic aggregate concrete was not considerably altered from that of the conventional concrete.

Binici (2007) studied the addition of 40-60% fine ceramic aggregate on the compressive strength of concrete at the age of 7, 28, 90 and 365 days. They reported an increase in compressive strength of concrete with the increasing content of ceramic aggregates. Ceramic aggregate concrete with 60% sand substitution resulted in highest compressive strength at all curing ages up to 365 days. The compressive strength of specimen containing 50% and 60% ceramic aggregate was found to be higher about 1.31 and 1.52 times that of control concrete samples.

Medina et al. (2012) found that compressive strength of coarse recycled ceramic aggregates was better than that of control concrete. The compressive strength increased by 12% at 28 days of age. As shown in Table 6 when recycled ceramic aggregate was utilised in the mix, compressive strength bested that of conventional concrete at all ages.

Higashiyama et al. (2012) studied the addition of 100% fine recycled ceramic aggregate as substitution for natural sand on the compressive strength of cement mortar at 7, 28 and 90 days. Furthermore, ceramic powder was used to replace 10%, 20% and 30% of cement by weight. Increase in the ceramic aggregate content resulted in greater compressive strength of cement mortar, the use of ceramic powder in addition to cement also yielded in higher strengths.

Halicka et al. (2013) investigated the concrete mixture containing both fine and coarse recycled ceramic aggregate after exposure to high temperature (1000°C). The compressive strength of concrete containing ceramic aggregates was better than that of the conventional concrete. High alumina cement was used due to expected resistance to high temperatures.

Corominas and Etxeberria (2014) reported that samples of concrete having 15 and 30% natural sand replaced with fine recycled ceramic aggregates showed enhanced compressive strength compared to control concrete sample at all curing age. At 28 days, the concrete produced with fine recycled ceramic aggregates achieved almost 10% higher strength values than that of the control mixture.

Gonzalez et al. (2014) explored the effect of sanitary ware recycled coarse ceramic aggregates with 100% replacement of natural aggregates and reported that ceramic aggregate concrete exhibited compressive strength nearly equal to the control concrete specimens. They concluded that the incorporation of 100% of recycled ceramic aggregates did not have a negative effect on the compressive strength of concrete.

Alves et al. (2014) reported that utilisation of 20%, 50% and 100% fine ceramic aggregate in concrete, the compressive strength was found to be almost 32.5%, 33.5% and 42.5% lower than that of reference concrete mix at 28 days. The reduction in compressive strength is due to higher water absorption of fine ceramic aggregates resulting in the increase of effective water/cement ratio, which contributed to the reduction of strength.

Higashiyama et al. (2014) explored the potential of utilising ground granulated blast furnace slag as a cement replacement in mortar containing 100% fine recycled ceramic aggregates. The mortar with 15% and 30% GGBS replacement did not exhibit the strength loss at any age compared to ceramic mortar without GGBS. Some retardation of compressive strength was observed in the 45% GGBS replacement at the early stages. At the later age of 91 days, all

ceramic mortar samples with GGBS have higher compressive strength than ceramic mortar without GGBS.

Zegardlo et al. (2016) studied the effect of 100% sanitary ware ceramic coarse aggregate on the compressive strength of high strength concrete. They reported an increase of 24.74% in compressive strength on using 100% sanitary ware coarse aggregate. The better physical properties of raw ceramic aggregate were considered to be the determining factor of concrete compressive strength.

Rashid et al. (2017) reported that upto 30% coarse sanitary ware aggregate can be incorporated in concrete mixes with positive effects on compressive strength. The roughness of ceramic aggregate creates a better interfacial transition zone between aggregate surface and cement mortar. The porous structure of raw aggregate also releases water thus initiating internal curing which results in higher compressive strength.

2.3.2.3 Flexure strength

Correia et al. (2005) observed that flexural strength of coarse recycled ceramic aggregate concrete was inferior to the flexural strength of control concrete specimen. The modulus of rupture decreased by 25% on 100% replacement of natural aggregates with coarse ceramic recycled aggregates.

Senthamarai and Manoharan (2005) demonstrated that the flexural strength of coarse recycled ceramic aggregate concrete was nearly equivalent to the control concrete specimen. They studied six different water/cement ratios at the age of 28 days.

Corominas and Etxeberria (2014) found that the flexural strength of fine recycled ceramic aggregates concrete was higher than that the reference sample. They observed that for 15% substitution, the increase in tensile strength is almost 28% and with the substitution of 30% the increase is 1.2%.

Gonzalez et al. (2014) studied the influence of coarse recycled ceramic aggregate on the hardened properties of concrete. They reported that the flexural strength of 100% ceramic aggregate concrete was greater than control mix concrete.

Zegardlo et al. (2016) found that 100% coarse sanitary ware ceramic aggregate results in 34.25% higher flexural tensile strength. The better interfacial zone between aggregate and mortar provided prolonged resistance against tensile loading.

2.3.2.4 Split tensile strength

Senthamarai and Manoharan (2005) studied coarse ceramic aggregate concrete with six different water/cement ratio. The concrete containing coarse ceramic aggregate had splitting tensile strength less than conventional concrete.

Medina et al. (2102) observed that up to 25% coarse aggregate substitution in concrete, there was an increase in split tensile strength and it increased considerably with the higher substitution of coarse ceramic aggregate content. As shown in Table 7 the maximum increase in the split tensile strength was 25% for 25% substitution of ceramic aggregates at the age of 28 days.

Alves et al. (2014) found that splitting tensile strength of fine ceramic aggregate concrete specimen were lower than reference concrete specimen at the age of 28 days. At replacement ratio of 100% maximum loss of 33.8% was observed.

Corominas and Etxeberria (2014) observed that fine ceramic aggregate concrete exhibited increased tensile splitting strength when compared to reference concrete. With 30% replacement of sand with ceramic aggregate, tensile splitting strength of concrete increased by 2.33%.

Gonzalez et al. (2014) found that 100% coarse ceramic aggregate concrete have 8.89% lower split tensile strength than reference concrete made with constant water/cement ratio.

2.3.2.5 Modulus of elasticity

Senthamarai and Manoharan (2005) reported that modulus of elasticity of concrete decreased with the incorporation of 100% coarse ceramic aggregate. The decreased modulus of elasticity was also a result of higher water/cement ratio. The modulus of elasticity of ceramic aggregate concrete varied from 22.2 to 16.1 GPa which was 13.6% to 2.4% lower compared to control concrete.

Alves et al. (2014) reported that modulus of elasticity of fine ceramic aggregate concrete declined from 38.3GPa to 28.3 GPa with the increase from 0% to 100% of the fine recycled ceramic aggregate content. The replacement ratio of 100% had a maximum loss of 26%.

Corominas and Exeberria (2014) observed that the modulus of elasticity of concrete at the age of 28 days curing decreased slightly when fine ceramic aggregate was substituted 15% whereas when the replacement was 30% the values of modulus of elasticity is nearly equal to that of control concrete mix.

2.3.2.6 Abrasion resistance

Correia et al. (2005) demonstrated that concrete having coarse recycled ceramic aggregate have far better abrasion resistance than reference concrete. They observed the variation of average loss in thickness by abrasion with proportion to ceramic aggregates. As the percentage of ceramic aggregates increases the loss in thickness reduces. The variation curve is almost linear.

Binici (2007) found that the resistance to abrasion improved as the percentage of fine ceramic aggregate was increased at all ages. The ceramic concrete had abrasion values 30% lower than the conventional aggregate.

Alves et al. (2014) found that the usage of ceramic aggregate in concrete caused a decrease in abrasion resistance. For a replacement of 100% recycled ceramic aggregates, a loss of 49.8% was observed. However, the differences in abrasion resistance were smaller for higher replacement ratios.

2.3.2.7 Microstructure

Medina et al. (2012) investigated the changes in microstructure when the natural coarse aggregate is substituted by recycled ceramic aggregate. The ITZ between the ceramic aggregate–paste becomes more compact, narrower and less porous than the natural aggregate–paste interface as the ceramic aggregates present a chemical composition similar to pozzolanic materials. The incorporation of ceramic aggregates results in superior specific surface area than natural aggregates due to its more irregular shape. The bond between recycled ceramic aggregate and cement paste is better due to irregularity in the shape of ceramic aggregates.

Zegardlo et al. (2016) observed better cohesion between ceramic coarse aggregate and cement mortar. The mechanical hook phenomenon due to angularity of ceramic aggregate created a trap area for mortar paste and resulted in dense microstructure of concrete.

2.3.2.8 Permeability

Binci (2007) observed that increase in fine ceramic aggregate content in concrete increases the chloride ion penetration resistance. The specimen with 60% fine ceramic aggregate were having lower chloride penetration depth than that of control concrete.

Senthamarai et al. (2011) demonstrated that with a decrease in water-cement ratio the permeability reduces. As shown in Fig. 6 and 7, the concrete mix of 100% coarse ceramic aggregate concrete the mix with lowest water-cement exhibits lowest permeability values. The permeability of ceramic aggregate concrete was higher than that of the conventional concrete mix.

Medina et al. (2012) investigated the oxygen permeability of recycled ceramic aggregate concrete, slight increments of 1.42% and 2.55% for 20% and 25% replacement were reported. The resistance to oxygen penetration decreased with rising porosity.

Medina et al. (2012) investigated the water permeability of ceramic aggregate concrete. The observed results were that the higher porosity of recycled ceramic aggregate did not affect the permeability of concrete. The concrete mixes with ceramic aggregate had higher sorptivity than control concrete mix. The values were under 3 $mm/h^{0.5}$, which indicate recycled ceramic aggregates as durable materials. The maximum water penetration depth in ceramic aggregate concrete was comparable to control concrete. Though, the mean value of the former was higher, it never exceeded 30 mm.

Higashiyama et al. (2012) found that at constant water/cement ratio, mortar containing ceramic powder and fine ceramic aggregate exhibited enhanced resistance to chloride ion penetration as compared to control mortar mix.

Corominas and Etxeberria (2014) observed that at the constant water-cement ratio, the resistance to chloride ion penetration of the concrete mixes reduced with an increased percentage of fine recycled ceramic aggregate replacement of river sand at the age of 28 days. However, at the age of 180 days the concrete mixtures prepared with fine ceramic aggregate exhibited the highest resistance to chloride penetration. The reduction of total charge in concrete was by 52% and 70% for 15% and 30% replacement of natural sand by fine ceramic aggregate.

Higashiyama et al. (2014) found that replacing cement by GGBS in 100% fine ceramic aggregate mortar paste decreased the penetration depth of chloride in mortar by half. The replacement level of 15% was sufficient to efficiently resist the chloride ingress.

Medina et al. (2016) investigated the chloride ion permeability of concrete incorporating 20% and 25% coarse ceramic aggregates. The pore system of concrete was influenced by high porosity of ceramic aggregates as an increase was observed with higher percentage replacement. This high pore system of the concrete caused 4% and 8% higher chloride penetration in concrete containing 20% and 25% ceramic aggregates.

Zegardlo et al. (2016) reported that incorporation of 100% sanitary ware ceramic coarse aggregate in concrete results in increased water absorption and depth of water penetration. The higher water absorption of the ceramic aggregate as well as the concrete voids due to angularity of aggregate leads to higher ingress of water.

2.3.2.9 Freeze thaw resistance

Medina et al. (2013) observed that the ceramic aggregate concrete had good performance and durability in environmental locations with frequent freezing and thawing cycles. The specimens observed had a maximum crack of 1.99 μm after 56 freezing and thawing cycles.

2.3.2.10 Electrical resistivity

Medina et al. (2016) substituted 20% and 25% natural coarse aggregate by ceramic aggregate. They observed that ceramic aggregate concrete displayed 17% and 31% higher resistivity than control concrete. The electrical resistivity was better with longer curing duration as it resulted in decline of large pores and better compact matrix.

Although there are several studies about the utilisation of sanitaryware and electrical insulator ceramic waste as aggregate in production of concrete. Almost none of the investigations have been found on the use of fine bone china ceramic waste as aggregate. This presents a major opportunity of research, given the characteristics of such ceramic materials, where their greatest objective is to confront and offer solutions to the environmental challenges that frequently used non-recycled materials imply.

CHAPTER 3

MATERIALS CHARACTERISATION

3.1 INTRODUCTION

In this chapter, a brief description of cement and admixtures will be presented, as their technical information can be consulted in the appendixes of this document. In the case of aggregates, the complete programme of characterisation will be presented, focussing on the chemical properties, physical properties and composition.

The materials used in this study are presented below:

- Tap water
- Ordinary Portland cement (43 grade)
- Superplasticising admixture (Auramix 400)
- Natural fine aggregate (NFA)
- Fine bone-china aggregate (FBA)
- 10mm and 20mm natural coarse aggregate (NCA)

3.2 CEMENT AND ADMIXTURE

43 grade ordinary Portland cement as per the specifications of BIS 8112 (2013) has been used in the experimental programme. Its technical sheet is presented in Appendix A.

Admixture from Fosroc company, a superplasticiser based on polycarboxylates have been used in this study. The technical sheets for admixture can be consulted in Appendix B.

3.3 AGGREGATES

The fine aggregates selected for this research were both natural and FBA. The coarse portion (>4.75 mm) comprised of only natural aggregates, while the fine portion (≤4.75 mm)

comprised of natural and/or fine bone-china ones. Two natural coarse aggregates, one natural fine aggregate (river sand) and bone-china based fine aggregate have been used. Since FBA are obtained from industrial sources its chemical analyses have been obtained to understand its basic properties. The evaluation of specific gravity and water absorption followed the BIS 2386-3 (2016). The particle size distribution of the aggregates has been obtained through BIS 383 (2016). All the test were carried out with at least three duplicate samples and under laboratory conditions.

3.3.1 Origin of FBA

The FBA used in this study come from waste and discarded ceramic tableware products (Fig. 3.1).

The FBA has been produced by means of crushing the waste tableware products. The crushed material was subjected to the particle size distribution test before choosing the final diameter of roller opening size and amount of passing through the crushing system. A pictographic diagram of the process is shown in Fig. 3.2.

(a) Ceramic waste as obtained

(b) Roller crusher

(c) FBA aggregate pile

Fig. 3.1 Process of production of FBA

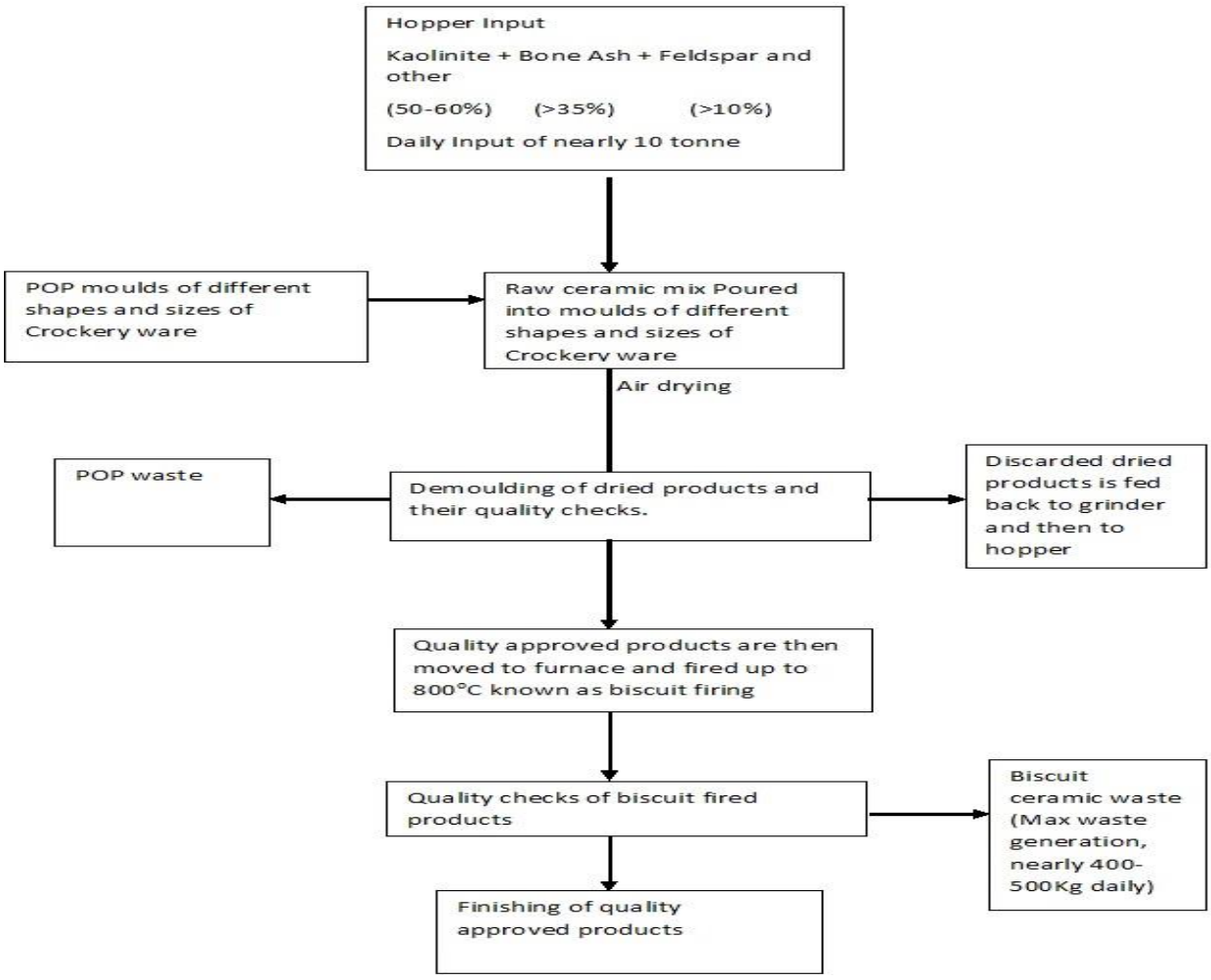

Fig. 3.2 Fine bone china table ware production and waste generation hotspots

3.3.2 FBA chemical properties

The X-rays diffraction (XRD) and X-ray fluorescence (XRF) were done on FBA samples to detect and determine their mineralogical and elemental compositions. The XRD diffractograms are presented in Fig. 3.3. XRF results are presented in Table 3.1.

From Fig. 3.3, the crystalline phases of tricalcium phosphate (T) and anorthite (A) were observed with small amounts of quartz (Q), aluminosilicate (AS), and phosphorus oxide (P). The overlapping of tricalcium phosphate and anorthite suggests a similarity in their crystal lattice spacing. XRD results indicate that the bone china ceramic aggregate has a high crystalline phase content with the slight presence of the glassy phase.

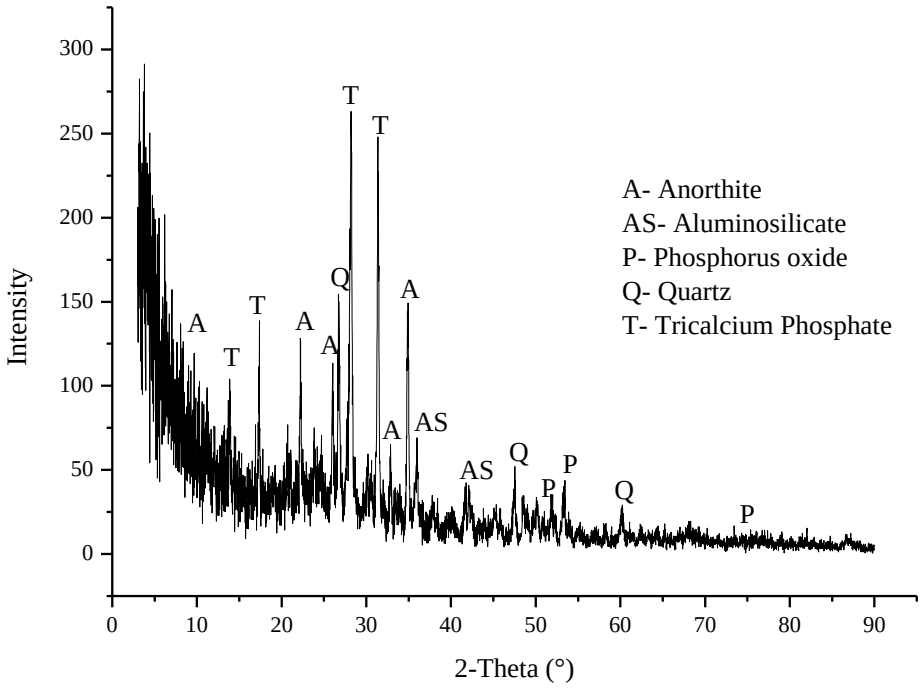

Fig. 3.3 XRD spectra of FBA

Table 3.1 XRF analysis of FBA ad NFA used in this study

Compound	FBA Sample	NFA Sample
Al_2O_3	23.86%	9.81%
CaO	24.15%	1.15%
SiO_2	28.86%	81.67%
MgO	2.8%	0.75%
Fe_2O_3	5.41%	2.11%
K_2O	1.58%	2.52%
P_2O_5	10.99%	-

Na_2O	0.54%	-
BaO	0.70%	-
MnO	0.01%	-
SrO	0.04%	-
TiO_2	0.55%	-
ZnO	0.01%	-
NiO	0.001%	-
CuO	0.01%	-
LOI	0.5%	0.2%

The above presented XRF analysis (Table 3.1) shows that FBA has nearly equal quantities of silica, calcium and aluminium followed with phosphorus and other minority elements, whereas NFA present silica as their main constituent, followed by alumina and other traces of elements.

3.3.3 Structure of FBA

Fig. 3.4(a) shows the bone china aggregate used in this study. A scanning electron microscope (SEM) study of bone china ceramic was conducted to examine its microstructure, which is presented in Fig. 3.4(b). JEOL JSM-7600F field emission SEM (FE-SEM) was used in the image processing study. From the images, it can be inferred that bone china ceramic is composed of the infused layers of calcium and silica. In addition, angularity in particles can be observed with sharp cleavages and elongation. The presence of calcium can be observed in the brighter areas of the image. The dark areas show closed and semi-closed pores of different shapes and sizes.

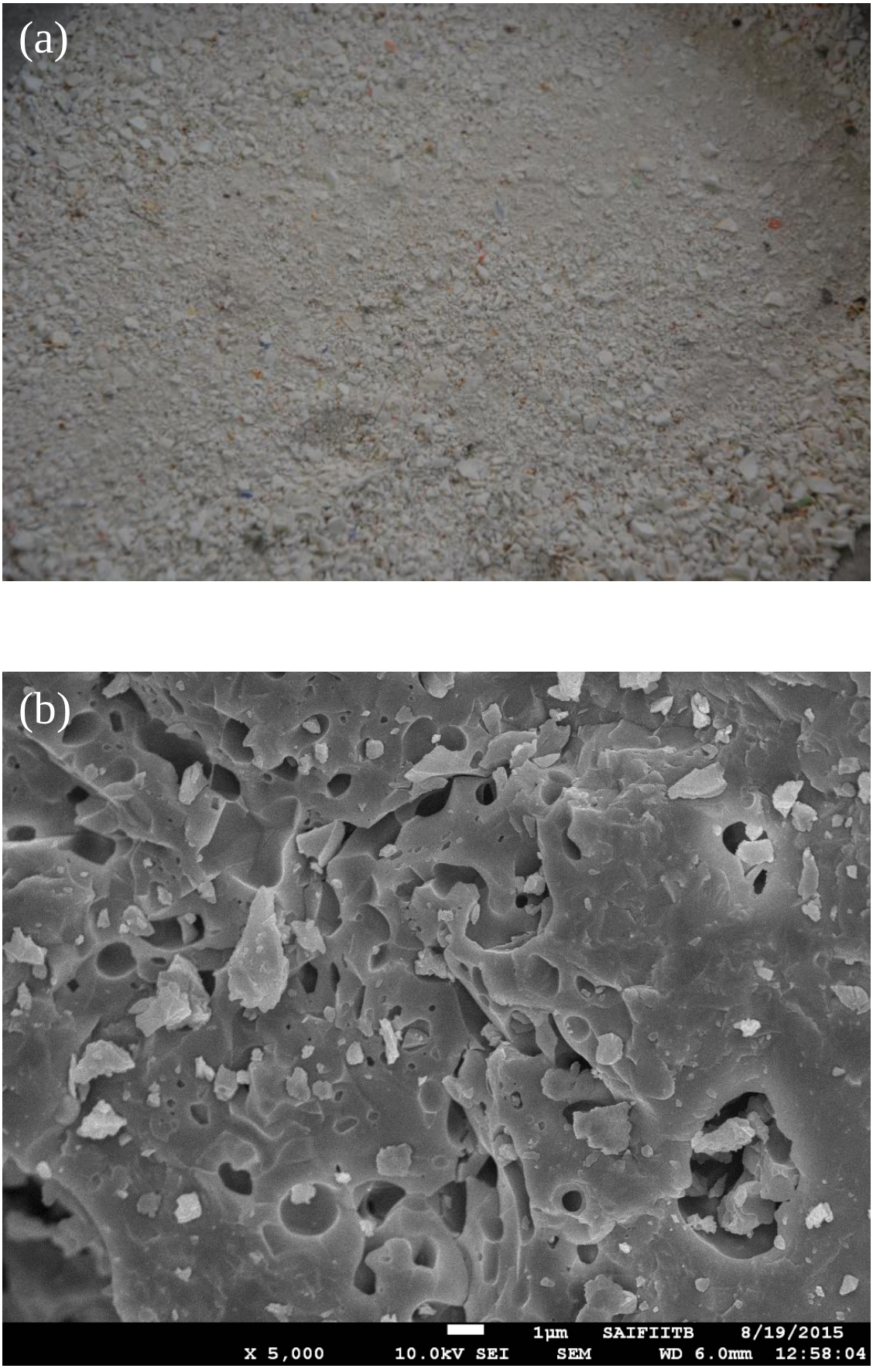

Fig. 3.4 (a) FBA **(b)** Microstructure of FBA

3.3.4 Thermal properties of FBA

Thermo gravimetric analysis (TGA) was done on samples of both ceramic and natural sand as shown in Fig. 3.5. The samples were exposed upto 900°C with a rate of 30°C/min. The mass loss of the sample were plotted against the rise in temperature. Natural sand sample show mass loss when temperature reaches 700°C, on the other hand ceramic sand show no mass loss upto 900°C. The results obtained shows that FBA can be used to develop fire/elevated temperature resistant concrete.

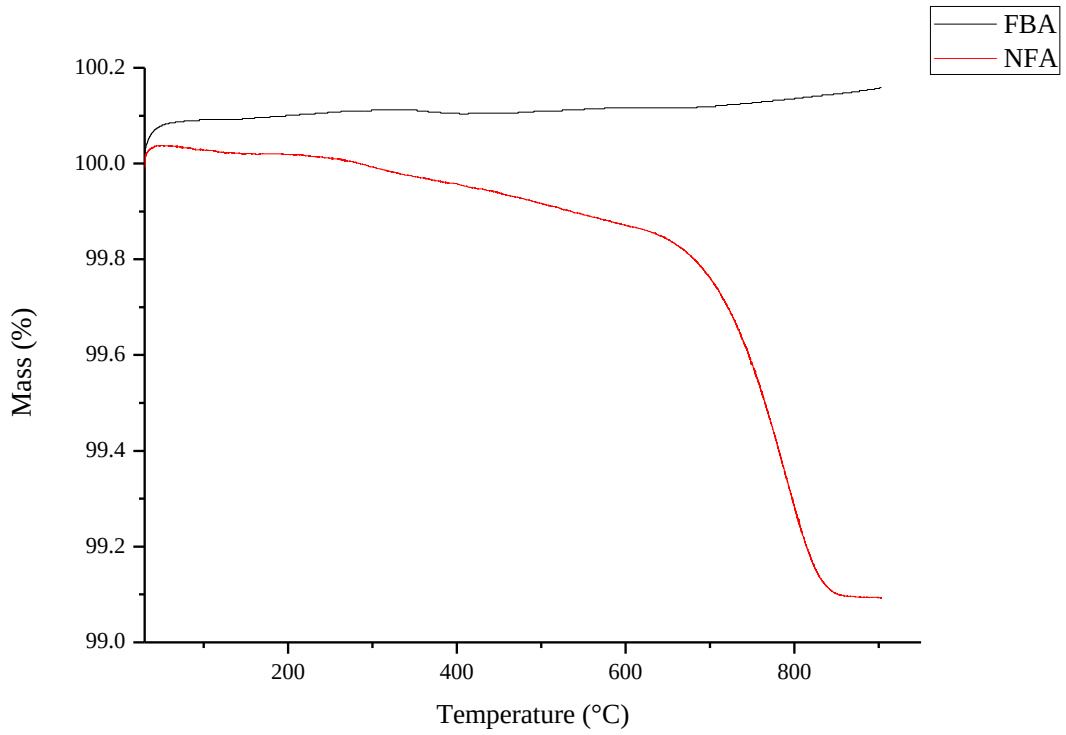

Fig. 3.5 TGA curve for FBA and NFA

3.3.5 Aggregates physical properties

3.3.5.1 Specific gravity and water absorption

This section deals with obtaining the specific gravity and water absorption of the aggregates.

Specific gravity of aggregates were tested according to the pycnometer procedure as per BIS 2386 (2016). The procedure followed is also instrumental in determining the water absorption capacity. Table 3.2 shows the results of the test.

Table 3.2 Specific gravity and water absorption of the aggregates

Aggregate	Specific gravity (kg/m^3)	Water absorption (%)
NFA	2.6	1.0
FBA	2.3	2.5
NCA	2.7	0.5

From the above listed results it can be observed that the specific gravity of different aggregates present little differences with each other and the absorption values have higher differences. The higher water absorption results are due to the presence of P_2O_5 in FBA which acts as water desiccator and enhances the water absorption capacity of aggregate (Kotoh et al. 1990). Each concrete mix used in this investigation has incorporated these results in their formulation.

3.3.5.2 Particle size distribution

The particle size distribution of fine aggregate provides the distribution of different sizes of specific aggregate, by means of sieve separation following the specifications of BIS 383 (2016). Both NFA and FBA used in the study conforms to the Zone II of the Indian specification and standard (BIS 383:2016). The particle size distribution is presented in Fig. 3.6.

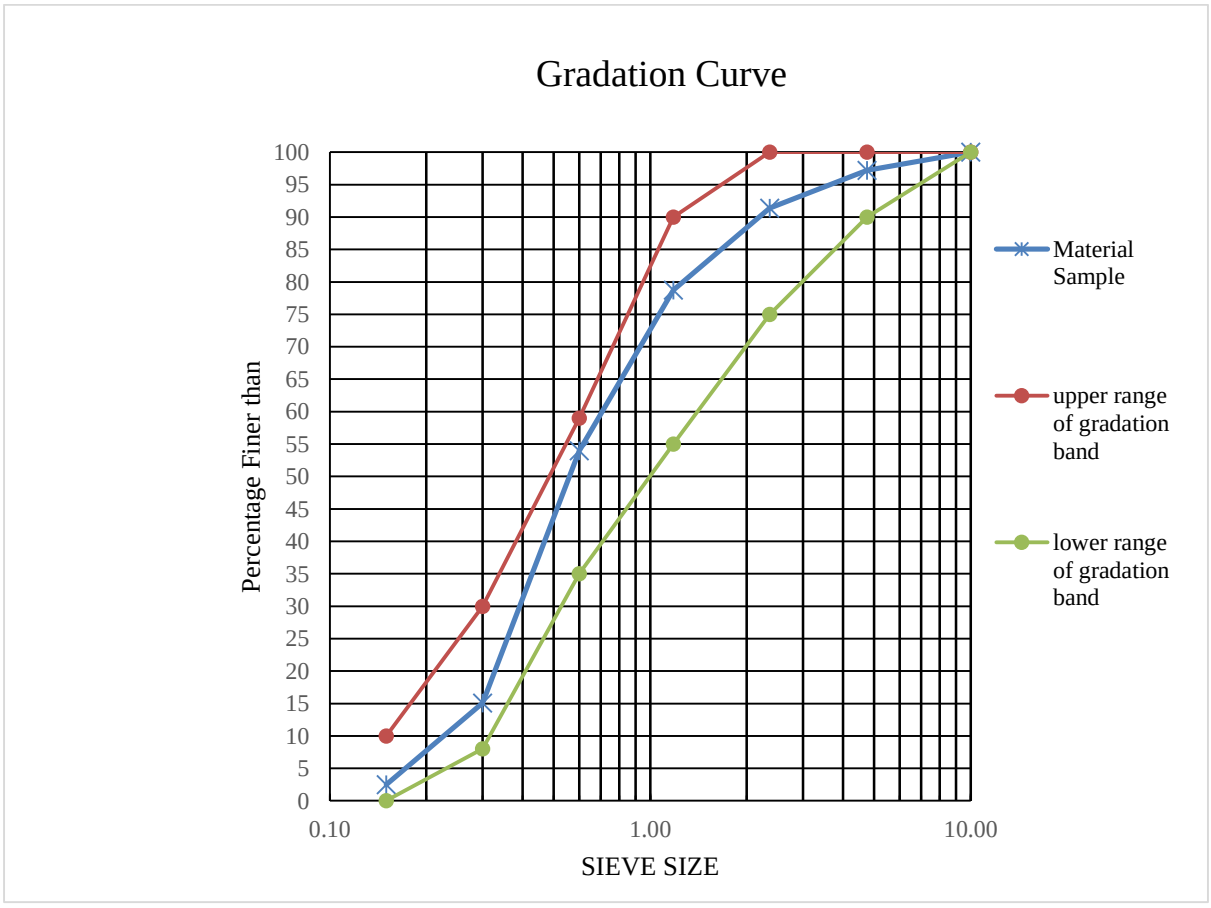
Gradation Curve
Percentage Finer than
100
95
90
85
80
75
70
65
60
55
50
45
40
35
30
25
20
15
10
5
0
0.10
1.00
10.00
SIEVE SIZE
Material Sample
upper range of gradation band
lower range of gradation band

(a)

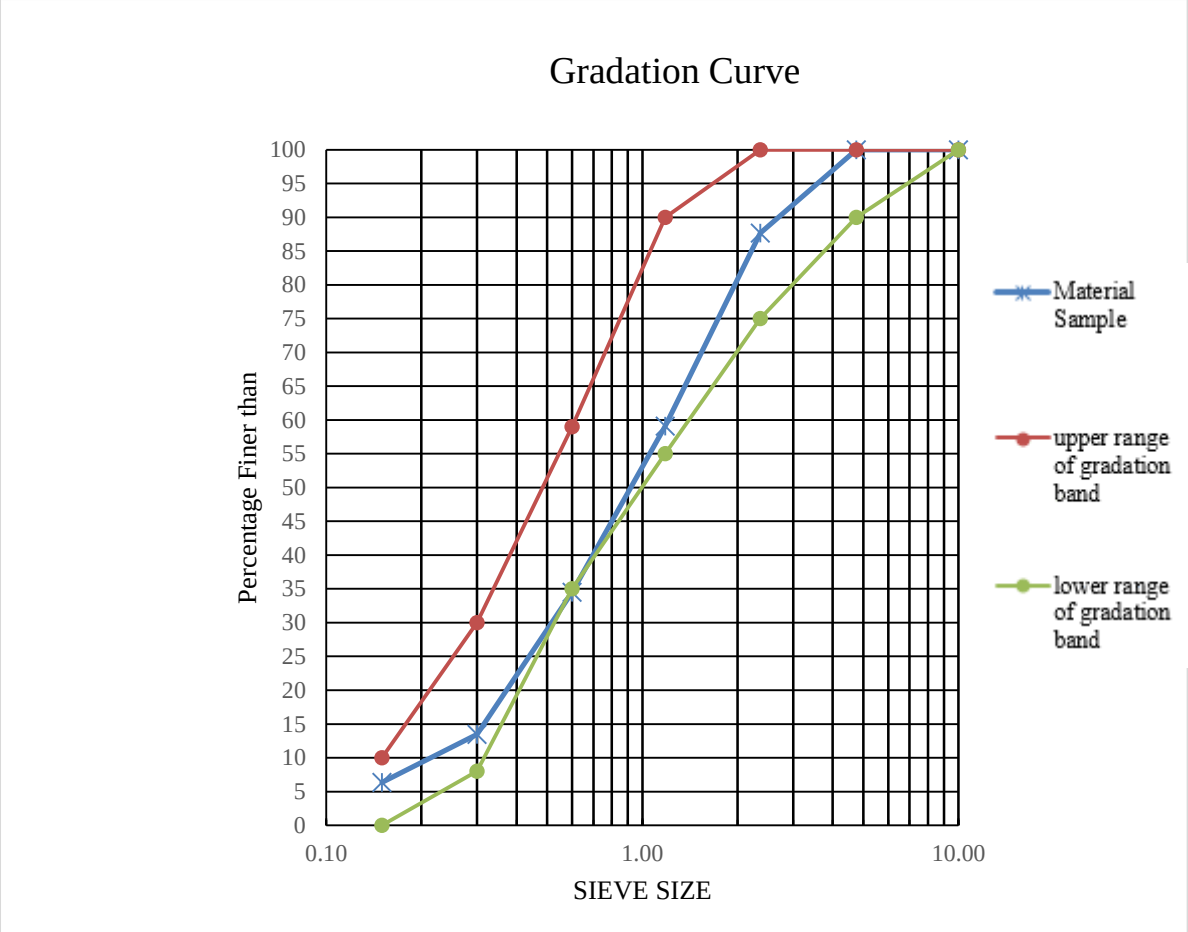

(b)

Fig. 3.6 Particle size distribution of fine aggregate: **(a)** NFA; **(b)** FBA

3.4 POZZOLANIC BEHAVIOUR

3.4.1 Pozzolanic activity (Frattini test)

The guidelines specified in BS EN 196-5 (2011) were followed. 20 gram test samples containing 20% FBA and 80% OPC were made and mixed with 100 gm distilled water. The samples were properly sealed in plastic bottles and were kept in an oven at 40° C for 15 days. The samples were then vaccum filtred through 2.7 µm nominal pore size diameter filter paper (Whatman No. 542) and were cooled to ambient temperature in sealed Buchner funnel. The filtrate was analysed for OH^- by titration against dilute hydrochloric acid solution with methylorange indicator. The filtrate solution was also analysed for Ca^{2+} by pH adjustment to

12.5, followed by titration with 0.003 mol l^{-1} of ethylenediaminetetra-acetic acid (EDTA) solution using Patton and Reeders indicator. The filtrate solution was standadised for dilute HCl and EDTA solution using calcium carbonate and sodium carbonate solutions respectively. The data points that lie above saturation line (lime activity curve defined in BS EN 196-5: 2011) indicate no pozzolanic activity and those lying below the saturation line indicate pozzolanic activity. The procedure assumes that no other source of soluble calcium influences the system.

3.4.2 Pozzolanic activity (Saturated lime test)

In presence of pozzolanic material, the calcium hydroxide reacts with pozzolana to dissolve until the pozzolana or portlandite is exhausted. The sample preparation was done by adding 1 gm of material to a plastic bottle containing 75 ml of saturated lime solution. The lime solution was prepared by dissolving 2 gm of hydrated lime in 1l ml of distilled water. The sealed plastic bottles were placed in an oven at 40°C for 1, 3, 7 and 28 days. The samples at respective testing dates were filtered and titrated for OH^- and Ca^{2+} using the procedure mentioned in frattini test. The Ca^{2+} ions interact with test material or water, the quantity of lime consumed by the test materials can be quantified. The results reported is the % CaO removed at the respective testing period.

3.4.3 Pozzolanic activity (Strength activity index)

The specifications of ASTM C311 (2016) were followed to obtain strength activity index (SAI) of aggregate. The control sample was prepared by mixing 500 gm OPC cement, 1375 g graded standard sand and 242 ml water. Test samples were prepared by replacing 20% OPC cement with natural sand and FBA aggregate. The water/cement ratio was altered to obtain similar flow values as that of control sample. Mortar samples were cast into six 50 mm cubes and were demoulded after 24 hours and placed in curing tank for 7 and 28 days. The samples were tested at 7 and 28 days for compressive strength. The strength acivity activity index is reported as :

SAI= (A/B)×100

Where A is average compressive strength of test mix cube and B is average compressive strength of control mix.

3.4.4 Pozzolanic behaviour of FBA

Figs. 3.7-3.9 presents the pozzolanic activity of fine aggregates. As shown FBA exhibit slightly higher pozzolanic activity than NFA. The chemical composition of fine bone china aggregate consituting mainly of SiO_2, CaO and Al_2O_3, permits slight pozzolanic behaviour of the raw material. From Fig. 3.7 (frattini test), the concentration of CaO and OH was plotted on the lime activity curve. For raw sand the corresponding values of CaO and OH are 45.56 mmol/L and 11.34 mmol/L respectively whereas for FBA the values for CaO and OH are 49.98 mmol/L and 8.752 mmol/L respectively. Results of FBA fall below the lime activity curve as shown in Fig. 3.7. The greater consumption of calcium hydroxide in the pozzolanic reaction due to FBA can be a suitable assessment of such behaviour. In saturated lime test, percentage of total CaO removed was calculated for 1, 3, 7 and 28 days. The decrease in CaO content in solution is due to consumption of $Ca(OH)_2$ caused by pozzolanic reaction. Higher level of CaO reduction was observed for FBA sample. The reduction observed for natural sand was 24.52%, 31.13%, 27.42% and 25.32% for 1, 3, 7 and 28 days respectively. For FBA, the reduction observed was 37.9%, 53.71%, 70% and 67.26% for 1, 3, 7 and 28 days respectively (Fig 3.8). Fig. 3.9 shows the compressive strength observed in strength activity index test for NFA and FBA. The strength activity index ratio observed for FBA was higher than 0.75 required to be classified for pozzolanic material as per ASTM guidelines. The results obtained from all three methods can be used to confirm that introduction of FBA plays a significant role in formation of hydration products.

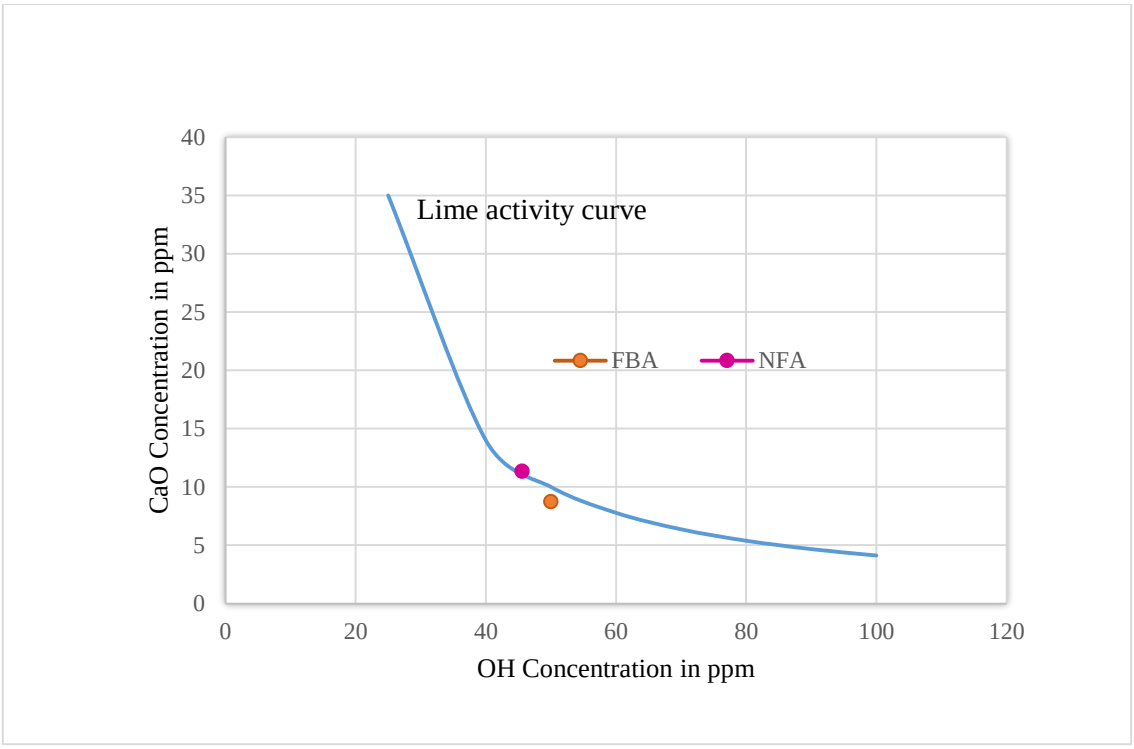

Fig. 3.7 Frattini test results for FBA and NFA at 15 days

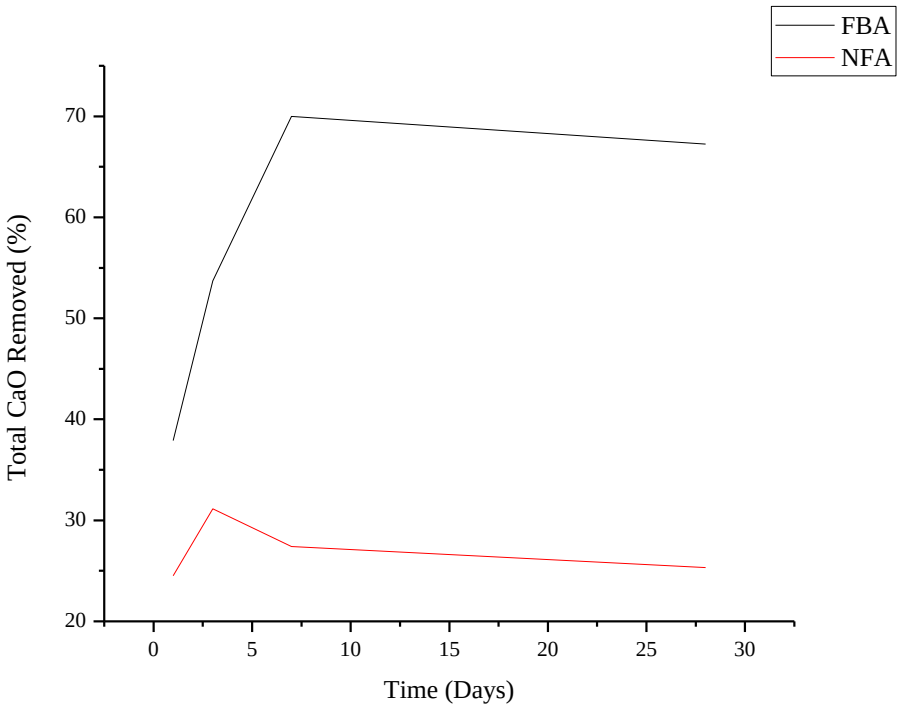

Fig. 3.8 Saturated lime test results for FBA and NFA at 1, 3, 7 and 28 days

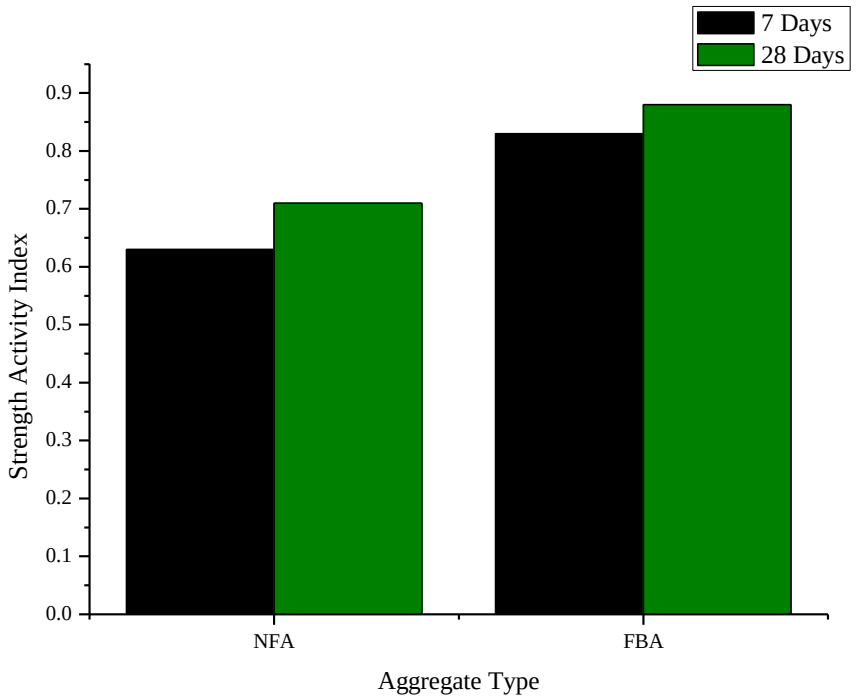

Fig. 3.9 Strength activity index for FBA and NFA at 7 and 28 days

3.5 CONCRETE MIX DETAILS

Three experimental programme of concrete mix proportion were designed according to BIS 10262 (2009) for three water cement (w/c) ratio of 0.35, 0.45 and 0.55. In all three mixes 100% NFA was replaced by FBA with increments of 20%. To maintain a constant workability (compaction factor of 0.9-0.95) the dosage of superplasticiser was varied as shown in Table 3.3. The three w/c ratios were designated as series A (0.35), series B (0.45) and Series C (0.55). Series A was designed for M30 grade of concrete and water content was varied for rest two series, i.e B and C. To compensate for water absorption of aggregate extra water was added at the time of mixing.

Table 3.3 Concrete mix proportions

Mix	Cement (kg/m^3)	NFA (kg/m^3)	FBA (kg/m^3)	Coarse aggregate (kg/m^3)	Water (kg/m^3)	Superplasticiser (%)
A0	383	821	0	1095	147.73	0.5
A20	383	656.8	147.78	1095	149.78	1.0
A40	383	492.6	295.56	1095	151.84	1.0
A60	383	328.4	443.34	1095	153.89	1.0
A80	383	164.2	591.12	1095	155.94	2.2
A100	383	0	738.9	1095	157.99	2.4
B0	383	821	0	1095	186.03	0.10
B20	383	656.8	147.78	1095	188.08	0.10
B40	383	492.6	295.56	1095	190.14	0.15
B60	383	328.4	443.34	1095	192.19	0.15
B80	383	164.2	591.12	1095	194.24	0.20
B100	383	0	738.9	1095	196.29	0.20
C0	383	821	0	1095	224.33	0
C20	383	656.8	147.78	1095	226.38	0
C40	383	492.6	295.56	1095	228.44	0
C60	383	328.4	443.34	1095	230.49	0.05
C80	383	164.2	591.12	1095	232.54	0.10
C100	383	0	738.9	1095	234.59	0.10

3.6 CONCRETE MIX ELABORATION

Three concrete mixes were prepared using different w/c ratio and varying percentage of FBA. The materials were first weighed and put into the concrete mixer, starting with coarse aggregates followed with fine aggregates, cement and water. The admixture was introduced after 1-2 minutes of wet mixing. The admixture was properly mixed in small amount of water taken from initial mixing water. When concrete mix showed desired and uniform distribution, the concrete specimens for different tests were casted and cured. The curing process was done by leaving the specimen mould in the laboratory for 24 hours, covered with plastic sheets to prevent evaporation. Afterwards, the specimens were de-moulded and were cured in water for 28 days or until testing.

3.7 CONCLUSIONS

The properties of concrete making materials were evaluated by evaluating their specific gravity, water absorption, particle size distribution, chemical composition, thermal response and microstructure. The following conclusions are drawn:

1. The chemical composition of FBA contains no toxic element and can be beneficial in hydration mechanism of concrete.
2. Particle size distribution of FBA conform to the requirements of Indian standard for fine aggregate.
3. The FBA have higher roughness and angularity than NFA.
4. Micro pores are observed in FBA which may increase the water absorption of raw aggregate.

CHAPTER 4

FRESH STATE AND MECHANICAL PROPERTIES

4.1 INTRODUCTION

The fresh and mechanical properties of concrete are the early stage indicators of the quality of concrete designed for specific requirements. Compressive strength of concrete is the most important of all properties as it provides a wide array of knowledge regarding the performance of concrete on its mechanical properties. However, some specific applications and situations demand a better understanding of other parameters, like the elastic modulus, abrasion resistance and density. Also, determining the fresh state properties such as slump, air content, bleeding and fresh density gives us an idea of the flowing behaviour, entrapped air and water loss of the material in its fresh state, which is of importance when the working and placement of the mix is done.

4.1.1 Objectives

The main objective of this chapter is to obtain and discuss some of the fresh state and mechanical properties of concrete containing FBA.

The specific objectives being covered from the previously defined are:

1. To state an experimental procedure adopted to determine the fresh state and mechanical properties of concrete mixes.
2. To determine and analyse the influence of the FBA on the compaction factor, air content, bleeding, fresh density, hardened density, compressive strength, split tensile strength, flexural strength, modulus of elasticity, and abrasion resistance, of the concrete mixes.

3. To establish the effects of utilising FBA concerning these tests, when compared to NFA.

4.1.2 Program of the study

The above presented objectives will be covered by presenting the experimental programme and its results.

In the first stage, the methods and standards followed for experimental programme will be presented. Next, the results obtained will be presented along with the overall analysis of the results. Finally, the conclusions of the chapter will be presented.

4.2 METHODOLOGY

The assessment of fresh state and mechanical properties of concrete mixes was done by various experimental programmes. The fresh state properties were measured immediately after the mixing process was completed. The hardened state mechanical properties were measured after 7, 28, 56 and 90 days of curing. In case of mechanical properties of concrete mixes, three samples of each mix for one of the tests were used to obtain required information and to prevent inconsistencies of the final reported values, the presented results correspond to the average values.

4.3 FRESH STATE PROPERTIES

4.3.1 Experimental programme

In the present study, the workability of fresh concrete was examined by compaction factor test as per BIS 1199 (1959). Suitable dosage of superplasticiser was administered to maintain the compaction factor of 0.9 or higher. The air content and fresh density of concrete were determined per BIS 1199 (1959). The loss of water through bleeding was determined as per the specifications of ASTM C232 (2009).

4.3.2 Results and discussion

4.3.2.1 Workability

The water demand to achieve desired workability of concrete depends upon the fines percentage and characteristics of aggregates. The workability of concrete is the basic indicator of the quality for placement and ease of workmanship.

The results of compaction factor test measurements of various concrete mixes are shown in Table 4.1. It can be observed that required dosage of superplasticiser increases as the content of FBA increases in fresh concrete mix. The increase in surface area due to angularity and roughness of FBA particles, causes decrease in workability. The roughness and angularity of FBA also causes increased inter particle friction that restricts the workability of fresh concrete mix. The angularity of FBA increases the amount of paste required to cover the aggregate surface causing difficulty in achieving the desired workability. High water absorption by the semi closed pores of the FBA, also reduces the free water for particle lubrication. In chemical composition of FBA 10.99% of P_2O_5 was observed. The desiccating nature of P_2O_5 enhances the need for water to attain desired workability.

Table 4.1 Workability of FBA concrete mixes

Mix No.	**CF**	**Mix No.**	**CF**	**Mix No.**	**CF**
A0	0.93	B0	0.94	C0	0.96
A20	0.93	B20	0.93	C20	0.95
A40	0.92	B40	0.93	C40	0.94
A60	0.92	B60	0.93	C60	0.94

A80	0.92	B80	0.93	C80	0.94
A100	0.92	B100	0.93	C100	0.93

4.3.2.2 Air Content

The entrapment of air can happen intentionally or unintentionally either during mixing and placement of concrete. Small, well dispersed air can be helpful in providing adequate workability, reduction in segregation and early age resistance to freeze thaw effect.

Fig. 4.1 shows the air content test results for fresh concrete mixes containing FBA. The concrete mixes with higher w/c have higher air content due to the formation of air pockets or bubbles in fresh mix. B0 and C0 concrete mixes have 9.1% and 15.5% higher air content than A0 mix. Introduction of FBA in concrete mixes results in decrease of air content. The concrete mixes containing 100% FBA recorded the lowest values of air content.

The air content of concrete mixtures containing 20%, 40%, 60%, 80% and 100% bone china aggregates decreased by 1.3%, 3.9%, 4.74%, 5.6% and 9.1% for concrete series A; 3.9%, 7.9%, 8.7%, 10.7% and 11.8% for concrete series B; and 5.9%, 7.5%, 8.6%, 11.2% and 13.8% for concrete series C, respectively. The higher dosage of the superplasticizer also reduced the air content, as the low viscosity led to the escape of air from fresh mixed bone china ceramic concrete. Increased bleeding from bone china ceramic concrete mixtures also lowered the air content, because the movement of water molecules by capillary action reduced the formation of air pockets. Similar observations were made when the air content was measured using the gravimetric method. The results of the gravimetric method are listed in Table 4.2. The values obtained using the gravimetric method were higher than those obtained using the pressure meter method. The percentage difference between the values obtained using two methods is also presented in Table 4.2.

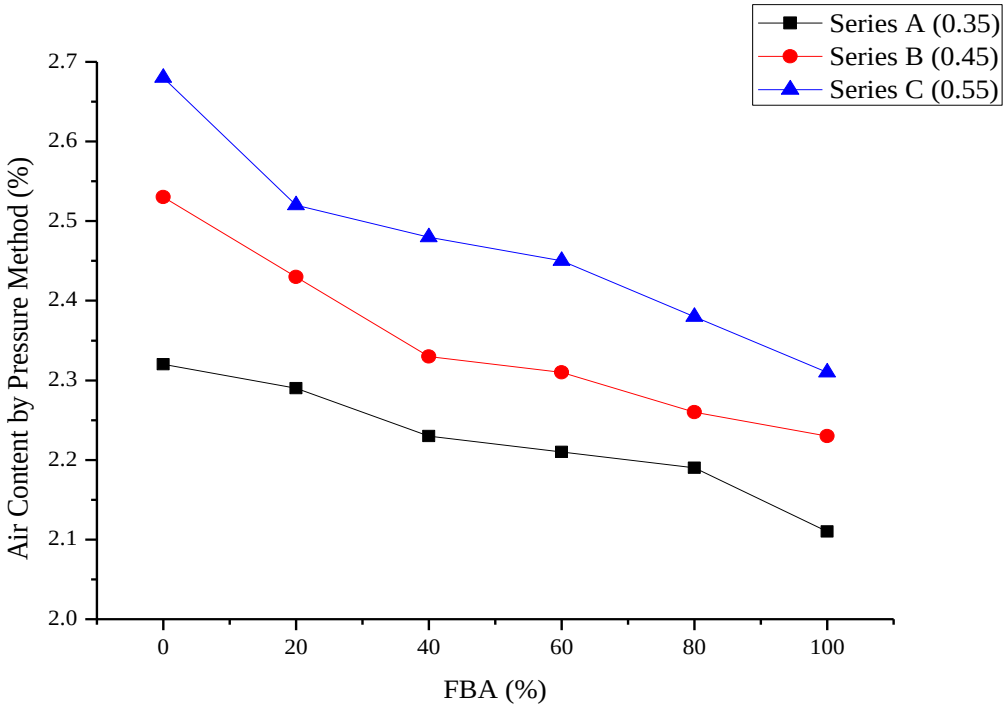

Fig. 4.1 Air content (%) of FBA concrete mixes

Table 4.2 Air content by gravimetric method and percentage difference from pressure method

Mix	Air content (%)	Difference between gravimetric method and pressure method (%)
A0	2.46	+6.03
A20	2.39	+4.37
A40	2.30	+3.14
A60	2.28	+3.17
A80	2.26	+3.20
A100	2.17	+2.84
B0	2.64	+4.35
B20	2.59	+6.58
B40	2.38	+2.15

B60	2.37	+2.60
B80	2.35	+3.98
B100	2.29	+2.69
C0	2.77	+3.36
C20	2.63	+4.37
C40	2.61	+5.24
C60	2.57	+4.90
C80	2.43	+2.10
C100	2.37	+2.60

4.3.2.3 Bleeding

After placement of concrete, the process of segregation starts due to difference in weights of the constituent materials. Water being the lightest constituent material rises to the top of surface giving the effect of bleeding. Too much bleeding of water may result in imbalance of water to cement ratio and formation of voids left behind due to rising effect of water.

The effect of FBA on the bleeding of concrete is presented in Fig. 4.2. The total water loss caused by bleeding was 0.16% for the control mixture A0, 0.13% for B0, and 0.87% for C0. The total water content in the control concrete mixture C0 was higher than that in A0 and B0, leading to high water loss from bleeding. The bleeding in all three FBA concrete mixtures containing 100% bone china aggregates was 2.09%, 1.68%, and 2.1%, respectively. On incorporation of 100% FBA into concrete, a higher volume of total water was added to the mixture to compensate for the water absorption of bone china aggregates, resulting in increased bleeding of the water content. The internal water absorbed by FBA is gradually released back into the concrete mixture, which causes an increase in the bleeding of the water content.

Corominas and Etxeberria (2014) observed similar behavior for ceramic aggregate. In addition, high dosages of the superplasticizer used to produce the desired workability in FBA concrete mixtures resulted in high water loss due to bleeding. The higher dosage of the superplasticizer also caused a delay in the setting time, resulting in the longer duration of bleeding. Further, the FBA are lighter than those in NFA. This leads to the formation of laitance on the top surface of freshly mixed bone china ceramic concrete, causing an increase in the amount of water from bleeding.

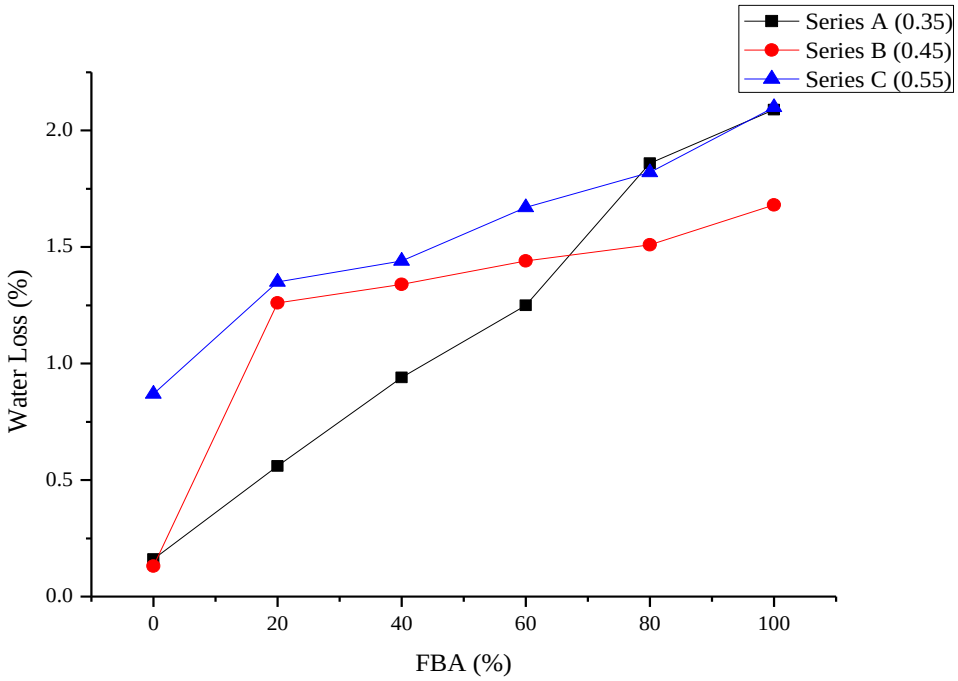

Fig. 4.2 Bleeding water loss in FBA concrete mixes

4.3.2.4 Fresh density

The effect of FBA on the fresh density of the concrete mixtures of all series is illustrated in Fig. 4.3. The fresh density of control mixtures was 2490 kg/m^3, 2450 kg/m^3, and 2410 kg/m^3 for A0, B0, and C0 respectively. Almost comparable increase in the fresh density of concrete mixtures was observed after the incorporation of FBA. Depending on the content of FBA the fresh density of FBA concrete mixtures varied between 2.01% and 8.03% for series A, between 2.45% and 6.12% for series B, and between 1.04% and 7.26% for series C compared with that

of particular control mixtures. As shown in Fig. 4.3, the fresh density of concrete mixtures increased by an average value of 7% when 100% FBA were used. The addition of higher doses of superplasticizer into fresh concrete mixtures containing FBA resulted in better consolidation due to lower viscosity that causes an increase in fresh density of concrete.

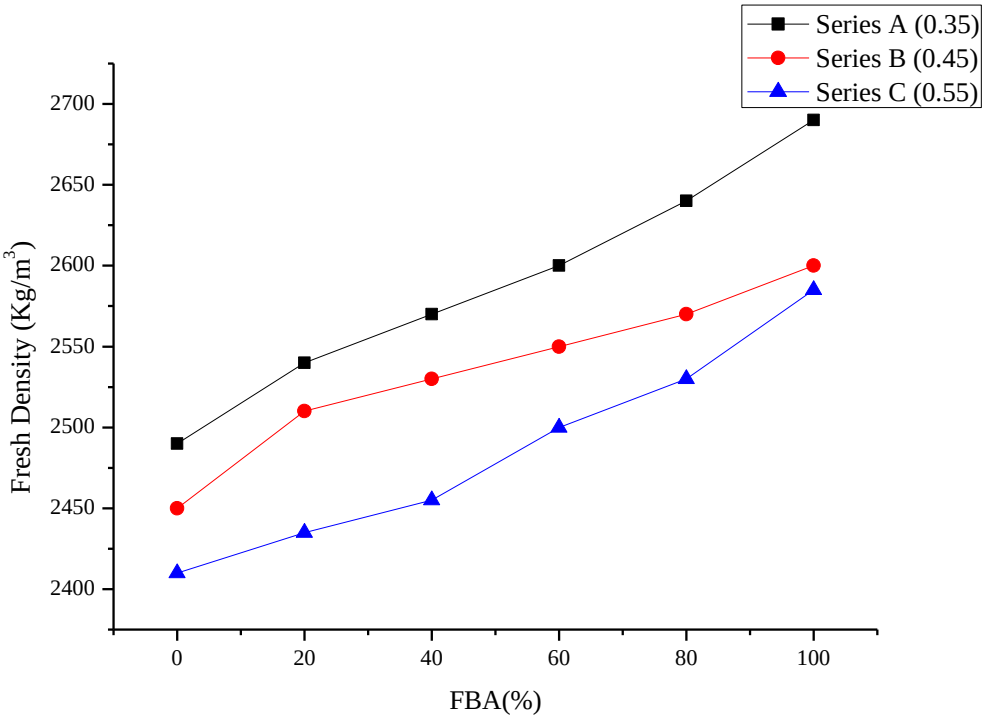

Fig 4.3 Fresh density of FBA concrete mixes

4.4 MECHANICAL PROPERTIES

4.4.1 Experimental Programme

4.4.1.1 Density

Density of hardened concrete was measured as per the specifications of BIS 516 (2013). An average of 3 samples of 150 mm cube was considered in reporting the final values.

4.4.1.2 Compressive strength

The compressive strength was performed on three 100 mm concrete cubes at 7 days, 28 days, 90 days and 180 days water cured specimens as per the guidelines of BIS 516 (2013). A compression testing machine having a capacity of 2000 kN was used throughout the study.

4.4.1.3 Split tensile strength

Split tensile strength was determined on three 150 mm concrete cubes at 28 days water cured specimens as per the specifications of BIS 5816 (2004). The split tensile strength test was performed on 1000 kN universal testing machine throughout the study.

4.4.1.4 Flexural strength

The flexural test was performed on 100 mm×100 mm×500 mm concrete beams. Flexural strength was determined for three specimens at 28 days and 56 days of water curing age as per the specification of BI 516 (2013). A flexural testing machine of 200 kN with four point loading configuration was used throughout the study.

4.4.1.5 Static modulus of elasticity

The static modulus of elasticity was measured as per the specification of ASTM C469 (2014). Cylindrical specimen of 150 mm diameter and 300 mm height were used at 28 days curing age. Specimens were tested on a compression testing machine of 2000 kN capacity with longitudinal

compressometer and lateral extensometer attachments. The rate of loading was kept at 240±35 kN/m^2/s. The modulus of elasticity was then calculated by the following equation:

$$E_s = \frac{(\sigma_2 - \sigma_1)}{(\varepsilon_2 - 0.000050)} \quad (4.1)$$

4.4.1.6 Abrasion resistance

Abrasion resistance was measured on 100 mm size concrete cubes at 28 days of curing age. Initial weight (w_1) before testing and final weight (w_2) after testing was recorded. Each specimen was exposed to 20 gram of abrasive powder on abrasion testing machine. The speed of abrasion disc was kept at 30 rev/min. The specimen was turned by 90° in the clockwise direction after every twenty two revolutions and was further exposed to twenty gram of abrasive powder. The similar cycle was repeated nine times leading to a total of 220 revolutions.

The abrasion resistance was calculated using the following equation:

$$t = \frac{(w_1 - w_2)V_1}{w_1 A} \quad (4.2)$$

Where, t = depth of wear, V_1 = initial volume of the specimen in mm^3, and A = surface area of the specimen in mm^2.

4.4.2 Result and discussion

4.4.2.1 Density

Fig. 4.4 shows the results of hardened density for FBA concrete for concrete mix series A, B and C at 28 days of curing age. It can be observed from the Fig. that there is a slight decrease in the density of concrete as the percentage replacement of FBA is increased. The specific gravity of FBA (2.3 kg/m^3) is slightly lower than that of NFA (2.6 kg/m^3). The small change in density of hardened concrete can be attributed to the above mentioned factor. Another reason

for low density of FBA concrete is the angularity and roughness of raw aggregate, the angularity of FBA can create pores and voids between the cement matrix, therefore, the amount of cement paste required to cover the FBA is higher. As the highest decrease in density is nearly 3% at 100% replacement level at w/c it is safe to say that the voids formed due to angularity will have no major detrimental effect on other properties of hardened concrete.

It is also observed from Fig 4.4, that on increasing the water cement ratio the density of concrete decreases at replacement levels. The presence of higher amount of water during mixing creates air bubbles and voids on hardening of concrete. The density of concrete is lowered due to the formation of such bubbles and voids.

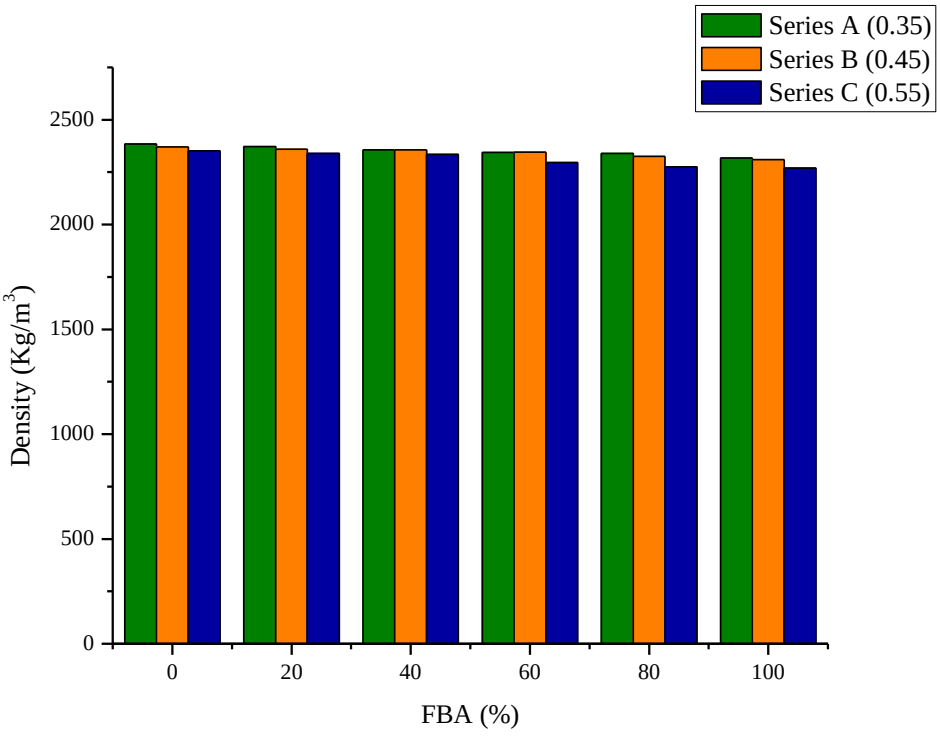

Fig. 4.4 Density of FBA concrete mixes

4.4.2.2 Compressive strength

The compressive strength of concrete is the deciding factor for its applicability and suitability. The compressive strength of FBA concrete for concrete mix series A, B and C at 7 days, 28 days, 90 days and 180 days curing age is shown in Figs. 4.5-4.8 respectively.

It is observed that the compressive strength of concrete increased with increase in percentage of FBA for all w/c. Compressive strength of concrete at 28 days (Fig. 4.6) was highest for concrete mixes containing 60% FBA. The compressive strength of 60% FBA concrete increased from 39 N/mm^2, 31.33 N/mm^2 and 22 N/mm^2 to 47.33 N/mm^2, 38.33 N/mm^2 and 35 N/mm^2 for concrete mix series A, B and C respectively.

For concrete specimens cured for 90 and 180 days the highest compressive strength observed was for mixes containing 100% FBA. It may be noted that compressive strength gain by concrete mixes containing FBA at various replacement level was also observed. In case of control concrete the compressive strength increased by 13.6%, 11.7% and 33.3% for A0, B0 and C0 respectively for 90 days of curing as compared to 28 days, whereas the observed increase for A100, B100 and C100 concrete mixes was 45.8%, 53.6% and 46.4% respectively. Similarly, for 180 days of curing age the compressive strength of control concrete increased by 31.4%, 30.9% and 55.1% for A0, B0 and C0 respectively as compared to 28 days, whereas the observed increase for A100, B100 and C100 concrete was 66.5%, 98% and 81% respectively.

Increase in compressive strength in the present study may be due to (i) the enhanced pozzolanic activity of the cement paste matrix because presence of FBA leads to higher quality of hydration products. Similar, observations were drawn by Medina et al. 2012 and Halicka et al. 2013 for sanitary ware ceramic aggregate. (ii) higher quality of hydration products creates strong bond between cement paste and aggregates. (iv) improved bond characteristics yield towards superior interfacial transition zone (ITZ) of the concrete (iii) lower amount of air

content in FBA concrete specimens creates a dense microstructure (iv) The water added to compensate the water absorption of FBA provides sufficient support to kick start the secondary hydration mechanism of the pozzolanic aggregates. (v) irregular shape if the FBA provides a superior surface area than NFA creating better bond between aggregate and paste.

The microstructural findings are discussed and further expanded in detail in Chapter 5.

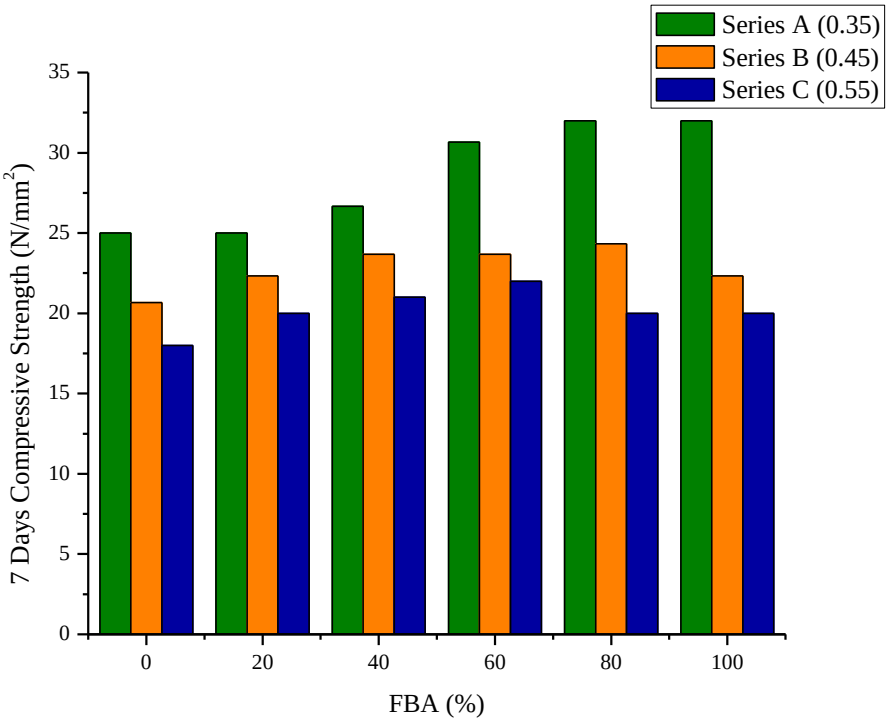

Fig. 4.5 7 day compressive strength of FBA concrete mixes

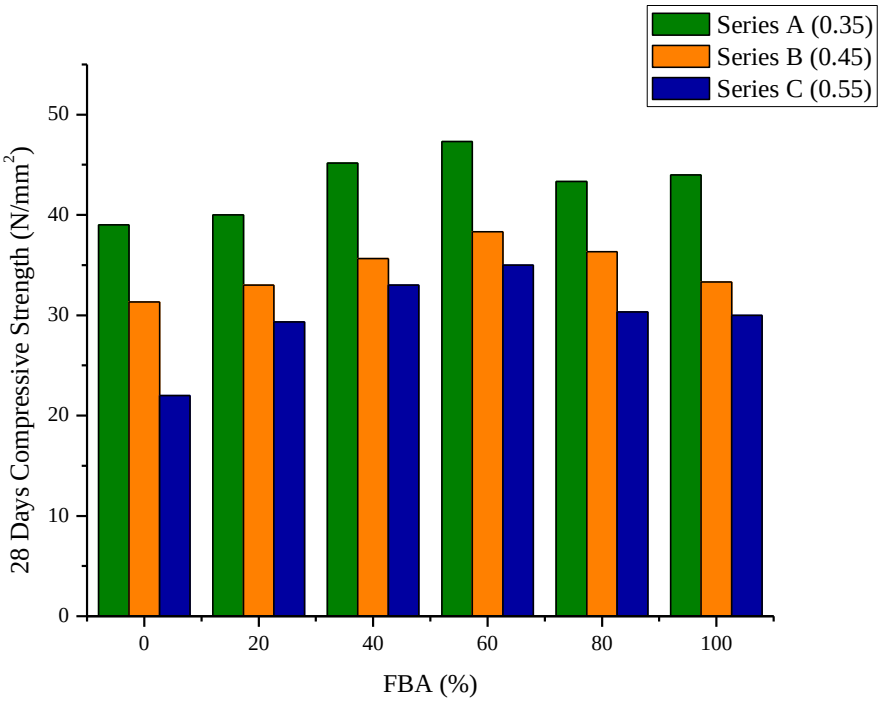

Fig. 4.6 28 day compressive strength of FBA concrete mixes

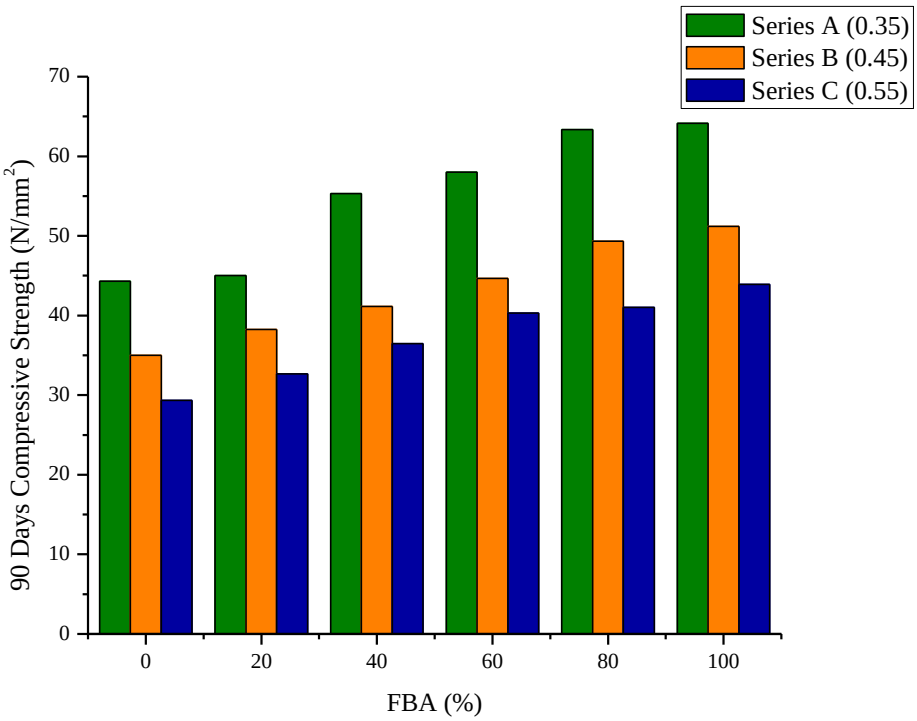

Fig. 4.7 90 day compressive strength of FBA concrete mixes

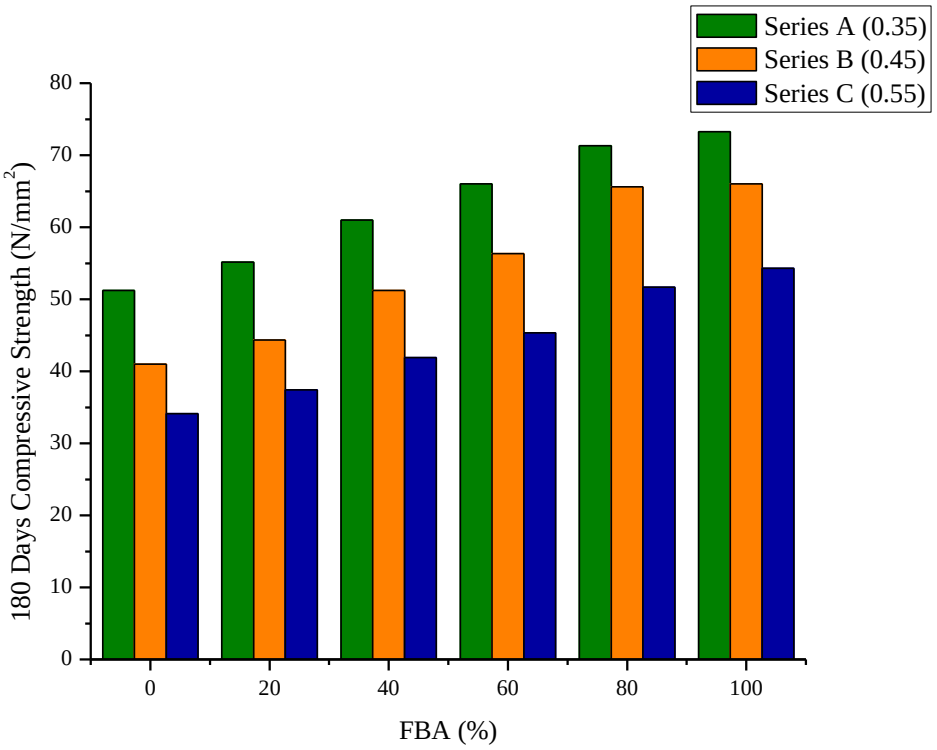

Fig. 4.8 180 day compressive strength of FBA concrete mixes

4.4.2.3 Split tensile strength and flexural strength

The split tensile and flexural strength of concrete is quite important in unreinforced structures under different loads. The strength development of split tensile and flexural strength is slower than compressive strength, it still follows the similar pattern. The 28 days split tensile strength for FBA concrete is shown in Fig. 4.9.

It is observed that the split tensile strength of concrete containing 100% FBA increased by 26.48%, 40.61% and 36.33% for concrete mix series A, B and C respectively.

The 28 days and 56 days flexural strength for FBA concrete is shown in Fig. 4.10-4.11. The results obtained for flexure strength follow a similar pattern as was observed in compressive and split tensile strength. The highest flexural strength was obtained at 80% FBA content at all w/c. At 28 days of curing the flexural strength of concrete increased from 4.37 N/mm^2, 3.51

N/mm^2 and 3.03 N/mm^2 to 5.81 N/mm^2, 4.38 N/mm^2 and 4.31 N/mm^2 for concrete mix series A, B and C respectively on 80% replacement of NFA by FBA.

The increase in split tensile and flexural strength of FBA concrete in the present study may be due to superior compressive strength behaviour; proper bonding between aggregate and cement paste and also due to dense and strong ITZ which resists the propagation of cracks as discussed and validated in Chapter 5.

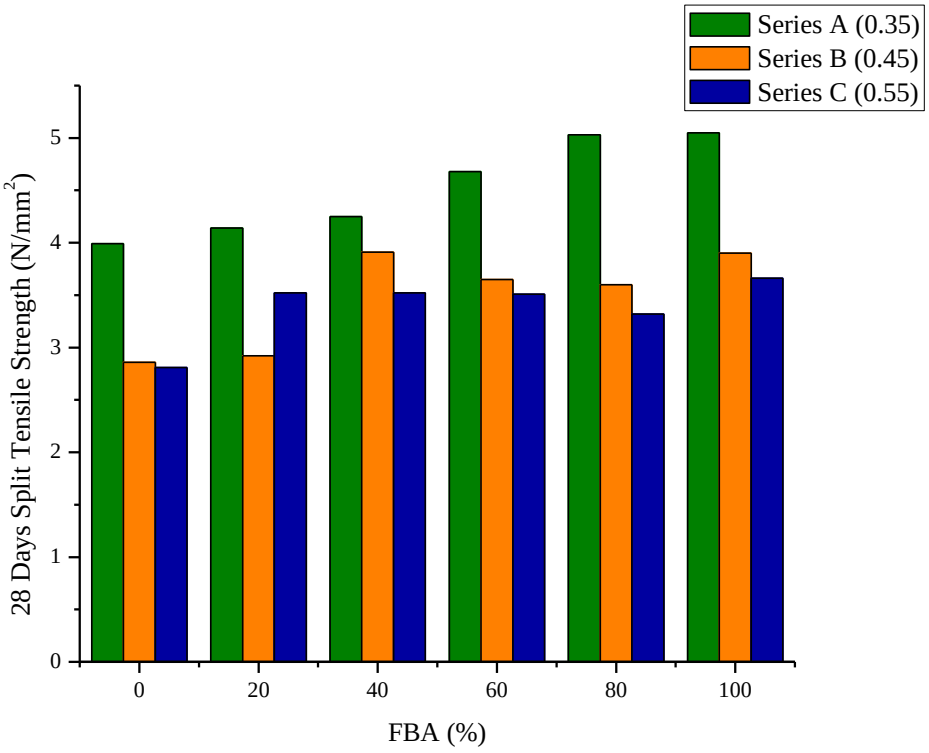

Fig. 4.9 28 day split tensile strength of FBA concrete mixes

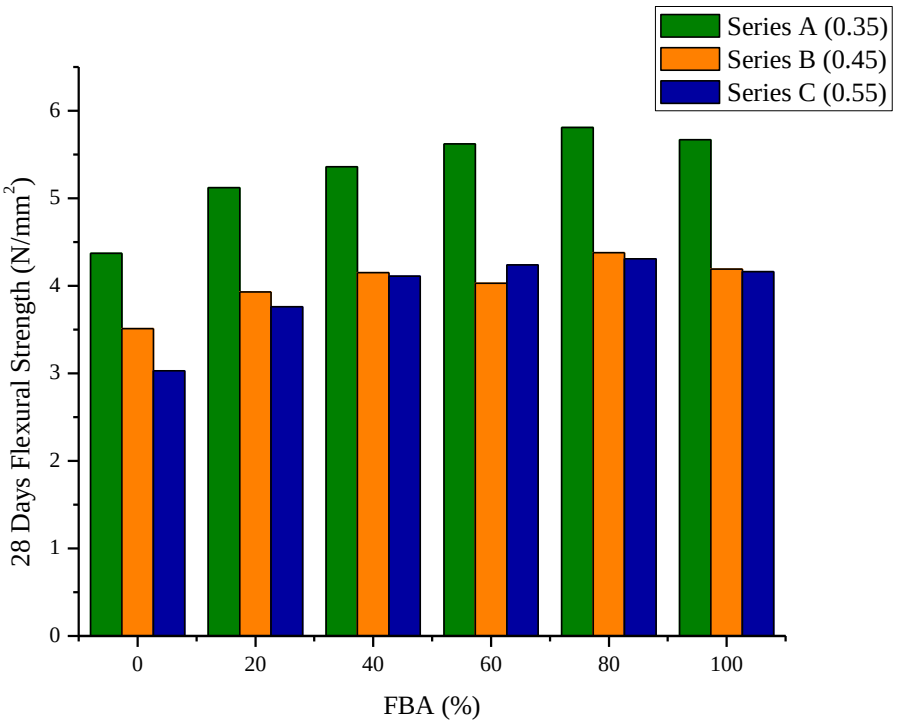

Fig. 4.10 28 day flexural strength of FBA concrete mixes

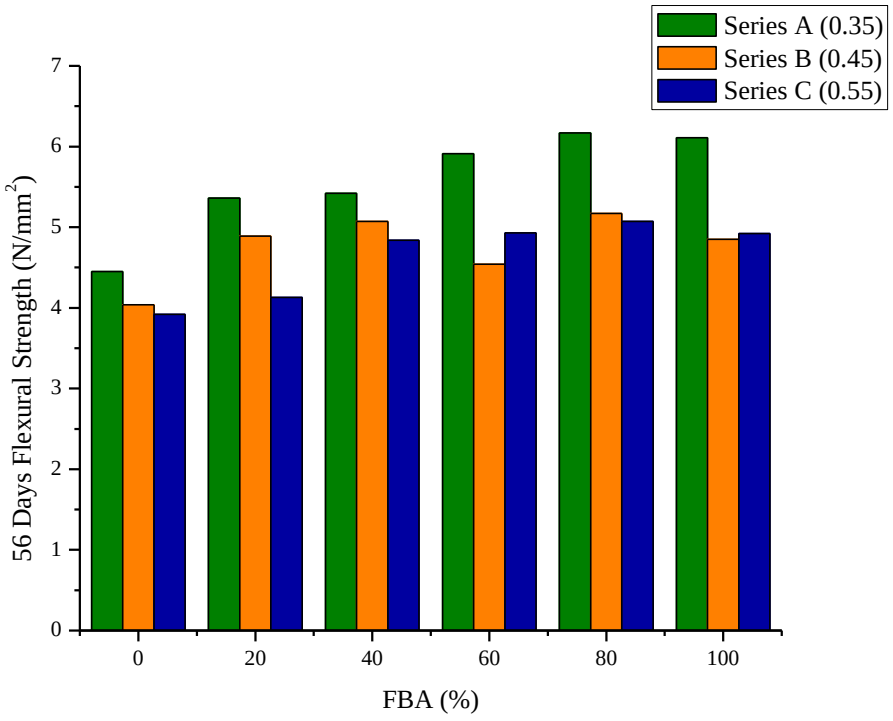

Fig. 4.11 56 days flexural strength of FBA concrete mixes

4.4.2.4 Static modulus of elasticity

The static modulus of elasticity provides flexibility of concrete depending upon the constituents of concrete. The higher values of static modulus of elasticity are generally related to higher stiffness of concrete. Higher stiffness restricts the deflection of a structure experienced during its service life.

The static modulus of elasticity for various FBA concrete mixes is shown in Fig. 4.12. An increase in the values of static modulus of elasticity was observed on introduction of FBA in concrete mixes. The static modulus of concrete decreased on increasing the water to cement ratio. The weakened microstructure due to excess water created poor interface between coarse aggregate and cement mortar paste lowering the static modulus of elasticity.

The main factors influencing modulus of elasticity of concrete are stiffness of coarse aggregate, stiffness of mortar paste, porosity and bond between aggregate and mortar paste. In this study the only parameter changing across mixes is the type of fine aggregate. The stiffness of mortar paste increases on replacing NFA with FBA. For series A and series B, 40% FBA concrete recorded highest modulus of elasticity. For higher percentage of FBA (60%, 80% and 100%), the angularity and roughness of raw aggregate creates voids in the concrete specimens which decreases the modulus of elasticity. For concrete series C the highest modulus of elasticity was observed for 100% FBA concrete. The higher amount of water available for hydration in C100 specimen creates a stronger microstructure. At lower percentage substitution (40%) and lower water to cement ratio, the roughness of FBA helps in increasing the interlocking and the contact area between aggregate and cement paste. Such behaviour facilitates uniform stress distribution with minimum deformation in dimensions.

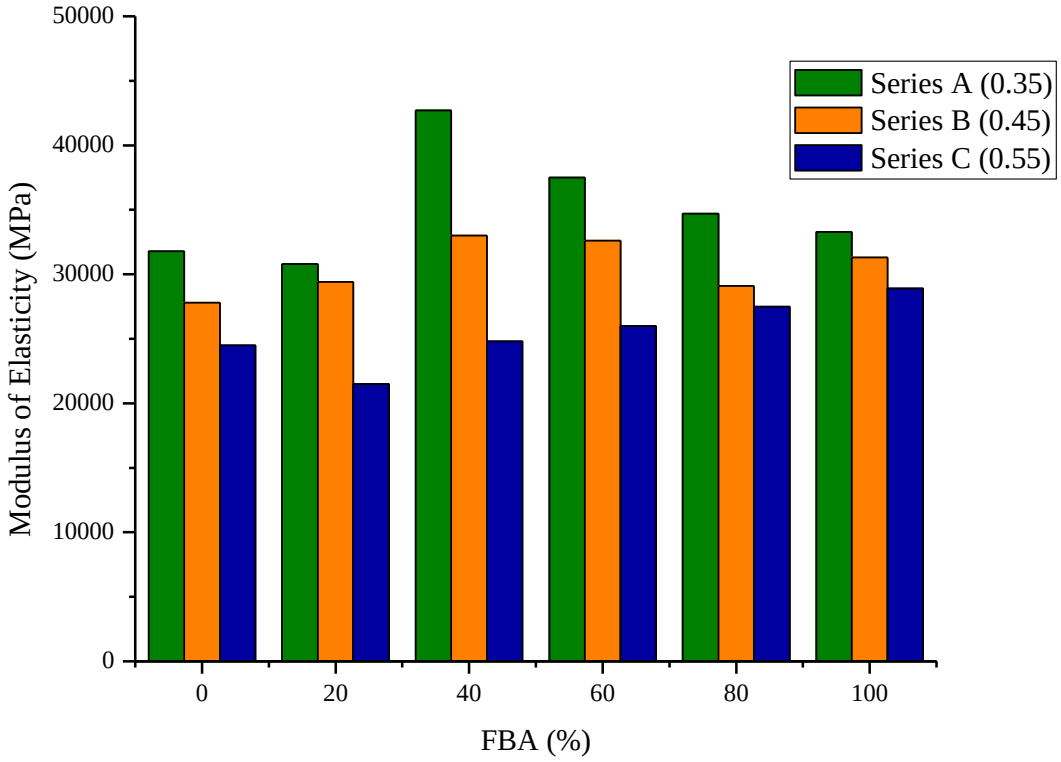

Fig. 4.12 Static modulus of elasticity of FBA concrete mixes

4.4.2.5 Abrasion resistance

Movement of various objects on the surface of concrete leads to deterioration of concrete due to wear. As this property is closely related to both types of aggregates the abrasion of concrete mixes was evaluated by measuring the depth of wear. As per the specification of BIS 1237 (2012) the depth of wear limit for general purpose tiles is 3.5 mm and for heavy duty applications the depth of wear should be less than 2 mm.

The variation in abrasion resistance of FBA concrete mixes is shown in Fig. 4.13. The depth of wear decreases slightly with the increase in FBA content. No clear trend or pattern is observed for abrasion resistance of FBA concrete. For series A the lowest value of depth of wear was observed at both 40% and 60% FBA content, whereas for series B and C the lowest

value of depth of wear was observed at 100% FBA content. Depth of wear is 0.96 mm for A0 specimen whereas the depth of wear marginally reduced to 0.9 mm for 40% and 60% replacement level of FBA in the concrete mix. It can also be observed that the maximum deterioration due to abrasion is observed in concrete mixes with w/c of 0.55. The highest value for depth of wear is 1.42 mm for C0 concrete mix which is still less than the permissible limits (BIS 1980).

The higher strength and hardness of raw FBA can be attributed to the superior resistance to abrasion of FBA concrete mixes. Halicka et al. (2013) also observed similar behaviour for sanitary ware ceramic concrete mixes. The higher adhesion characteristics between cement paste and aggregate creates a stronger surface characteristic. The lower pores in the cement matrix create a dense concrete microstructure which resists the chipping action of fine aggregates. The lower values observed for 0.55 w/c series C mixes can be due to the poor quality of cement mortar paste which deteriorates substantially when exposed to abrasive conditions. Another possible phenomenon controlling the abrasion resistance of concrete is the ratio of $Ca(OH)_2$ crystal to CSH gel. As both crystal and gel are products of hydration reactions they both are directly proportional to each other. The crystal structure of $Ca(OH)_2$ requires larger area to grow as compared to CSH gel. In concrete specimens containing FBA the concrete matrix provides sufficient distance for crystal growth due to the rough and angular nature of aggregate. Similar observations were reported by various other studies considering pozzolanic material (Acharya and Patro 2016; Ardalan et al. 2017; Rashad 2013).

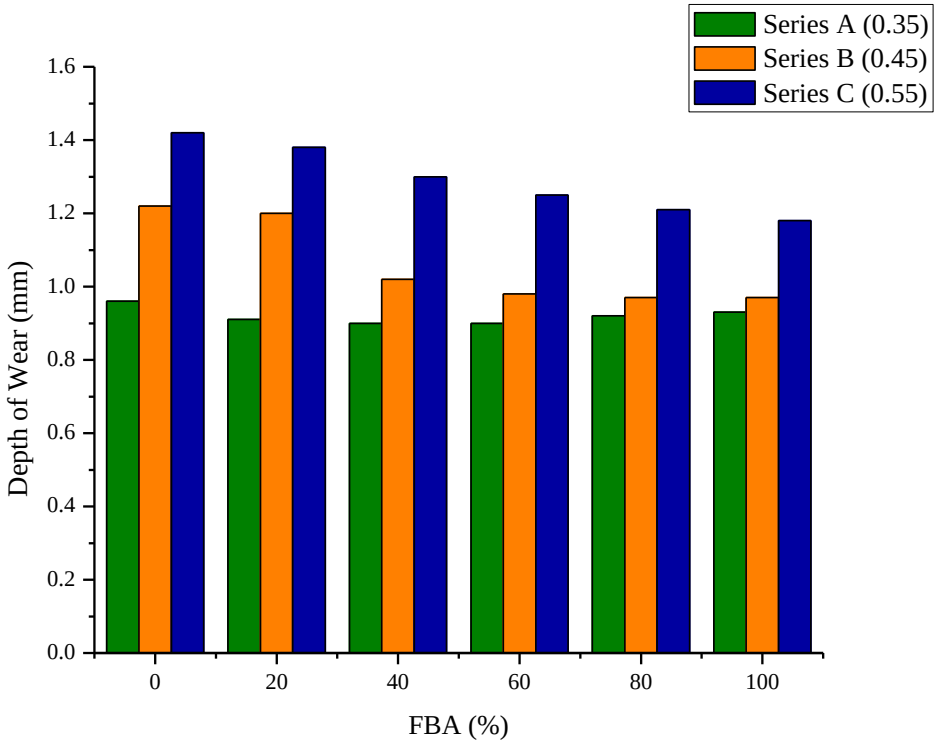

Fig. 4.13 Depth of wear of FBA concrete mixes

4.5 CONCLUSIONS

Figs. 4.14-4.16 presents the fresh and mechanical indices for concrete series A, B and C respectively. The nomenclature followed in indices are such that values higher than 1 indicate better performance for respective FBA concrete.

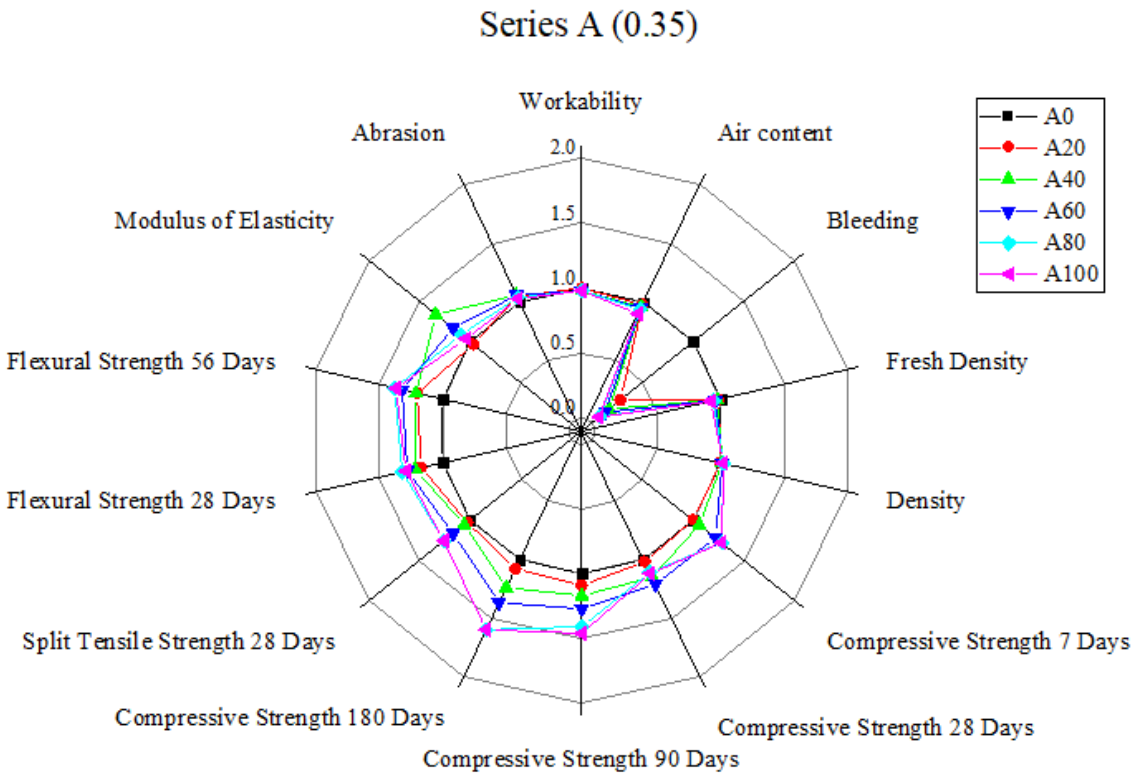

Fig. 4.14 Fresh and Mechanical properties indices of FBA concrete for series A (0.35)

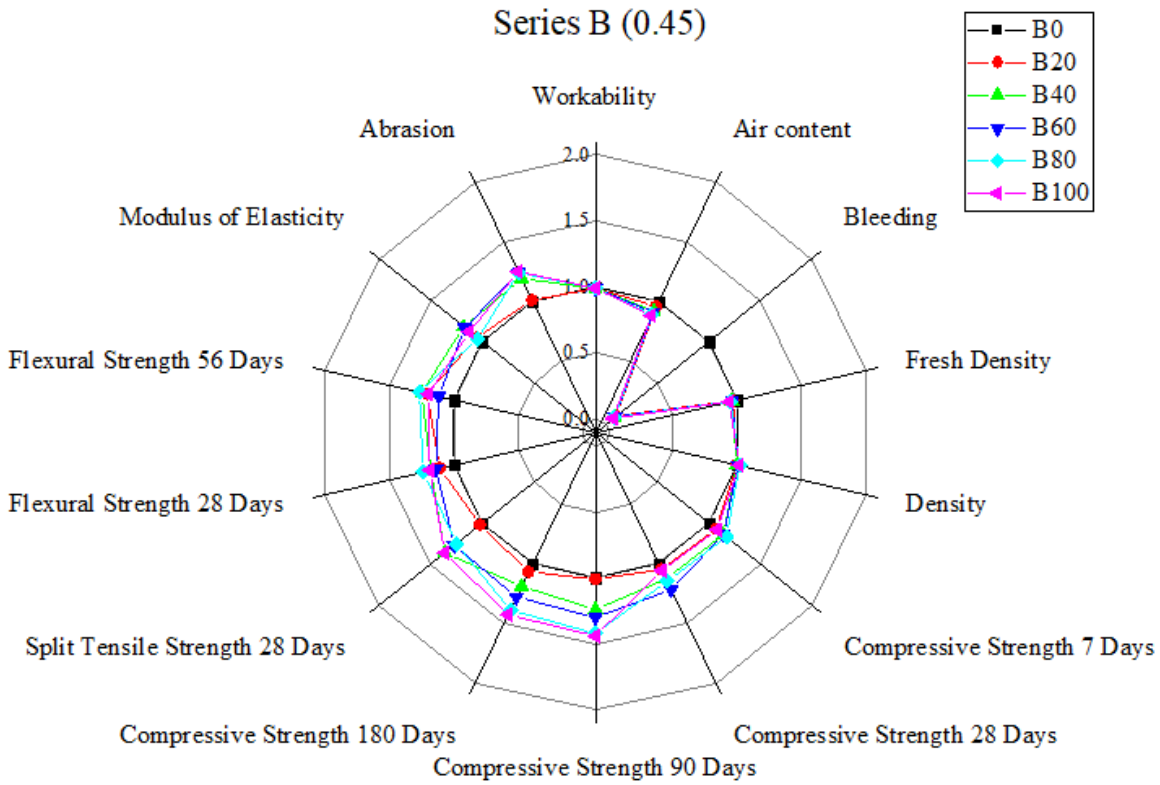

Fig. 4.15 Fresh and Mechanical properties indices of FBA concrete for series B (0.45)

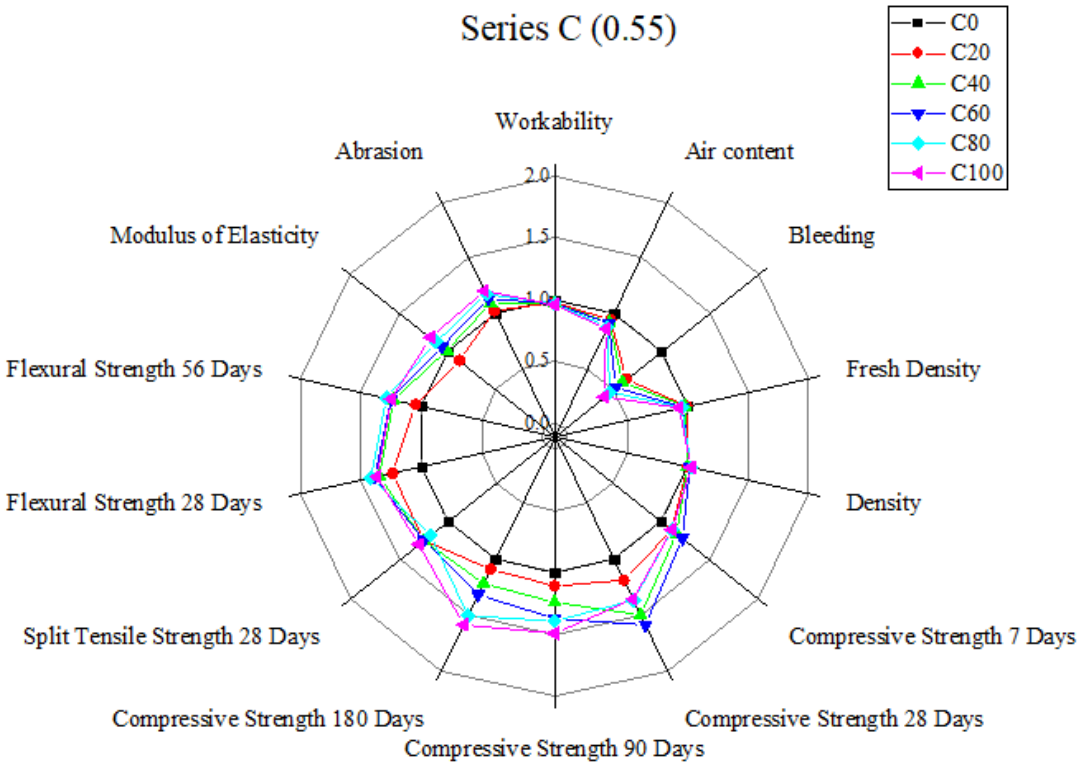

Fig. 4.16 Fresh and Mechanical properties indices of FBA concrete for series C (0.45)

The compatibility and influence of FBA in concrete mixes on selected fresh state and hardened state properties were observed. Following conclusions are drawn:

1. Partial and complete replacement of NFA by FBA demands increased dosage of superplasticiser to maintain the workability of fresh concrete mixes.
2. The air content of fresh concrete mixes containing FBA decreases due to higher quantity of water and superplasticiser in FBA concrete as compared to NFA concrete.
3. The higher dosage of superplasticiser coupled with increased water demand of FBA results in higher bleeding losses for concrete mixes.
4. Fresh density of FBA concrete mixes is higher due to greater amount of water demand of FBA.
5. Hardened state density of FBA concrete mixes was lower than control concrete mixes.

6. The compressive strength at 28 days of curing is highest in concrete mixes incorporating 60% FBA.
7. For 365 days compressive strength the highest value was observed at 100% FBA concrete mixes.
8. For split tensile and flexural strength the highest value was observed at 80% replacement of NFA by FBA.
9. The static modulus of concrete increased for FBA concrete indicating higher stiffness of concrete.
10. No significant effect on abrasion properties was observed. Although, the superior hardness of FBA resulted in slightly better performance in concrete mixes.

As seen in the different experimental programme for fresh properties, concrete mixes containing FBA are more prone to water loss through bleeding, have low air content and require higher doses of superplasticiser to maintain desired workability. The mechanical properties of hardened FBA concrete exhibited superior compressive, split tensile and flexural strength at all ages of curing. The values of static modulus of elasticity and abrasion indicated applicability for structural and pavement grade concrete.

CHAPTER 5

MICROSTRUCTURAL AND CHEMICAL PROPERTIES

5.1 INTRODUCTION

The microstructural and chemical properties of concrete provide an insight on the micro/nano structure and the intensity, bond, chain length and phase of hydration products. The observations drawn from these properties can provide gainful prediction for strength and durability parameters of concrete.

As discussed in 'Chapter 3' FBA exhibited slight pozzolanic activity, such behaviour of aggregate influences the hydration reaction and the resultant products. To maintain brevity and conciseness of the study only 28 days cured samples of 'Series A' having water to cement ratio of 0.35 were subjected to microstructural and chemical investigations.

5.1.1 Objectives

The main objectives of this chapter is to observe and analyse the micro/nano structural and chemical properties of concrete samples containing various amount of FBA.

The specific objectives being covered from previously defined are:

1. To adopt a suitable experimental procedure for observing and analysing micro/nano structure properties of concrete mixes obtained by lateral force microscopy (LFM).
2. To study the chemical properties of hydration products specifically calcium silicate hydrate (CSH) in concrete mixes.
3. To determine the intensities of hydration products in concrete mixes by X-ray diffraction (XRD) method.
4. To determine the bond behaviour of hydration products in concrete mixes by Fourier transformation infrared spectroscopy (FT-IR).

5. To determine the hydration percentage and chain length of CSH by solid state nuclear magnetic response spectroscopy (NMR).
6. To determine the phases of CSH in concrete mixes by X-ray photoelectric spectroscopy (XPS).

5.1.2 Program of the study

The above presented objectives will be covered by presenting the experimental outline, instrument details and its results.

On first stage the experimental method adopted along with the details of the instruments will be presented. Afterwards, the general outline of results will be presented and will be then assessed by subdividing them into different variables/parameters. Finally, the conclusions of the chapter will be drawn.

5.2 EXPERIMENTAL PROGRAMME

5.2.1 Lateral force microscopy (LFM) imaging

The atomic force microscope used to obtain LFM images was Multimode 8 HR AFM system (Bruker) with silicon tip attached to cantilever arm. The images were obtained in tapping mode at scan ranges of 10 µm. The specific scan range was selected to obtain proper surface structure of ITZ. The optical microscope connected to AFM system was used to select the appropriate region of the ITZ. A total of 6 scans were considered to study the ITZ of all mixes. The rest of the images and the values extracted at different scan ranges (5 µm and 2 µm) are presented in Appendix C.

NanoScope Analysis was employed to obtain the final processed images, measurement of crack dimension, width of unhydrated cement particles and to calculate the roughness value at the scan range. Higher roughness value generally depicts higher porosity and lower amount of CSH

gel resulting in weak ITZ (Li et al. 2014). In the surface topography LFM images, bright areas represent unhydrated cement particles while the darker areas represent voids/pores and cracks. The roughness distributions in the scanned samples have been provided at an interval of 1/3rd from top to bottom of the images.

The dark areas in the LFM images represent pores/semi filled pores in the scan area of the samples. These pores have negative height values and were analysed for their count, density, diameter and area using the particle analysis feature of nanoscope analysis. The threshold height parameter (0.0 nm for pores) was utilised to highlight the specific areas with that characteristics.

The concrete samples were cut with precision saw to achieve 10 mm×10 mm×10 mm size. The samples were then cleaned with acetone and kept at 100°C in an oven for 48 hours. The polished smooth sample of size 10 mm×10 mm×2 mm were obtained by wet grinding on Buhler disks with paper grits of 120, 320, 800, 1000 and 1500 respectively. The samples were grinded for 10 minutes on 120 grit paper to reduce the depth and for 5 minutes on each grit paper to achieve smooth and plane surface. For polishing the surface of grinded samples, Buhler auto-polisher was used with velvet paper, diamond suspension liquid of 1µm gradation and consistency paste. The rotation speed was kept in between 200 to 250 RPM (Revolutions per minute) and each sample was polished for 25 minutes. Epoxy impregnation was not done to maintain the undisturbed topographic characteristics of ITZ. The polished samples were then cleaned with acetone and were kept in oven for 72 hours at 100°C temperature.

5.2.2 Scanning electron microscopy (SEM) imaging

Nova Nano FE-SEM 450 was used to obtain backscattered electron (BSE) images of the samples to select the ITZ regions of concrete samples. The polished specimens were cleaned with acetone to remove any dust or foreign particles on the surface of the specimens. In this

study the objective of SEM imaging was to obtain an interface between coarse aggregate and cement paste having entrapped fine aggregates. The BSE imaging was done to select an interface between mortar paste and aggregate having no voids or cracks. Fig. 5.1 presents the BSE images of the samples used in this study. The red lines highlighted along the ITZ layer provide an optimum surface (free of voids and cracks) to conduct the microscopic investigation.

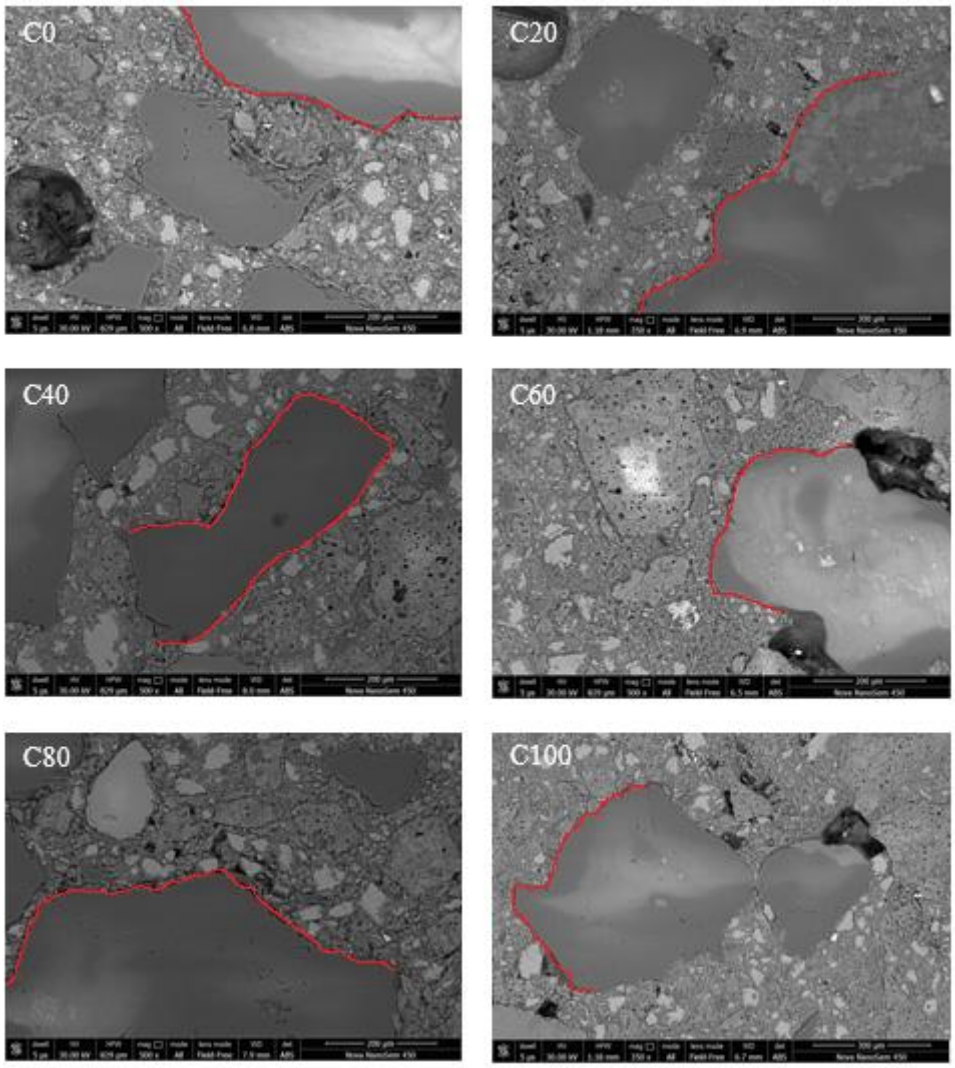

Fig 5.1 SEM BS images of the concrete samples

5.2.3 XRD measurements

XRD measurements were carried out on PANalytical X pert PRO powder diffractometer. The measurements were taken in the range of 5° to 90° with step size of 0.03° (2θ) and scan step time of 0.6 seconds. 5 gram powdered samples of each mix proportion were subjected to the scan. X'pert highscore with ICDD 2003 database was used to examine and analyse the XRD diffractograms of each sample.

5.2.4 FT-IR measurements

To identify the bond behaviour of concrete before and after incorporation of FBAs, a FT-IR spectrum 2 (Perkin Elmer) was used in this study to obtain the FT-IR spectra of the samples. The scans were recorded over the range of 400 to 4000cm^{-1} with spectral resolution of 4cm^{-1}. Linear baseline correction of the spectra was done automatically. The characteristics peaks observed at different wave number are presented in Table 5.1.

5.2.5 NMR measurements*

All NMR measurements were done on Varian Mercury-Plus NMR spectrometer with 5mm multi-nuclear CP-MAS probe. 10 KHz was the sweep width and pulse length was 7 μs. The 29Si chemical shifts were referenced against an external sample of talc at -98.1 ppm relative to tetramethylsilane (TMS) at 0 ppm. Mestranova software package was used for deconvulation and to analyse the NMR spectra.

*NMR results for sample containing 100% FBA was not obtained due to instrumentation issue.

5.2.6 XPS measurements

A pellet sample (5 mm×5 mm×1 mm) was used for XPS measurements. The XPS analysis was carried out on an XPS system using monochromatic Al Kα radiation hv=1486.7eV. The samples were deposited on a carbon tape and degassed overnight in XPS chamber to minimise air contamination. Pass energy of 50 eV was maintained to carry out the survey analysis.

Table 5.1. FTIR absorbance peaks

Wave number (cm^{-1})	**Functional Bond**	**Assinged to**	**Reference**
1641, 3000–3750	O–H	$Ca(OH)_2$	(Lavat et al. 2009; Lodeiro et al. 2009; Rubio et al. 1997; Villain et al. 2007)
1324–1576, 1640-1800	CO	$CaCO_3$	(Lodeiro et al. 2009)
852, 890–1079	Si–O	CSH	(Rubio et al. 1997; Villain et al. 2007)
450–650, 796	Si–O–Si	SiO_2	(Lodeiro et al. 2009; Rubio et al. 1997)
1100–1150	S–O	SO_4	(Mollah et al. 2000)
2850-2925	CH_2/CH_3	Methyl and Methylene	(Chollet and Horgnies 2011)

5.3 RESULTS AND DISCUSSIONS

5.3.1 LFM imaging

5.3.1.1 Surface topography

The surface topography of sample provide the irregularities and variations in the horizontal and vertical dimensions. The selected scan range of these samples help in describing the irregularities by roughness distribution of the surface profile.

In Fig. 5.2 the roughness distribution of A0 sample at 10 μm scan range with surface topography is shown. The bright spots observed in Fig. 5.2 are unhydrated cement particle. The biggest unhydrated cement particle at upper right corner in Fig. 5.2 has a diameter of 0.784

μm. As stated earlier, the dark spots seen in the image depict pores or voids present in the ITZ layer. The roughness distribution curves show high undulations/variations in surface roughness; this is caused by pores and staggered distribution of ITZ layer across the scan range.

The surface topography along with roughness distribution of A20 sample is shown in Fig. 5.3. As it can be observed from the image that introduction of 20% FBA results in a relatively smooth surface topography of the ITZ layer, Medina et al. (2012) in their study speculated a more compact and non-porous CSH gel in the ITZ layer on incorporating pozzalanic sanitary ware coarse aggregates. The size of unhydrated cement particles is less as compared to A0 sample although the number of such particles is comparable in both the samples. A crack is observed (approximately 32 nm deep) in the ITZ layer on the top right corner of Fig. 5.2 which can be due to improper bond between cement paste and aggregate leading to development of crack during the cutting or polishing of the sample.

As observed in Fig. 5.3 the surface topography of A40 sample is smoother than A0 and A20 samples. No pores and unhydrated cement particles are observed in the scan range. It can be assumed that the quality of compactness and distribution of CSH gel in A40 sample is superior to the earlier counterparts. The grain type structure of CSH gel is evident from the surface topography images. The roughness distribution curve of image shows a smooth waveforms with less undulations along the surface. The enhanced pozzolanic activity due to introduction of FBA results in a dense formation of CSH gel which leads to better ITZ properties of the sample.

The surface topography and roughness distribution of A60 sample is shown in Fig. 5.4. The surface topography images and roughness distribution curves at the scan range show smooth profile of the samples with few unhydrated cement particle. Since the quantity of natural sand is small in this sample, abundance of pozzolanic aggregate contributes to generation of CSH

gel in high amount. This indicates a smooth and dense ITZ layer with rich CSH gel. Peled et al. (2013) observed a cluster of grains of CSH gel in conventional cement mortar. However in this study of ceramic concrete samples the CSH structure observed is more suitably grouped together as a cloud.

Surface topography and roughness distribution curve of A80 sample is presented in Fig. 5.5. Despite repeated attempts a clear surface topography image of A80 could not be obtained. Some characteristic changes near the aggregate surface might be the reason for this anomaly. Over all the surface topography image show almost no voids and unhydrated cement particles. The high content of FBA helps in the dense structure of CSH gel leading to strong ITZ layer. The down side of high content of FBA is the angularity of the raw aggregate which contributes to slightly high roughness distribution of the sample containing 80% FBA than samples containing 20%, 40% and 60% FBA as seen in scan range.

The surface topography and roughness distribution of A100 sample containing 100% FBA are presented in Fig. 5.6. A particle is observed in the ITZ layer along with the grain of CSH gel. The particle observed can be of a small FBA or an agglomeration of fine powder of bone china ceramic aggregate. The roughness distribution curve of scan range also denotes presence of aggregate with high roughness. Another interesting observation from the images that can be drawn is the presence of pores in the sample. Although ample amount of CSH gel is observed, roughness of the fine bone china aggregate creates pores in the cement matrix which results in loss of compressive strength.

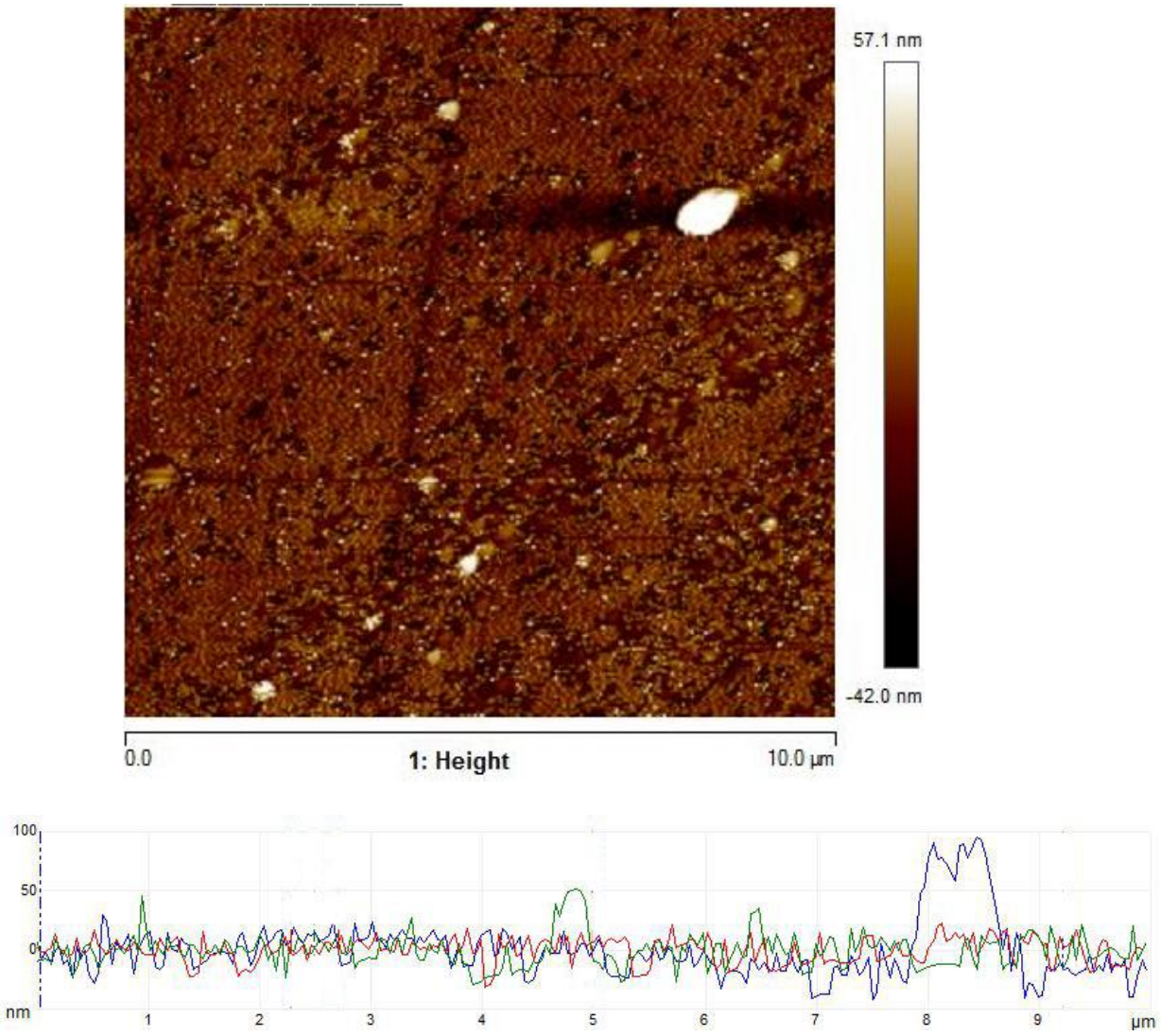

Fig. 5.2. Surface topography with roughness distribution of A0 sample ITZ at 10 µm scan range

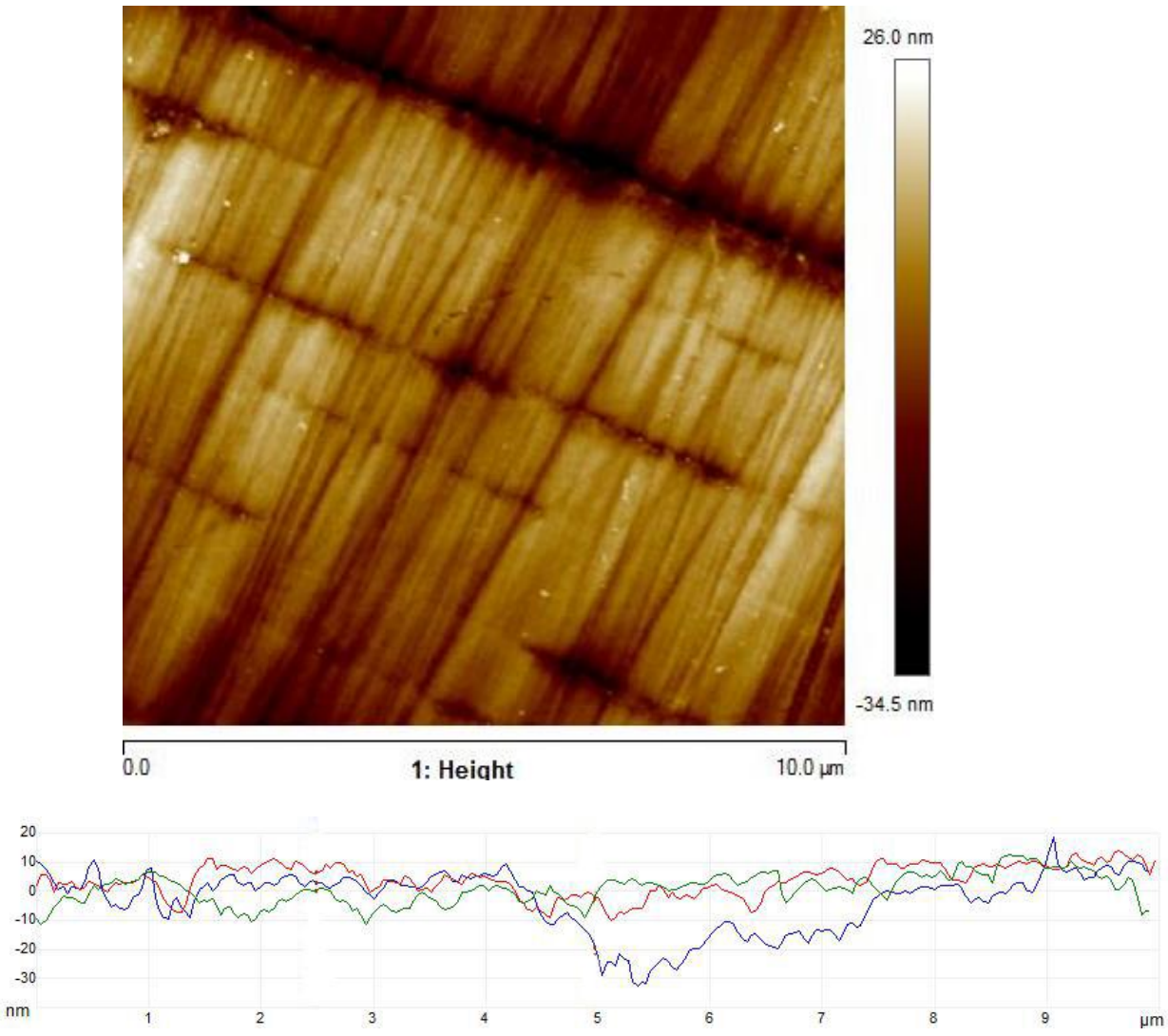

Fig. 5.3 Surface topography with roughness distribution of A20 sample ITZ at 10 µm scan range

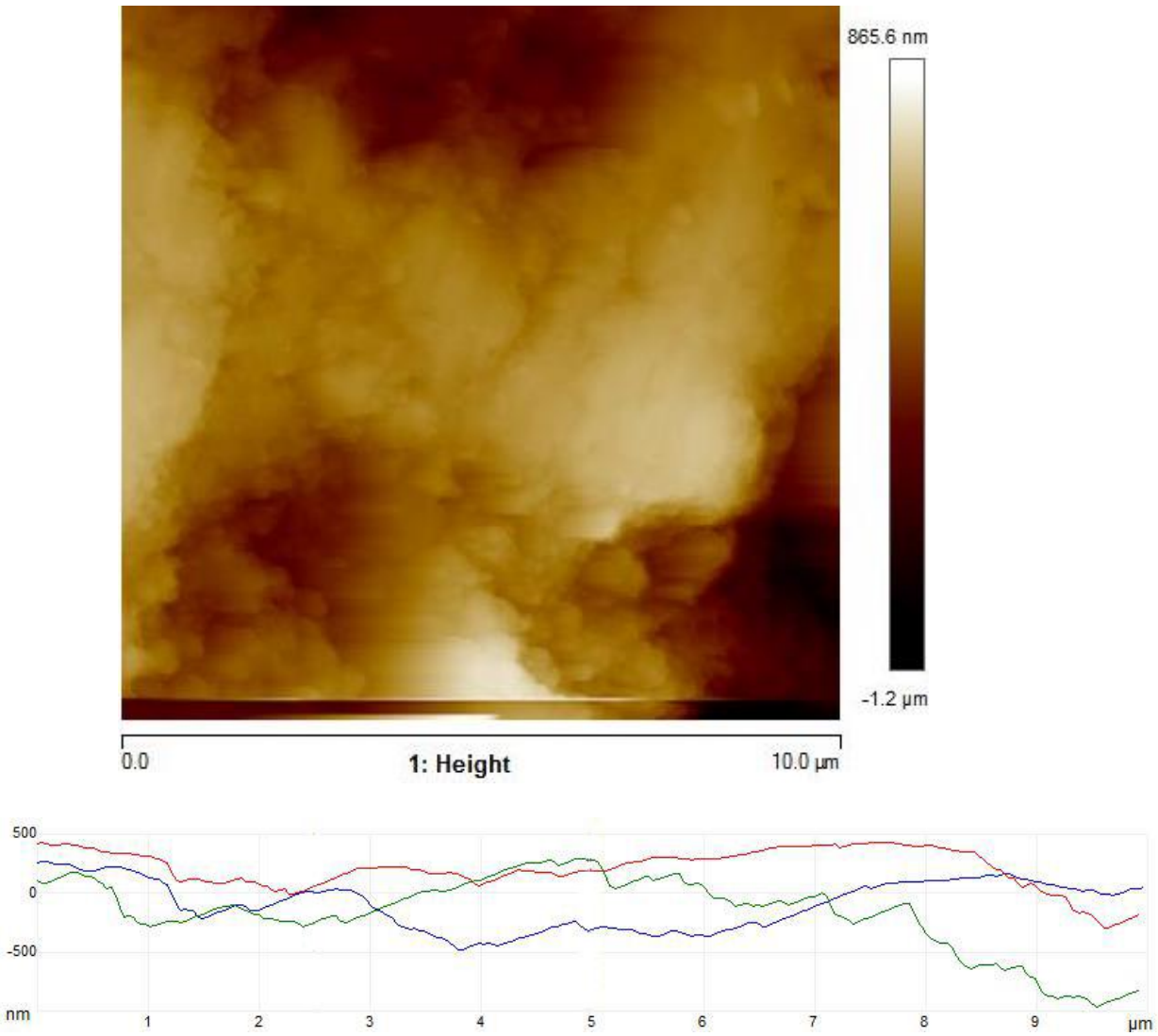

Fig. 5.4 Surface topography with roughness distribution of A40 sample ITZ at 10 µm scan range

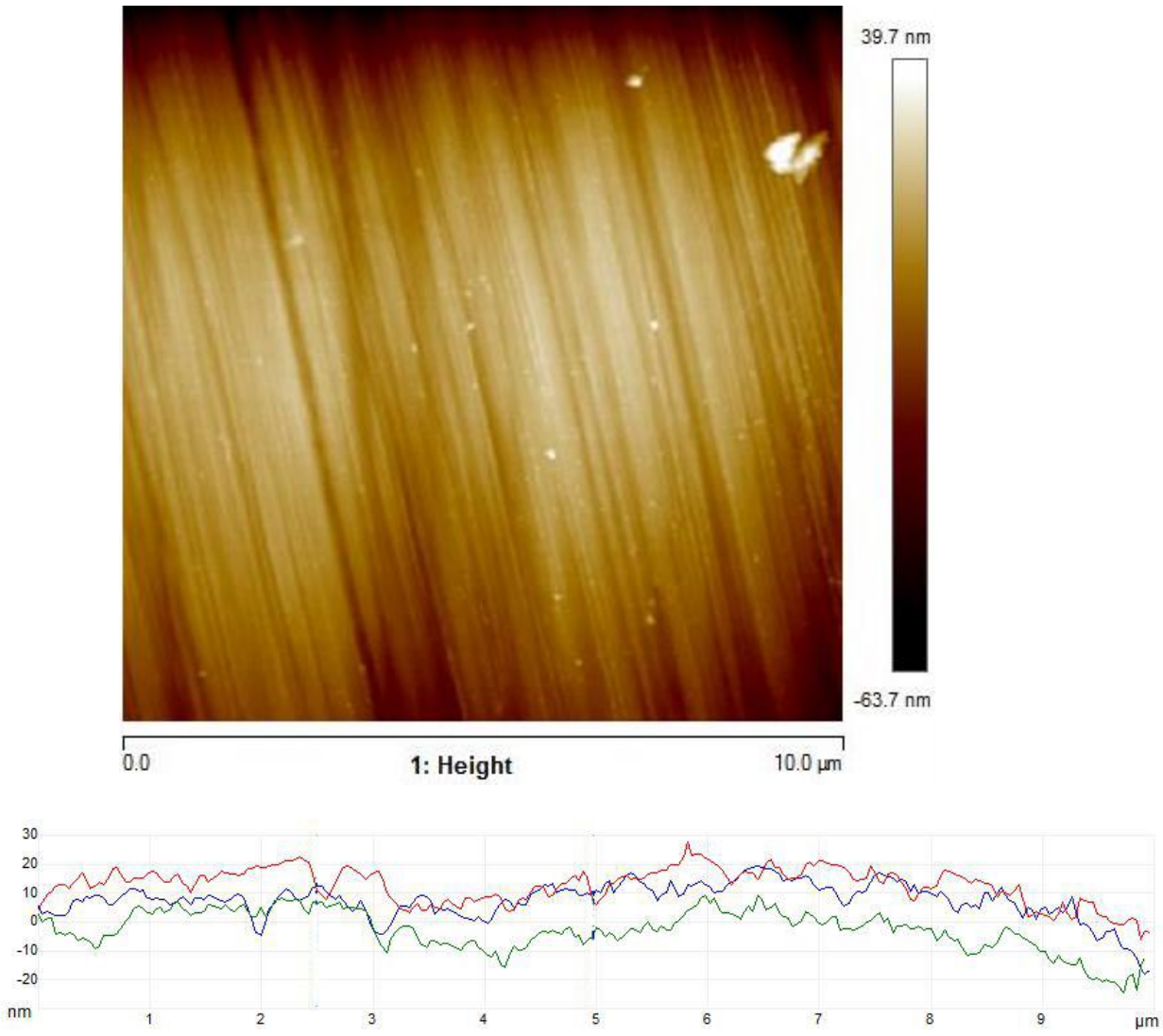

Fig. 5.5 Surface topography with roughness distribution of A60 sample ITZ at 10 µm scan range

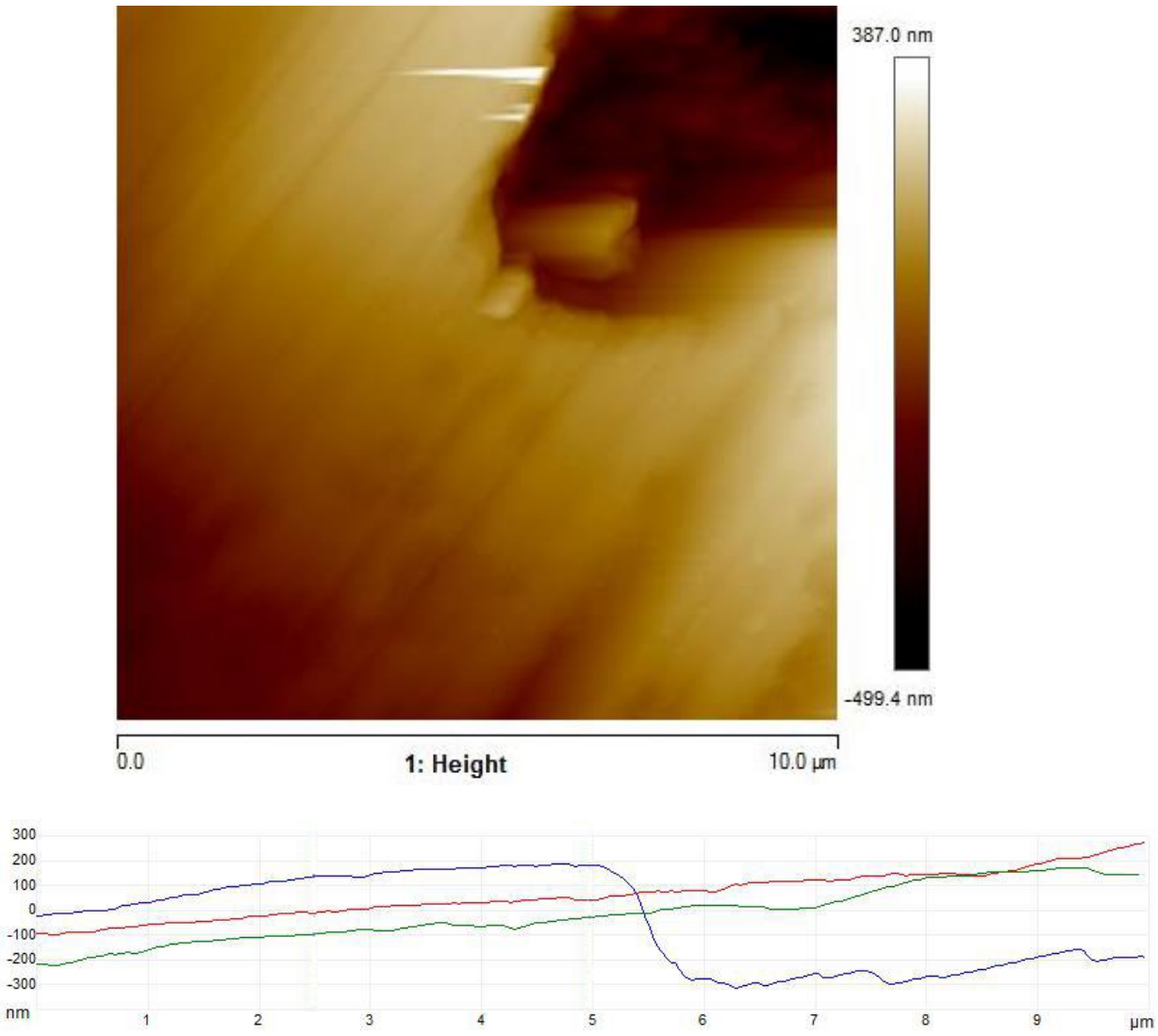

Fig. 5.6 Surface topography with roughness distribution of A80 sample ITZ at 10 µm scan range

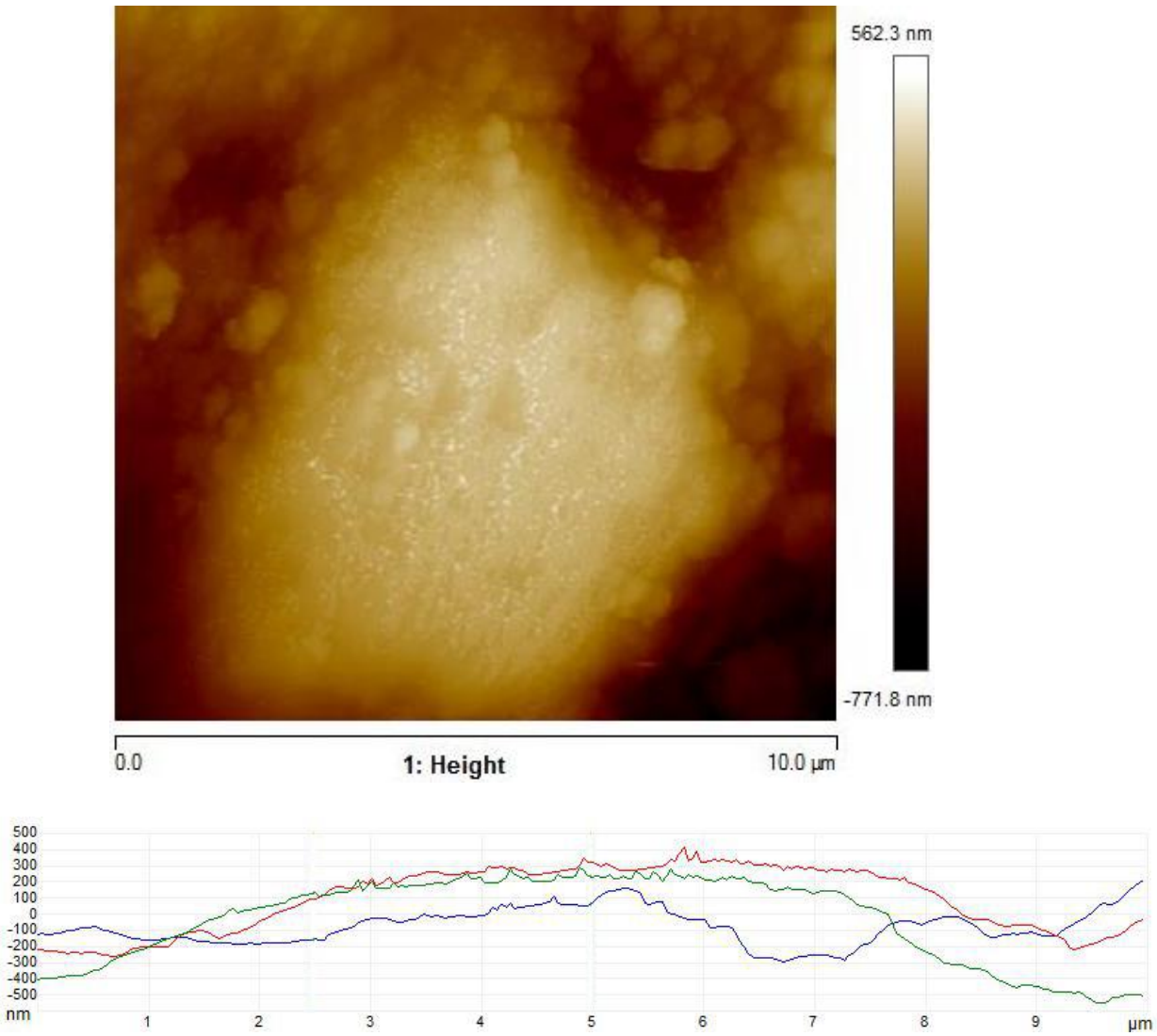

Fig. 5.7 Surface topography with roughness distribution of A100 sample ITZ at 10 µm scan range

5.3.1.2 Phase

The phase image obtained is due to the shift between the tip response and driving force generates phase image and contains information about the variations in mechanical properties of the sample. The 3D rendered images of phase provides an enhanced look on the features present in the observed sample.

Fig. 5.8 shows the 2D and 3D phase image of A0 sample. The 2D phase image shows CSH grains and their distribution across the scan range. The 3D phase image shows high roughness which indicate improper distribution of CSH gel across the ITZ layer. It can also be stated that such high roughness can also be interpreted as relatively weak ITZ layer.

Fig. 5.9 shows the 2D and 3D phase characteristics of the A20 sample. The uniform distribution of grains can be observed in the 2D image. The phase spectra of the A20 sample 3D image is nearly equal to the spectra of A0 sample. It can be observed that the addition of 20% FBA has a slightly positive effect on the densification of ITZ layer and has more pronounced CSH grains in the cement paste.

The 2D and 3D phase image of A40 is shown in Fig. 5.10. The scan image show homogenous distribution of CSH grains which indicate a proper bonding between cement paste and aggregate leading to better performance in compressive strength.

As shown in 2D phase image of A60 in Fig. 5.11, the structure of a CSH has many layers grouped together to form a mass. The 3D phase image also concur the theory of having a dense and uniformly distributed CSH grains across the ITZ layer.

Fig. 5.12 show the 2D and 3D phase image of A80 sample. 2D phase image of scan range confirms a change in phase along the ITZ layer on nearing the aggregate which was also observed in surface topography image. From the 3D phase image it can be observed that the CSH grain distribution is uniform with high coarseness of the particle leading to roughness.

Fig. 5.13 show the 2D and 3D phase characteristics of A100 sample. 2D phase image shows the phase characteristics across the scan range, the ceramic aggregate with different phase can be clearly observed in the image. The 3D phase image show uniform presence of CSH gel across the scan range.

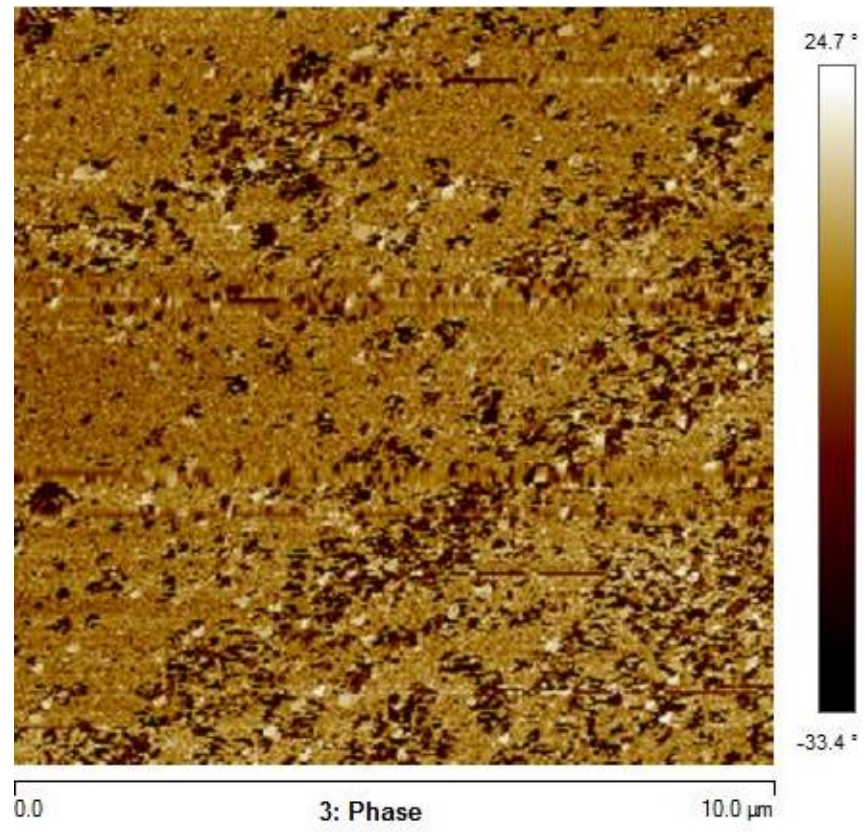

Fig. 5.8 Phase characteristics with grain distribution of A0 sample ITZ at 10 µm scan range

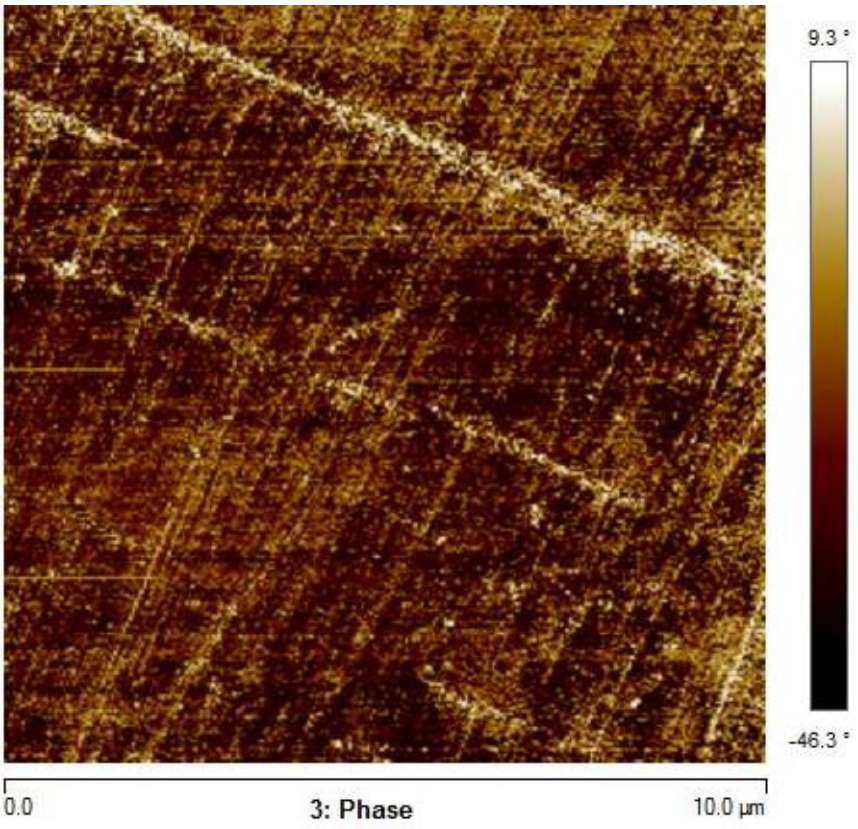

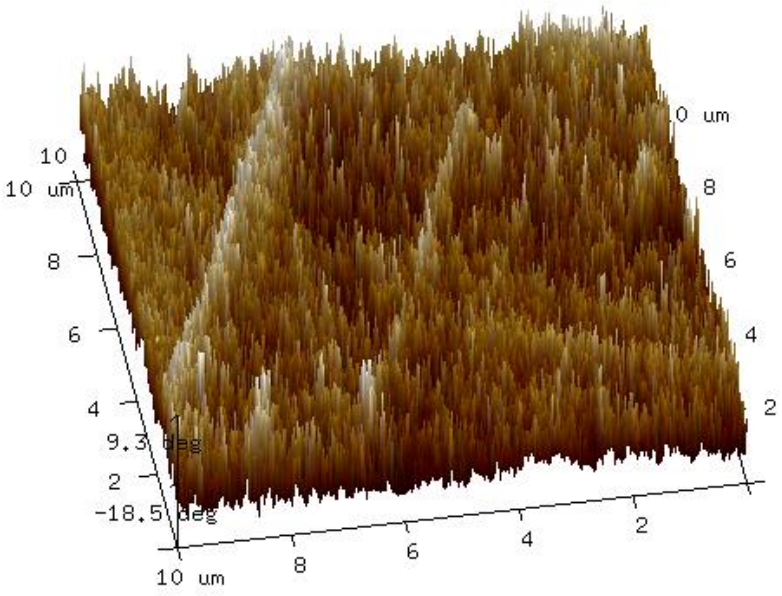

Fig. 5.9 Phase characteristics with grain distribution of A20 sample ITZ at 10 µm scan range

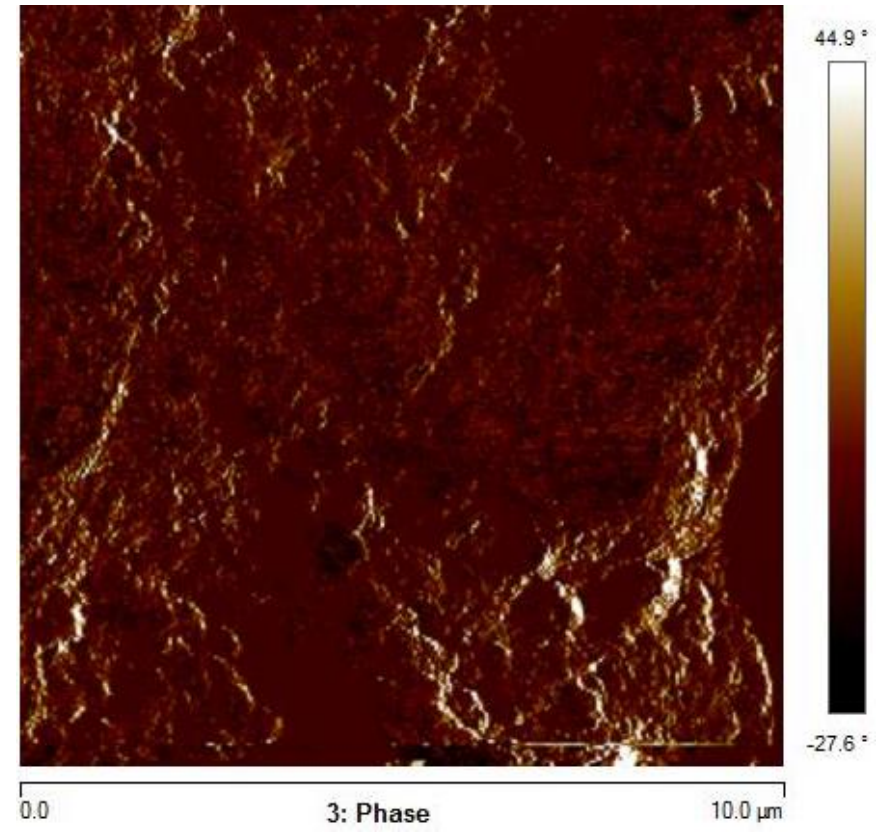

Fig. 5.10 Phase characteristics with grain distribution of A40 sample ITZ at 10 µm scan range

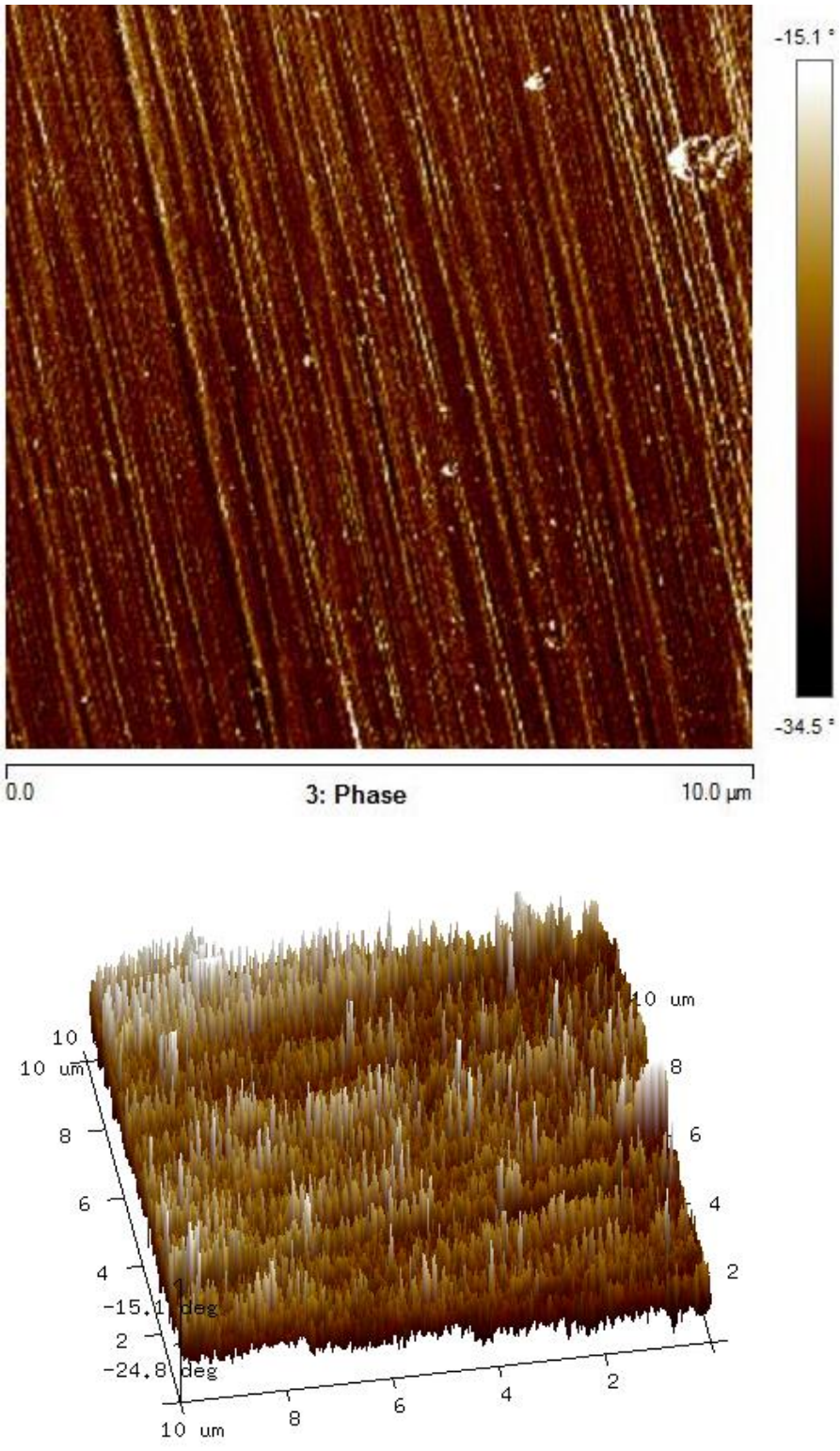

Fig. 5.11 Phase characteristics with grain distribution of A60 sample ITZ at 10 µm scan range

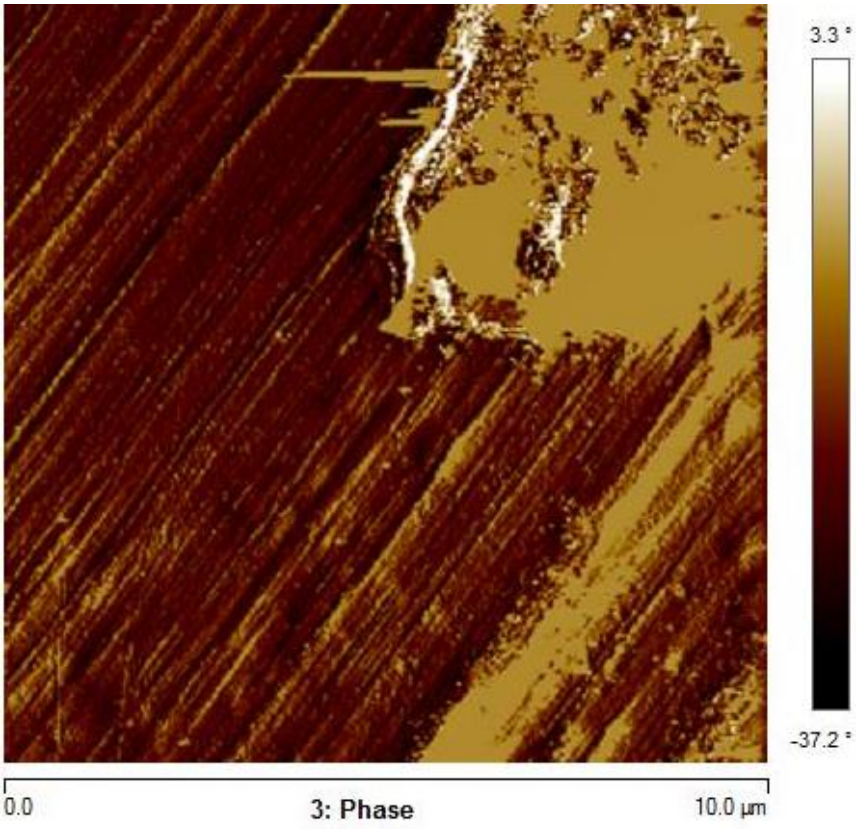

Fig. 5.12 Phase characteristics with grain distribution of A80 sample ITZ at 10 µm scan range

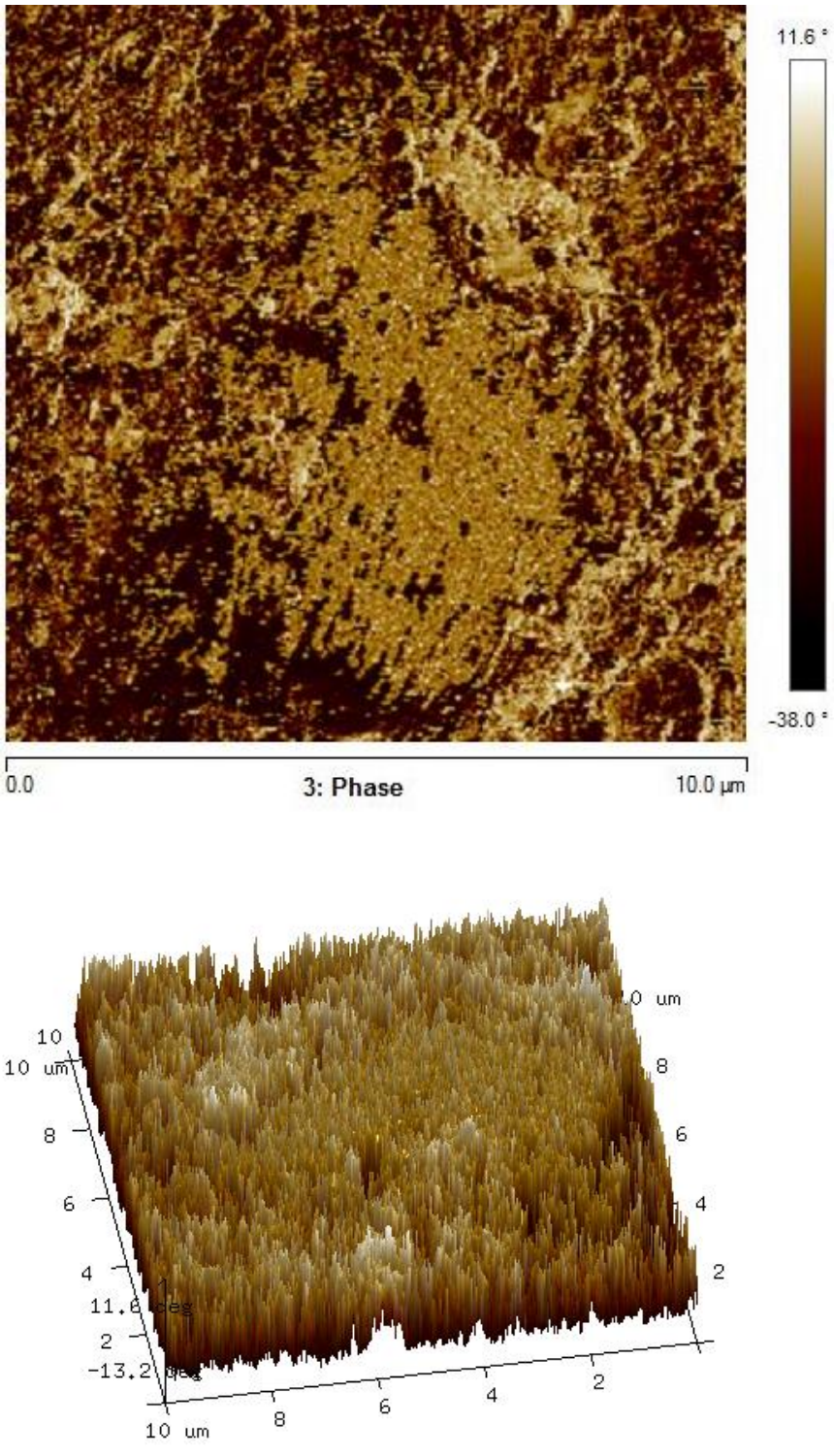

Fig. 5.13 Phase characteristics with grain distribution of A100 sample ITZ at 10 µm scan range

5.3.1.3 Roughness

Nanoscope analysis software was used to evaluate the surface roughness on the surface topographical images of scanned samples. The value of the roughness is calculated by taking the average value of the surface height deviations between highest and lowest data points. It may be noted that average roughness value considers height variations in the surface of the sample (Szyszka et al. 2016). Fig. 5.14 presents the average value of roughness obtained from the analysis of the samples. It can be observed that inclusion of FBA lowers the average roughness value of concrete. This change in average roughness value can be linked to compressive strength values of the concrete. A60 sample containing 60% fine bone china aggregate has the highest compressive strength and lowest average roughness value (Fig. 5.14). Similar relations regarding roughness value and compressive strength were observed by Xiao et al. (2013) for concrete containing recycled coarse aggregate. The introduction of fine bone china aggregate at 20% replacement of natural sand in concrete matrix creates a favourable hydration reaction mechanism forming a denser CSH gel structure. Similarly, at higher replacement percentages the quality of CSH gel and ITZ layer keeps on improving till 60% replacement. . It may be noted that the presence of fine bone china aggregate at any replacement percentage demonstrates the above mentioned phenomenon leading to decrease in pores and unhydrated cement particles.

After 60% replacement, the amount of angular particles of fine bone china aggregate create slightly higher deviation in surface profile leading to small rise in average roughness value. However, even higher replacement percentage of FBA (60% and 80%) provides a much smoother surface of FBA concrete than control concrete.

The roughness of concrete samples mainly depend upon the ITZ and quality of CSH gel of the hydration products. The lower values of roughness usually relate to superior strength and durability characteristics (Papadakis et al. 1999). The roughness values observed in FBA

concrete depict denser and compact ITZ between aggregates and cement paste. The slight pozzolanic activity of the FBA helps in formation of refined CSH gel. Such positive influence of FBA creates a strong and resilient microstructure.

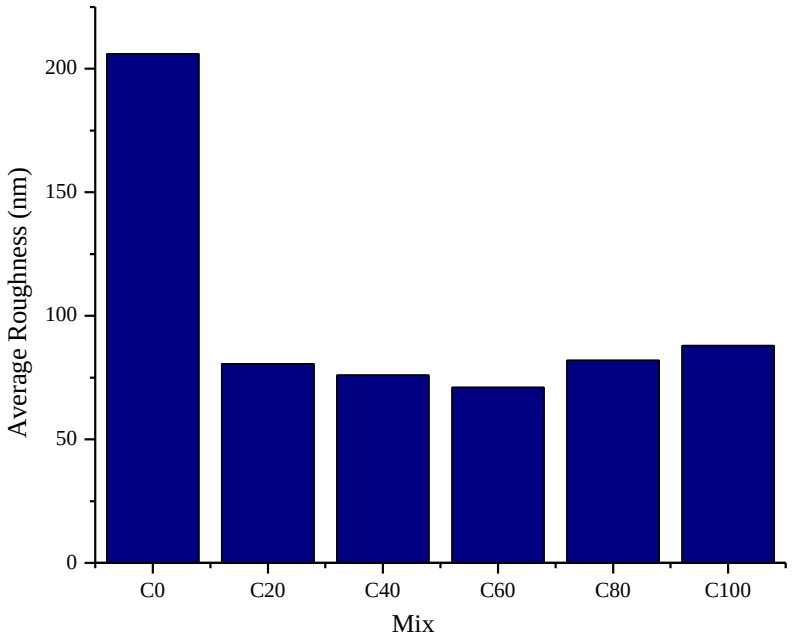

Fig. 5.14 Average roughness of concrete samples

5.3.1.4 Capillary pore analysis

Figs. 5.15-5.32 shows the LFM images on which particle analysis was carried out on the concrete samples. The blue highlighted portion in the images show areas having capillary pores of height less than 0 nm. The other darker areas observed in the images can be the interfaces between nano particles of the hydration products (Li et al. 2015). The presence of higher amount of capillary pores and interface joints in the concrete matrix can be interpreted as weaker microstructure due to lower quality of hydration products.

Table 5.2-5.6 shows the total count, density, height, area and diameter of the capillary pores concrete samples. The results show that the control concrete sample (A0) has higher area and

diameter of capillary pores in hydration products (CSH gel) in all scan ranges. Samples A60, A80 and A100 shows no capillary pores in 10 µm scan range. However, at lower scan range of 2 µm, the capillary pores can be observed for A60, A80 and A100 sample.

The reduction in total count of capillary pores in FBA concrete shows the positive influence of FBA on the development of hydration products (Table 5.2). These capillary pores exist in the hydration products and provide an important role in the transport properties of concrete. (Thomas et al. 1999). The reduction of capillary pores implies higher amount of CSH gel in the concrete matrix which promote superior ITZ properties of concrete.

The density of capillary pores increases as the scan range is reduced from 10µm to 2µm (Table 5.3). Such observations can be due to the reduction of the scanned surface area in the lower scan ranges (5 µm and 2 µm). The FBA concrete recorded lower density of capillary pores than control concrete. Pozzolanic behaviour of the ceramic aggregate can be the instrumental factor in generating denser CSH gel in concrete (Higashiyama et al. 2012; Medina et al. 2012).

The average, minimum and maximum depth of the capillary pores for various concrete mixes at different scan ranges are shown in Table 5.4. The values of depth reported is relative to the threshold height. The reduction in average depth of capillary pores provides insight on the quality of CSH gel as the samples with lower average depth of capillary pores can be considered as semi-filled pores. The higher values of depth can be interpreted as poor structure of CSH gel. The lower depth values for fine bone china aggregate concrete can be due the internal curing effect provided by the raw aggregates on release of the absorbed water.

Table 5.5 shows the average, minimum and maximum area covered by the capillary pores in the respective scan ranges. Previous studies have established that the outward growing nature of CSH gel provides adhesion characteristics and higher resistance to transportation of adverse chemicals by reducing porosity (Alderete et al. 2017; Barbhuiya et al. 2015; Thomas et al.

1999; Wang and Park 2015; Wang et al. 2012). The reduction of capillary pore area in A20, A40, A60, A80 and A100 samples implies higher volume of CSH gel with fewer pores in its structure.

Table 5.6 shows the average, minimum and maximum diameter of the capillary pores in the respective scan ranges. The compactness of the CSH gel can be interpreted from the diameter of pores (Oltulu and Şahin 2014). Lower diameter of gel pores generally results in a well compact CSH gel formation. The higher compactness of CSH gel provides a closely packed ITZ of concrete. It can be stated that introduction of FBA enhances the compactness of CSH gel. The lower average diameter of gel pore in CSH provides enhanced durability characteristics against harmful external agents.

A40 sample shows slightly increased total count, density, average height and average diameter of capillary pores in CSH gel at the 10 µm scan range than other samples of FBA concrete. However, the values of the parameters is less than control concrete, and the values for 5 µm and 2 µm scan range follow the similar trend as for other samples of FBA concrete the results observed for 10 µm scan range can be considered as an irregularity.

Table 5.2 Total count of capillary pores in FBA concrete

Mix	Total Count			
	Average	**Minimum**	**Maximum**	**Sigma**
10µm				
C0	89.000	89.000	89.000	0.000
C20	3.000	3.000	3.000	0.000
C40	1.000	1.000	1.000	0.000
C60	0.000	0.000	0.000	0.000
C80	0.000	0.000	0.000	0.000
C100	0.000	0.000	0.000	0.000
5µm				
C0	67.000	67.000	67.000	0.000
C20	4.000	4.000	4.000	0.000
C40	5.000	5.000	5.000	0.000
C60	10.000	10.000	10.000	0.000
C80	1.000	1.000	1.000	1.000
C100	0.000	0.000	0.000	0.000
2µm				
C0	133.000	133.000	133.000	0.000
C20	5.000	5.000	5.000	0.000
C40	7.000	7.000	7.000	0.000
C60	2.000	2.000	2.000	2.000
C80	1.000	1.000	1.000	0.000
C100	1.000	1.000	1.000	0.000

Table 5.3 Density of capillary pores in FBA concrete

Mix	Density (/μm^2)			
	Average	**Minimum**	**Maximum**	**Sigma**
10μm				
C0	0.890	0.890	0.890	0.000
C20	0.030	0.030	0.030	0.000
C40	0.010	0.010	0.010	0.000
C60	0.000	0.000	0.000	0.000
C80	0.000	0.000	0.000	0.000
C100	0.000	0.000	0.000	0.000
5μm				
C0	2.680	2.680	2.680	0.000
C20	0.160	0.160	0.160	0.000
C40	0.200	0.200	0.200	0.000
C60	0.400	0.400	0.400	0.000
C80	0.040	0.040	0.040	0.040
C100	0.000	0.000	0.000	0.000
2μm				
C0	32.864	32.864	32.864	0.000
C20	1.260	1.260	1.260	0.000
C40	1.764	1.764	1.764	0.000
C60	0.504	0.504	0.504	0.000
C80	0.252	0.252	0.252	0.000
C100	0.252	0.252	0.252	0.000

Table 5.4 Depth of capillary pores in FBA concrete

Mix	Depth (nm)			
	Average	**Minimum**	**Maximum**	**Sigma**
10µm				
C0	-21.912	-30.461	-8.954	3.420
C20	-5.902	-7.554	-2.623	2.319
C40	-92.012	-92.012	-92.012	0.00
C60	0.000	0.000	0.000	0.000
C80	0.000	0.000	0.000	0.000
C100	0.000	0.000	0.000	0.000
5µm				
C0	-21.907	-27.655	-7.282	4.810
C20	-3.242	-4.609	-2.207	0.943
C40	-21.688	-34.118	-7.118	9.167
C60	-1.241	-2.871	0.0047	0.969
C80	-2.773	-2.773	-2.773	0.000
C100	0.000	0.000	0.000	0.000
2µm				
C0	-20.932	-29.789	-6.945	3.971
C20	-1.998	-3.230	-1.118	0.700
C40	-4.317	-10.733	-0.482	3.460
C60	-0.892	-1.637	-0.146	0.745
C80	-3.829	-3.829	-3.829	0.000
C100	-1.210	-1.210	-1.210	0.000

Table 5.5 Area of capillary pores in FBA concrete

Mix	Area (nm^2)			
	Average	**Minimum**	**Maximum**	**Sigma**
10µm				
C0	127933.805	38146.973	736999.500	128858.383
C20	48319.500	47302.246	48828.125	719.306
C40	189208.984	189208.984	189208.984	0.00
C60	0.000	0.000	0.000	0.000
C80	0.000	0.000	0.000	0.000
C100	0.000	0.000	0.000	0.000
5µm				
C0	35624.719	9536.743	265121.469	45201.547
C20	33092.500	17166.137	59127.809	15743.139
C40	21362.305	12969.971	37765.504	9158.452
C60	55046.082	10299.683	230789.188	63891.578
C80	9918.213	9918.213	9918.213	0.000
C100	0.000	0.000	0.000	0.000
2µm				
C0	6020.645	1543.815	82377.945	10191.881
C20	3064.306	1877.341	5208.108	1214.575
C40	3607.610	1695.663	7388.247	1738.339
C60	4239.158	1574.544	6903.772	2664.614
C80	5268.668	5268.668	5268.668	0.000
C100	1816.782	1816.782	1816.782	0.000

Table 5.6 Diameter of capillary pores in FBA concrete

Mix	Diameter (nm)			
	Average	**Minimum**	**Maximum**	**Sigma**
10µm				
C0	371.517	220.387	968.699	157.689
C20	248.030	245.412	249.339	1.851
C40	490.824	490.824	490.824	0.00
C60	0.000	0.000	0.000	0.000
C80	0.000	0.000	0.000	0.000
C100	0.000	0.000	0.000	0.000
5µm				
C0	189.110	110.193	581.002	97.960
C20	199.960	147.840	274.379	46.377
C40	161.503	128.506	219.282	33.410
C60	233.916	114.516	542.079	123.976
C80	112.376	112.376	112.376	0.000
C100	0.000	0.000	0.000	0.000
2µm				
C0	76.423	44.336	323.862	42.724
C20	61.329	48.891	81.432	11.864
C40	66.060	46.465	96.900	15.149
C60	69.265	44.775	93.756	24.491
C80	81.904	81.904	81.904	0.000
C100	48.096	48.096	48.096	0.000

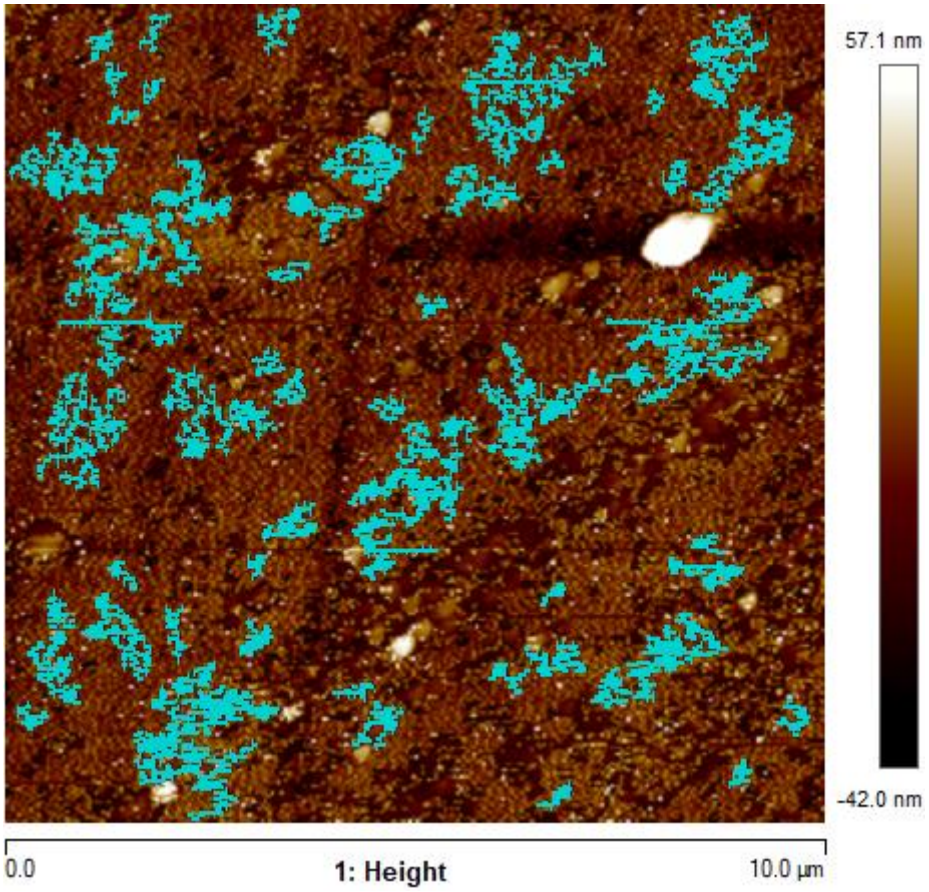

Fig. 5.15 LFM image of A0 sample at 10 µm scan range with capillary pores highlighted in blue

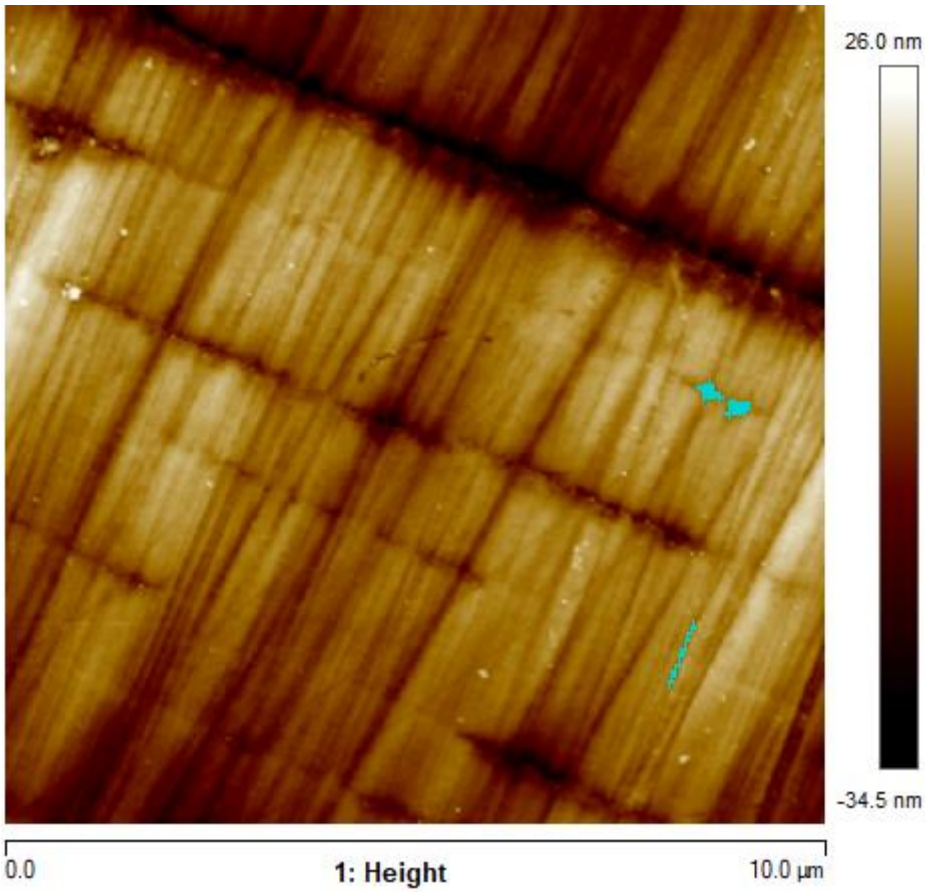

Fig. 5.16 LFM image of A20 sample at 10 µm scan range with capillary pores highlighted in blue

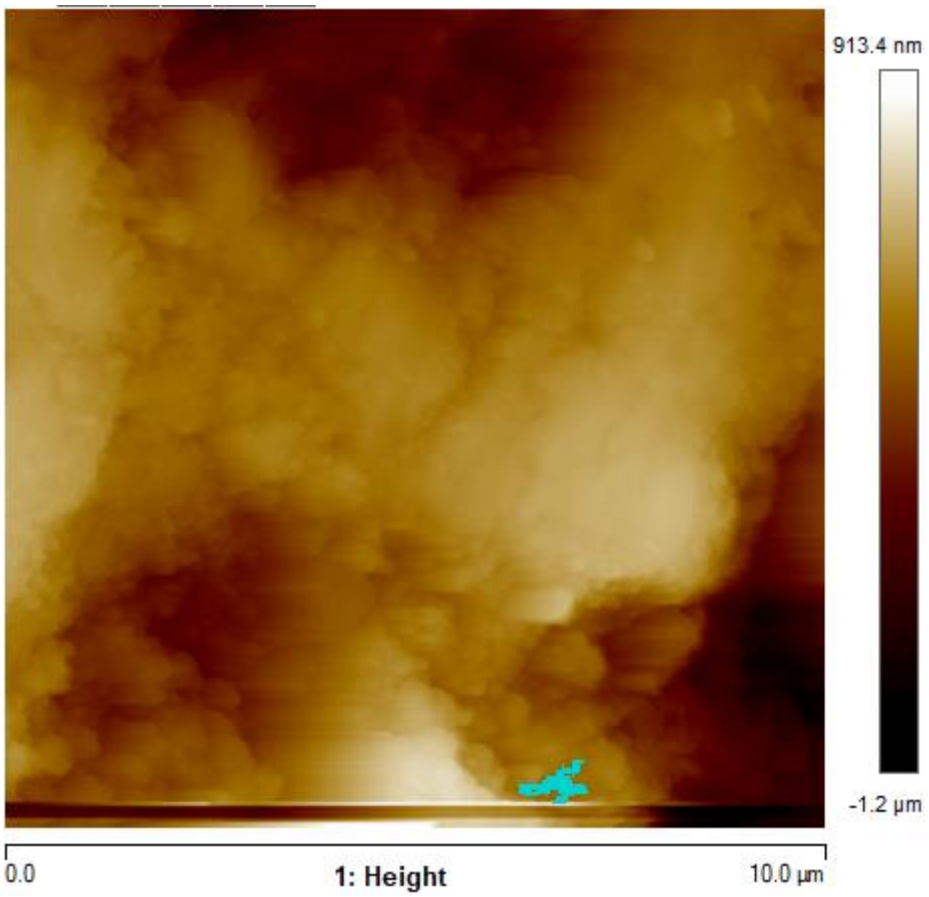

Fig. 5.17 LFM image of A40 sample at 10 µm scan range with capillary pores highlighted in blue

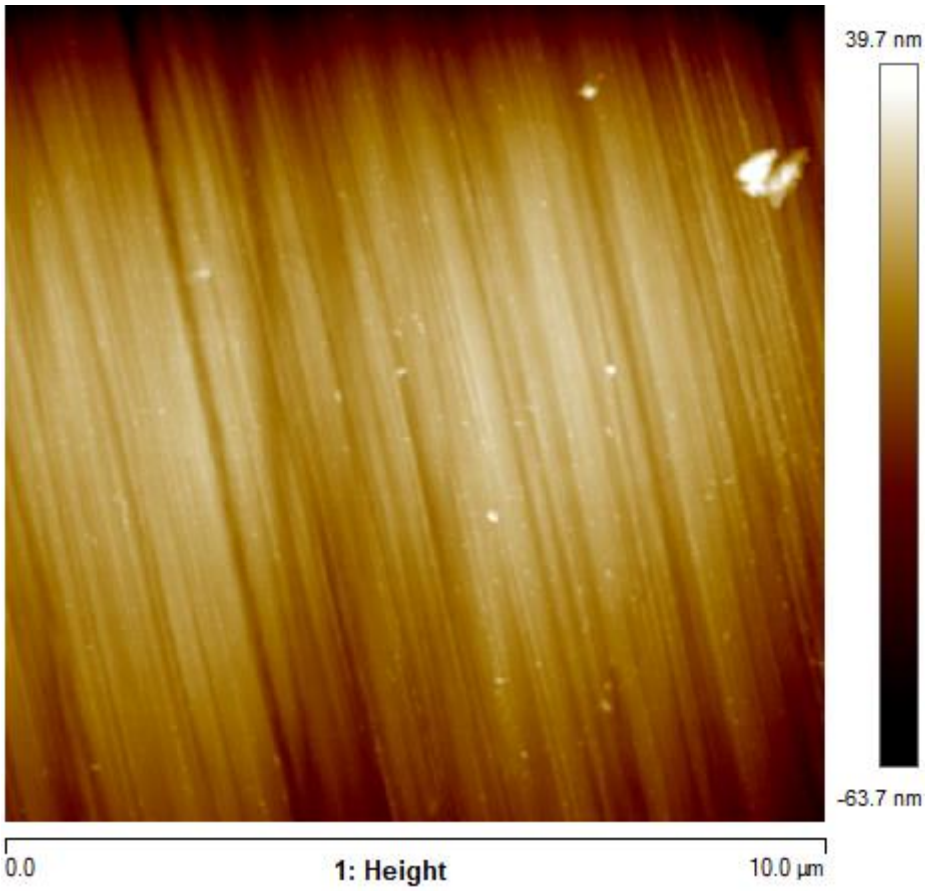

Fig. 5.18 LFM image of A60 sample at 10 µm scan range with capillary pores highlighted in blue

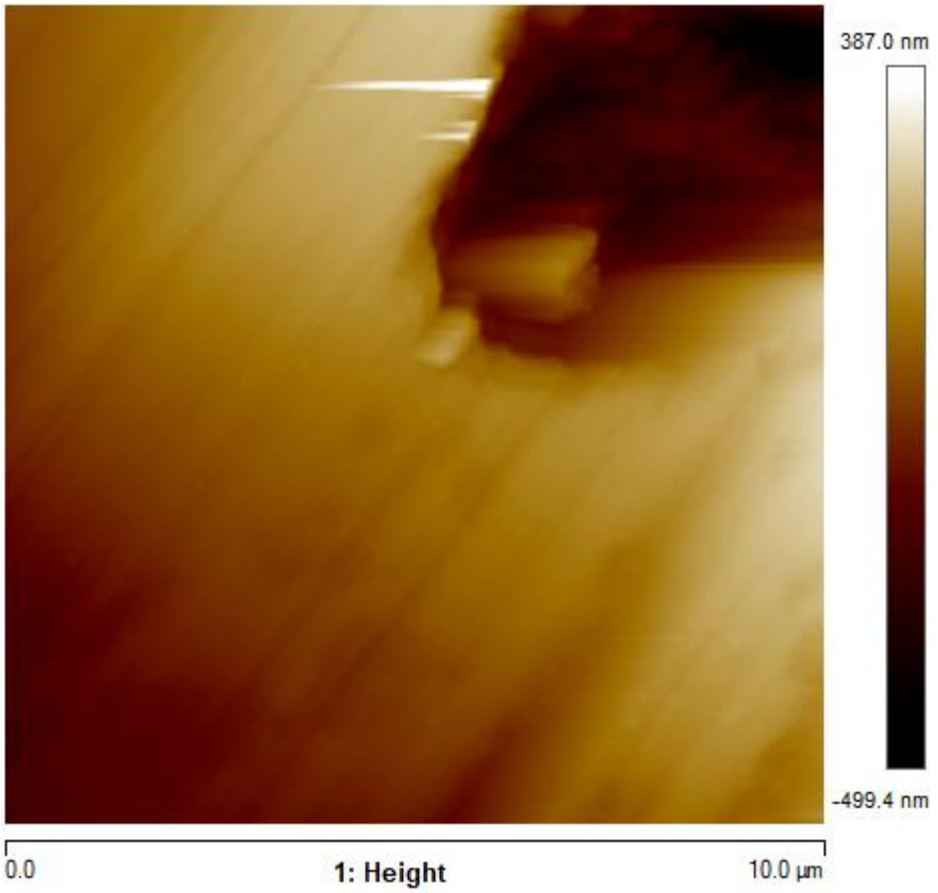

Fig. 5.19 LFM image of A80 sample at 10 µm scan range with capillary pores highlighted in blue

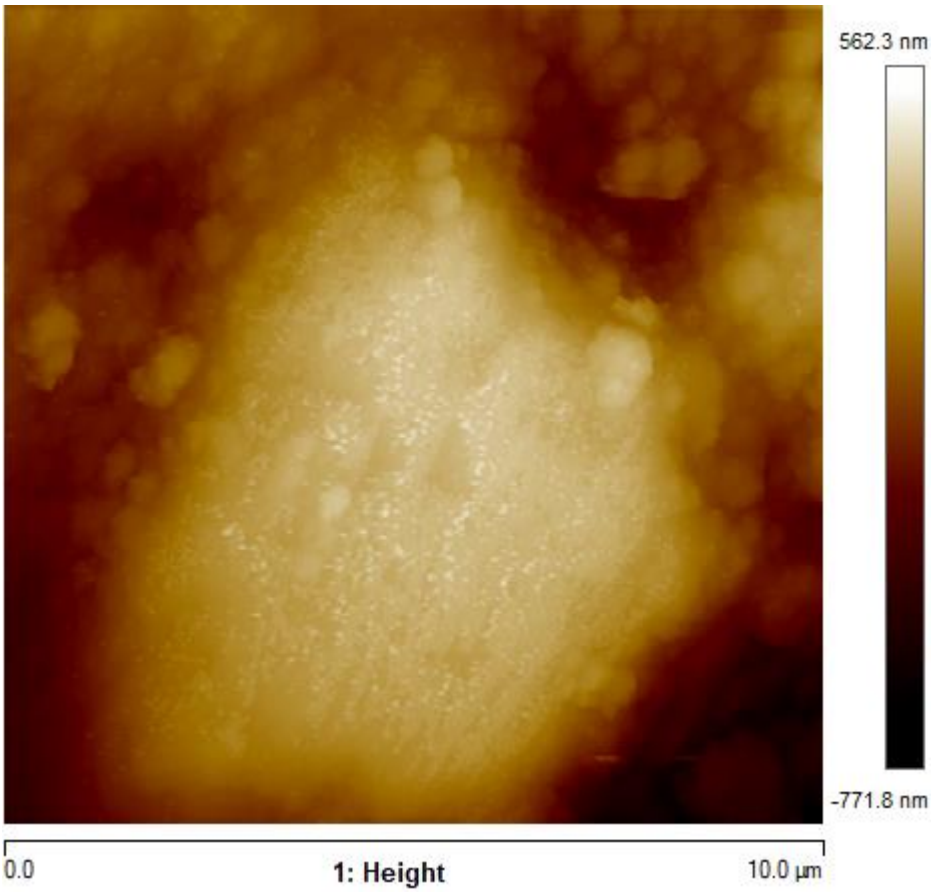

Fig. 5.20 LFM image of A100 sample at 10 µm scan range with capillary pores highlighted in blue

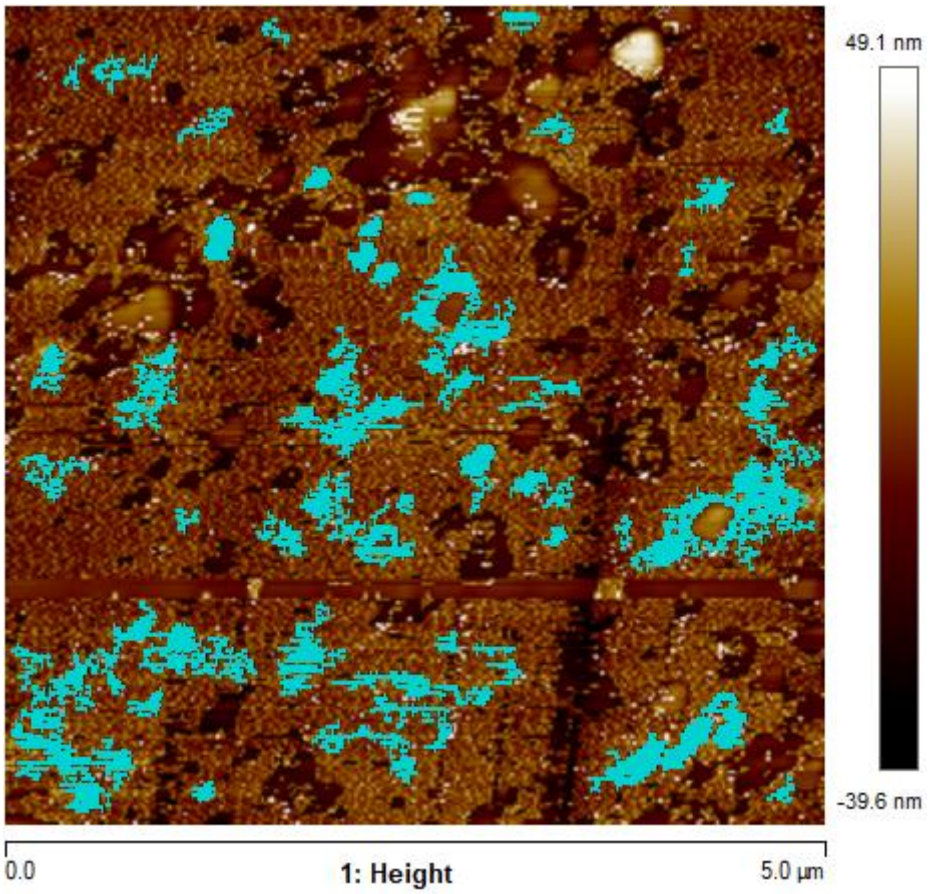

Fig. 5.21 LFM image of A0 sample at 5 µm scan range with capillary pores highlighted in blue

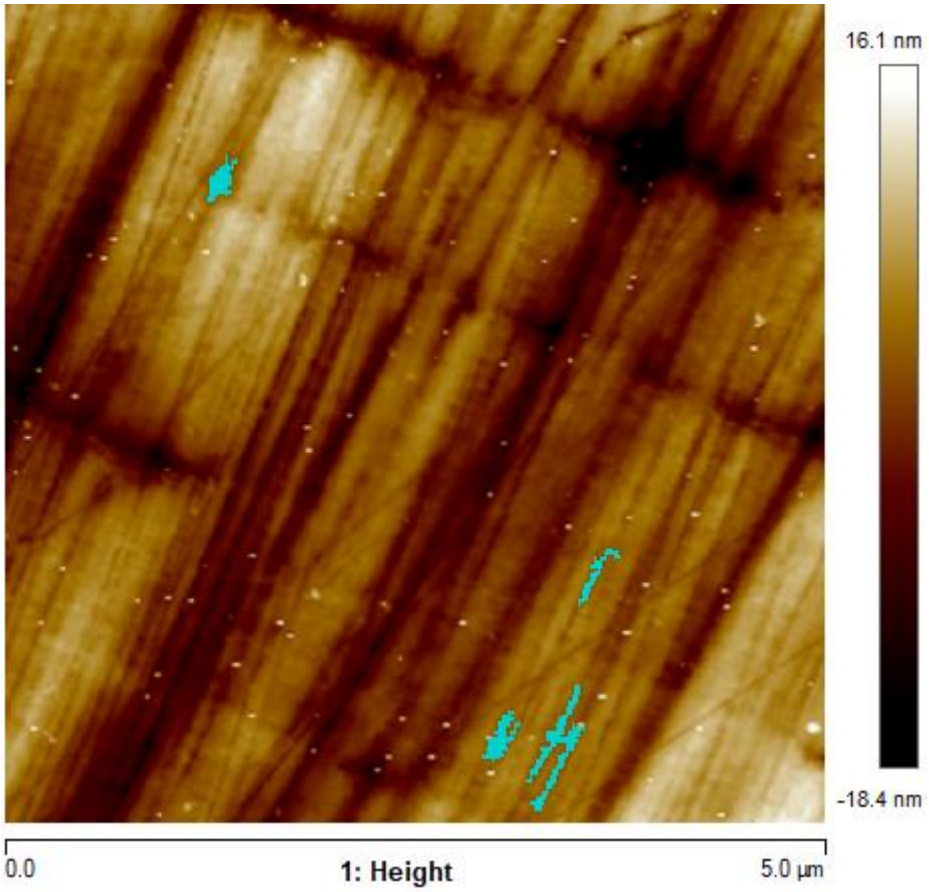

Fig. 5.22 LFM image of A20 sample at 5 µm scan range with capillary pores highlighted in blue

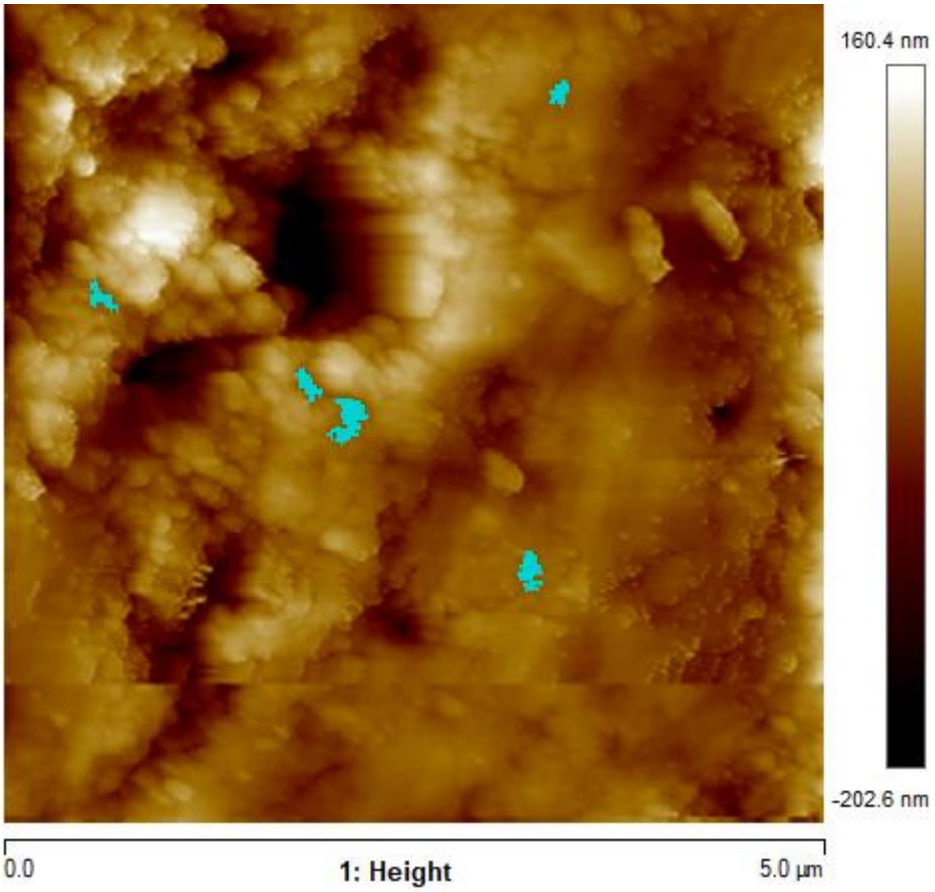

Fig. 5.23 LFM image of A40 sample at 5 µm scan range with capillary pores highlighted in blue

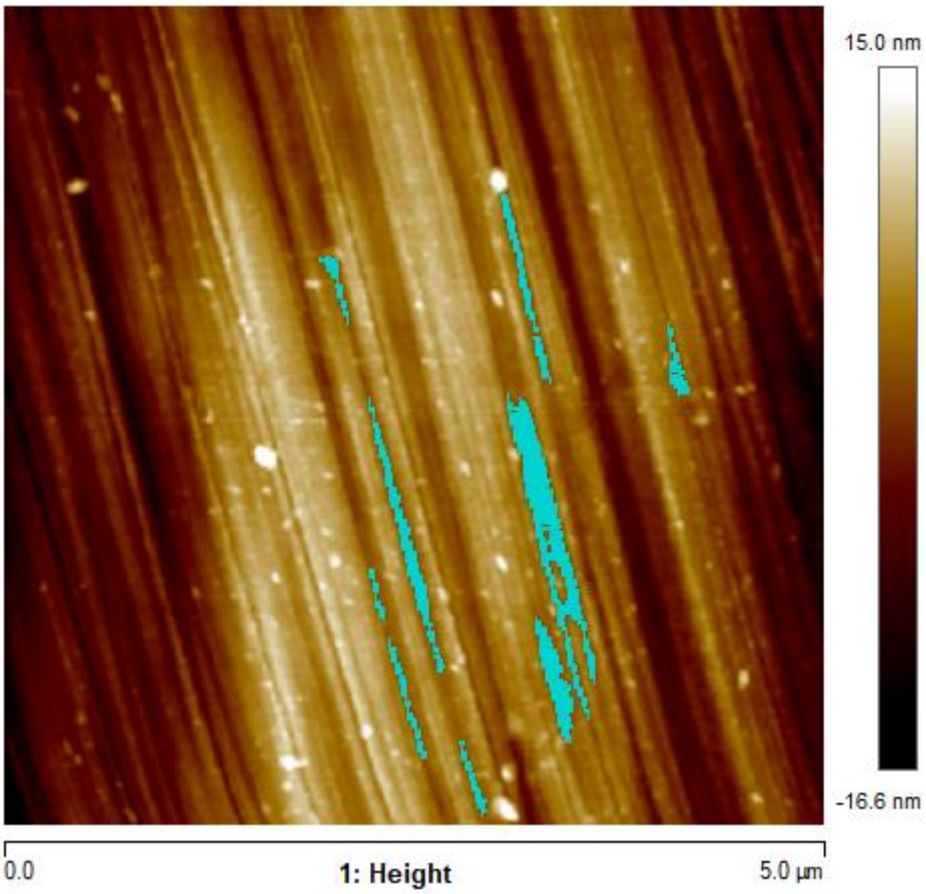

Fig. 5.24 LFM image of A60 sample at 5 µm scan range with capillary pores highlighted in blue

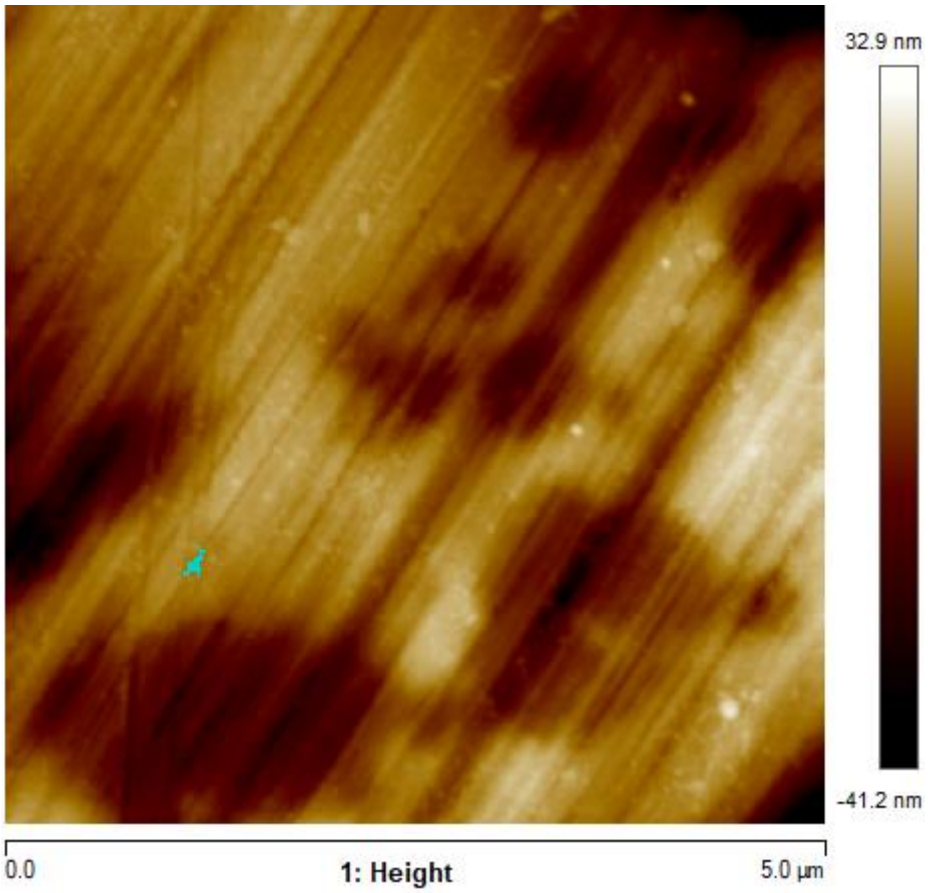

Fig. 5.25 LFM image of A80 sample at 5 µm scan range with capillary pores highlighted in blue

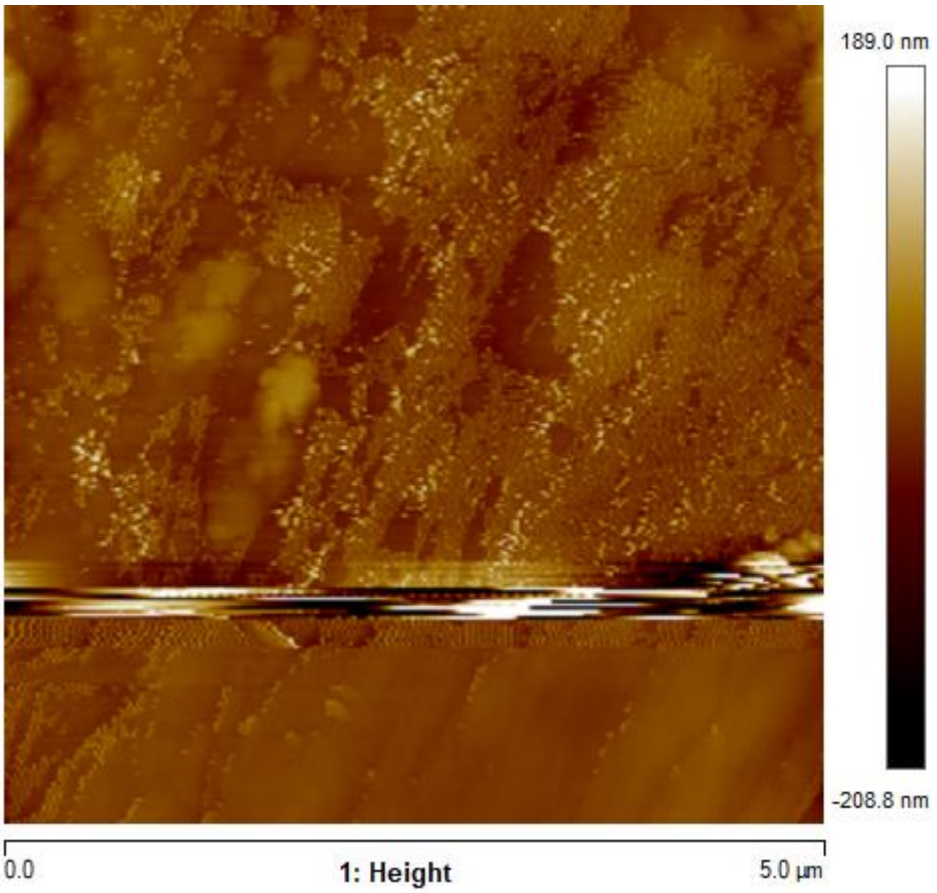

Fig. 5.26 LFM image of A100 sample at 5 µm scan range with capillary pores highlighted in blue

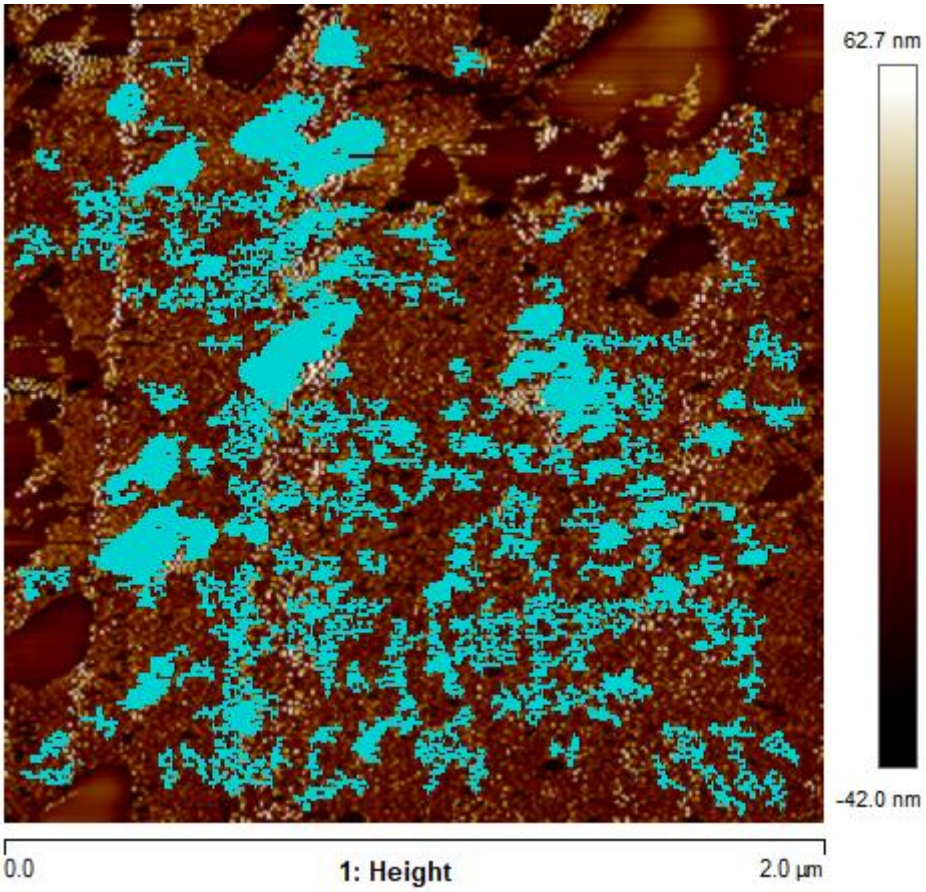

Fig. 5.27 LFM image of A0 sample at 2 µm scan range with capillary pores highlighted in blue

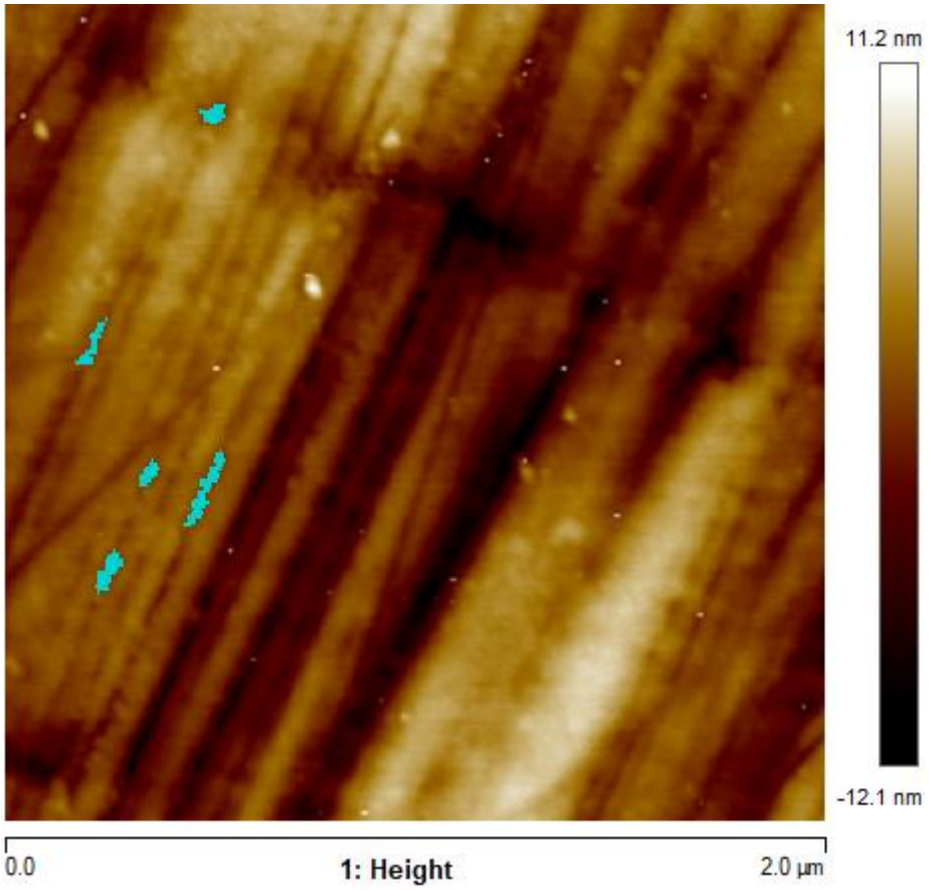

Fig. 5.28 LFM image of A20 sample at 2 µm scan range with capillary pores highlighted in blue

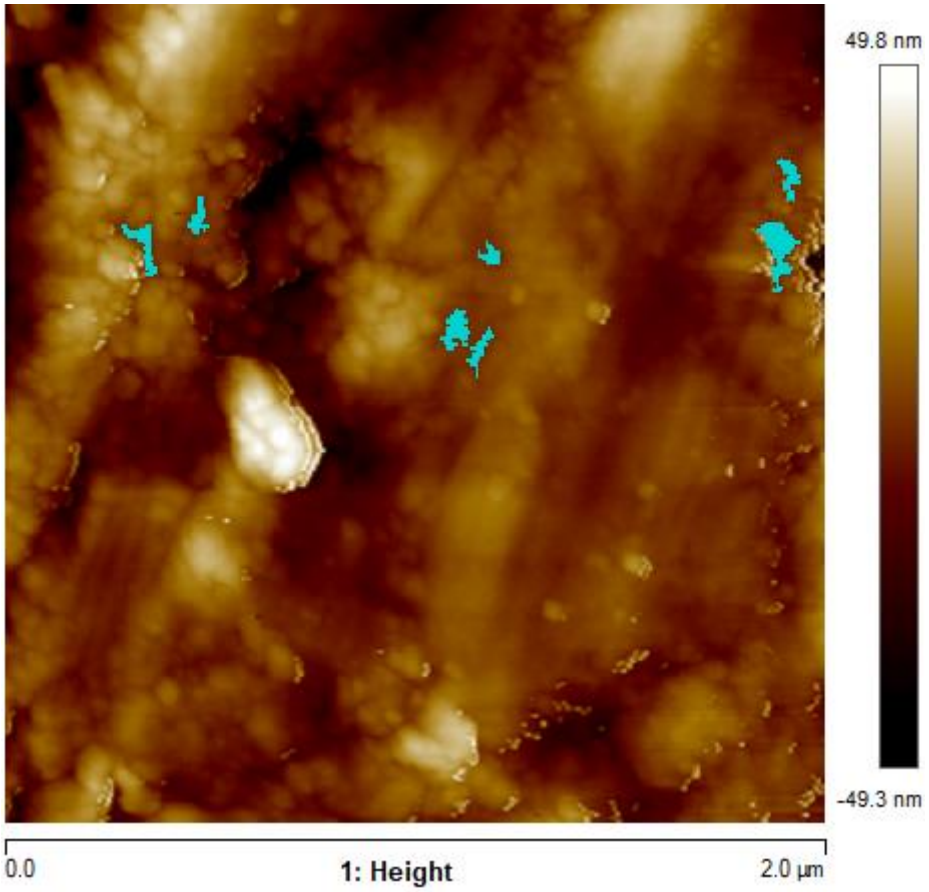

Fig. 5.29 LFM image of A40 sample at 2 µm scan range with capillary pores highlighted in blue

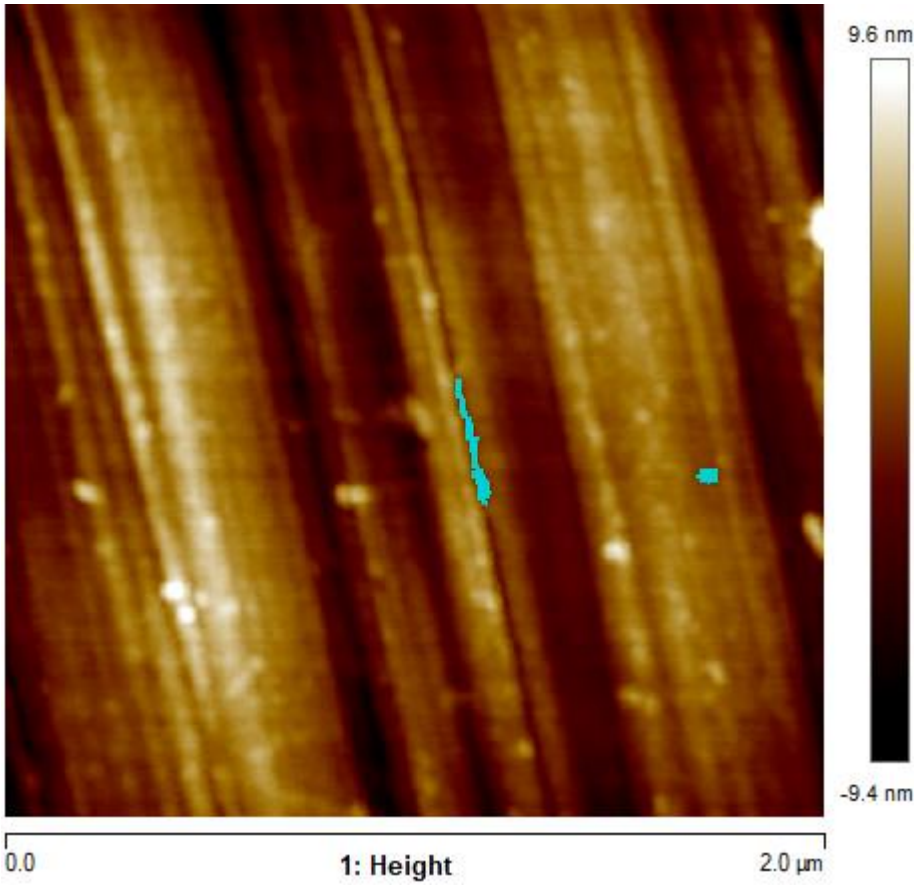

Fig. 5.30 LFM image of A60 sample at 2 µm scan range with capillary pores highlighted in blue

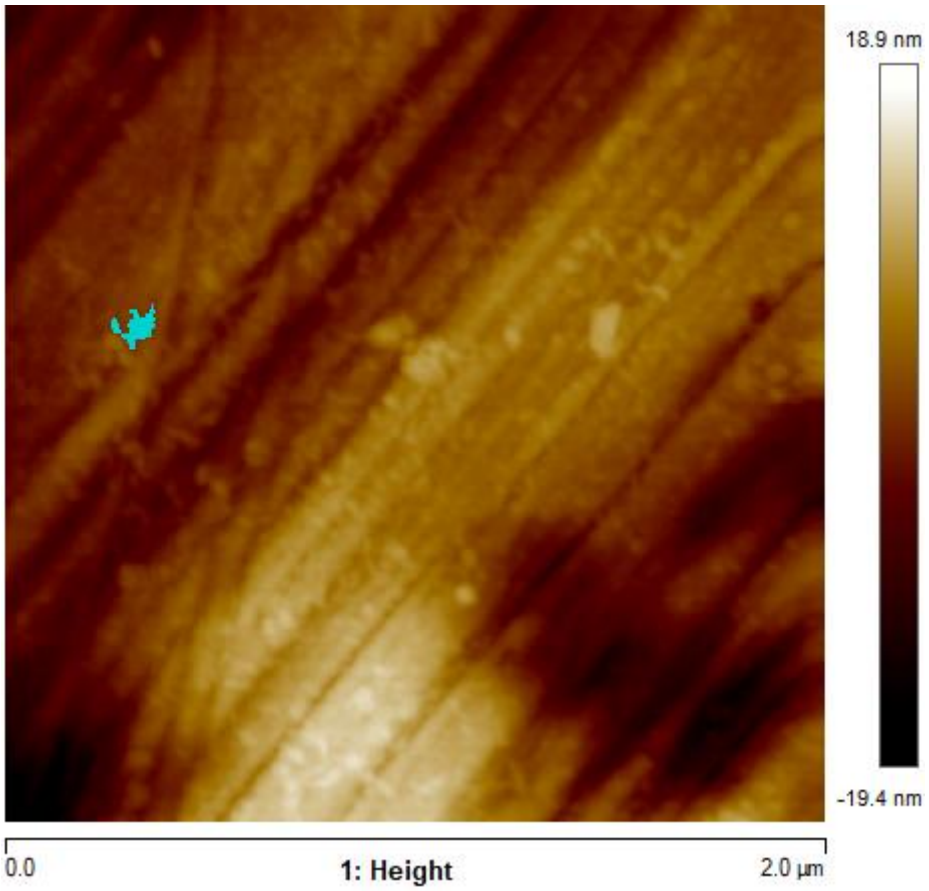

Fig. 5.31 LFM image of A80 sample at 2 µm scan range with capillary pores highlighted in blue

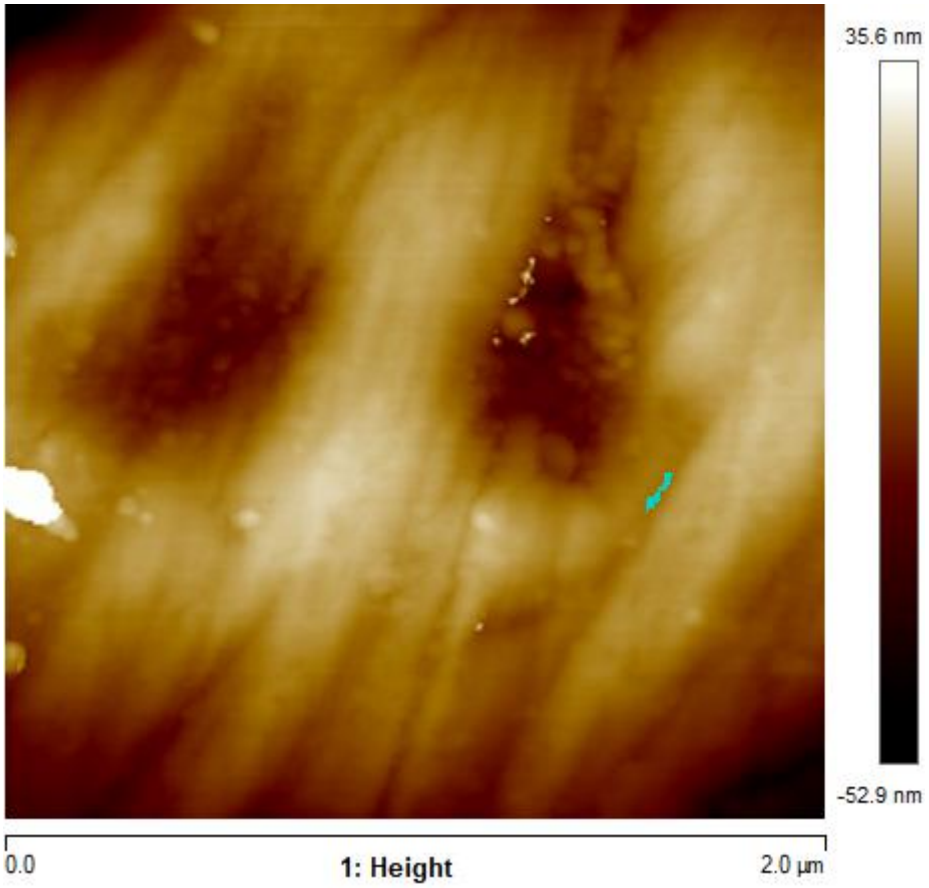

Fig. 5.32 LFM image of A100 sample at 2 µm scan range with capillary pores highlighted in blue

5.3.2 XRD measurements

The X-ray diffraction pattern and analysis of concrete mixes at 28 days are shown in Fig. 5.33. The analysis described below is with respect to different compound formed in hydrated cement concrete.

5.3.2.1 Silica (quartz)

As shown in Fig. 5.33, the peak of silica (SiO_2) for A0 mix was observed at 36.5131 (2 theta) having intensity count of 1063.59. The introduction of FBA in concrete mixes results in siginificant variation of peak values for A20, A40, A60, A80and A100 mixes. In case of A20 mix, peak value increases to 1548.66 (at 2 theta 20.9517) whereas for A40 mix the peak value was 1958.62 (at 2 theta 26.7511). Finally, the peak values for A60 mix was 727.03 (at 2 theta 26.6080) which further decreases to 428.12 (at 2 theta 26.6387) for A80 mix and 478.94 (at 2 theta 26.9153) for A100 mix. The presence of silica particles helps in densification of the concrete matrix and formation of calcium silicate hydrate (CSH) gel leading to enhanced interfacial transition zone (ITZ) of the aggregate cement paste matrix. Since the maximum compressive strength was observed at mix A60 it can be stated that optimum utilisation of silica is obtained at 60% replacement of natural sand by FBA.

5.3.2.2 Calcium silicate hydrate (CSH)

The most important compound governing the properties of concrete, formed after hydartion reaction is calcium silicate hydrate. Higher concentration of CSH results in superior ITZ layer which leads to higher compressive strength properties of concrete. XRD analysis (Fig. 5.33) of concrete mixes shows the peaks of CSH gel at different positions with different intensities. A60 mix has the highest peak value of CSH gel whereas A0 mix has large number of CSH peaks with lower intensity. Intensity peaks of CSH in A60 mix for 2 theta value of 27.4627, 27.9760, 30.9487 and 34.1395 are 472.60, 107.69, 766.06 and 111.67 respectively. For A0 mix, prominent intensity peaks of CSH observed are 573.67, 53.18, 360.44 and 61.60 at 2 theta

26.5942, 32.1552, 34.0828 and 41.0864 respectively. Highest concentration of CSH gel is present in A60 mix compared to other mixes which results in higher compressive strength of A60 mix.

5.3.2.3 Portlandite

Portlandite reduces the pore volume of the concrete matrix due to its crystal form. In general, the presence of portlandite in optimum amount contributes slightly in strength development and reduction of voids. The higher or lower content of potlandite can result in loss of durability or higher permeability values. In case of A0 mix, XRD patterns (Fig. 5.33) of the sample show presence of portlandite with highest peak intensity of 227.93 at 2 theta 18.0020. For A20 mix, peak value of 518.92 was observed at 36.5945 (2 theta) which is higher than A0 mix. Highest peaks of portlanite for A40, A60, A80 and A100 were observed as 117.43, 72.34, 195.97 and 49.46 at 2 theta of 18.148, 36.5033, 18.0384 and 36.8272 respectively. From the compressive strength results, it can be safely said that A60 mix has the optimum amount of portlandite compared to other mixes.

5.3.2.4 Ettringite

Reaction of calcium aluminate and calcium sulfate (both present in Portland cement) forms ettringite. The needle shaped ettringite crystals are formed in cracks and voids present in the ITZ layer. The controlled presence of ettringite crystals helps in reduction of voids and densification of concrete matrix (Johansen et al. 1993; Thomas et al. 2008). XRD analysis (Fig. 5.33) of concrete samples for A0 to A100 mixes ettrengite peak intensity values are 53.18, 124.26, 56.32, 121.84, 41.57 and 32.20 respectively. 2 theta position for these observed peaks are 32.1552, 45.8395, 39.5888, 29.4398, 47.2305 and 45.9467. In case of A60 mix, another peak of intensity 107.69 at 27.9760 (2 theta) is also observed. The concentration of ettringite crystals is highest in case of A60 mix, resulting in dense and superior concrete matrix.

5.3.2.5 Alumina, calcite and dolomite

Higher alumina content in concrete samples provides positive influence on the initial strength gaining mechanism of concrete matrix but also weakness the resistance capacity of concrete against sulphate attack. As shown in XRD analysis of the concrete mixes, the alumina content is very less as compared to silica. The alumina content is therefore expected to barely influence the development of compressive strength in concrete. XRD analysis (Fig. 5.33) shows slightly high intensity peaks of calcite and dolomite in concrete samples incorporating fine bone china aggregtaes. For calcite, observed highest intensity values for A0-A100 mixes are 81.05, 139.79, 115.03, 54.50, 103.23 and 30.90 at 2 theta 47.1003, 29.5455, 29.5871, 42.4383, 41.1652 and 36.0052 respectively. Whereas for dolomite, highest intensity values are 24.51, 63.36, 71.06, 67.45, 67.06 and 11.06 at 2 theta 67.3231, 81.1627, 60.0052, 59.9526, 50.1647 and 81.4790 respectively. From the observed intensity peaks, it can be concluded that the presence of small amount of alumina, calcite and dolomite does not have any significant effect on the performance of concrete.

5.3.2.6 Sodium oxide, potassium oxide and magnesium oxide

Sodium oxide and potassium oxide also known as alkali oxides in higher quantity have been found to react with some coarse aggregtaes and cause alkali aggregate reaction and also causes delay in the hydration rate of concrete. Magnesium oxide causes slight decrease in strength of concrete and increses the setting time of concrete. Higher quatitites of magnesium oxide can also cause unwanted expansion in concrete. As shown in XRD analysis (Fig. 5.33), the introduction of fine bone china aggregte in the concrete mix causes reduction in the quantity of alkali oxides and magnesium oxide. Further, they are not traceable when the content of FBA is higher than 40%.

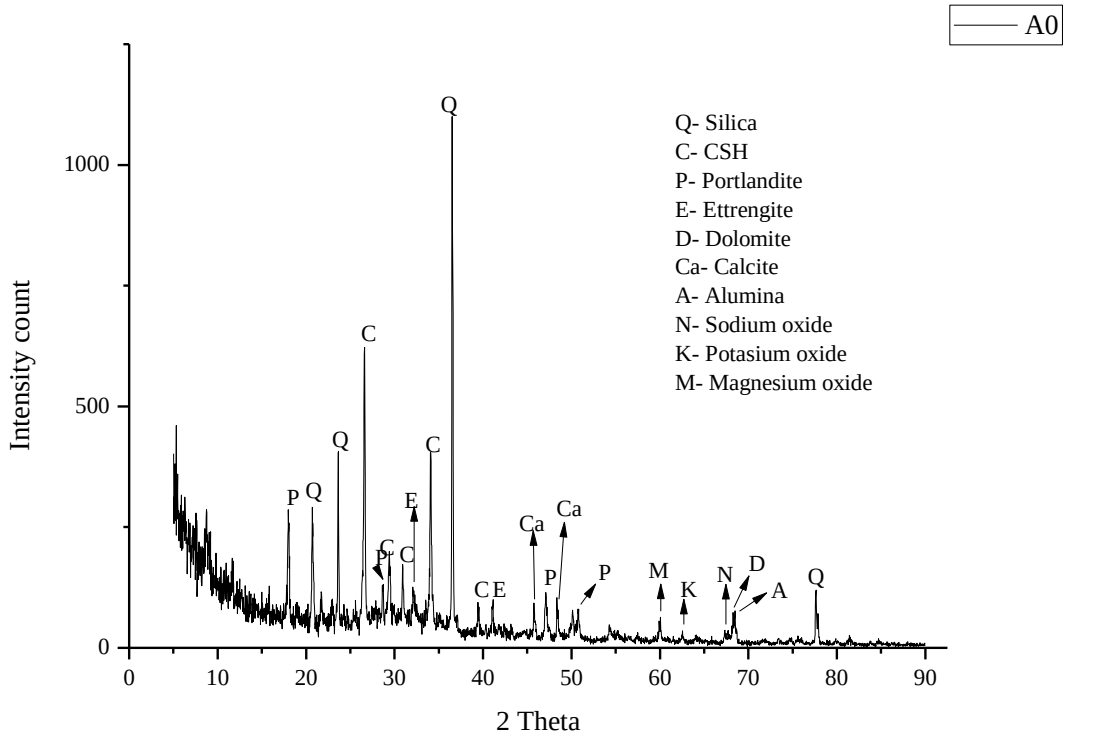
A0
Intensity count
2 Theta
Q- Silica
C- CSH
P- Portlandite
E- Ettrengite
D- Dolomite
Ca- Calcite
A- Alumina
N- Sodium oxide
K- Potasium oxide
M- Magnesium oxide

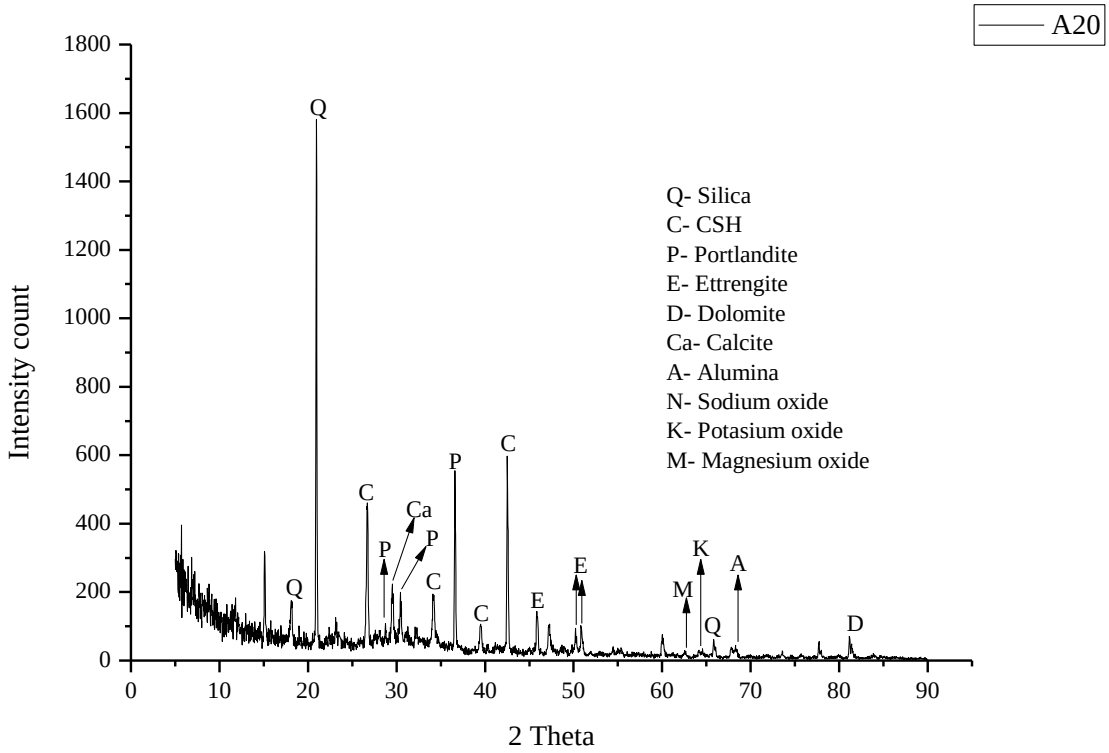
A20
Intensity count
2 Theta
Q- Silica
C- CSH
P- Portlandite
E- Ettrengite
D- Dolomite
Ca- Calcite
A- Alumina
N- Sodium oxide
K- Potasium oxide
M- Magnesium oxide

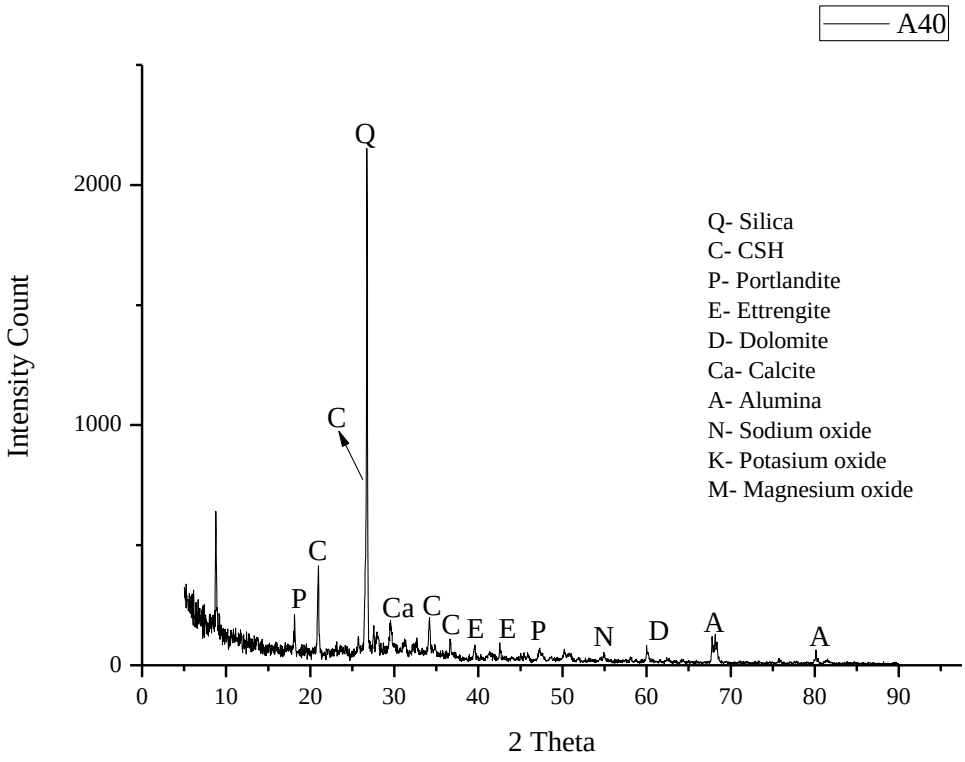
A40
Intensity Count
2 Theta
Q- Silica
C- CSH
P- Portlandite
E- Ettrengite
D- Dolomite
Ca- Calcite
A- Alumina
N- Sodium oxide
K- Potasium oxide
M- Magnesium oxide

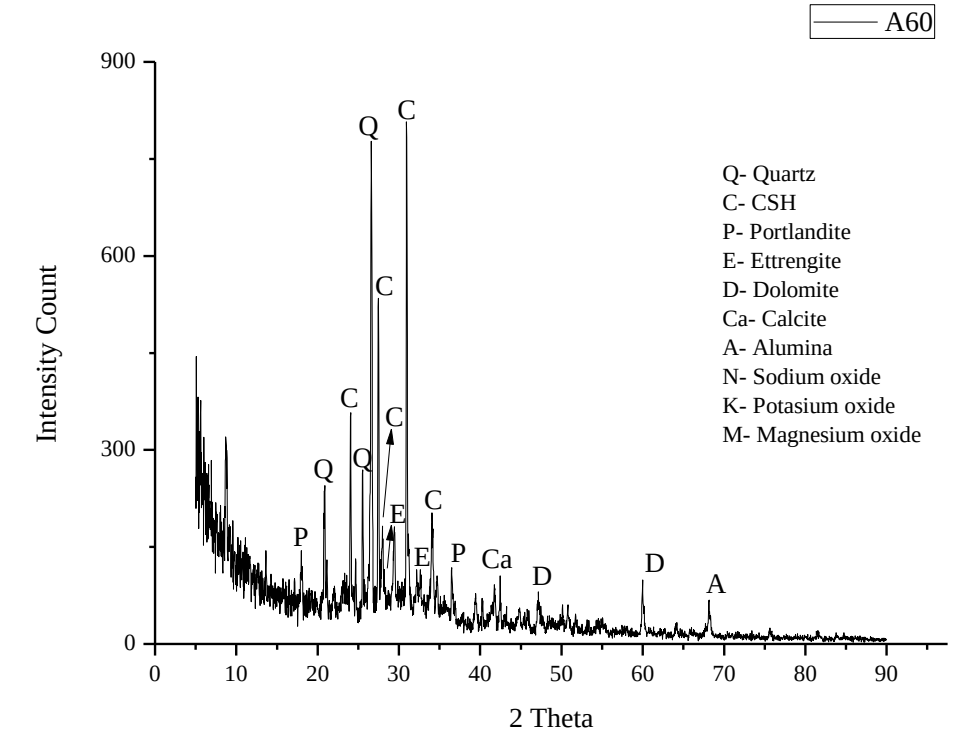
A60
Intensity Count
2 Theta
Q- Quartz
C- CSH
P- Portlandite
E- Ettrengite
D- Dolomite
Ca- Calcite
A- Alumina
N- Sodium oxide
K- Potasium oxide
M- Magnesium oxide

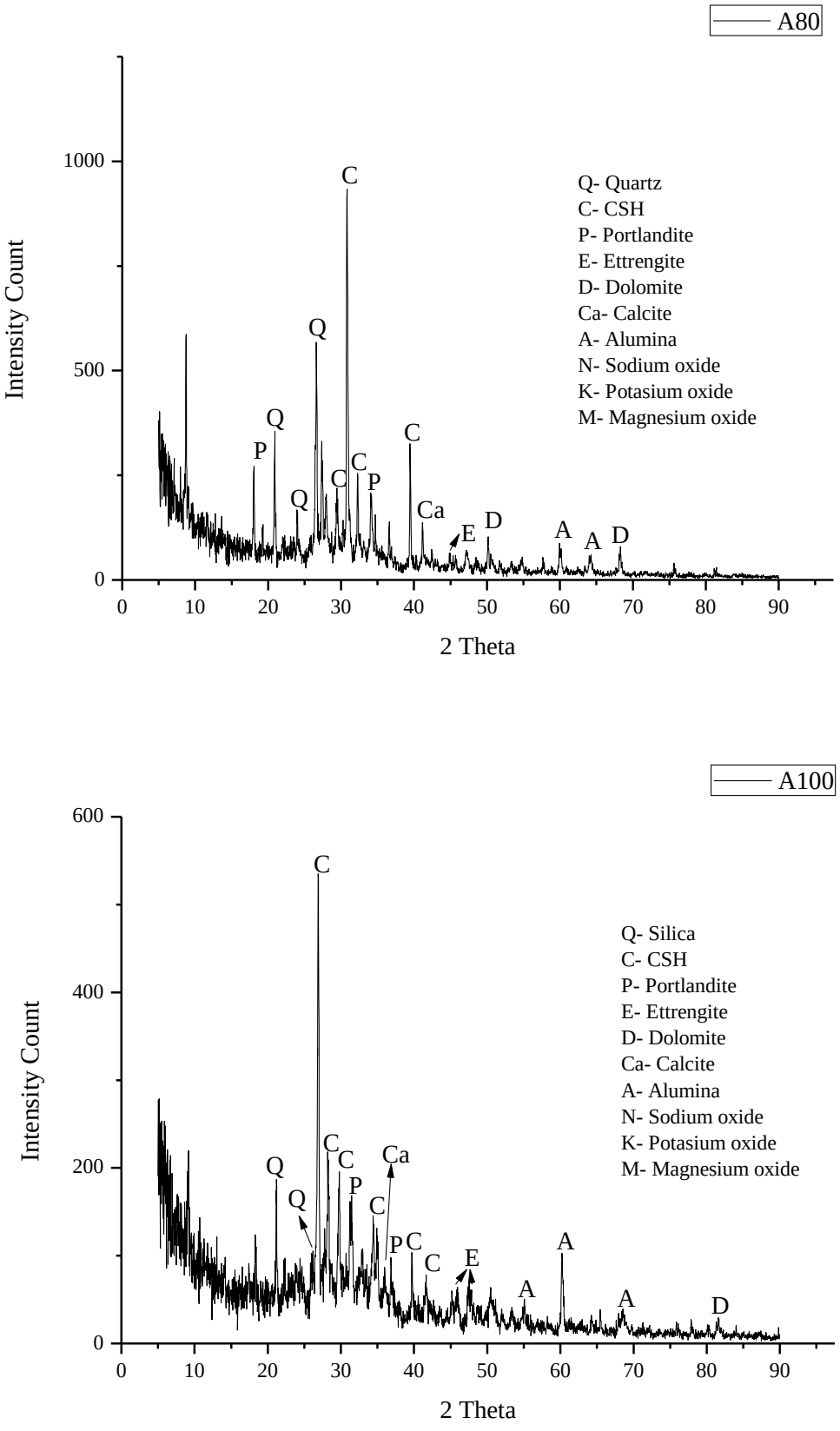

Fig. 5.33 XRD spectra of FBA concrete mixes

5.3.3 FT-IR measurements

The FT-IR spectra of the concrete samples are shown in Fig. 5.34. The spectral changes and relative shifts of the peaks can provide valuable prespective in understanding the strength gaining mechanism of concrete samples. The spectral data is discussed in two parts.

5.3.3.1 (>2000cm^{-1}) bond bands

This region holds crucial information regarding the hydration mechanism of cement paste. It can be seen in Fig. 5.34 that two bands of $Ca(OH)_2$ are present in the spectra. The broad shoulder of the band shows the complete formation of $Ca(OH)_2$ atrributed to OH bond. The observed wave number for $Ca(OH)_2$ band are 3369.34, 3368.95, 3367.14, 3356.15, 3370.71 and 3510 cm^{-1} for A0, A20, A40, A60, A80 and A100 respectively. It is observed that incorporation of FBA causes slight relative shift in the peaks. On close examination it was found that for A60 mix, the $Ca(OH)_2$ wave number shifted by nearly 13 cm^{-1}. Such shift towards lower peak number symbolises decrease in bond length leading to weaker bonds. Since the shifts observed for $Ca(OH)_2$ band are not high and the peaks maintain the similar intensity structure it can be said that they have little influence on the strength gaining characteristics of the concrete samples incorporating FBA.

Another weak band at 2893 cm^{-1} is observed in all the concrete samples. The intensity of the band and wave number of the band is nearly similar in all the samples. This band is commonly attributed to methyl and methylene groups and the presence of organic compounds in demoulding oil are responsible for this bond band in all the concrete mixes (Chollet and Horgnies 2011).

5.3.3.2 (<2000 cm^{-1}) bond bands

Calcium carbonate ($CaCO_3$) in all the specimens results from the carbonation of calcium hydroxide. The wave number at which the CO bond appears are 1416.15, 1417.28, 1425.03, 1368.15, 1415.50 and 1437.9 cm^{-1} for A0, A20, A40, A60, A80 and A100 respectively. A

second peak at around 1740 cm^{-1} wave number is observed in the concrete samples containing FBA. The introduction of FBA in the concrete mixes results in higher intensity of $CaCO_3$ with higher wave number. The abundance of cacium hydroxide in the FBA concrete leads to formation of $CaCO_3$ upon carbonation.

The peaks observed at wave number 992.40, 1032.37, 988.08, 968.17 , 989.78 and 1024 cm^{-1} for A0, A20, A40, A60, A80 and A100 respectively are attributed to calcium silicate hydrates (CSH). It is observed that except for A20 mix all the other FBA concrete samples show lower wave number when compared with control concrete sample. This observation is helpful in concluding that the bond length of the CSH polymer is shorter when FBA is used and it also causes mass reduction of the polymer molecules. The gain in compressive strength when fine bone china aggregtae is used can be due to a second peak of CSH observed at 1210.43, 1213.66, 1215.81 and 1214.16 cm^{-1} wave number for A20, A40, A60 and A80 respectively. The occurrence of second peak of CSH polymer at a higher wave number can lead to a better compressive strength in the samples containing FBA. Similar observations were made by different authors on incorporating recycled aggregates and geopolymer concrete (Adak et al. 2107; Bulatović et al. 2017).

The wave number corresponding to SiO_2 covers numerous peaks in the band of (410-780) cm^{-1}. From the spectral patterns it is observed that the intensity of SiO_2 content reduces slightly when fine bone china is used to replace natural sand but the wave numbers for bond bands are nearly similar in all cases.

The lack of SO_4 bond band at wave number 1100-1150 cm^{-1} can be due to absence of thaumasite or ettrengite formation.

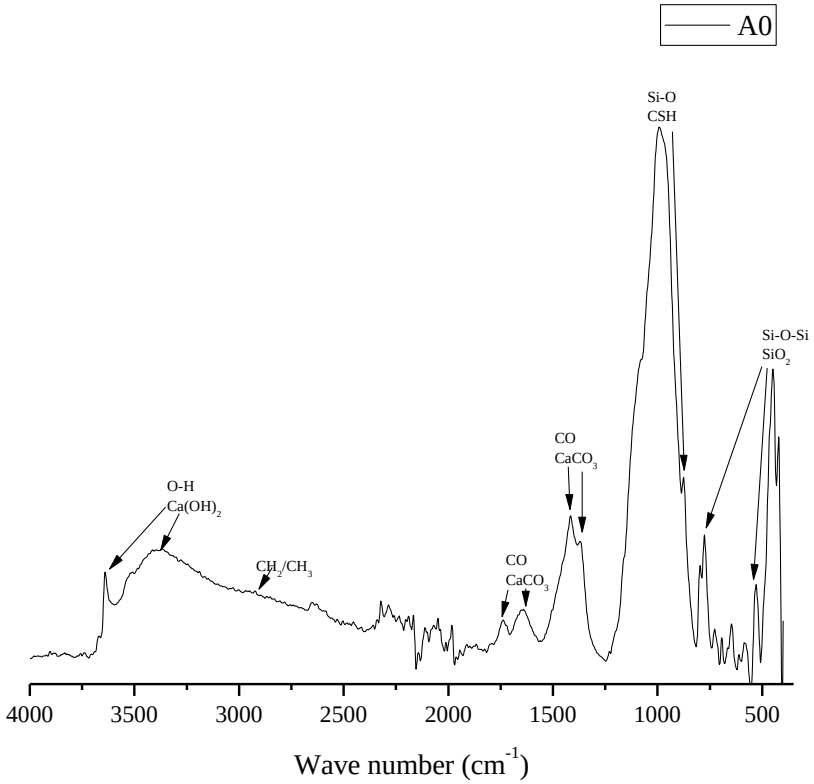
A0
Si-O
CSH
Si-O-Si
SiO2
CO
CaCO3
O-H
Ca(OH)2
CH2/CH3
CO
CaCO3
4000
3500
3000
2500
2000
1500
1000
500
Wave number (cm-1)

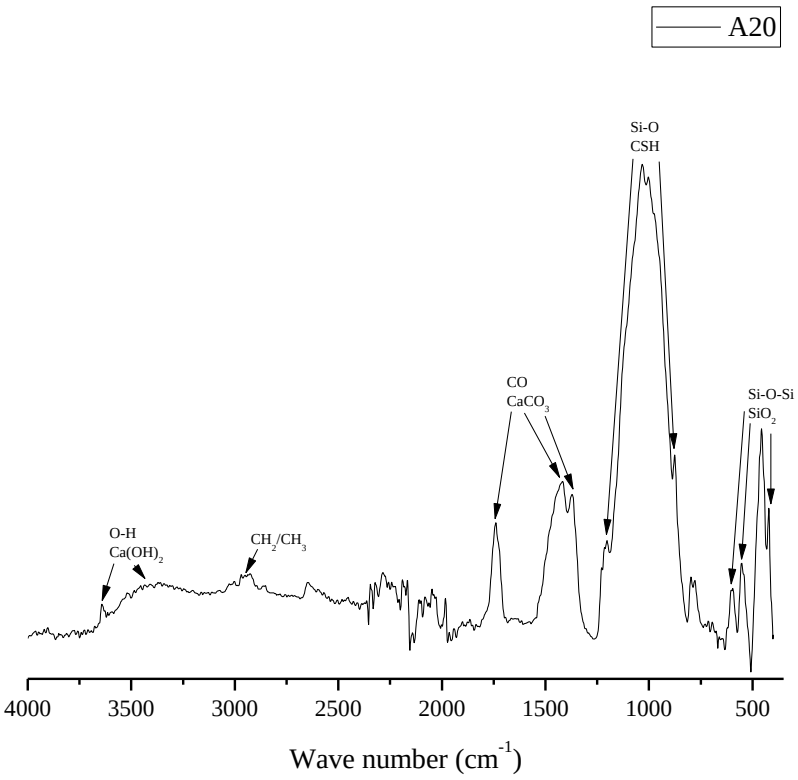
A20
Si-O
CSH
CO
CaCO3
Si-O-Si
SiO2
O-H
Ca(OH)2
CH2/CH3
4000
3500
3000
2500
2000
1500
1000
500
Wave number (cm-1)

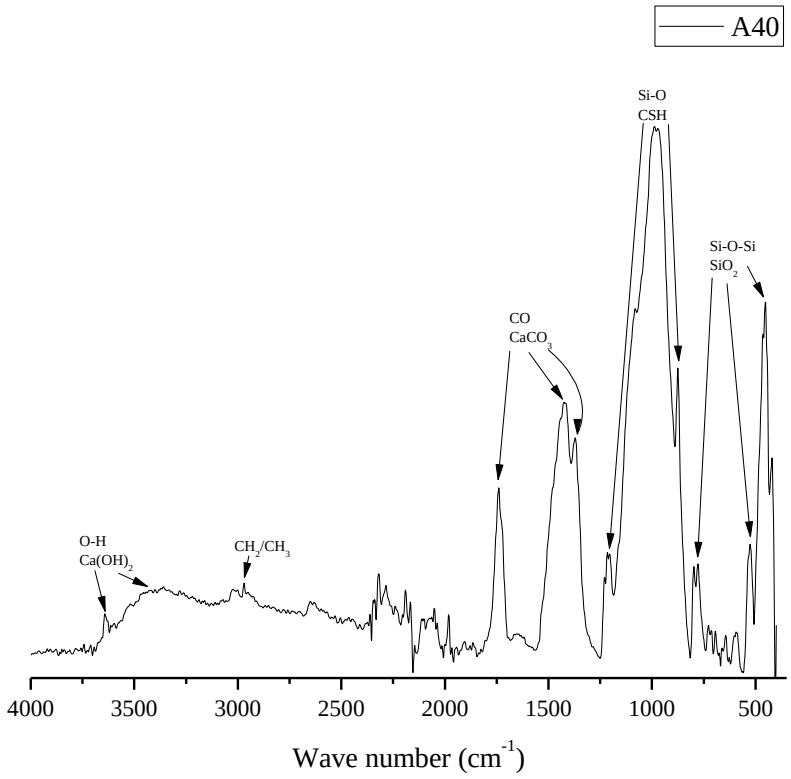
A40
Si-O
CSH
Si-O-Si
SiO2
CO
CaCO3
O-H
Ca(OH)2
CH2/CH3
4000
3500
3000
2500
2000
1500
1000
500
Wave number (cm-1)

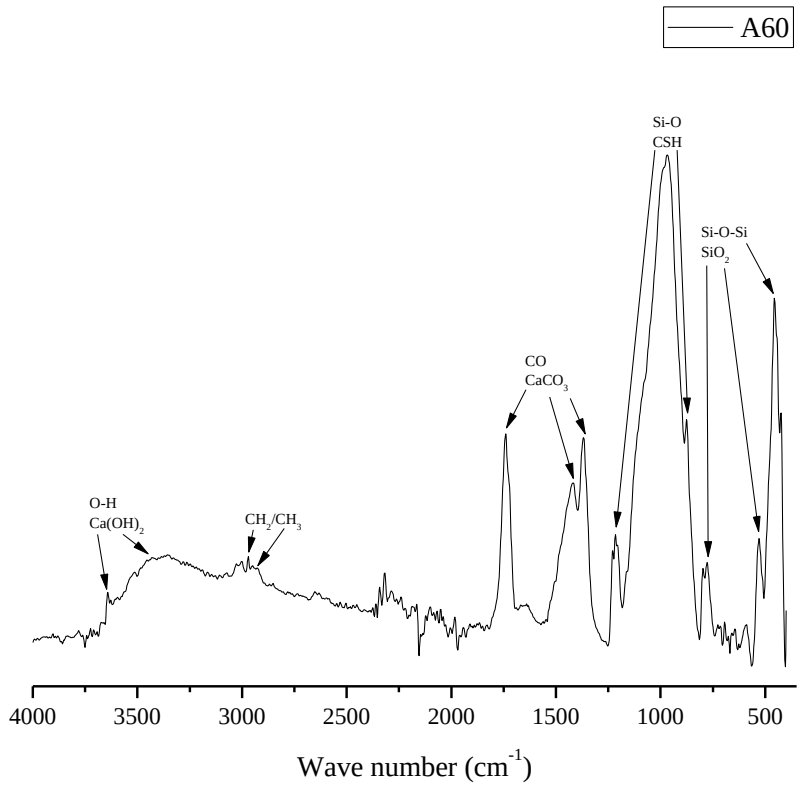
A60
Si-O
CSH
Si-O-Si
SiO2
CO
CaCO3
O-H
Ca(OH)2
CH2/CH3
4000
3500
3000
2500
2000
1500
1000
500
Wave number (cm-1)

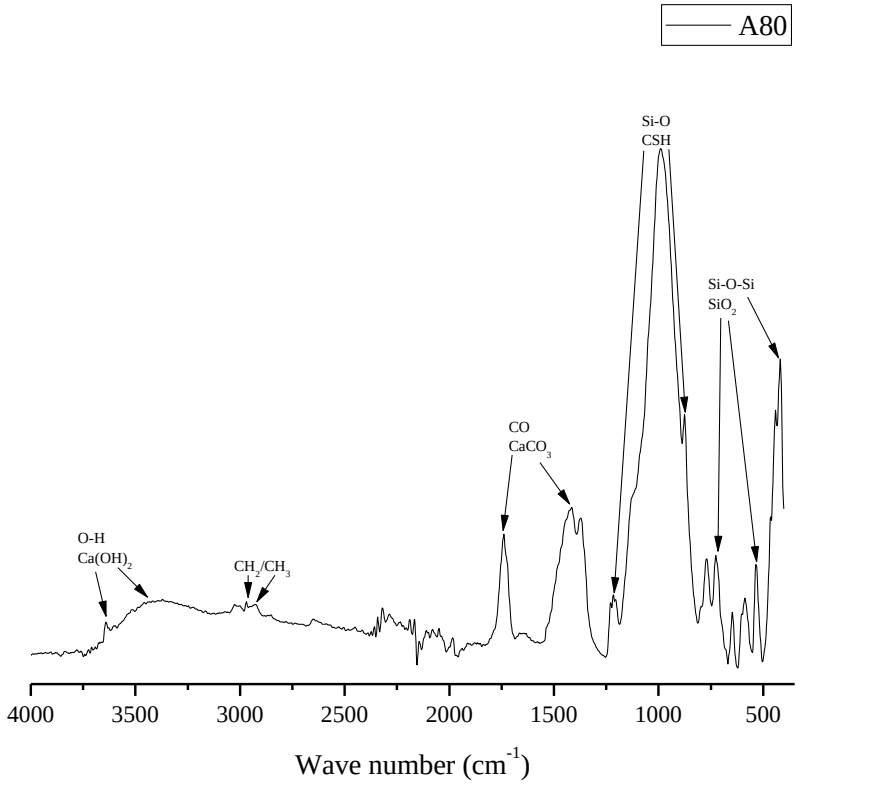

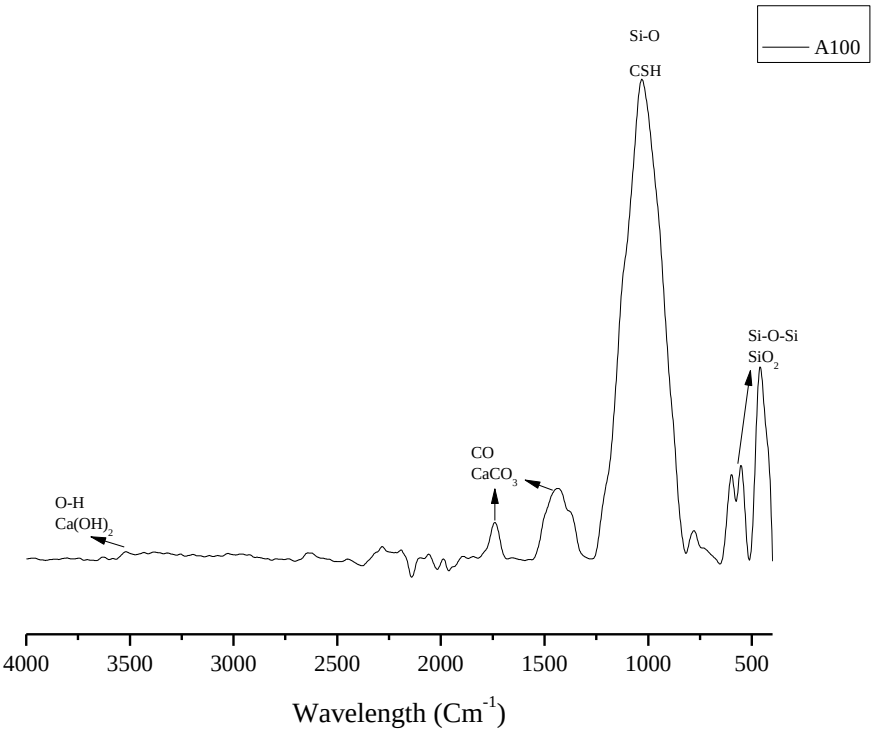

Fig. 5.34 FT-IR spectra of FBA concrete mixes

5.3.4 NMR measurements

Fig. 5.35 shows the ^{29}Si NMR spectra of concrete samples. Standard Q^n nomenclature was followed for peak assingment. Table 5.7 presents the information derived from ^{29}Si NMR spectra. The CSH polymerisation and chain length values derived from ^{29}Si NMR spectra are useful in understanding the influence of fine bone china ceramic aggregate on the formation of CSH gel. The peak corresponding to Q^3 is indicative of the coarse aggregate and the Q^4 peak usually corresponds to crystalline silicate or quartz from natural sand or FBA.

5.3.4.1 Q^0 peak

The Q^0 peak is indicative of unhydrated cement particles. In concrete mix samples the Q^0 peak is observed at -68.45, -67.68, -68.35, -68.83 and -73.45 ppm for A0, A20, A40, A60 and A80 mixes. It can be observed from Table 5.7 that the introduction of FBA results in higher degree of hydration lowering the unhydrated cement particles.

5.3.4.2 Q^1 and Q^2 peak

CSH polymer behaviour can be predominentely assesed by Q^1 and Q^2 peak. The relatively broadened peaks in the NMR spectrum are a result of poor crystalline structure of CSH. Q^1/Q^2 ratios were 0.934, 0.938, 0.903, 0.902 and 0.940 in A0, A20, A40, A60 and A80 mixes concrete respectively. Since lower Q^1/Q^2 ratio indicate higher degree of polymerisation it can be stated that 40% and 60% utilisation of FBA results in higher degree of CSH polymerisation resulting in dense and compact matrix. Another valuable observation from the spectra is yielding of average silicate chain length. It can be seen in Table 5.7 that the introduction of 40% and 60% FBA causes slight increase in chain length. The pozzolanic behaviour of FBA coupled with higher degree of hydration results in higher chain length. At 80% utilisation of FBA, the lesser amount of free silica results in minor decrease of chain length and increase in Q^1/Q^2 ratio. Similar observations were obtained by other authors incorporating differernt

pozzolanic materials in cement concrete mixes (Muller et al. 2015; Wang et al. 2013; Zanni et al. 1996).

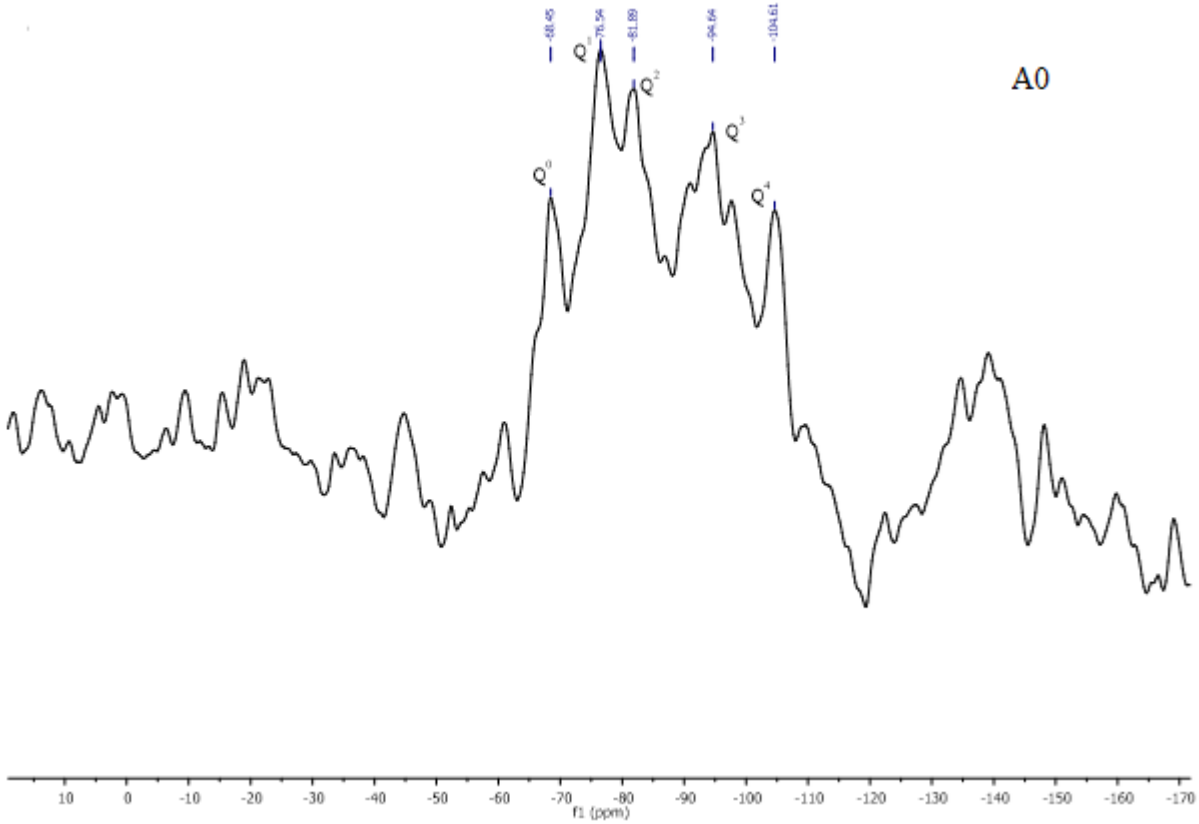

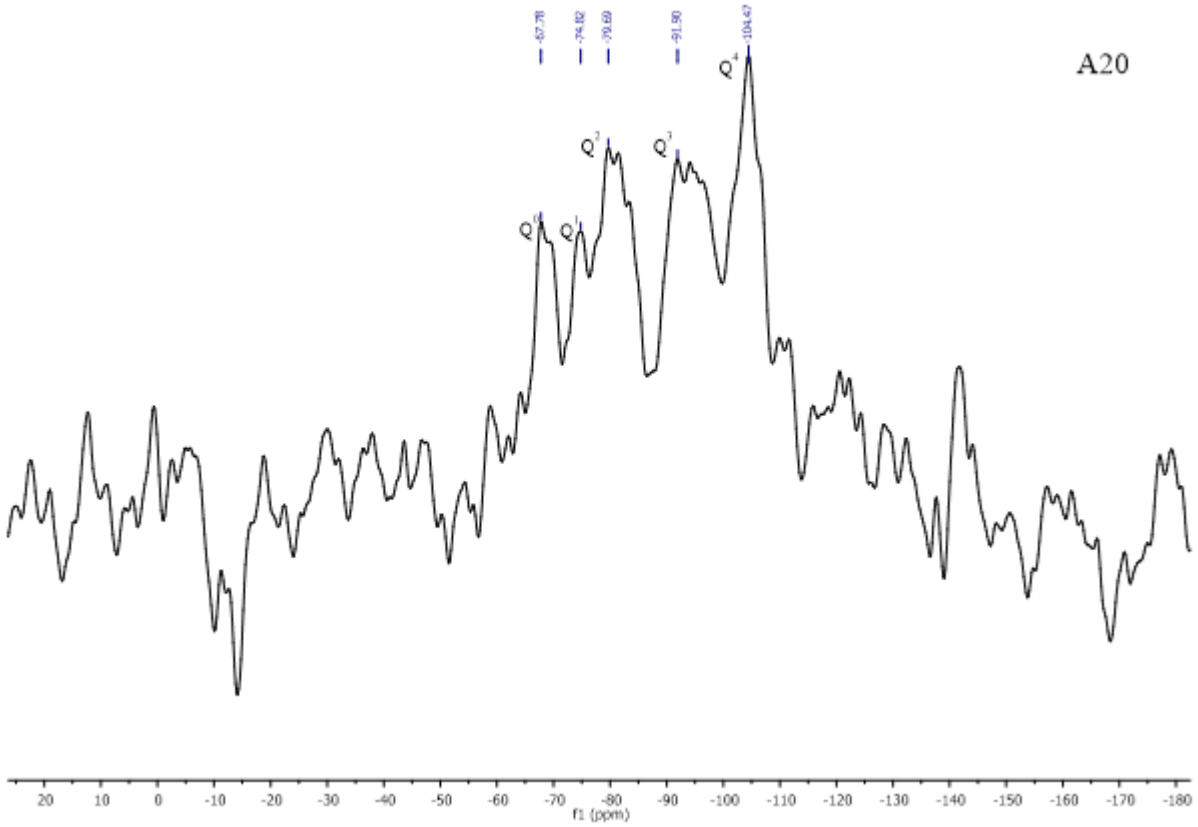
A20
-67.78
-74.82
-79.69
-91.90
-104.47
Q4
Q3
Q2
Q1
Q0
20 10 0 -10 -20 -30 -40 -50 -60 -70 -80 -90 -100 -110 -120 -130 -140 -150 -160 -170 -180
f1 (ppm)

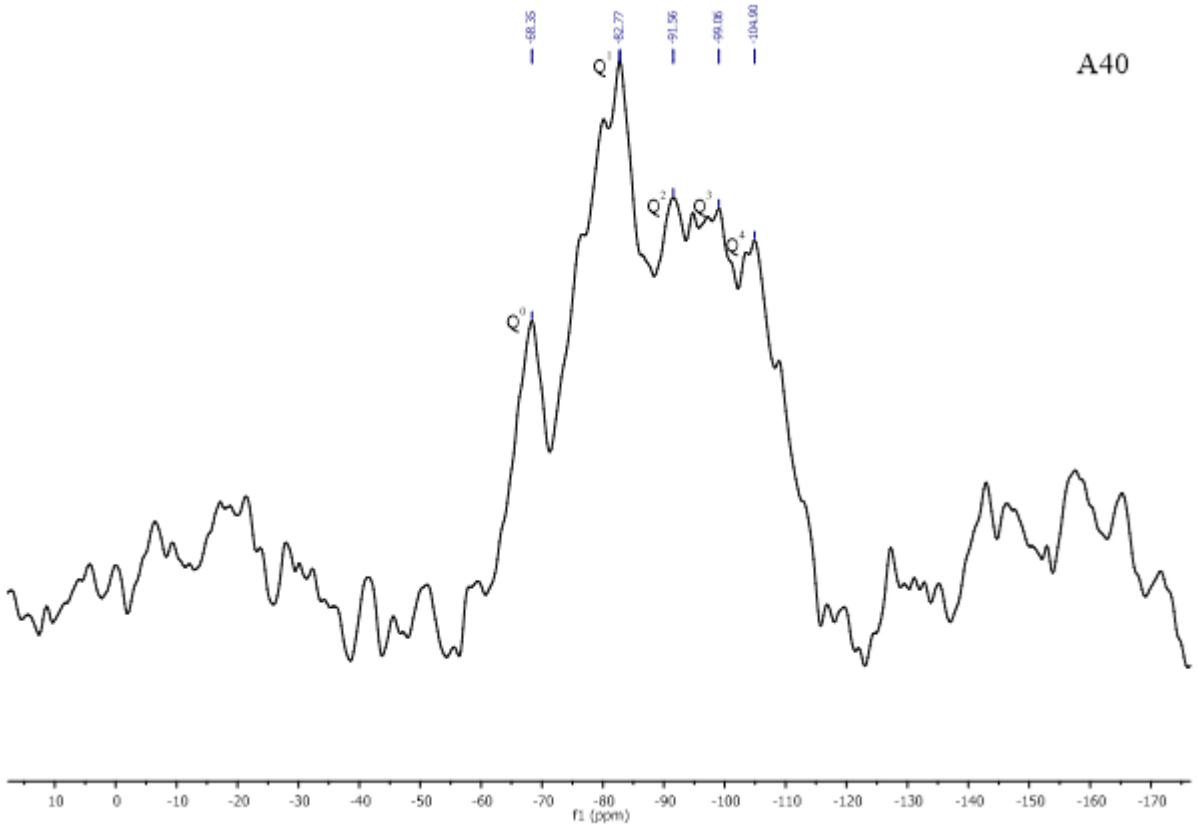
A40
-68.35
-82.77
-91.56
-99.06
-104.90
Q1
Q2
Q3
Q4
Q0
10 0 -10 -20 -30 -40 -50 -60 -70 -80 -90 -100 -110 -120 -130 -140 -150 -160 -170
f1 (ppm)

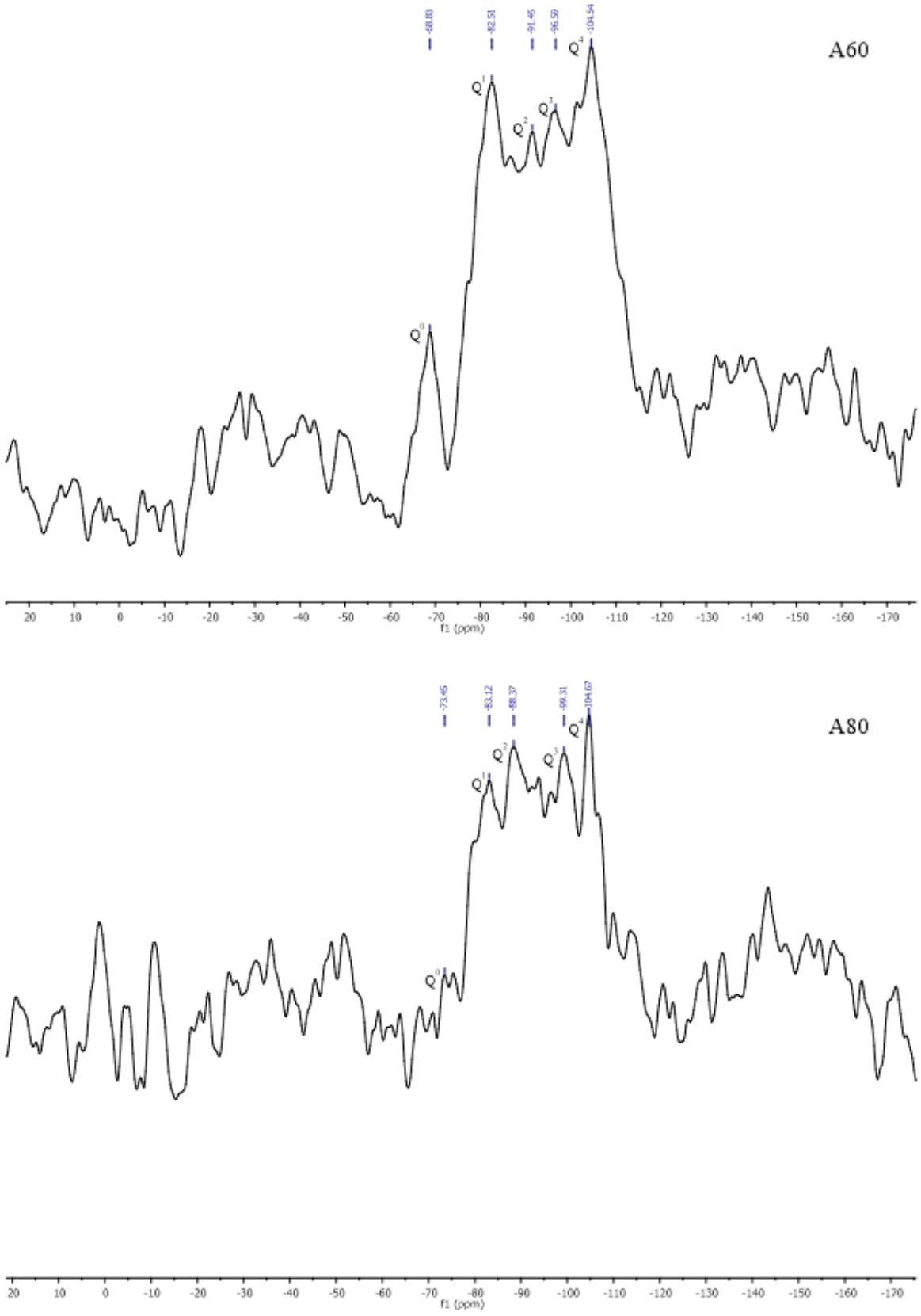

Fig. 5.35 ^{29}Si NMR spectra of FBA concrete mixes

Table 5.7 Information obtained from ^{29}Si NMR spectra of concrete samples

Mix	**Degree of hydration (%)**	**Q^1/Q^2**	**Chain Length**
A0	47.7	0.934	4.13
A20	66.5	0.938	4.13
A40	73.4	0.903	4.21
A60	85.3	0.902	4.22
A80	82.4	0.940	4.13

5.3.5 XPS measurements

Fig. 5.36 shows the photoelectron spectra of control and FBA concrete. Table 5.8 presents the atomic percentage, Ca/Si (C/S) and O/S (O/Si) ratio for control and FBA concrete. The C/S values for concrete samples vary greatly along various concrete mixes and their composition. A quick observation of Fig. 5.36 shows that on increasing the content of FBA the intensity and atomic percent (Table 5.8) of calcium increases. Since the composition of concrete mixes varied in type of fine aggregate only, consideration of the binding energies only can lead to biased observations. To understand the influence of FBA on concrete hydration products, both binding energy and atomic percent parameters are to be considered for assessment of various samples.

The calcium (Ca2p, Ca2s and Ca2p1/2) indicates presence of various phases of calcium silicate hydrate (CSH) in FBA concrete matrix. As the crystallisation of CSH gel increases the ratio of C/S also increases. The observed C/S ratios of A0, A40, A80 and A100 indicates formation of Phyllosilicates (ranging between 0.36-0.65). Phyllosilicates are characterised by sheet like structure. The phase observed in the samples shows the evolving stage of CSH gel as the hydration mechanism will transform the Phyllosilicates to the next crystalline stage of

Inosilicates (ranging between 0.74-1.04). The C/S ratio of A20 and A60 indicates formation of chain silicates (Inosilicates). The Inosilicates provide stronger and fairly long bond length of Si-O. The formation of Inosilicates in concrete samples containing FBA and the higher values of C/S ratio can provide substantial proof of formation of higher and stable phase of CSH gel in concrete matrix after 28 days of curing.

Another observations that can be drawn from the XPS spectra and Table 5.8 is the O/S ratio. Increase in O/S ratio due to introduction of FBA in the concrete mix leads to lower binding energy in silicon. Increase in C/S ratio due to introduction of FBA in the concrete mix leads to dominance of non-bridging oxygen which balance out by forming Ca-O-Si. These two characteristics also substantiate the stable nature of CSH gel formed in fine bone china concrete matrix.

As observed in Table 5.8, the atomic percent of carbon increases on increasing the content of FBA in concrete. As stated earlier, fine bone china aggregate creates favourable hydration mechanism leading to higher and stable CSH gel. Another product of hydration mechanism is calcium hydroxide or portlandite. Since concentrations of CSH and portlandite are directly proportional to each other it can be said that formation of portlandite also increases in fine bone china aggregate concrete. The atmospheric carbon dioxide reacts with the surface of concrete breaking down portlandite into calcium carbonate. Since the observed values of atomic percentage of carbon are not very high for FBA concrete and the hydration products are of better quality and phases, it can be said that degradation of concrete surface will not affect the service life requirements of concrete.

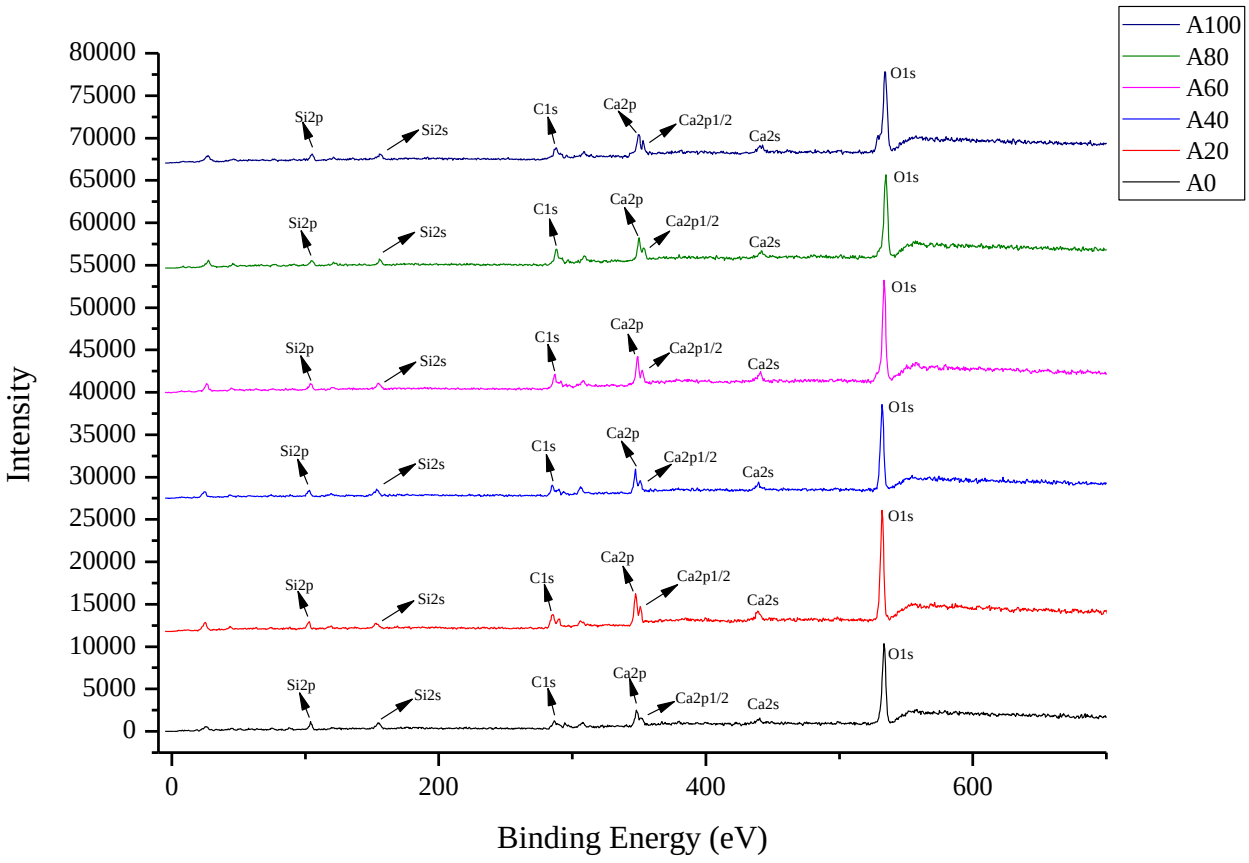

Fig. 5.36 XPS spectra of FBA concrete mixes

Table 5.8 XPS observations obtained for different elements in FBA concrete mixes

Mix	Ca2p	Ca2s	Ca2p1/2	Si2p	Si2s	C1s	O1s	C/S	O/S
	Atomic percent								
A0	3.82	2.07	5.20	36.29	6.81	7.26	38.52	0.36	0.50
A20	5.43	3.44	7.01	26.59	4.02	12.58	40.90	0.74	0.76
A40	5.12	3.05	6.34	21.46	10.28	11.37	42.35	0.65	0.76
A60	5.58	4.12	7.37	22.45	6.38	12.91	28.84	1.04	1.23
A80	4.84	1.76	5.29	26.15	6.93	15.64	39.36	0.51	0.67
A100	4.71	1.97	7.96	34.64	5.10	10.25	35.64	0.52	0.51

5.4 CONCLUSIONS

Fig. 5.37 presents the micro/nano structural and chemical indices for concrete series A. The nomenclature followed in indices are such that values higher than 1 indicate better performance for respective FBA concrete. The indices covered in Fig. 5.37 are roughness determined from LFM measurements, degree of hydration and CSH chain length determined from NMR measurements and C/S ratio determined form XPS measurements. For A100 sample degree of hydration and CSH chain length was not available due to instrumentation issue and are shown at the centre of indices plot.

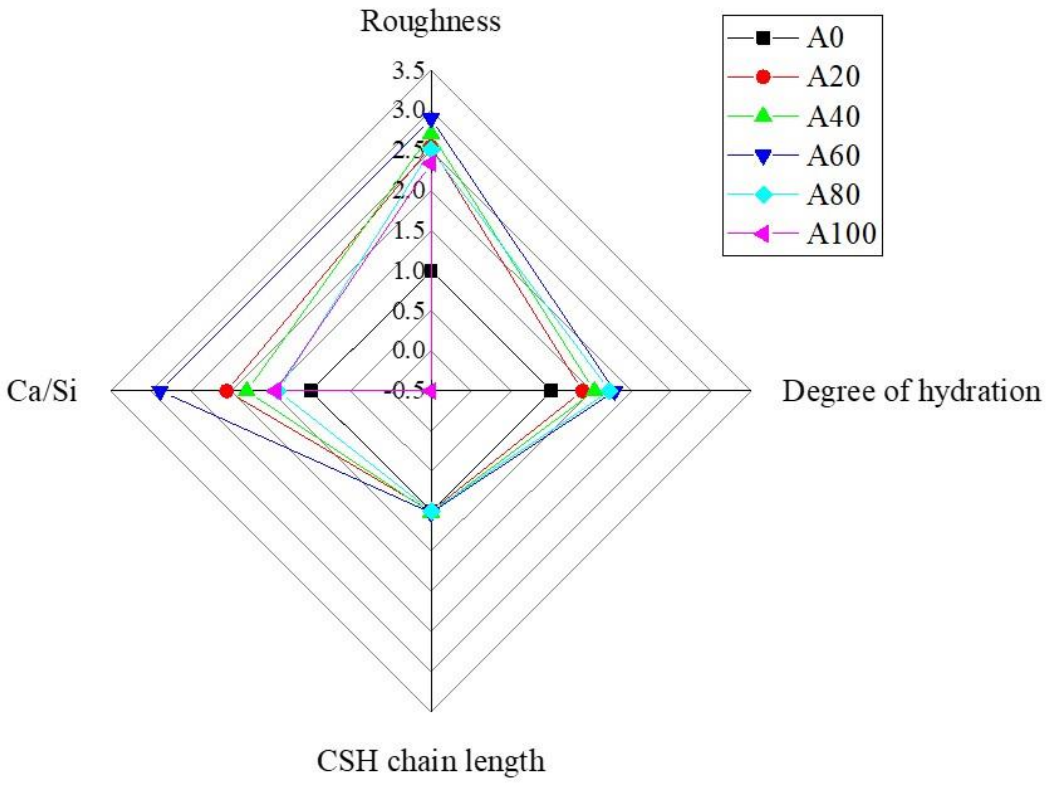

Fig. 5.37 Micro/nano structural properties indices of FBA concrete for series A (0.35)

Influence of FBA on selected micro/nano structural and chemical properties of concrete were observed. Following conclusions are drawn:

1. Concrete samples with FBA have lower pores and unhydrated cement particles than control concrete.
2. The incorporation of FBA results in dense formation of CSH gel with enhanced ITZ layer.
3. Incorporation of 80% and 100% FBA causes slight increase in roughness of the ITZ layer.
4. XRD analysis revelaed that increase of FBA content in concrete cuases decrease in free silica content. The higher count of CSH observed from XRD confirms slight pozzolanic properties of FBA aggregate. The deleterious compounds were present in insignificant amount and have no harmful effects on the properties of concrete.
5. FT-IR analysis showed a second peak of CSH bond band at higher wave number. The presence of second peak provides support for the higher compressive strength observed in FBA concrete mixes.
6. Quantitative analysis of ^{29}Si NMR spectra shows higher degree of hydration in concrete samples containing FBA. The higher chain length observed in sample containing 40% and 60% FBA results in superior compressive strength characteristics.
7. The XPS analysis show slight pozzolanic behaviour of FBA leading to stable and higher phases of CSH gel.

As observed from the micro/nano structural and chemical properties, concrete containing FBA have superior ITZ characteristics with denser, stronger and stable amount of CSH gel. The amount of gel pores gradually decrease with increase in FBA content in concrete. The internal curing effect of FBA creates favourable hydration conditions in concrete mixes causing higher degree of hydration.

CHAPTER 6

DURABILITY PROPERTIES: WATER RESISTANCE

6.1 INTRODUCTION

The ability of concrete to resist the actions generated by its surrounding provide valuable information to predict its service life. The water resistance parameter of concrete helps in determining the life span of structure, and also the repair and maintenance required.

The durability properties of concrete have close relation with mortar paste of concrete, so for investigating the alternative for fine aggregate having high water absorption analysing the water resistance properties of concrete is of utmost importance.

6.1.1 Objectives

The general objectives of this chapter are to observe and analyse the water based durability properties of concrete mixes comprising of partial or full replacement of NFA by FBA.

The specific objectives being covered from previously defined are:

7. To lay out the experimental programme for determining some water resistance based durability properties of concrete mixes.
8. To observe and analyse the obtained values for each concrete mix and provide a comparative understanding of different concrete mixes.
9. To provide specific discussions regarding the observed phenomenon in different concrete mixes.

6.1.2 Program of the study

The above mentioned objectives will be addressed by outlining the proposed experimental programme and its results.

In first step the methodology adopted for the investigation will be presented, highlighting the codal provisions followed. Afterwards, each result of the experimental programme will be presented by specific property. In the end the conclusions arising from the chapter will be drawn.

6.2 EXPERIMENTAL PROGRAMME

6.2.1 Total porosity, apparent density and water absorption

The total porosity, apparent density and water absorption was carried out as per ASTM C642 (2013). Three 100 mm cubic specimens having no visible cracks and broken edges were selected. The following equations were used to evaluate the total porosity, apparent density and water absorption:

Total porosity (%) = $\frac{(C-A)}{(C-D)} \times 100$

Apparent density = $[\frac{A}{(A-D)}]\rho$

Absorption after immersion (%) =$\frac{(B-A)}{A} \times 100$

Where ρ is density of water; A is oven dry mass of specimen; B is saturated surface dry mass of specimen; C is saturated surface dry mass after boiling of specimen; D is suspended mass of specimen.

6.2.2 Sorptivity

The sorptivity test was carried out as per the specifiations of ASTM C1585 (2013). Three 100 mm cubic specimens having all four sides coated with water proof material were placed such that only 3-5 mm height of their bottom surface was in contact with water.

6.2.3 Resistance to water penetration

The resistance to water penetration was carried out as per DIN 1048 (1991). Three 150 mm cubic specimens were oven dried at 60°C for 5 days. The specimens were exposed to water pressure of 0.5 N/mm^2 for 72 hours. The depth of water penetration was recorded by splitting the specimens into two halves and measuring the value to the nearest 0.1 mm.

6.2.4 Chloride ion diffusion

Resistance to chloride ion diffusion was obtained by steady state chloride diffusion test. 50 mm thick cylindrical samples having a diameter of 65 mm were used. The cylindrical samples were obtained by core cutting a 150 mm cube, the procedure was followed to get samples with no visible thick deposition of cement paste on the surface. The upstream (anode) and downstream cell of the cell were filled with 3% NaCl solution and distilled water respectively. A constant potential of 30 V DC was maintained throughout the 72 hours of test duration.

The initial chloride concentration of upstream cell was measured by titrating a 10 mL sample and adding 4-5 drops of KCr as indicator. The amount of AgNO3 required to change the colour of sample to reddish brown was recorded.

The chloride diffusion coefficient (D_{sm}) in m^2/s was evaluated by using the Nernest-Planck's equation (Andrade 1993):

$$D_{sm} = \frac{RTL}{zF\Delta Ec}J \tag{5.1}$$

Where, R = gas constant (R=8.314 J/K mol^{-1}), T = average value of initial and final temperature (K), L = thickness of the specimen (mm), z = absolute value of ion valence (for chloride, z=1), F= faraday constant (F= 9.648×10^4 J/(V mol), ΔE = absolute value of the potential difference between the upstream solution and the downstream solution, c = activity of chloride ions, J = unidirectional flux of species j (mol/cm^{2}s) which depends upon the monitored chloride ions.

6.2.5 Drying Shrinkage

To measure drying shrinkage, three prisms of size 75 mm×75 mm×300 mm were cast and were tested following the guidelines of ASTM C157 (2008). After 28 days of curing the specimens were dried for few hours and brass studs were attached at a distance of 212±1 mm on the top of the specimens. Initial reading after 24 hours of drying period of adhesive used for mounting the studs. A mechanical strain gauge with least count of 0.002 mm was utilised to observe the variations in reading at 7, 15, 30, 45, 60, 90, 180 and 270 days of initial reading.

6.3 RESULTS AND DISCUSSION

6.3.1 Total voids, apparent density and water absorption

The total voids, apparent density and water absorption of concrete mixes is shown in Figs. 6.1-6.4. The total voids of the concrete mixes was found to change with the increase in the content of FBA. The highest value for total voids of concrete was observed at 100% FBA content as 11.03%, 12.4% and 13.25% for series A, B and C respectively. The value of total voids gradually increased on increasing the FBA and water content.

The apparent density (Fig. 6.2) observed for concrete mixes shows an increase in its value as content of FBA is increased. As discussed earlier that to compensate for higher water absorption of FBA extra water was added into the mix. The presence of extra water in the concrete mix creates a favourable hydration mechanism leading to enhanced pozzolanicc activity that creates a denser, better and higher polymerised CSH gel. The powers law (1955) by TC powers speculates that the amount of calcium hydroxide converted to CSH gel in a known volume space will result in increased apparent density. For series A, the highest increase of 2% was observed for A80 and A60 mixes, for series B, the highest increase of 8.2% was observed for B80 mix and for series C, the highest increase of 8.4% was observed for C40 mix.

Fig. 6.3 shows the values observed for water absorption of various concrete mixes. The increase in total porosity and apparent density results in higher water absorption characteristics of concrete mixes containing FBA. The highest value of water absorption was observed at 100% FBA content for Series A and B. For series C the highest value of water absorption was observed at 80% FBA content.

In the present study the increase in total voids, apparent density and water absorption of FBA concrete mixes may be due to (i) High angularity and roughness of raw aggregate leading to gaps in cement paste matrix (ii) the higher bleeding observed in fresh state causes development of capillaries which helps in internal curing effect and are partially filled by the outward growing nature of CSH gel (iii) The extra water in the concrete mixes to maintain the standard w/c leads to development of voids or pores which increases the total porosity and water absorption of FBA concrete mixes.

Various authors (Medina et al. 2014; Alves et al. 2012; Senthamarai et al. 2011) observed similar results for water absorption values of concrete mixes containing different types of ceramic waste aggregate.

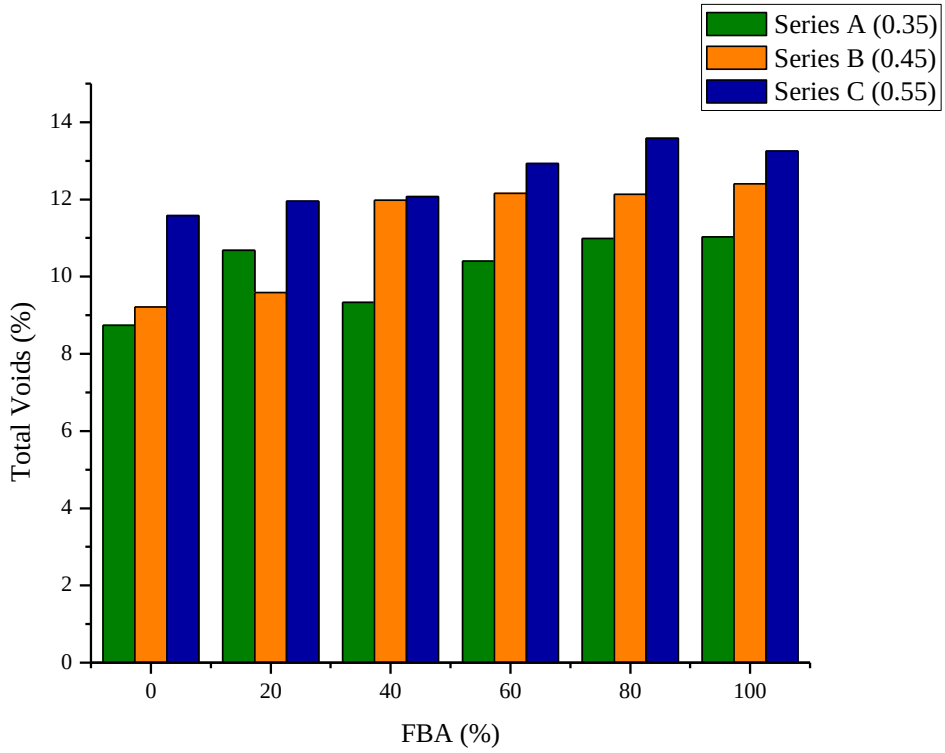

Fig. 6.1 Total voids of FBA concrete mixes

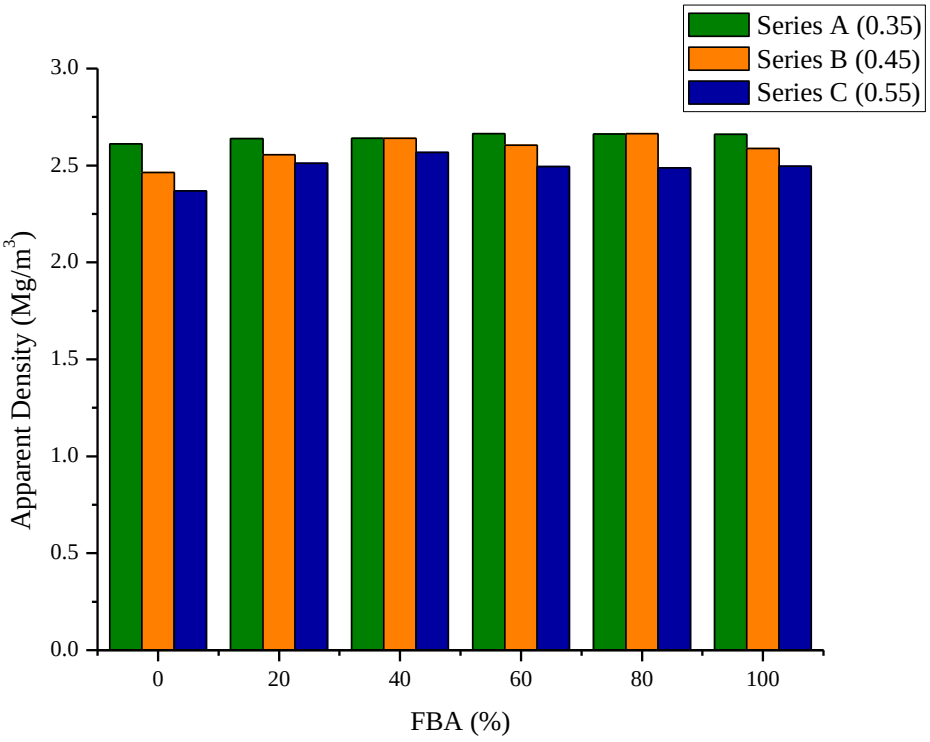

Fig. 6.2 Apparent density of FBA concrete mixes

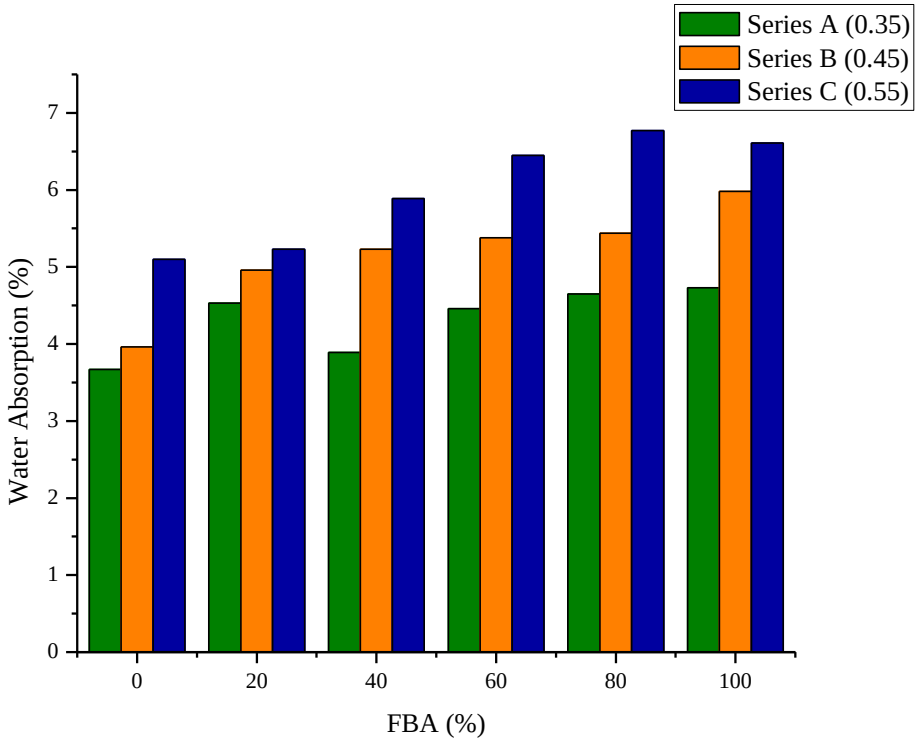

Fig. 6.3 Water absorption of FBA concrete mixes

6.3.2 Sorptivity

Figs. 6.4-6.6 shows the capillary rise values observed for concrete mix series A, B and C respectively. The initial and secondary absorption values are presented in Table 6.1. On close observation, there seems to be an important influence by the amount of FBA in the concrete mix and the w/c.

The sorptivity values for concrete mixes containing FBA in series A remains lower than control concrete throughout the testing duration. For concrete mix series A, the minimum values for sorptivity was for A60 mix. The reduction observed was 35.3%, 57.6%, 69.2%, 68.4%, and 63% for A20, A40, A60, A80 and A100 concrete mixes respectively. For concrete mix series B, the values observed were in slight disagreement with that of series A. The sorptivity values of concrete mix B40 and B60 were higher than control concrete for 24 hours observation. The final increase observed for mixes B40 and B60 was 11.2% and 2.1% than control concrete. For

concrete mix series C, the values were in agreement to that of series A. The values of sorptivity for FBA concrete mixes were lower than that of control concrete.

The slower rate of water absorption or sorptivity of FBA concrete mixes observed in the present study may be due to (i) The growth of CSH gel in the capillaries creates a filler effect restricting the capillary rise of water (ii) The roughness of raw FBA creates an interconnected network of capillaries that behaves like maze to restrict the upward rise of water (iii) the angularity of raw FBA creates a porous structure which results in slightly increased values at 80% and 100% FBA content.

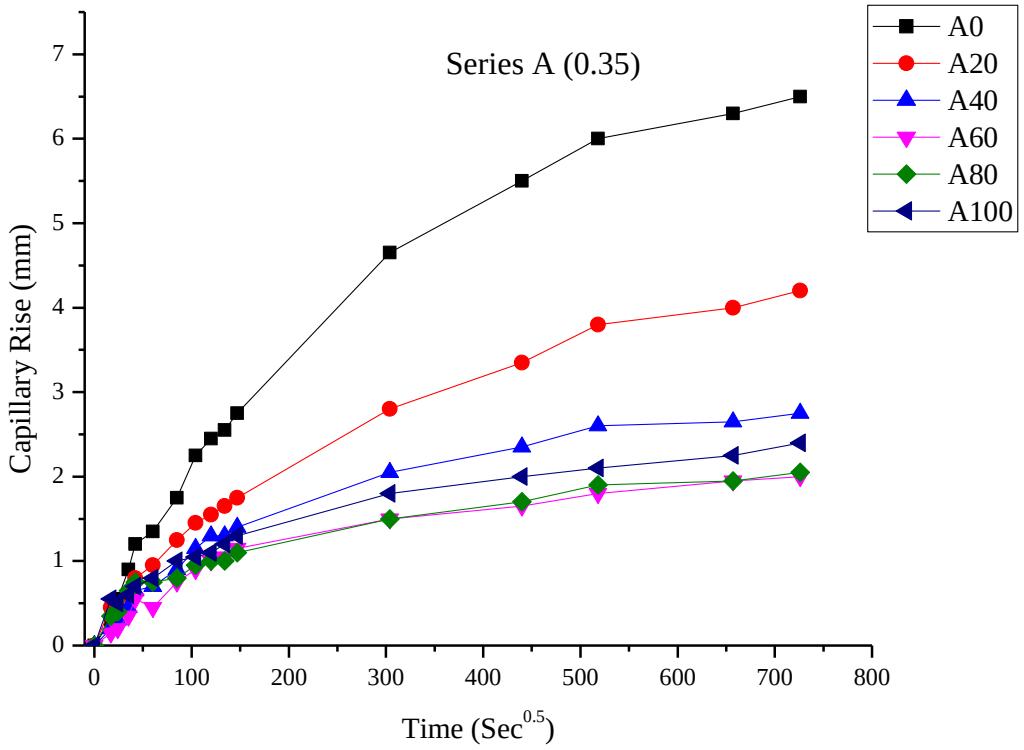

Fig. 6.4 Capillary rise of FBA concrete mixes (Series A)

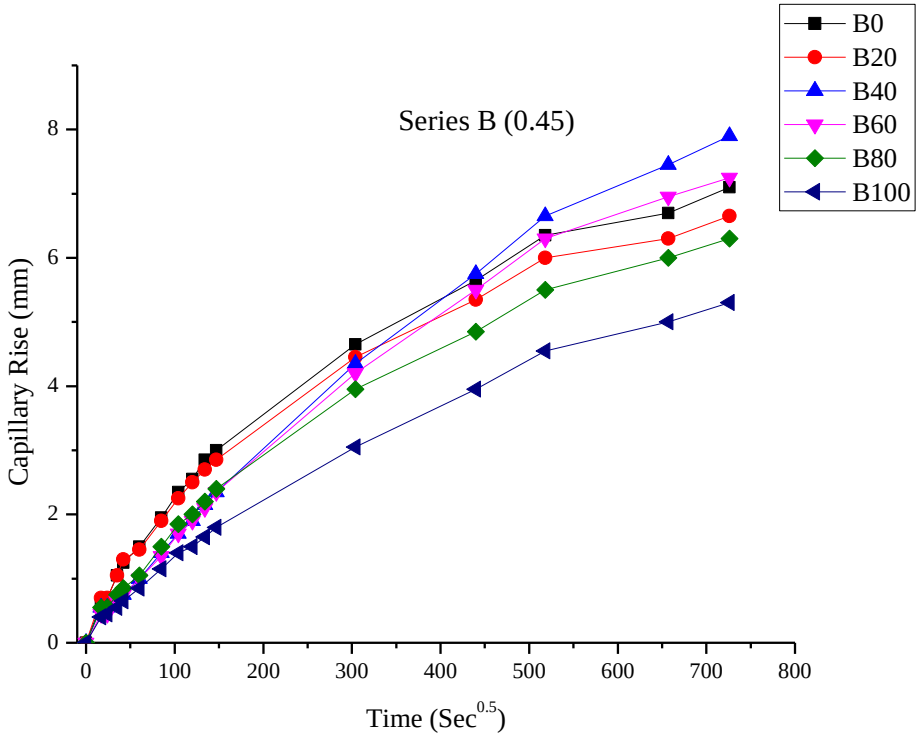

Fig. 6.5 Capillary rise of FBA concrete mixes (Series B)

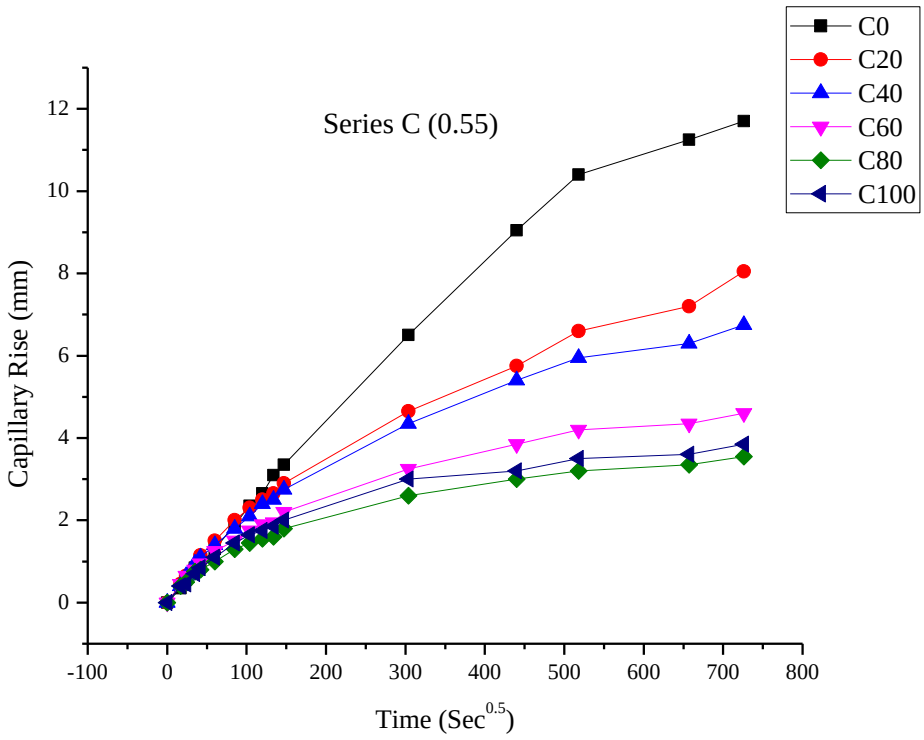

Fig. 6.6 Capillary rise of FBA concrete mixes (Series C)

Table 6.1 Initial and secondary rate of absorption of FBA concrete mixes

Mix	Initial rate of absorption ($mm/s^{0.5}$)	Secondary rate of absorption ($mm/s^{0.5}$)
A0	0.016305	0.004083
A20	0.009895	0.003149
A40	0.008179	0.001536
A60	0.006759	0.001195
A80	0.004881	0.001237
A100	0.006093	0.001389
B0	0.018637	0.00547
B20	0.017238	0.004907
B40	0.015051	0.008094
B60	0.015345	0.006876
B80	0.015179	0.00537
B100	0.011293	0.005097
C0	0.022852	0.011364
C20	0.018408	0.007815
C40	0.017309	0.005302
C60	0.017468	0.002952
C80	0.009983	0.002107
C100	0.011776	0.001992

6.3.3 Resistance to water penetration

The resistance to water penetration measured as depth of water penetration of FBA concrete mixes of different series is shown in Fig. 6.7. It can be observed that the depth of water penetration increased with the increase in FBA content for all concrete mixes.

The depth of water penetration in concrete increased by 23.3%, 32.17% and 8.71% for concrete mix series A, B and C respectively on 100% replacement of NFA by FBA. Ganjan et al. (2009) categorised depth of water penetration into three classes, (I) low permeability (<30 mm), (II) medium permeability (30-60 mm) and (III) high permeability (> 60 mm). The highest depth of water penetration observed was for C100 mix (53.6 mm). For series A the FBA concrete mixes A20 and A40 lied in class I low permeability bracket. Overall no FBA concrete mixes crossed over to class III permeability. Similar observations were made by Senthamarai et al. (2011) and Medina et al. (2013) on utilising electrical insulator and sanitary ware aggregate in concrete mixes.

The increase in depth of water penetration observed in this study may be due to (i) roughness and angularity of raw FBA can lead to development of voids (ii) the capillary network created due to bleeding of concrete leads to rise in depth of water penetration under pressure (iii) The higher amount of CSH gel generated in FBA concrete mixes also contain gel pores of different size (2.5-10 nm) (Thomas et al. 1999); the application of pressure on the concrete specimens creates an effect of moisture filled pores which can cause the discolouration effect observed after splitting of the specimens.

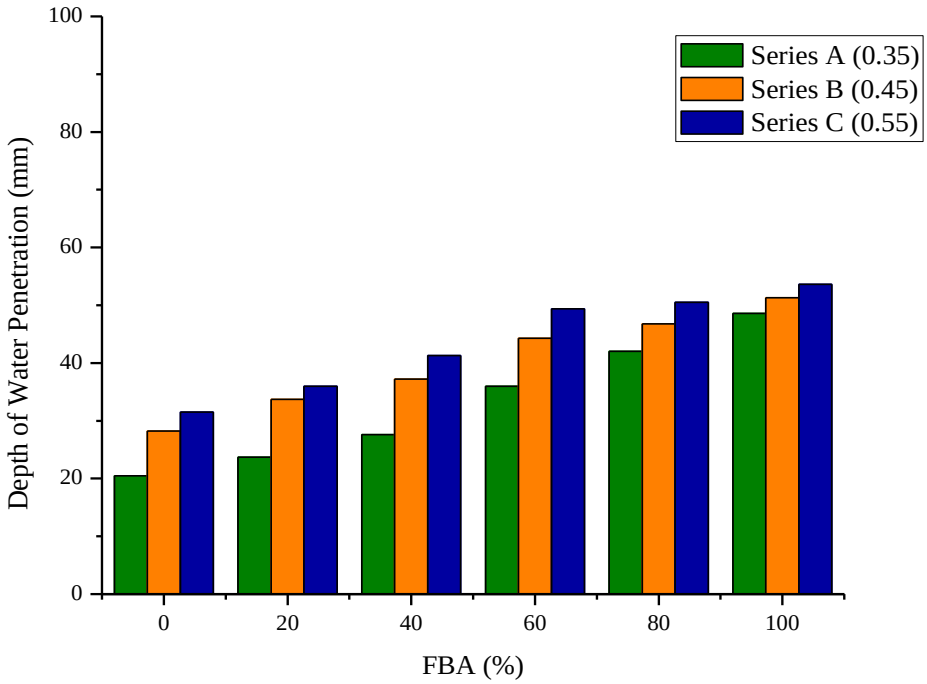

Fig. 6.7 Depth of water penetration of FBA concrete mixes

6.3.4 Chloride ion diffusion

The influence of FBA on the chloride ion diffusion of concrete is shown in Fig. 6.8. The concrete mixes containing FBA resulted in lower values of chloride ion diffusion. The chloride diffusion coefficient of concrete mix decreased by 27.54%, 9.22% and 10.31% for series A, B and C on 100% replacement of NFA by FBA.

It is also observed that the introduction of FBA higher than 20% in concrete mixes leads the chain of reduction in the chloride ion diffusion coefficients. The results obtained for chloride ion diffusion does not the follow the pattern observed in resistance to water penetration results. The pressure applied on the specimens neutralises the physical characteristics of FBA concrete and its contents.

The decrease in chloride ion diffusion coefficient observed in this study may be due to (i) The addition of FBA in concrete leads to reduction in amount of OH^- ions. The reduction of OH^- ions increases the chloride binding capacity of concrete causing decrease in chloride ion diffusion (ii) increase in amount of CSH gel restricts the transfer of chloride ions in FBA concrete mixes (iii) The dense and chemically stable and resilient structure of FBA provides a filter mechanism for blocking the ingress of chloride ions (iv) addition of tortuosity due to FBA also creates hindrance in the movement of chloride ions.

Various other authors (Binci et al. 2007; Higashiyama et al. 2012; Corominas and Etxeberria 2014) have observed lower values of chloride diffusion on utilisation of different types of ceramic waste aggregates at varying percentages in concrete and mortar mixes.

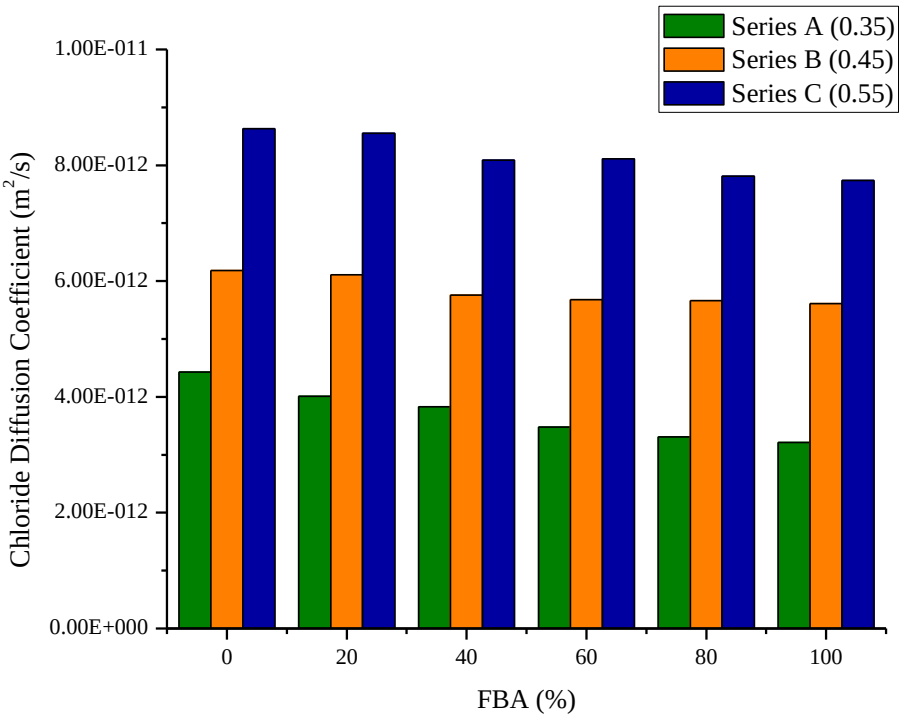

Fig. 6.8 Chloride diffusion coefficient of FBA concrete mixes

6.3.5 Drying Shrinkage

The movement of water in unsaturated air causes expansion or shrinkage of concrete. Figs. 6.9-6.11 shows the drying shrinkage behaviour of FBA concrete. It can be observed from Fig. 6.9 that shrinkage strain of A20 and A40 was higher than A0 till 60 and 45 days respectively. The entire drying period shrinkage strain values of A60, A80 and A100 were lower than that of A0 control concrete. For series B and series C the shrinkage strain of FBA concrete is lower to than that of equivalent control concrete. The reduced shrinkage strain exhibited by FBA concrete may be due to higher porosity of FBA. The water trapped by the raw FBA gets gradually released back in the concrete matrix to compensate for the drying of concrete specimens. During the process of internal curing, the pores release water back into the concrete mix thereby reducing the capillary stress.

Another possible reason might be the texture and shape of the aggregates. Since the only difference in the concrete mixes were the presence of FBA. The rough texture and angularity of FBA restricted the drying loss of water than the slightly smoother particles of NFA.

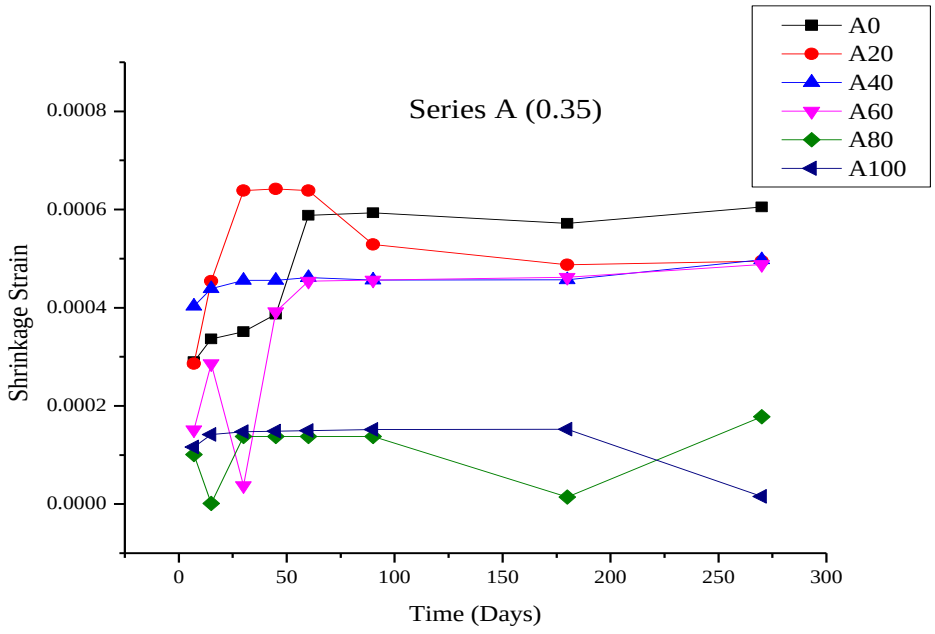

Fig. 6.9 Drying shrinkage of FBA concrete mixes (Series A)

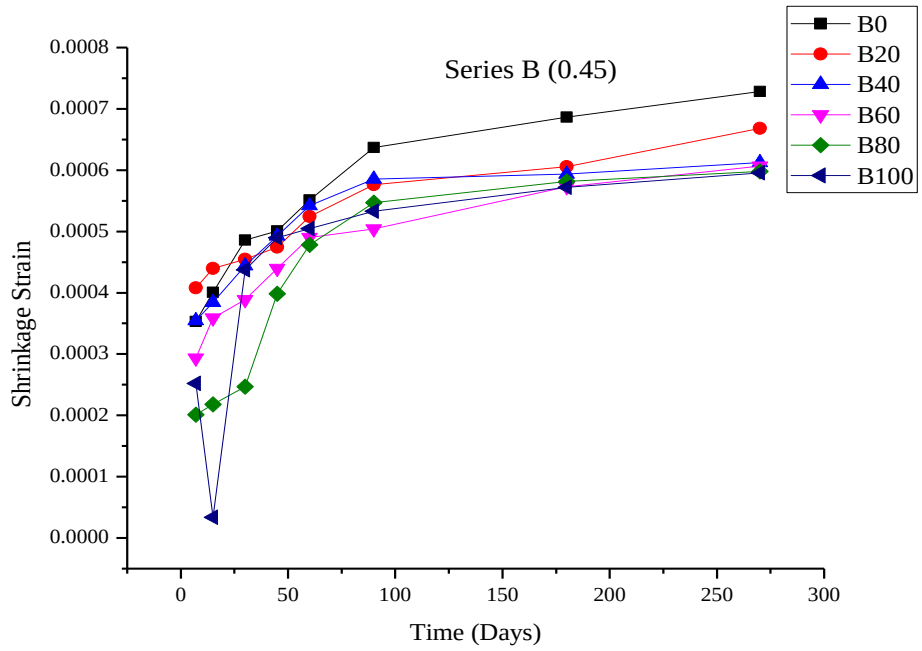

Fig. 6.10 Drying shrinkage of FBA concrete mixes (Series B)

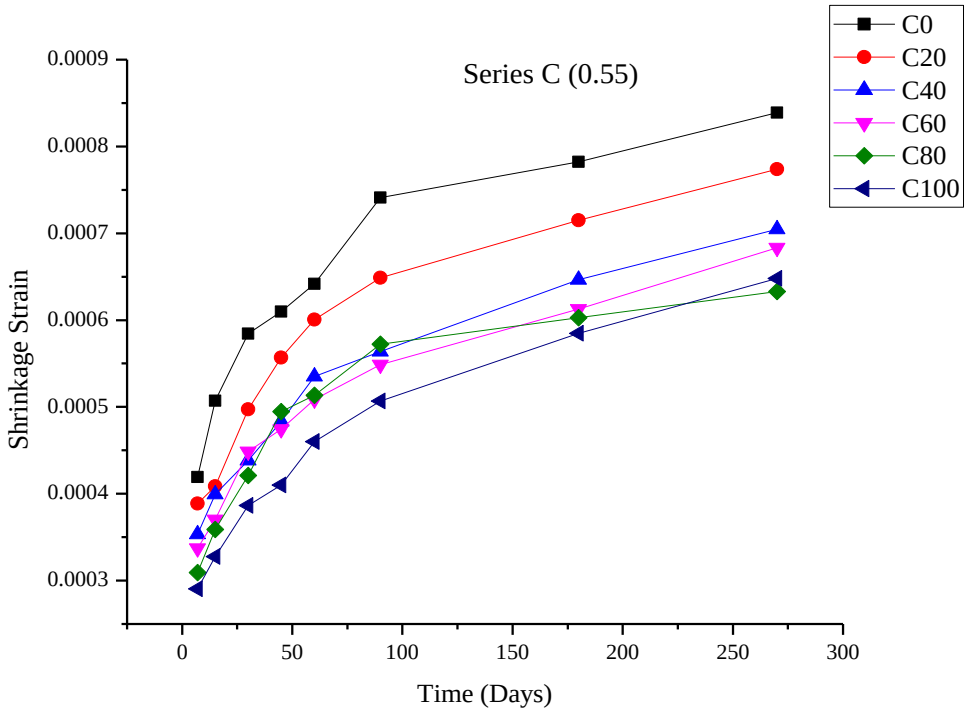

Fig. 6.11 Drying shrinkage of FBA concrete mixes (Series C)

6.4 CONCLUSIONS

Figs. 6.12-6.14 presents the water resistance durability indices for concrete series A, B and C respectively. The nomenclature followed in indices are such that values higher than 1 indicate better performance for respective FBA concrete. The indices for sorptivity and drying shrinkage are for final testing value observed, i.e. 5 days for sorptivity and 270 days for drying shrinkage.

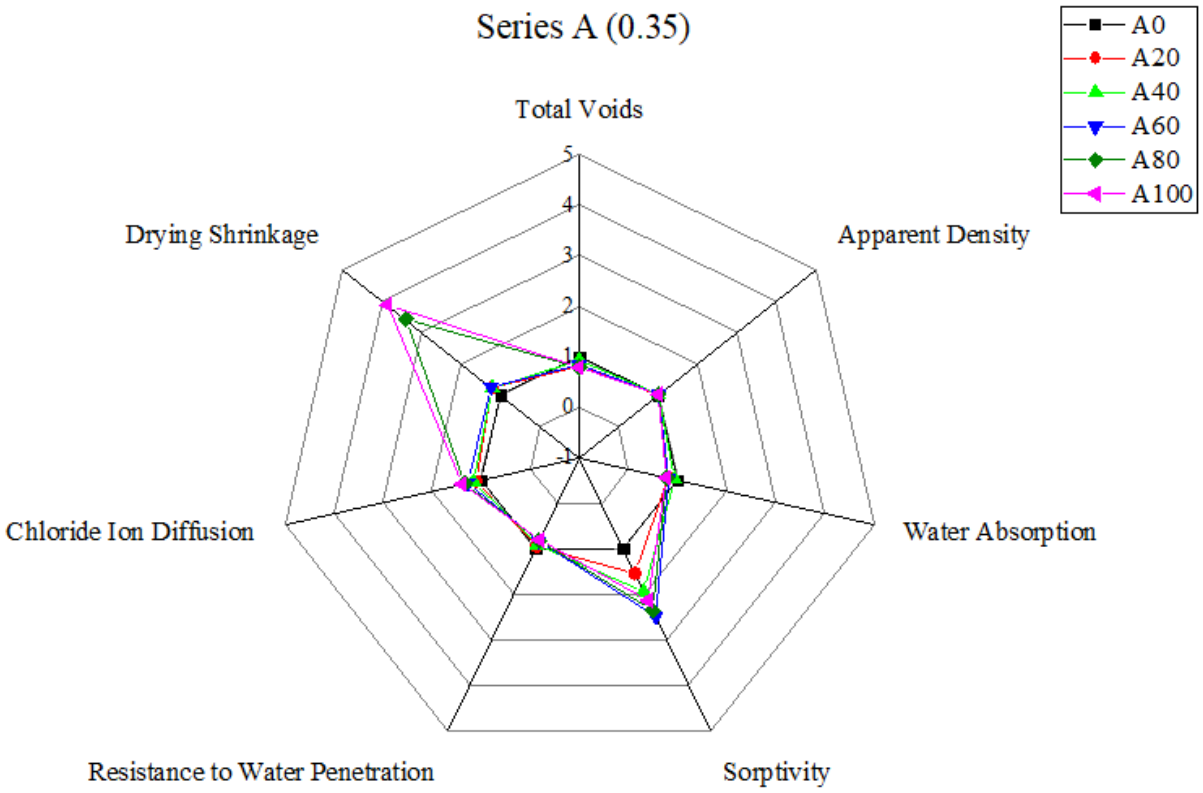

Fig. 6.12 Water resistance durability properties indices of FBA concrete for series A (0.35)

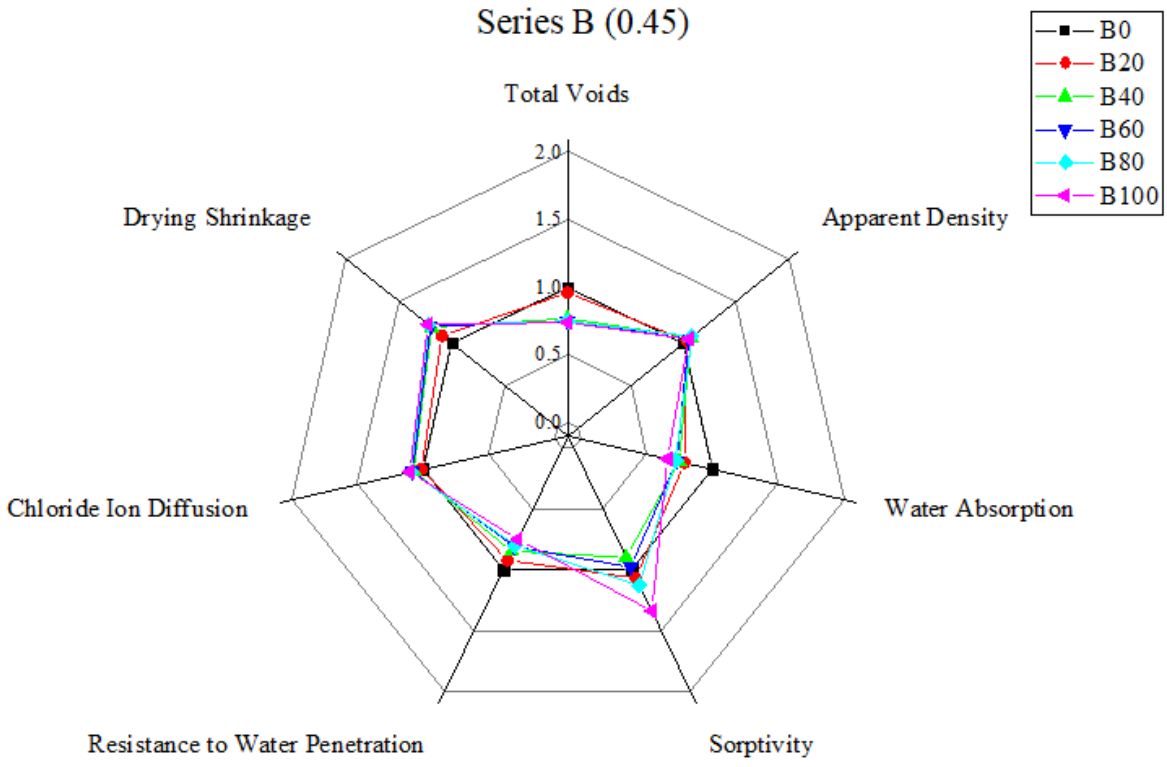

Fig. 6.13 Water resistance durability properties indices of FBA concrete for series B (0.45)

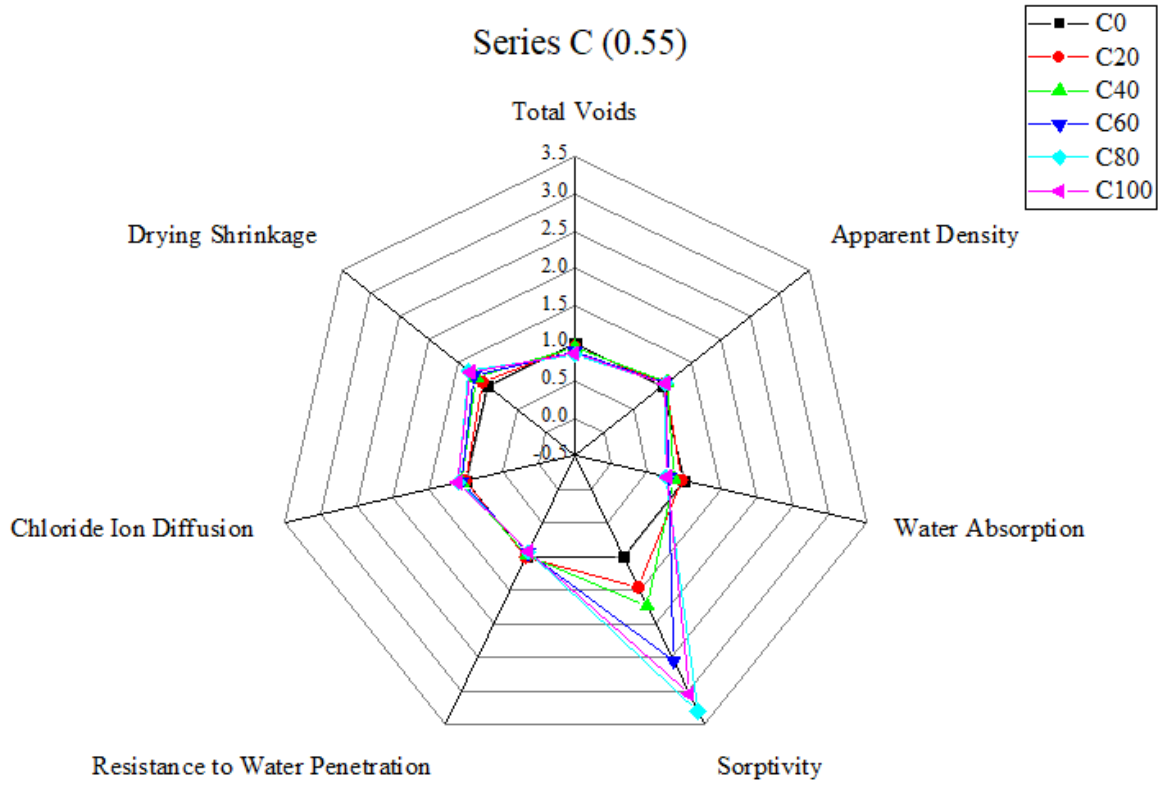

Fig. 6.14 Water resistance durability properties indices of FBA concrete for series C (0.55)

In general, it has been observed that, the replacement of NFA by FBA has slightly detrimental effect on total voids, water absorption and resistance to water penetration properties observed in this section. Following conclusions are drawn from the study:

1. The internal curing by mixing water results in voids and capillaries. The introduction of FBA in concrete mix demands increased mixing water leading to higher values of total voids.
2. The water absorption values of FBA concrete mixes are higher due to the increase in capillaries and total voids.
3. The capillary network and denser CSH gel of FBA concrete mixes limits the sorptivity values of specimens.
4. Higher values for depth of water penetration was observed for FBA concrete mixes. The roughness and angularity of raw FBA along with water filled CSH gel pores can lead to such aspect of water penetration.
5. The resistance to chloride ion penetration for concrete increased on introduction of FBA. The tortuosity and the denser CSH gel provided by the FBA are quite effective in confining the ingress of chloride ion in concrete matrix.
6. The dimensional stability exhibited by FBA concrete was better than control concrete. The porous nature of FBA significantly reduced the long term drying shrinkage of concrete.

The observations and conclusions drawn from the experimental programme of water resistance durability properties indicate that utilisation of FBA provides slightly high ingress of water into concrete than NFA concrete. To maintain serviceability life span of concrete structure FBA can be used upto 40% as fine aggregate.

CHAPTER 7

DURABILITY PROPERTIES: RESISTANCE TO ADVERSE CONDITIONS

7.1 INTRODUCTION

As discussed in the previous chapter the various aspects of durability of any unconventional concrete are always a subject of utmost importance and scrutiny. Concrete made with alternative materials can be regarded as durable if it retains its shape, quality and texture during adverse conditions such as freeze and thaw cycle, drying and wetting cycle, chloride penetration and corrosion.

The resistance of concrete against adverse conditions provide valuable insights regarding the repair and rehabilitation frequency of structure as well as identifying the particular type of concrete which can be recommended for hotspots having probability of single or multiple adverse conditions in local environment.

7.1.1 Objectives

The general objectives of this chapter are to observe and analyse the resistance of FBA concrete mixes against adverse conditions.

The specific objectives being covered from previously defined are:

1. To adopt suitable experimental programme to evaluate some adverse conditions durability properties of the concrete mixes.
2. To observe and analyse the obtained data for each concrete mix and provide suitable comparisons within and among different concrete mixes.

3. To provide specific discussions regarding the observed findings for different concrete mixes.

7.1.2 Program of the study

The aforementioned objectives will be addressed by describing the experimental protocol and its results. In first step the methodology adopted for the investigation will be presented, highlighting the provisions followed. Afterwards, each result of the experimental programme will be presented by specific property. In the end the conclusions arising from the chapter will be drawn.

7.2 EXPERIMENTAL PROGRAMME

7.2.1 Resistance to freeze and thaw

Resistance to freeze and thaw was measured by freezing and then thawing samples (100 mm cubes as per ASTM C666:2015) for 50 cycles. In a single cycle, the specimens were frozen at -20°C for 18 hours and were then thawed at 4°C for 6 hours. Weight loss and compressive strength of samples were determined after 50 cycles.

7.2.2 Resistance to drying and wetting

For drying and wetting test, 100 mm cube samples were kept under water at 20°C for 6 hours and then dried at 40°C. Final change in mass and compressive strength of samples was measured at the end of 25 cycles.

7.2.3 Resistance to chloride penetration

Resistance to chloride penetration was evaluated on 100 mm cubic samples. The cubes were submerged in 3% Sodium Chloride solution for 7, 28, 90 and 180 days. For measuring the depth of chloride penetration in concrete, the samples were split into two halves and were

sprayed with 0.1N silver nitrate. The presence of white precipitate due to formation of silver chloride was measured and reported as depth of chloride penetration.

7.2.4 Resistance to corrosion

Resistance to corrosion was evaluated upto 270 days of exposure. Samples of size 250 mm × 200 mm × 120 mm with pounding well on top were cast. After 28 days of curing, the samples were coated with epoxy paint on the vertical faces. The anode and cathode end of the specimen were connected by 100 Ω resistance. A pounding (3% sodium chloride solution) period of 14 days was followed as per the specifications of ASTM G109 (2013). At the end of each pounding period, the potential difference between the electrodes was measured. Macro cell current was evaluated as per ASTM G109 (2013). The half cell potential observations were made immediately after the macro cell readings as per the specifications of ASTM C876 (2015). The electrochemical potential of anode was measured relative to copper-copper (II) sulphate electrode.

7.3 RESULTS AND DISCUSSION

7.3.1 Resistance to freeze and thaw

The deterioration of concrete in cold climate is often attributed to the freeze and thaw cycles to which the samples are exposed during their lifetime. The damage caused by such phenomenon creates micro cracks which makes the concrete vulnerable to aggressive external agent attack. Internal stress generation has been found to be the main cause of frost damage. The findings reported briefly state that pressure and expansion due to ice formation and the pressure created by the growth of crystals in pores are the major sources for internal stress (Medina et al. 2013).

The mass variation of samples exposed to cycles of freeze thaw is presented in Fig. 7.1. For concrete mix series A the loss in mass reduced from 5.37% to 1.78% for A0 and A100 samples

respectively. For concrete mix series B the loss in mass reduced from 3.06% to 2.23% for B0 and B100 samples respectively. For concrete mix series C the loss in mass reduced from 1.86% to 0.52% for C0 and C100 samples respectively.

As discussed in chapter 6, the percent voids in concrete increases as concentration of FBA is increased. On freezing, the chemically bound water and moisture present in concrete matrix expands nearly by 9%. The constant expansion and contraction of water creates the scaling effect on the surface of concrete. The mortar adhered on the surface of concrete gets chipped of due to the stress. The rugged surface of concrete is a major cause of mass loss in concrete. For concrete samples containing FBA the higher percent of voids create an ice lens formation during freezing which ease out the internal stress on the mortar. The introduction of FBA in concrete results in higher percentage of voids due to the angularity and roughness of the raw aggregate. Another factor that influences the resistance to freeze thaw is the water to cement ratio. Higher water to cement ratio results in higher percentage of voids. Since series C has the highest water to cement ratio (0.55), the resistance to mass loss for freeze thaw is highest for this series.

The loss in compressive strength is due to weakened bond between aggregate and mortar paste caused by constant changes in internal stresses. Change in compressive strength after exposure to 50 cycles of freeze and thaw is shown in Fig. 7.2. It can be observed from Fig. 7.2 that the FBA concrete samples provide better resistance to freeze thaw attack. For concrete mix series A, the loss in compressive strength reduced from 23.08% to 9.09% for A0 and A100 samples respectively. For concrete mix series B, the loss in compressive strength reduced from 19.57% to 4.59% for B0 and B100 samples respectively. For concrete mix series C, the loss in compressive strength reduced from 11.36% to 2.23% for C0 and C100 samples respectively.

The better bond structure of ITZ (as observed in LFM imaging) provide higher restraint against cracking. The FBA provides extra pozzolanic behaviour during the hydration that results in higher amount of CSH gel. The CSH gel formed creates a superior bond between the aggregate and mortar paste. During freeze thaw action the bond between aggregate and mortar paste is able to resist the change in internal stress resulting in smaller loss in compressive strength of FBA concrete.

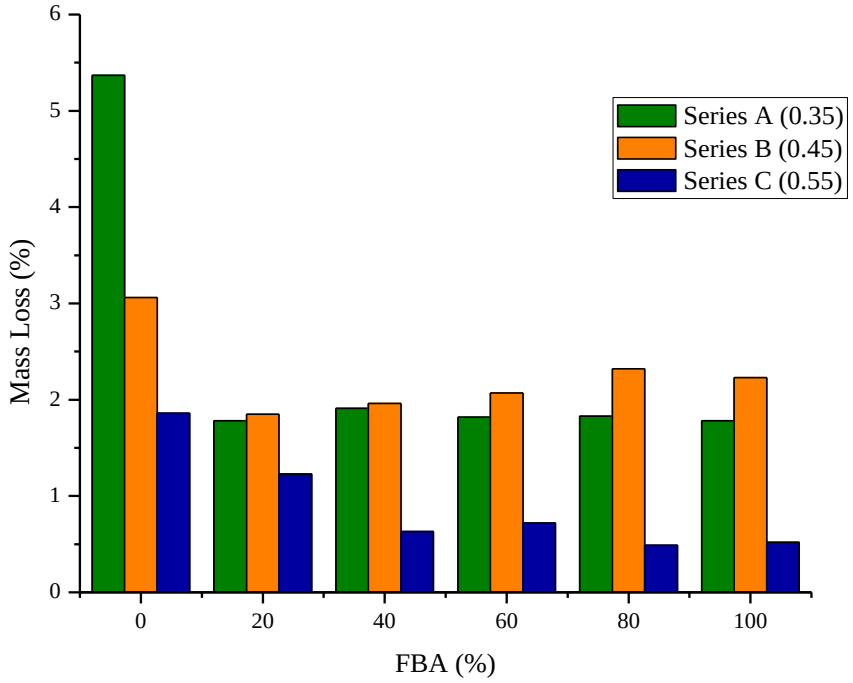

Fig. 7.1 Change in mass for FBA concrete exposed to freeze and thaw cycles

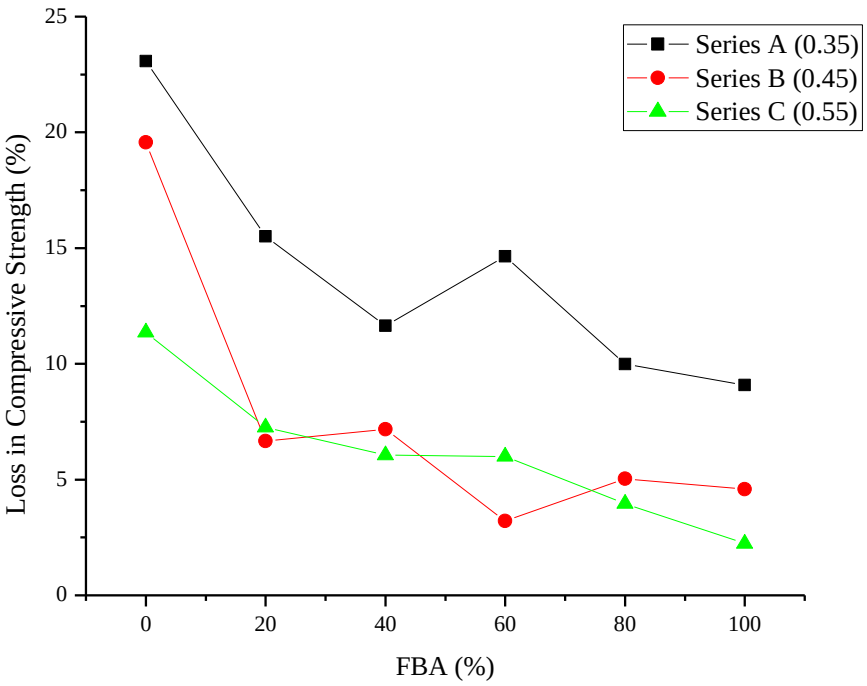

Fig. 7.2 Change in compressive strength for FBA concrete exposed to freeze and thaw cycles

7.3.2 Resistance to drying and wetting

The drying and wetting test provides suitable imitation of weather changes over different geographical areas. For a tropical country like India, the monsoon season provides daily rainfall with warm temperature durations. Exposure to drying and wetting makes concrete susceptible to external aggressive agents and may induce corrosion in reinforcement.

Loss in mass and compressive strength due to drying and wetting cycle is shown in Figs. 7.3-7.4. The mass loss observed remains more or less constant through the particular series mix. The increase in water to cement ratio increases the percent voids causing higher mass loss. The effect of FBA is slightly positive on resisting the action of drying and wetting cycles.

For loss in compressive strength the deterioration is severe in case of series C control concrete as water to cement ratio is increased. For series C, the loss observed is 32.5% as compared to

16% and 24.78% for series A and B. The lowest loss in compressive strength is observed for 100% FBA concrete.

The variations in temperature along with moisture content can be one of the probable causes for loss in strength. The ingress of cold water into the capillary pores of concrete matrix may cause slowing of the hydration process and may induce short term thermal shocks after exposure to higher temperature in the already hydrated concrete matrix. Another possible reason is the leaching out of $Ca(OH)_2$ in the form of lime. During the drying process the $Ca(OH)_2$ can decompose into CaO. This CaO reacts with water during wetting process to release heat and cause volume expansion. The volume expansion causes fissures at the ITZ of concrete and mortar paste. Furthermore the voids also create a zone of pressure difference due to entrapped air causing weakening of the hydration products.

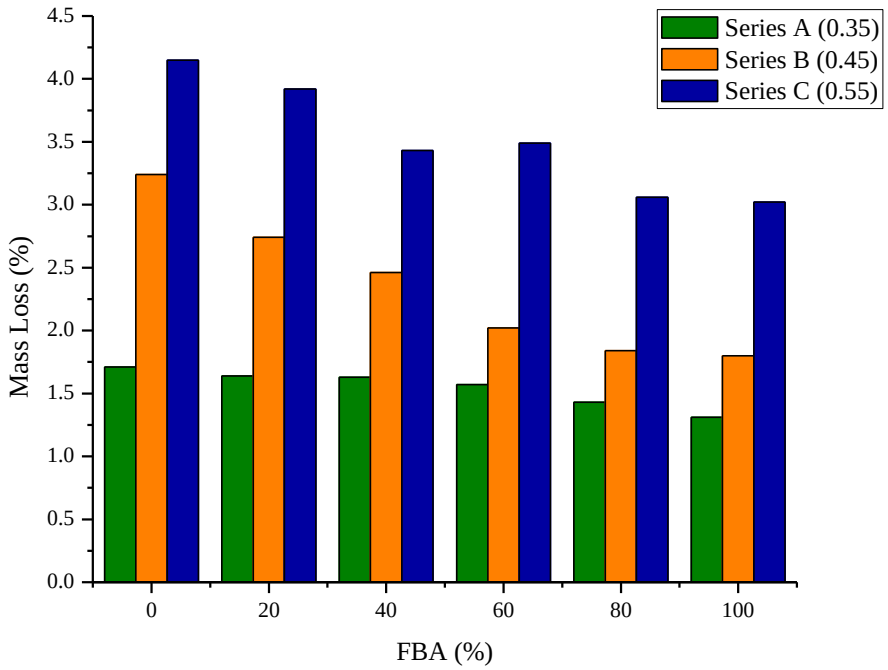

Fig. 7.3 Change in mass for FBA concrete exposed to drying and wetting cycles

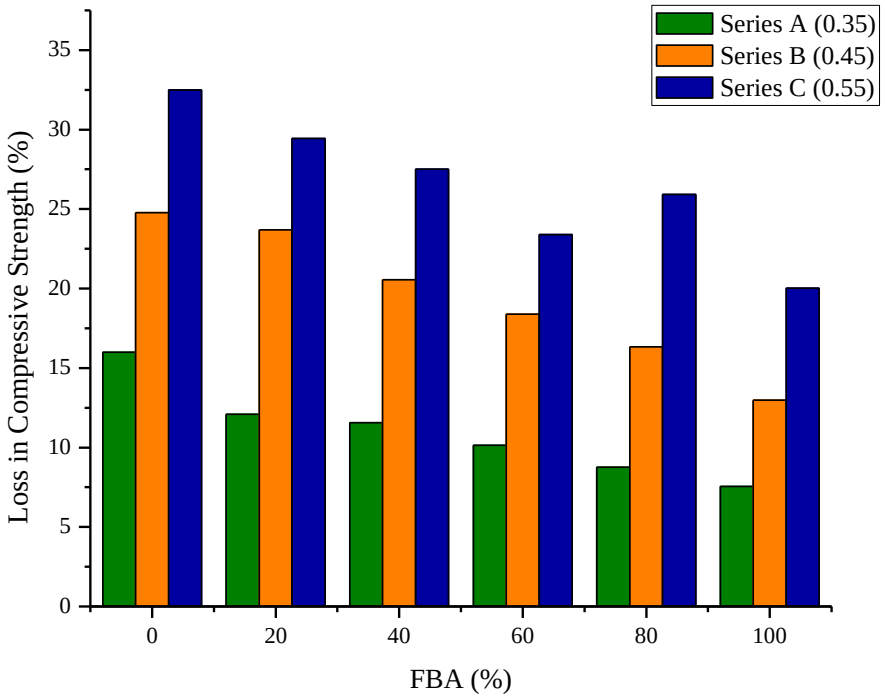

Fig. 7.4 Change in compressive strength for FBA concrete exposed to drying and wetting cycles

7.3.3 Resistance to chloride penetration

The observed chloride penetration depths for the concrete mixes are presented in Figs. 7.5-7.7. It was observed that increasing the FBA content, the depth of chloride penetration decreased. Considering the higher percentage of voids in FBA concrete, such behaviour can be attributed to the denser CSH gel in the microstructure. The pozzolanic activity of fine bone china aggregate also create a favourable reaction mechanism for Al_2O_3 and SiO_2 to form additional phases of AFm and AFt which provides resistance against chloride ions by ion exchange mechanism and forming Friedel's salt (Florea and Brouwers 2012; Suryavanshi et al. 1996).

The lowest chloride penetration depth was observed for concrete samples containing 100% FBA. For series A, B and C, the value observed for control concrete was 37 mm, 100 mm and 100 mm respectively at 180 days of chloride exposure. For 100% FBA concrete the depth of

chloride penetration recorded was 14 mm, 19 mm and 39 mm for series A, B and C respectively.

It can be stated that FBA provides higher resistance to concrete against chloride penetration. The use of other ceramic waste such as electrical insulator, sanitary ware or tile as aggregate exhibited both less and higher resistance to chloride penetration (Gomes and de Brito 2009; Higashiyama et al. 2012; Pacheco-Torgal and Jalali 2011). The advantage of chemically stable and resistant raw FBA is exhibited by its blocking of the chloride ions and adding a tortuosity in the microstructure of concrete.

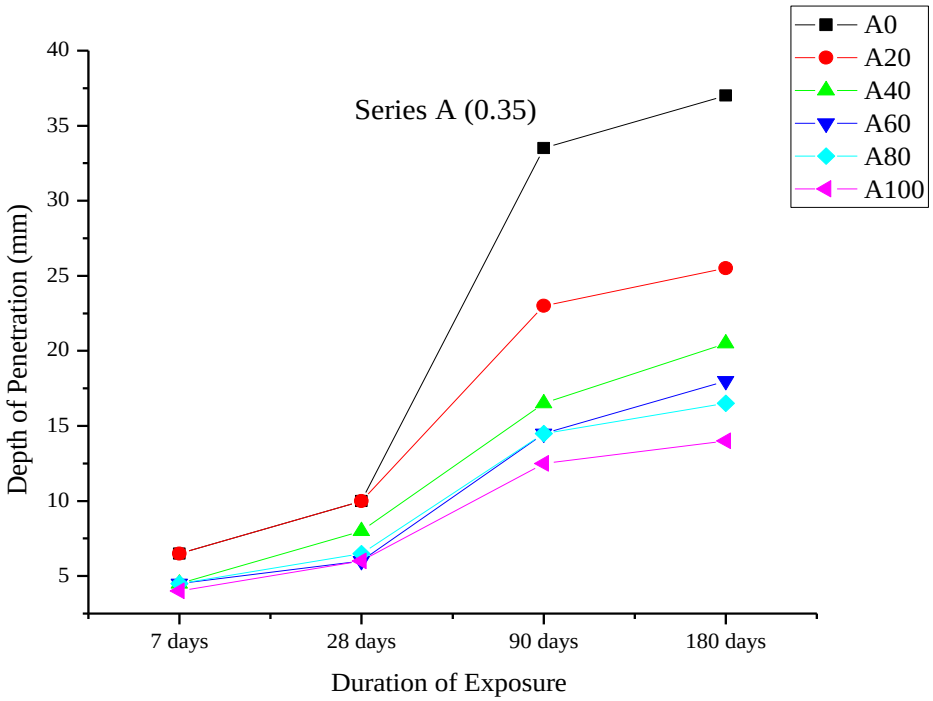

Fig. 7.5 Chloride penetration depths for FBA concrete mixes (Series A)

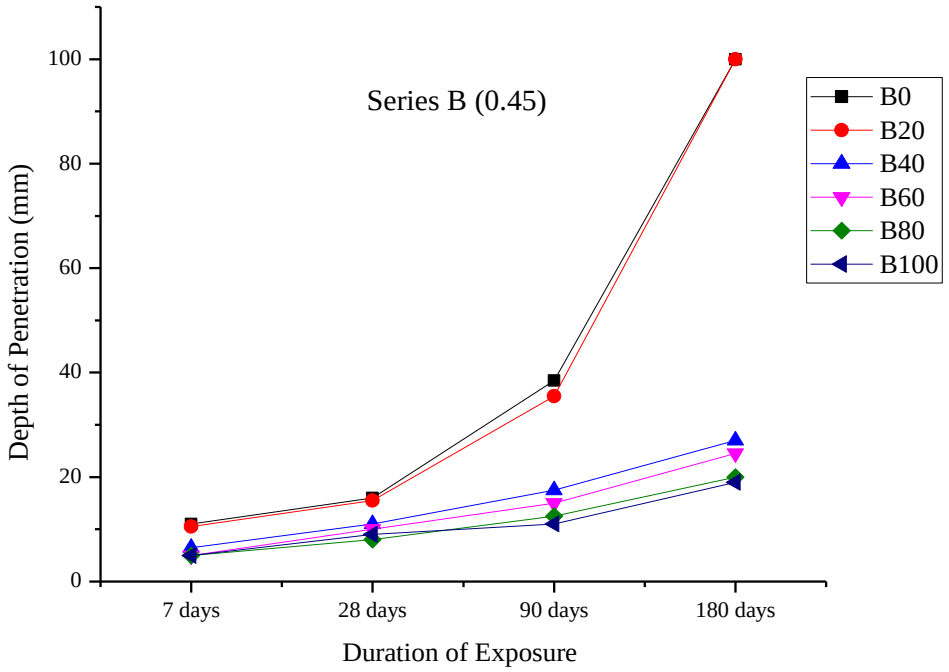

Fig. 7.6 Chloride penetration depths for FBA concrete mixes (Series B)

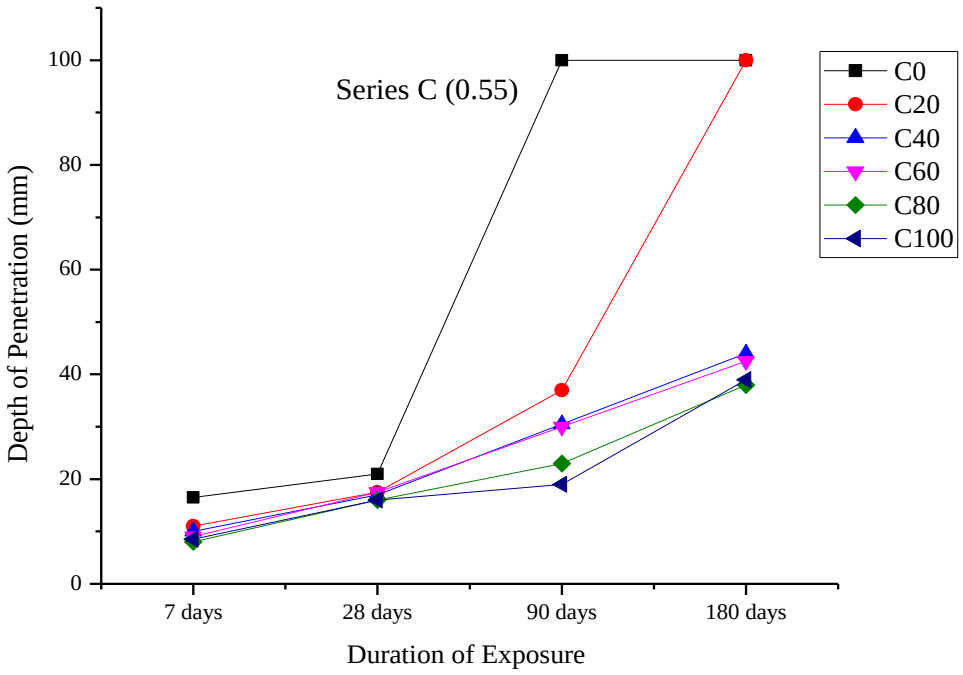

Fig. 7.7 Chloride penetration depths for FBA concrete mixes (Series C)

7.3.4 Resistance to corrosion

During chloride attack in concrete, the chloride ions are either absorbed by the CSH gel or they form Friedel's salt. The remaining free chloride ions initiate corrosion in reinforcement steel bars. The NaCl solution used for pounding provides the chloride ions that depassivate the rebar.

The results for macrocell current observed at different time periods for series A, B and C are shown in Figs. 7.8-7.10. Initiation of corrosion in rebar is indicated by macrocell current values higher than +10µA. Samples of series A and B showed values less than +10µA at the entire testing duration. Samples C0 and C20 recorded values of +11.15µA and +10.32µA respectively at 10 months of testing age. The values observed for fine bone china aggregate concrete show reduced corrosion activity. Higher amount of CSH gel in the microstructure provides suitable barrier for the ingress of chloride ions.

Figs. 7.11-7.13 present the half cell potential values observed for concrete series A, B and C. The values lower than -350 mV indicate 90% probability of corrosion. The results of half cell potential are in good agreement with that that of macrocell observations. The values of C0 and C20 specimen indicate initiation of corrosion at 9 months of exposure.

The highest probability of corrosion was observed in series C specimens. The weak microstructure along with higher void percent make the samples more susceptible to corrosion. FBA concrete having superior microstructure maintain higher resistance to corrosion despite having higher percentage of voids.

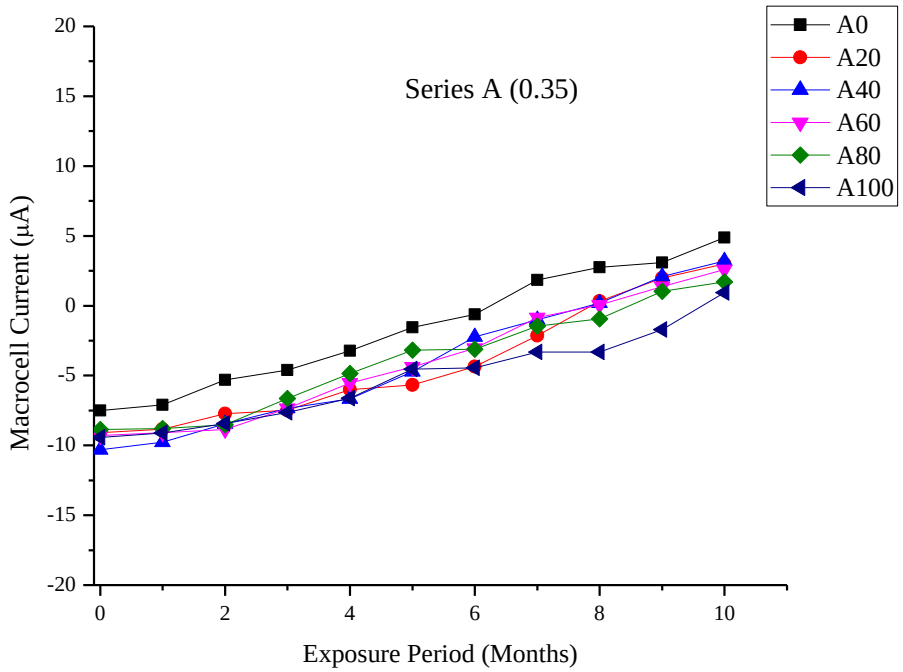

Fig. 7.8 Macrocell current of FBA concrete mixes (Series A)

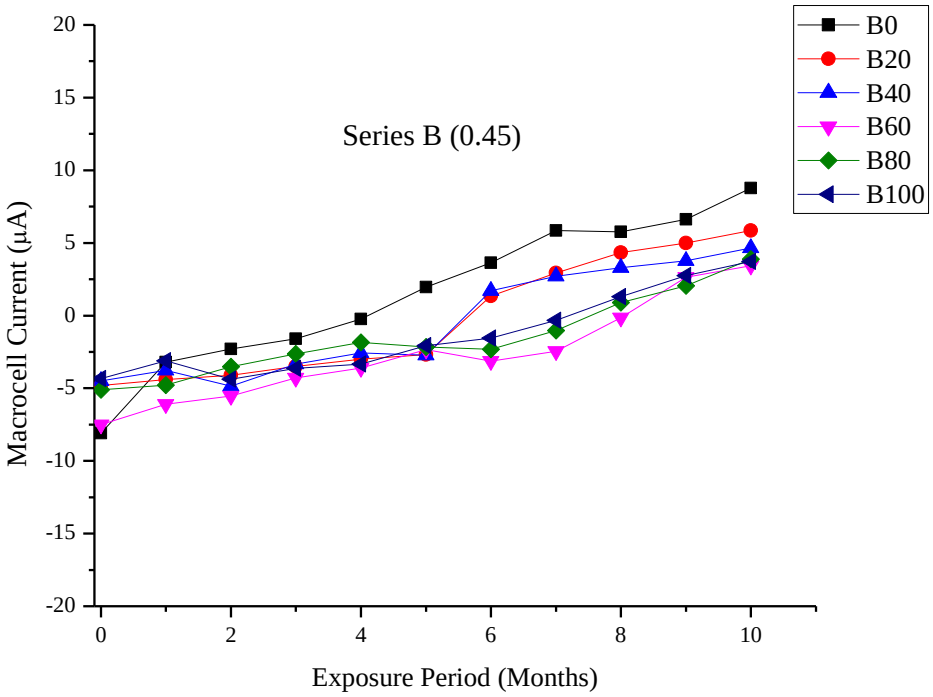

Fig. 7.9 Macrocell current of FBA concrete mixes (Series B)

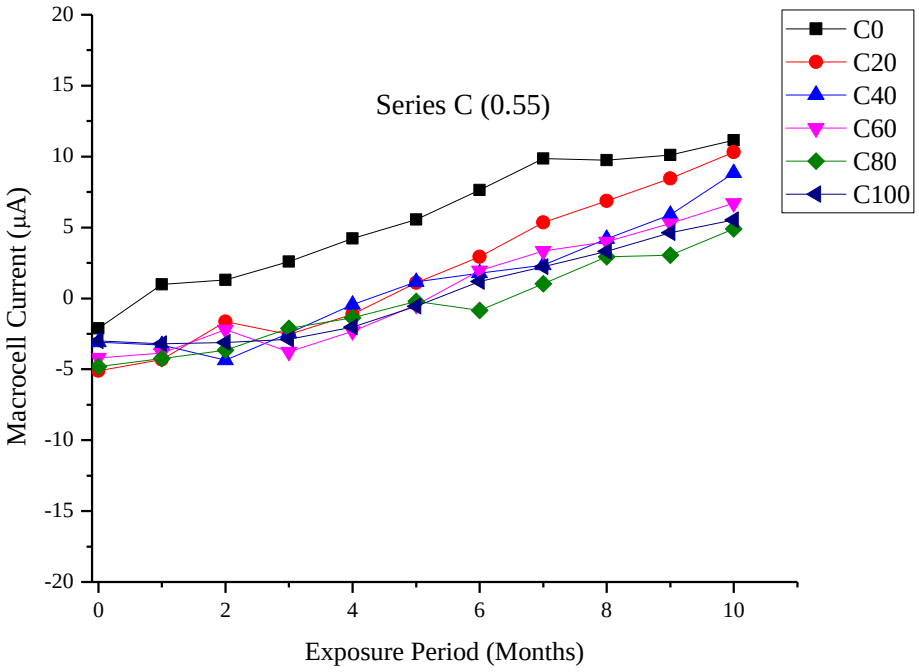

Fig. 7.10 Macrocell current of FBA concrete mixes (Series C)

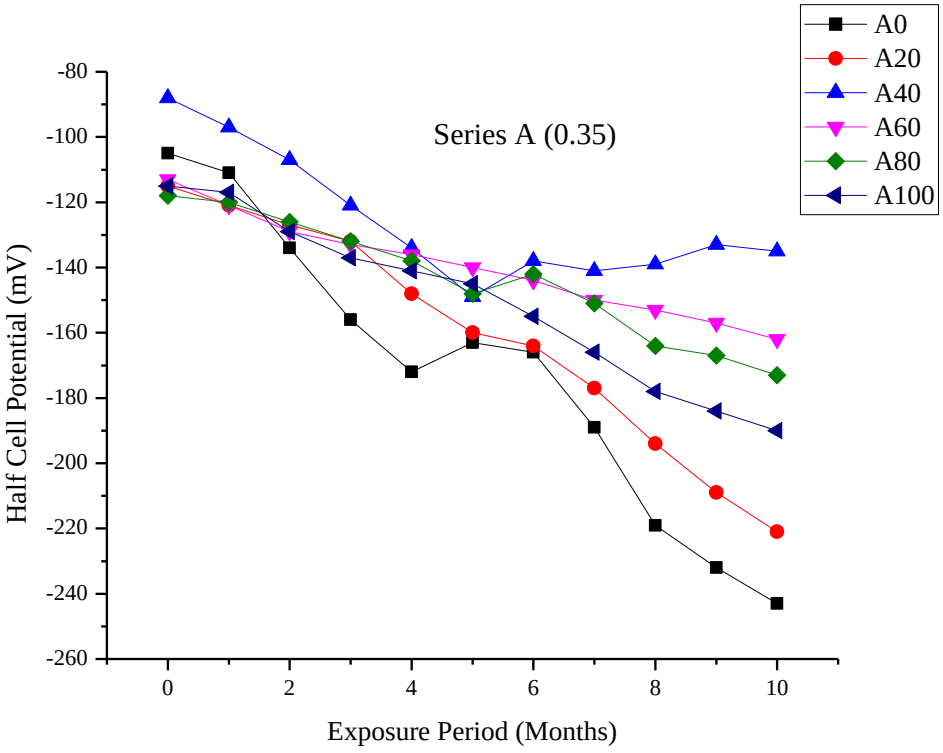

Fig. 7.11 Half cell potential of FBA concrete mixes (Series A)

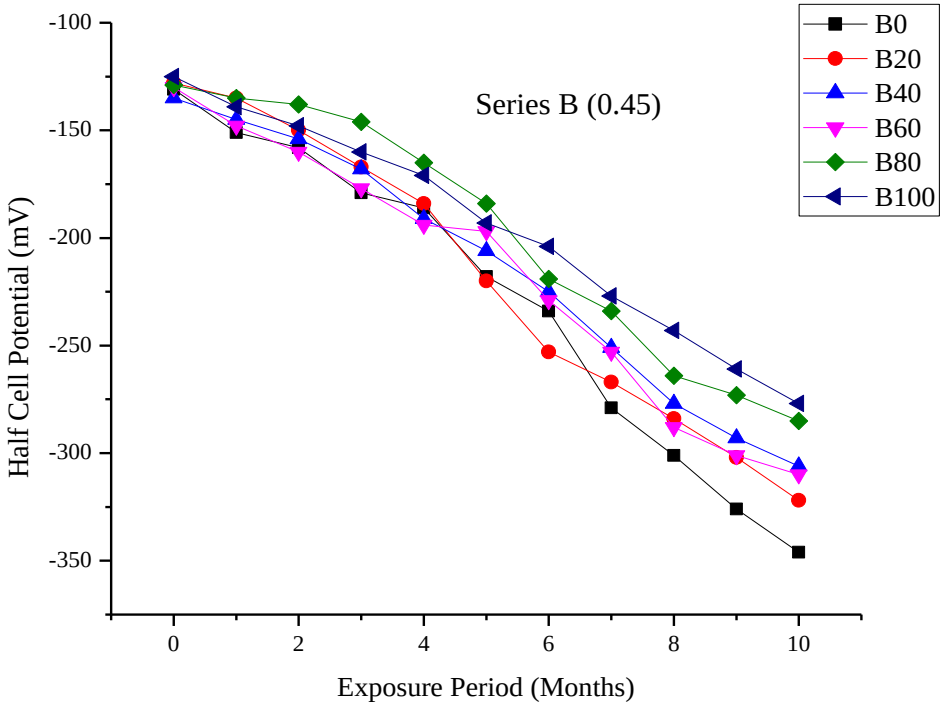

Fig. 7.12 Half cell potential of FBA concrete mixes (Series B)

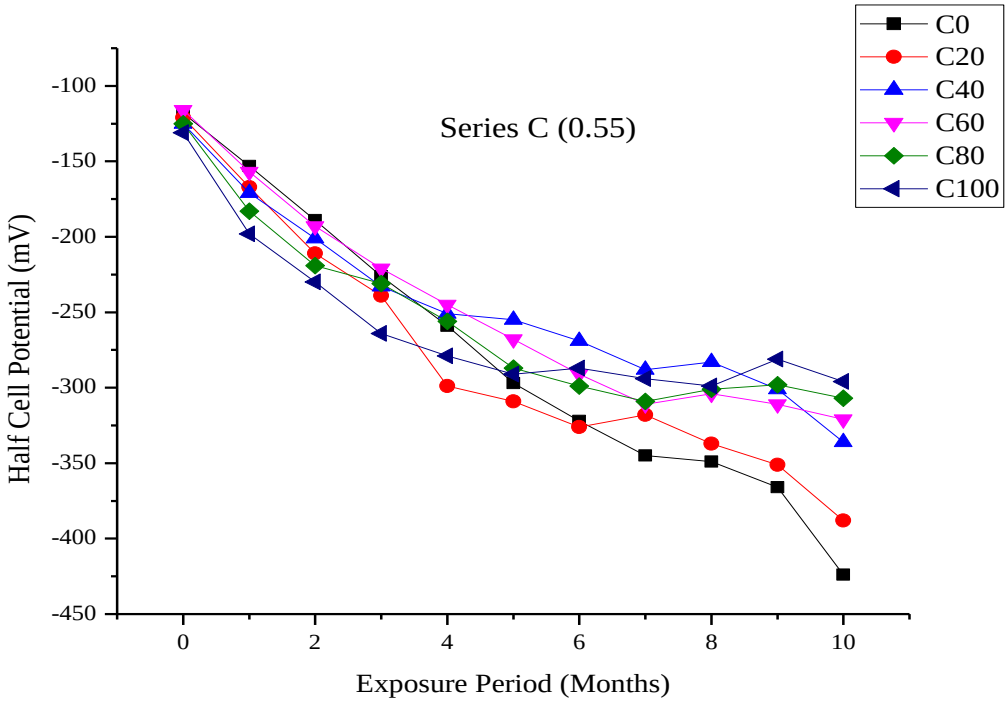

Fig. 7.13 Half cell potential of FBA concrete mixes (Series C)

7.4 CONCLUSIONS

Figs. 7.14-7.16 presents the resistance to adverse conditions durability indices for concrete series A, B and C respectively. The nomenclature followed in indices are such that values higher than 1 indicate better performance for respective FBA concrete. The indices for chloride penetration and corrosion are for final testing value observed, i.e. 180 days for chloride penetration and 10 months for corrosion.

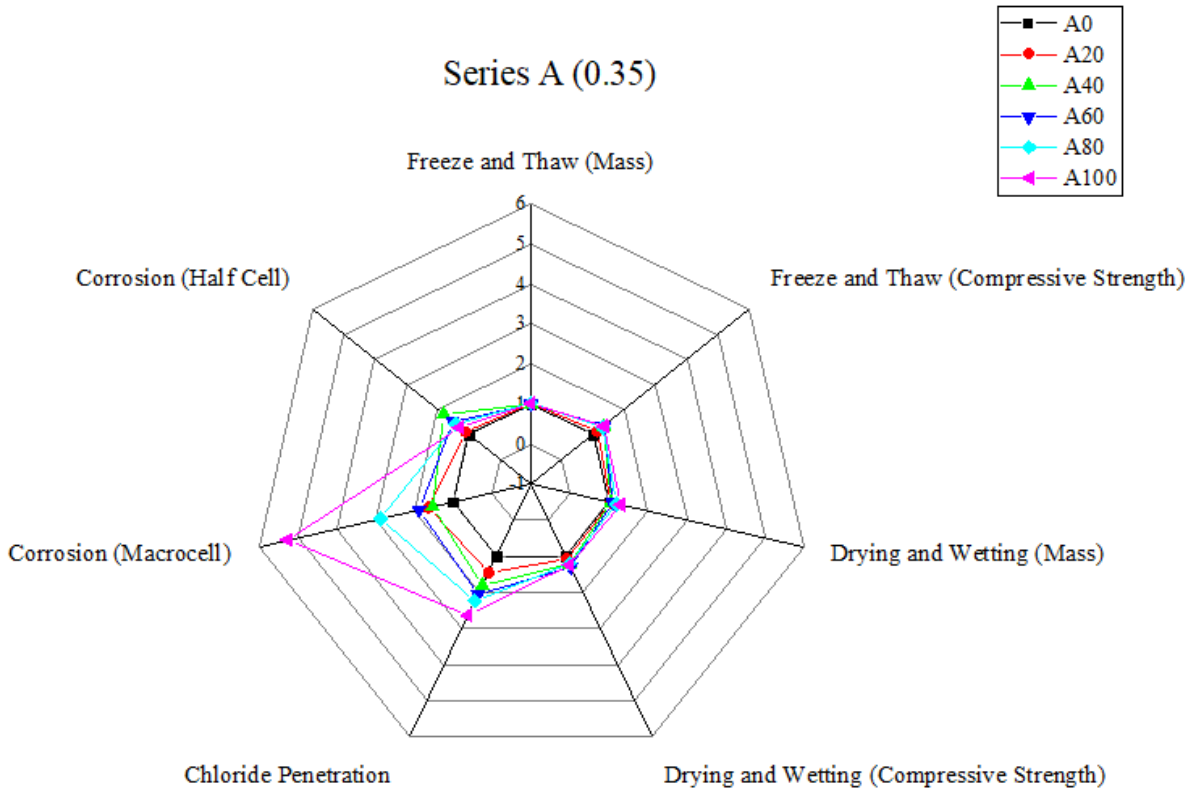

Fig. 7.14 Resistance to adverse conditions durability properties indices of FBA concrete (Series A)

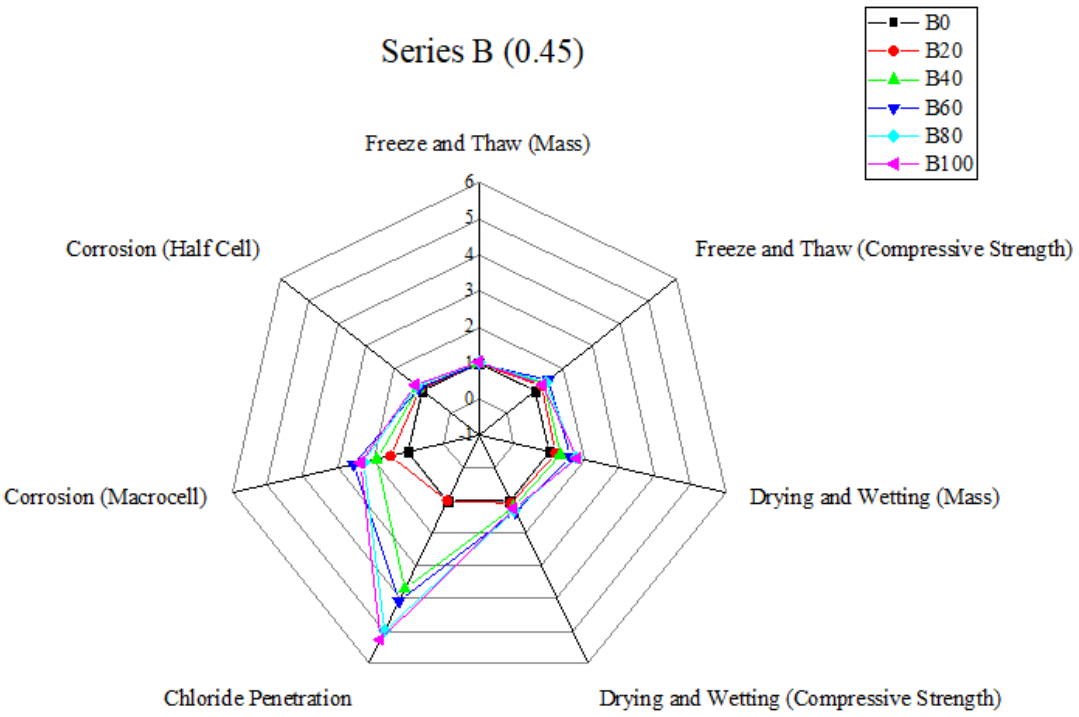

Fig. 7.15 Resistance to adverse conditions durability properties indices of FBA concrete (Series B)

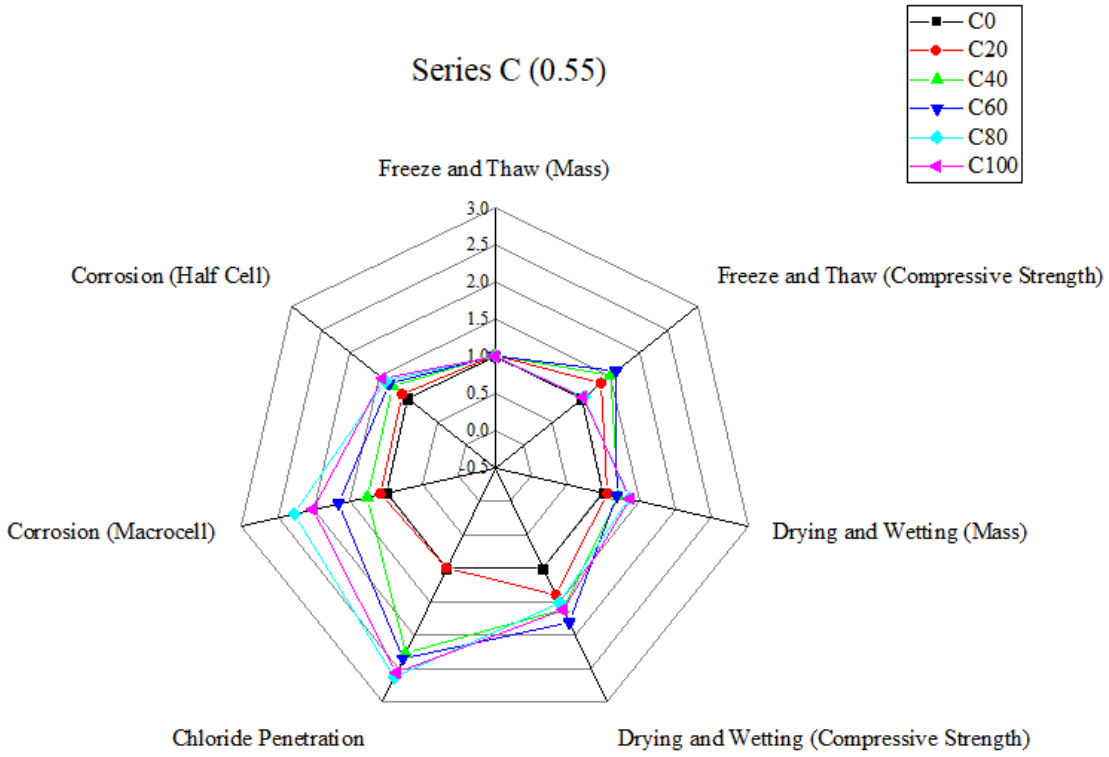

Fig. 7.16 Resistance to adverse conditions durability properties indices of FBA concrete (Series C)

As is seen from different experimental programme that FBA concrete exhibits superior durability characteristics than control concrete when exposed to adverse conditions. Following conclusions are drawn:

1. The higher percent voids in concrete due to FBA results in superior resistance to freeze and thaw action. The voids present act as an empty vessel that accommodates expansion of freezing water thus safeguarding the bond between aggregate and mortar paste from internal stress.
2. In drying and wetting test, the stable nature of FBA provided an important contribution by delaying the voluminous expansion of lime during wetting process.
3. The resistance to chloride penetration of FBA concrete was better than that of control concrete. The hydration products resisted the flow of chloride ions into concrete matrix by acting as a barrier.
4. Initiation of corrosion was not observed for any specimen series A (water to cement ratio 0.35) and B (water to cement ratio 0.45) samples for an exposure of 10 months. For series C (water to cement ratio 0.35), specimen C0 and C20 showed probability of corrosion for 9 months of exposure. Tortuosity in FBA concrete provided a resistant mechanism against corrosion initiation.

The observations and conclusions drawn from the experimental programme indicate that FBA as fine aggregate provides suitable resistance against extreme weather conditions and against chloride alkaline conditions. Replacement of NFA by FBA (40%-100%) can be recommended in climatic zones having adverse weather conditions.

CHAPTER 8

DURABILITY PROPERTIES: RESISTANCE AGAINST CHEMICAL ATTACK

8.1 INTRODUCTION

The range of properties exhibited by concrete makes it one of the most used man made material worldwide. However, on exposure to chemical attacks such as acid and sulphate the properties of concrete are severely compromised threatening the integrity and service life of structure. Non-conventional concrete mixes containing different types of waste material are always under scrutiny for their performance under chemical attack.

8.1.1 Objectives

The general objectives of this chapter are to observe and analyse the resistance of FBA concrete mixes against chemical attack (acid and sulphate).

The specific objectives being covered from previously defined are:

1. To adopt suitable experimental programme investigating acid and sulphate chemical attack durability properties of the concrete mixes.
2. To observe and analyse the obtained data for each concrete mix and provide suitable comparisons within and among different concrete mixes.
3. To provide specific discussions regarding the observed findings for different concrete mixes.
4. To investigate chemical changes by FT-IR and XPS measurements in concrete mixes exposed to chemical attack.

8.1.2 Program of the study

The aforementioned objectives will be addressed by describing the experimental protocol and its results. In first step the methodology adopted for the investigation will be presented, highlighting the provisions followed. Afterwards, each result of the experimental programme will be presented by specific property. In the end the conclusions arising from the chapter will be drawn.

8.2 EXPERIMENTAL PROGRAMME

8.2.1 Resistance to acid attack

Resistance to acid attack was carried out on 28 days cured 100 mm cubic samples (ASTM C267: 2012). After 28 days, the samples were marked and weighed for future reference. To simulate the acidic environmental conditions the samples were submerged in 3% sulphuric acid (H_2SO_4) solution upto 180 days. The sulphuric acid solution was regularly replenished to maintain homogeneity in the experiment. The deterioration of sample in mass and compressive strength was recorded at an interval of 7, 28, 90 and 180 days. At the 180 days exposure period the samples were visually assessed as per ASTM C672 (2012). A numerical scale was adopted for visual assessment from 0 (no scaling) to 5 (severe scaling).

8.2.2 Resistance to sulphate attack

Resistance to sulphate attack was carried out on 28 days cured 100 mm cubic samples. The resistance to sulphate attack was determined by immersing samples in 3% magnesium sulphate ($MgSO_4$) solution. The samples were properly marked and weighed for initial reference before allowing all the surfaces to be submerged in sulphate solution. The sulphate solution was replenished periodically to maintain the same concentration throughout the study. The exposure period to the sulphate solution was for 7, 28, 90 and 180 days. The compressive

strength after 7, 28, 90 and 180 days was carried out on three 100 mm cubic sample after recording their mass.

8.2.3 Chemical properties of concrete mixes

The concrete samples after 180 days of exposure to chemical attack were investigated for changes in the chemical structure. To maintain conciseness of the study, only selected samples (Series A) were investigated for changes in chemical structure of concrete on exposure to chemical attack.

To identify the bond behaviour of concrete before and after 180 days of chemical attack, a FT-IR spectrum 2 (Perkin Elmer) was used in this study to obtain the FT-IR spectra of the samples. The scans were recorded over the range of 400 to 4000cm^{-1} with spectral resolution of 4cm^{-1}. Linear baseline correction of the spectra was done automatically. The characteristics peaks observed at different wave number are presented in Table 8.1.

A pellet sample (5 mm×5 mm×1 mm) was used for XPS measurements. The XPS analysis was carried out on an XPS system using monochromatic Al Kα radiation hv=1486.7eV. The samples were deposited on a carbon tape and degassed overnight in XPS chamber to minimise air contamination. Pass energy of 50 eV was maintained to carry out the survey analysis.

Table 8.1 Assigned peaks in FT-IR spectra

Wave number (cm^{-1})	Functional Bond	Assinged to	Reference
1641, 3000–3750	O–H	$Ca(OH)_2$	(Lavat et al. 2009; Lodeiro et al. 2009; Rubio et al. 1997; Villain et al. 2007)
1324–1576, 1640-1800, 2501-2550	CO	$CaCO_3$	(Hughes et al. 1995; Lodeiro et al. 2009; Ylmén et al. 2009)
852, 890–1079	Si–O	CSH	(Rubio et al. 1997; Villain et al. 2007)
450–650, 796	Si–O–Si	SiO_2	(Lodeiro et al. 2009; Rubio et al. 1997)
1100–1150, 2330-2370	S–O	SO_4	(Mollah et al. 2000; Nasrazadani et al. 2016)
2850-2925	CH_2/CH_3	Methyl and Methylene	(Chollet and Horgnies 2011)

8.3 RESULTS AND DISCUSSIONS

8.3.1 Resistance to acid attack

8.3.1.1 Visual Assessment

Fig. 8.1 shows the visual appearance of concrete samples after 180 days of sulphuric acid exposure. Table 8.2 lists the visual appearance rating of concrete sample. Concrete samples containing FBA exhibit better and stable structural geometry than control concrete. The surface of samples containing 40%, 60%, 80% and 100% FBA although turned a little mellow; it exhibited structural integrity and almost no surface scaling. The visual observation of control concrete shows severe deterioration with extreme surface scaling. Overall, visual assessment shows that all the concrete mixes undergo variable degree of deterioration on exposure to acidic environment. The visual assessment of samples was sufficient to evaluate the performance of varying percentage of FBA concrete, and thus must be supplemented by more tangible indicator such as change in mass and compressive strength.

Fig. 8.1. Visual assessment of 180 days acid attack on FBA aggregate concrete

Table 8.2 Visual rating of deterioration of concrete mixes at 180 days acid exposure

Mix	**A0**	**A20**	**A40**	**A60**	**A80**	**A100**
Visual rating	5	4	2	2	2	2

8.3.1.2 Change in mass

It can be observed from Figs. 8.2-8.4 that despite the corrosive nature of acidic medium an increase in mass at 7 days and 28 days is detected. Such phenomenon can be due to formation of needle like ettrengite which at first develops in the empty void spaces of the matrix leading to increase in mass. Since percent voids is lowest in control concrete for all series of concrete mixes, at 28 days of exposure the samples of control concrete exhibits mass loss. At 180 days of exposure all the concrete mix samples showed mass loss of varying degree. The highest mass loss was observed for control concrete mix whereas the lowest value was observed for 80%-100% FBA concrete mix. For longer duration of acid exposure, the ettrengite being formed in the concrete matrix starts dissolving the calcium silicate hydrate (CSH) gel and the breakdown of calcium hydroxide to gypsum leads to mass loss. The gypsum formed by this phenomenon is deposited as a white substance (Fig. 8.1) on the surface of sample giving the mellow and softer layer on the sample. This layer gradually wears of the sample as the sulphuric acid is periodically replenished and gets deposited on the bottom of the container. On exposure to acidic medium the corrosive nature of acid starts eroding the exposed surface of concrete samples. Such simultaneous phenomenon's leads to loss in mass of concrete samples.

For concrete samples containing FBA, the quality and formation of CSH gel is higher than control concrete. The greater percent voids coupled with superior CSH gel in the concrete matrix leads to significantly lower mass loss. The higher, stable and durable nature of FBA than river sand provides superior resistance against corrosive nature of acidic medium.

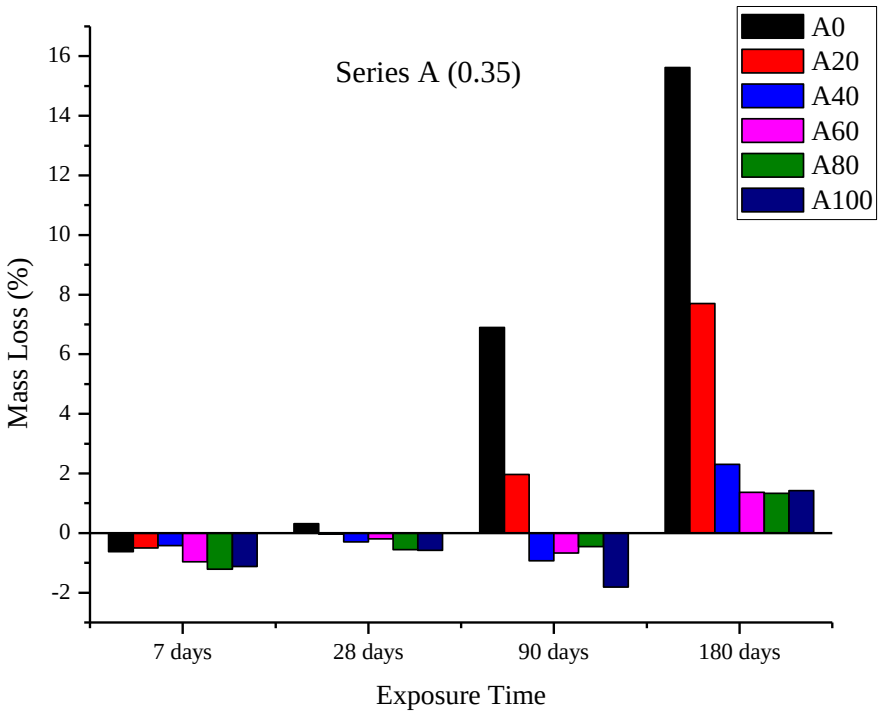

Fig. 8.2. Change in mass due to acid attack on FBA concrete mixes (Series A)

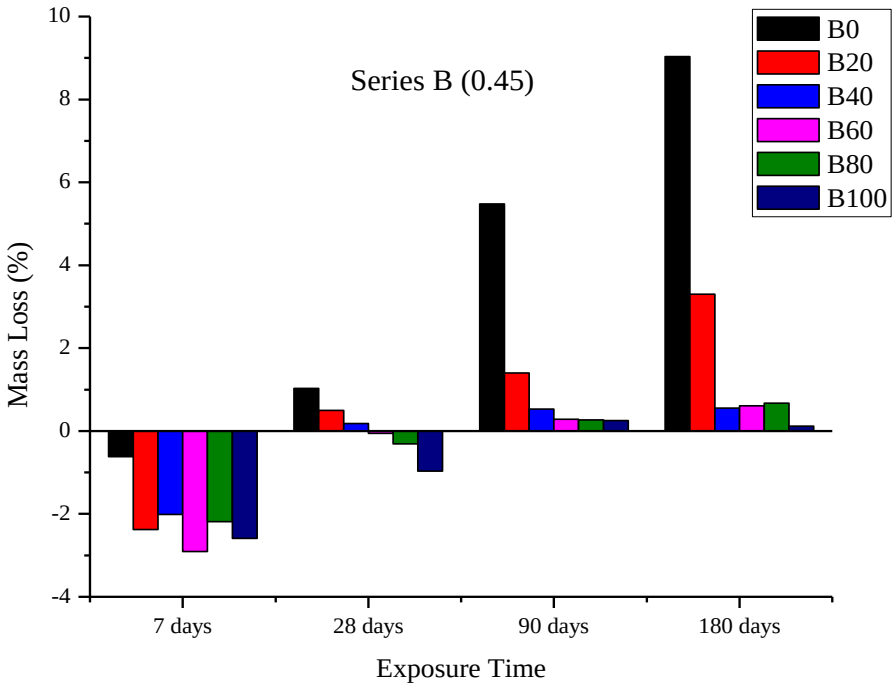

Fig. 8.3. Change in mass due to acid attack on FBA concrete mixes (Series B)

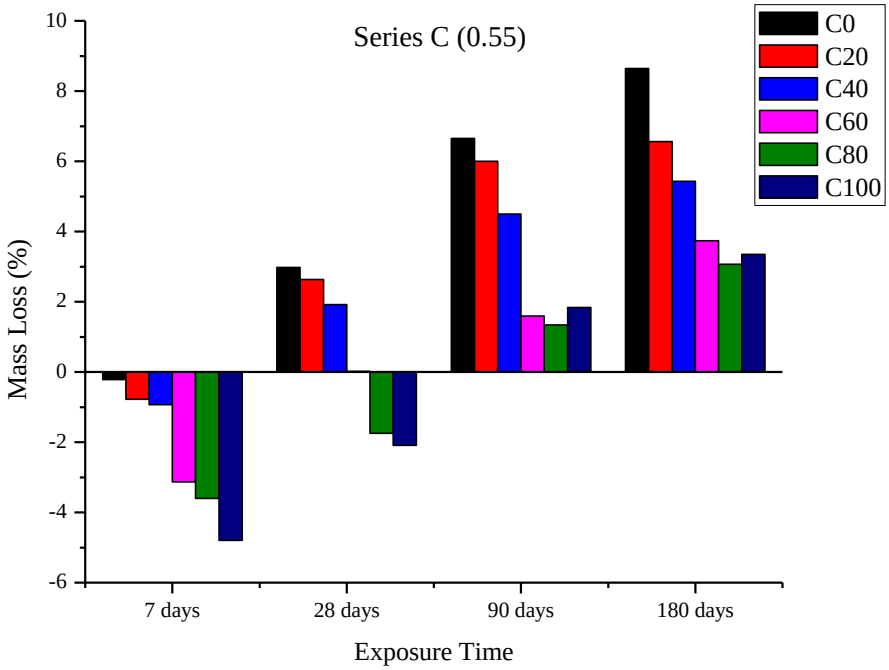

Fig. 8.4. Change in mass due to acid attack on FBA concrete mixes (Series C)

8.3.1.3 Change in compressive strength

The change in compressive strength of concrete samples at different durations of acid attack is shown in Figs. 8.5-8.7. It can be observed that at 7 days of acid exposure, sample of mix A80 and A100 exhibit increase in compressive strength. Overall the control concrete sample of all three series exhibit highest loss in compressive strength whereas sample of 100% FBA recorded lowest loss in compressive strength in respective series. The sulphuric acid attacks the calcium based hydration products forming calcium sulphate which then reacts with calcium aluminate phase forming calcium sulphoaluminate. The crystallisation of calcium sulphoaluminate causes volumetric changes and loss of bonding within the microstructure of concrete. In the present study decomposition of calcium hydroxide creates voids and the formation of calcium sulphoaluminates (needle shaped ettringite) creating a lack of binding CSH gel leading to severely flawed microstructure and surface structure. The above mentioned

phenomenon along with dissolution of calcium hydroxide to gypsum causes reduction in concrete compressive strength.

The better performance of FBA concrete mixes can be attributed to the enhanced microstructure of concrete and the higher quantity of hydration products in concrete matrix. Another possible aspect of improved resistance to acid attack can be the durable nature of raw bone china aggregate (Cook and Andrews 1945; Nyunin 1984). The stable structure of fine bone china aggregate creates a hindrance towards the corrosive nature of sulphuric acid thereby delaying the formation of calcium sulphoaluminate.

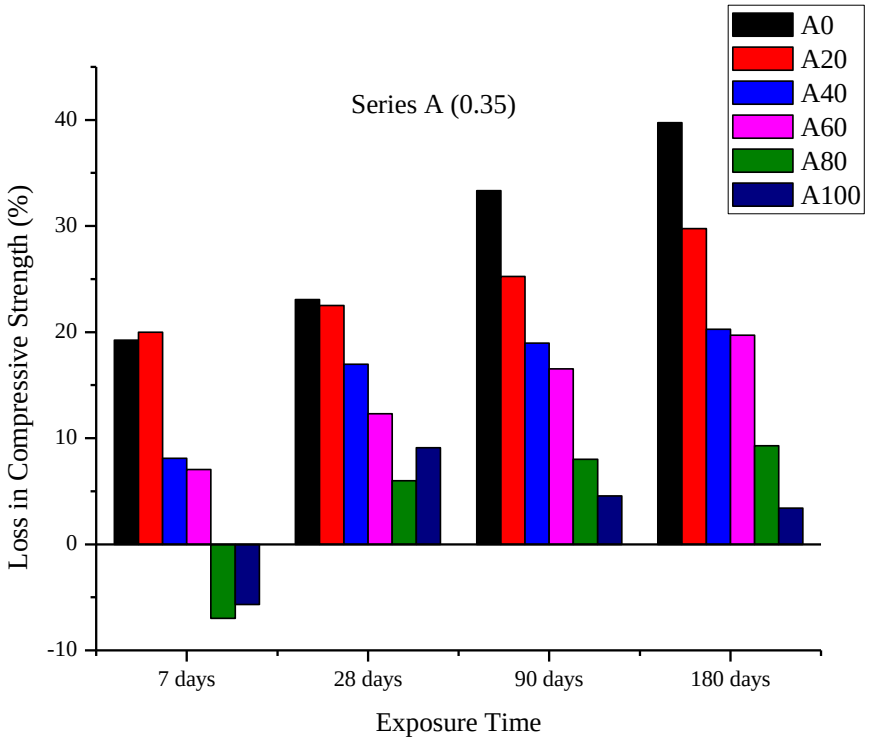

Fig. 8.5 Change in compressive strength due to acid attack on FBA concrete mixes (Series A)

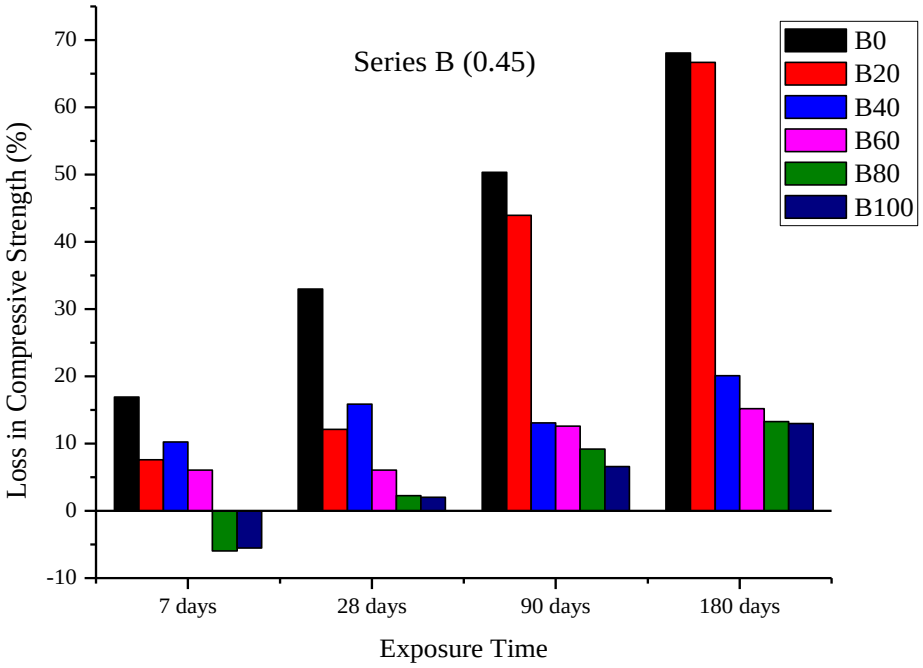

Fig. 8.6 Change in compressive strength due to acid attack on FBA concrete mixes (Series B)

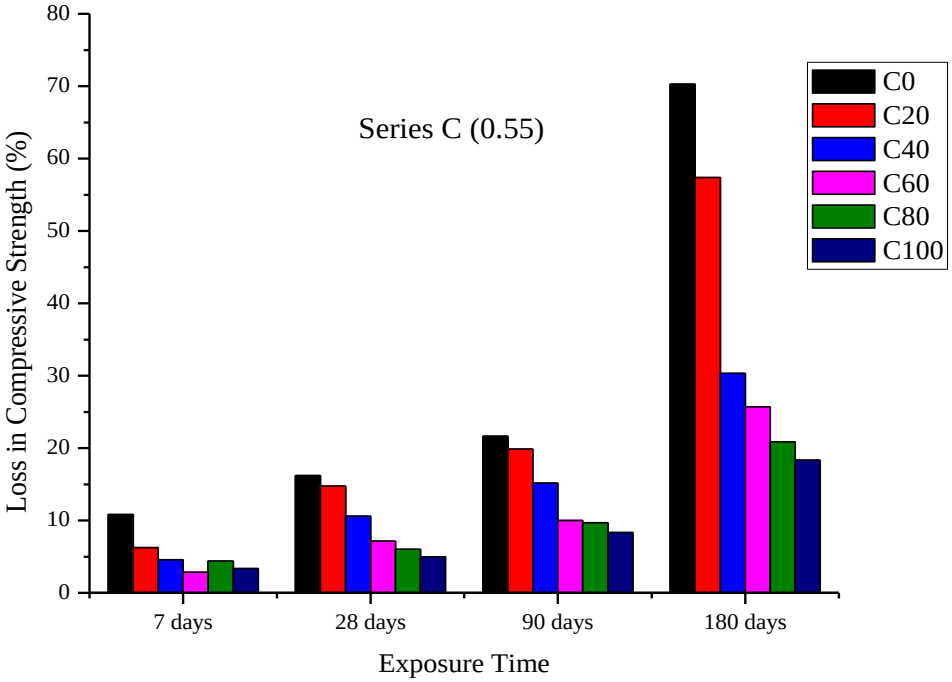

Fig. 8.7 Change in compressive strength due to acid attack on FBA concrete mixes (Series C)

8.3.1.4 Chemical properties

8.3.1.4.1 FT-IR measurements

Figs. 8.8-8.13 shows the FT-IR spectra of the concrete samples after 180 days exposure to sulphuric acid. The reaction of concrete samples in sulfuric acid showed disintegration of the CSH and calcium hydroxide phase bonds. A common observation for all concrete samples is the change in intensity for various bond bands on exposure to sulphuric acid.

For A0 unexposed sample the main binder CSH gel (992.40 cm^{-1}) was completely decomposed and a bond band of calcium sulfoaluminates or ettringite (1104.98 cm^{-1}) was observed. This observation is also consistent with the loss in compressive strength discussed in earlier section. The shoulder bond band of $Ca(OH)_2$ was nearly disintegrated into a much weaker and lower bond spectra. The bond bands of $CaCO_3$ registered an increased presence in the spectra of sulphuric acid exposed sample. For A0 acid exposed sample the peaks of calcium carbonate were observed at 1739.22 cm^{-1}, 1438.47 cm^{-1} and 1367.69 cm^{-1}. This shows an increased presence of calcium carbonate when compared to unexposed samples (1640.71 cm^{-1} and 1416.15 cm^{-1}). The increase can be attributed to the disintegration of calcium hydroxide into calcite due to carbonation. The weaker chemical structure of calcium hydroxide due to acid attack results in formation of gypsum (deposited as white layer on the surfaces of samples). The gypsum formed is also susceptible to carbonation from atmospheric CO_2 leading to formation of calcium carbonate (Azdarpour et al. 2014; Pérez-Moreno et al. 2015).

For concrete samples containing FBA a weaker CSH bond spectra was observed in all the mixes. No significant presence of calcium sulfoaluminates was observed. For concrete mixes A20 and A40 a bond is observed at wavelength 1092 cm^{-1} and 1082.13 cm^{-1} respectively. This bond band lies in the grey area of both CSH gel and calcium sulfoaluminates. It signifies the decomposition of CSH gel but still limited not to form calcium sulfoaluminates. In samples

A60, A80 and A100 bond bands for CSH were observed at 932.53 cm^{-1}, 1000.22 $cm^{-1}$and 1000.04 cm^{-1}. The intensity of CSH bond in these three samples is weaker than unexposed samples. For calcium carbonate similar observations can be drawn for both control concrete and FBA concrete.

For all acid exposed samples a bond peak is observed at wavelength 2990-3000 cm^{-1} that can be for the water component created on reaction between calcium hydroxide and sulphuric acid (Ariffin et al. 2013).

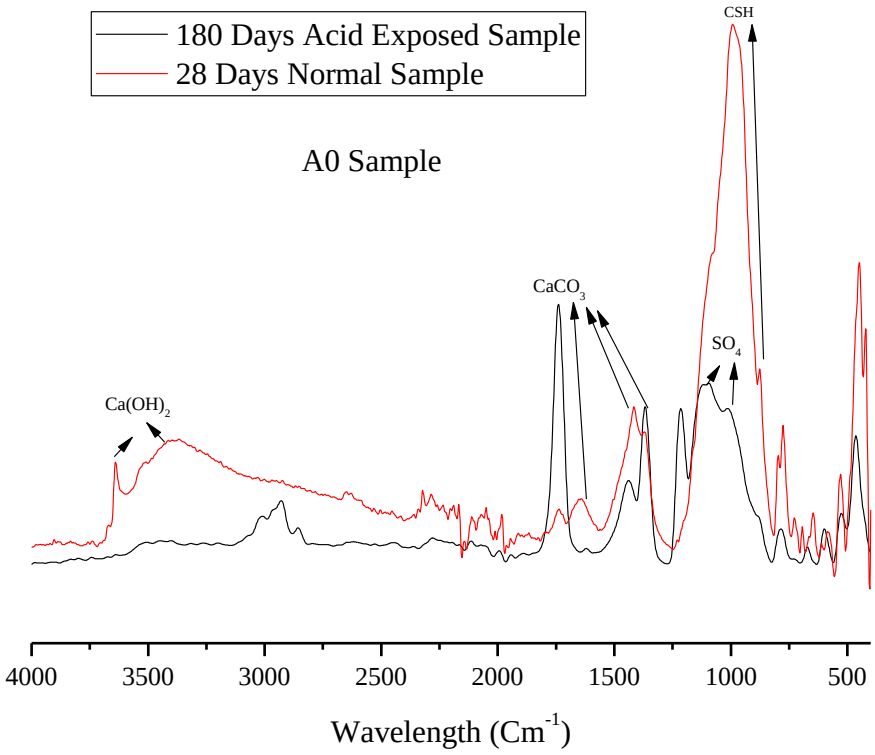

Fig. 8.8 FT-IR spectra of A0 concrete sample before and after 180 days exposure to acid attack

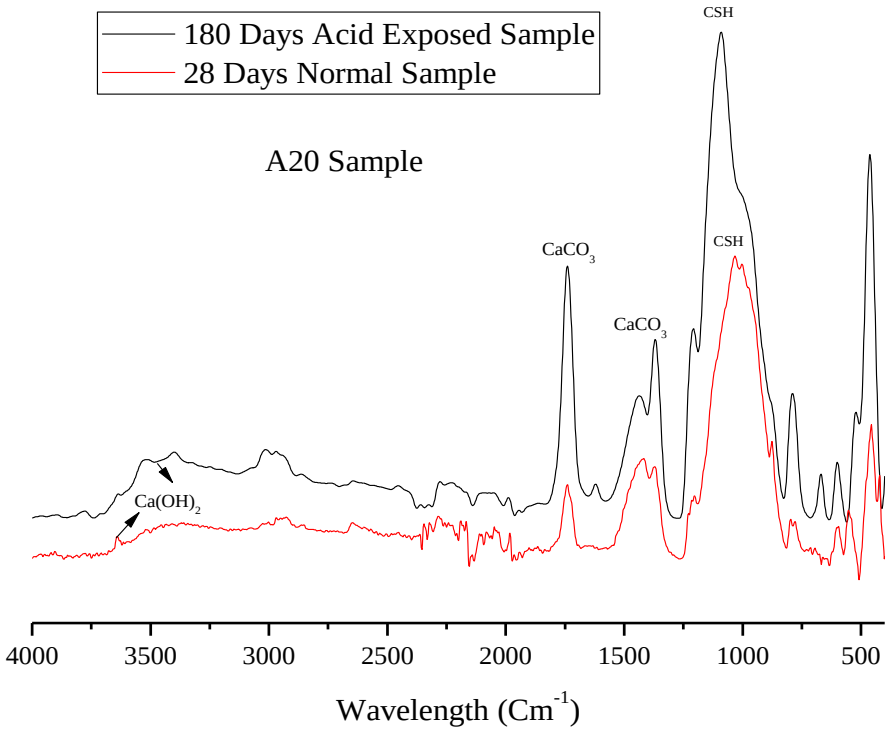

Fig. 8.9 FT-IR spectra of A20 concrete sample before and after 180 days exposure to acid attack

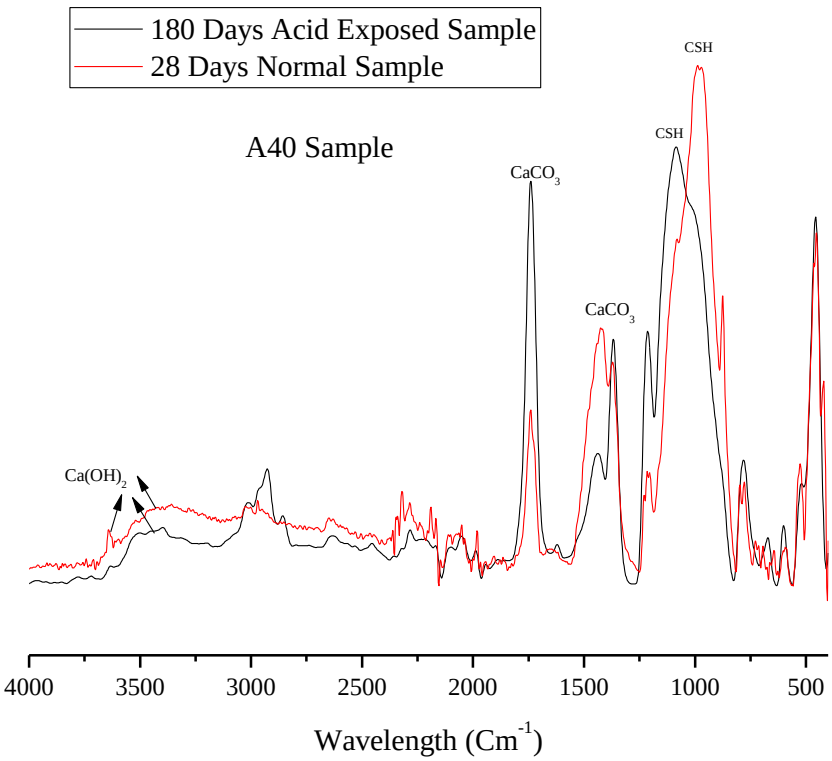

Fig. 8.10 FT-IR spectra of A40 concrete sample before and after 180 days exposure to acid attack

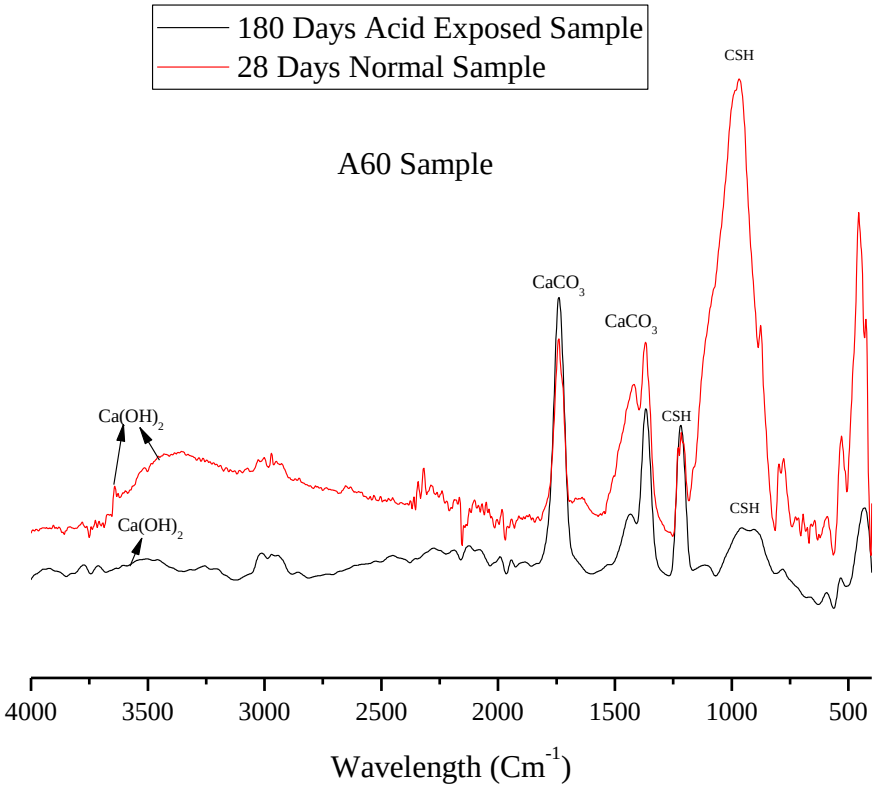

Fig. 8.11 FT-IR spectra of A60 concrete sample before and after 180 days exposure to acid attack

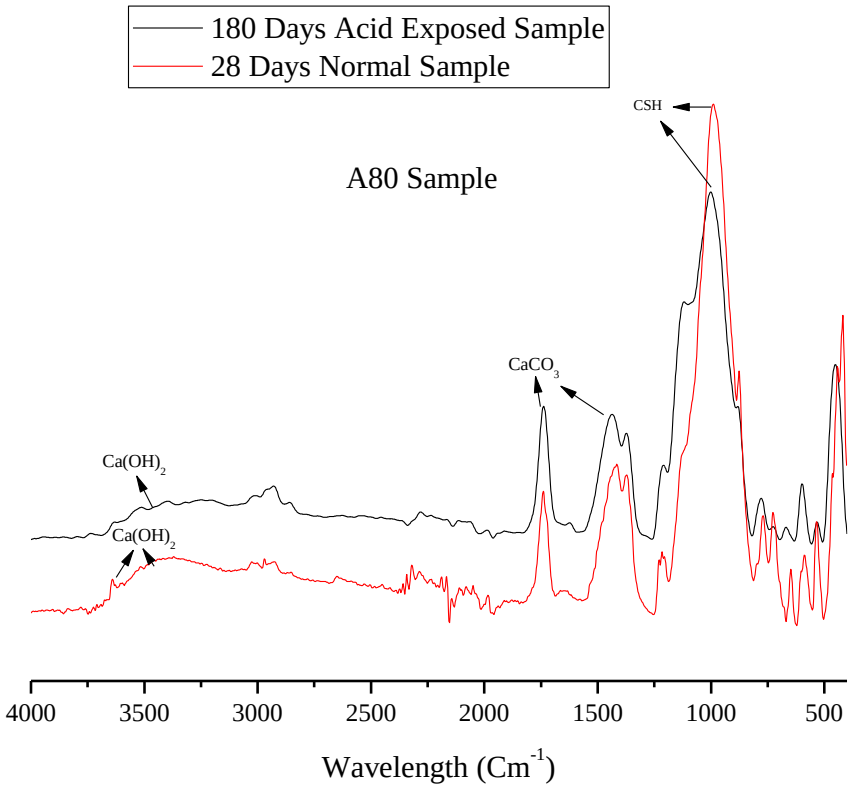

Fig. 8.12 FT-IR spectra of A80 concrete sample before and after 180 days exposure to acid attack

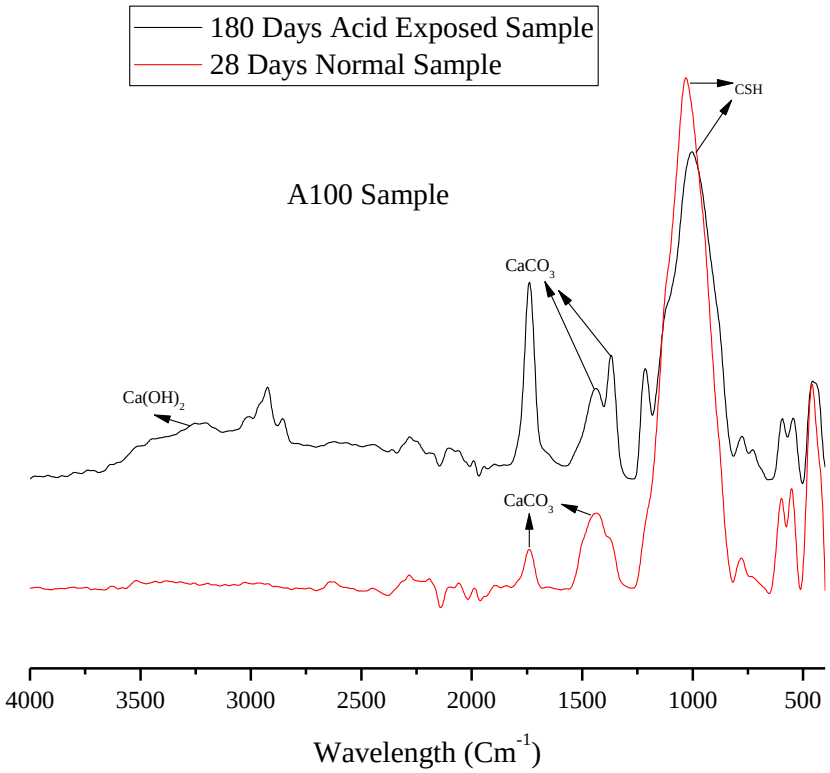

Fig. 8.13 FT-IR spectra of A100 concrete sample before and after 180 days exposure to acid attack

8.3.1.4.2 XPS measurements

The XPS measurements for 180 days acid exposed FBA concrete samples are shown in Fig. 8.14. The atomic percentage of elements observed in XPS spectra are presented in Table 8.3.

The atomic percentage of calcium (Ca2p, Ca2s and Ca2p1/2) is lowest for A0 sample, it signifies the corrosive nature of sulphuric acid which detoriates the hydration products of concrete (CSH and $Ca(OH)_2$). The intensities of all the hydration elements present in concrete indicates only trace amounts. The higher atomic percent of carbon shows the ingress of carbonation in control concrete. During acid attack the pH of concrete is lowered which results in increased carbonation of $Ca(OH)_2$ forming $CaCO_3$.

For concrete samples containing FBA the atomic percentage of hydration elements was higher than control concrete. The stable phase of CSH gel in FBA concrete resisted the ingress of acid to a much higher extent. The stable and durable nature of FBA also played an important role in preserving the Si2s element during acid attack. A80 sample exhibited showed unexpected poor performance in XPS measurement. It can be due to improper sampling or due to some impurity during the pellet making process. Nevertheless, rest of the FBA samples show considerable superior atomic percentage of hydration elements than control concrete. The observations drawn from these measurements can provide gainful knowledge on the decomposition of CSH and $Ca(OH)_2$. The lowered values of C1s indicate slower decomposition of $Ca(OH)_2$ into $CaCO_3$. The presence of FBA in concrete also helps in providing a tortuosity in the sample which delays the movement of acid in concrete thus maintaining higher atomic percentage of hydration products.

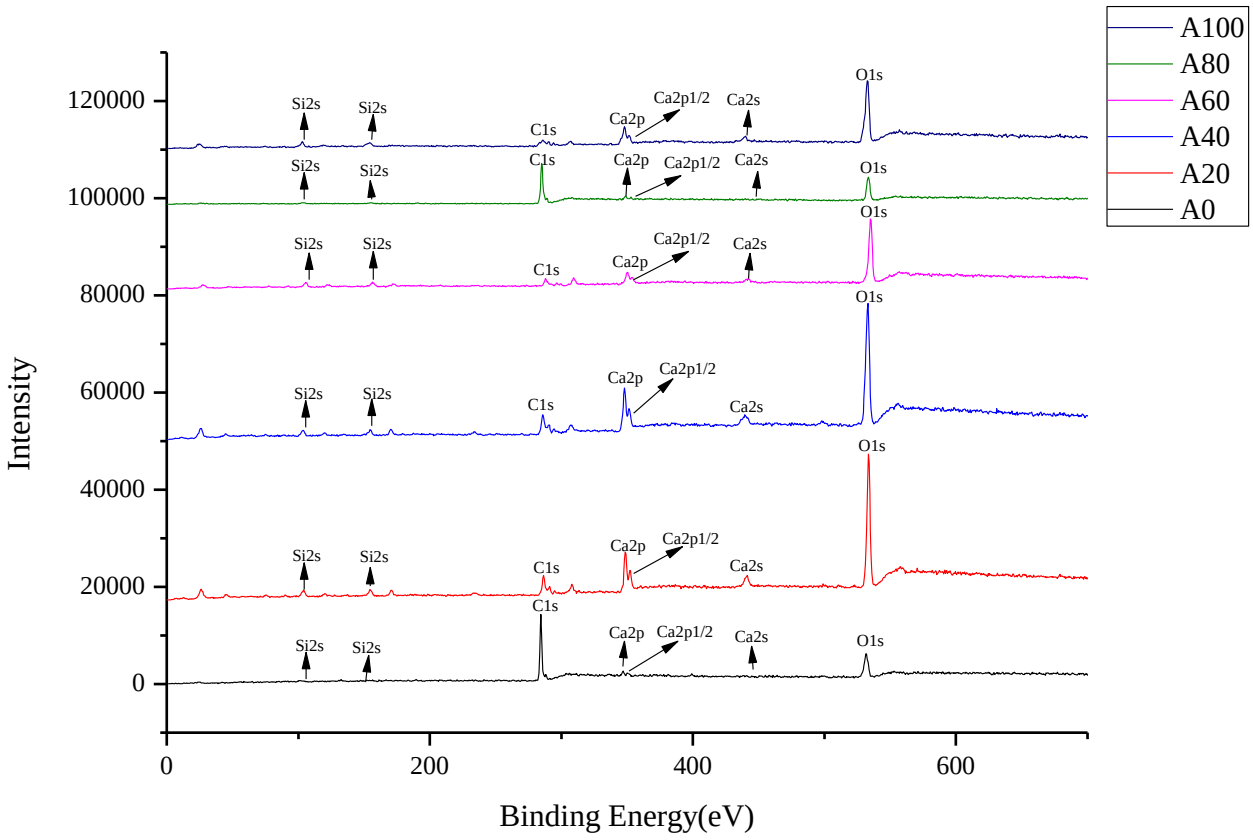

Fig. 8.14 XPS spectra of FBA concrete mixes exposed to 180 days of acid attack

Table 8.3 XPS observations obtained for different elements in FBA concrete mixes exposed to 180 days of acid attack

Mix	Ca2p	Ca2s	Ca2p1/2	Si2p	Si2s	C1s	O1s
	Atomic percent						
A0	1.11	0.62	2.13	1.46	0.55	84.01	10.09
A20	5.80	4.53	0.00	8.73	7.42	19.68	53.81
A40	8.24	2.80	4.83	8.61	4.65	18.73	52.11
A60	3.10	1.75	2.80	9.96	8.31	12.00	62.05
A80	0.91	0.89	2.43	1.91	1.91	76.60	15.33
A100	6.18	4.45	5.84	14.54	8.83	8.50	51.61

8.3.2 Resistance to sulphate attack

8.3.2.1 Change in mass

Figs. 8.15-8.17 shows the change in mass observed for samples of series A, B and C exposed to sulphate solution for 7, 28, 90 and 180 days. For all concrete mixes an increase in mass was observed till 28 days of sulphate exposure. For concrete mixes A80 and A100 in series A, the gain in mass continued till 90 days of exposure. The magnesium sulphate used to simulate the sulphate attack on concrete forms magnesium hydroxide which lowers the pH of the solution leading to formation of thaumasite and ettringite in the pores of the concrete samples. The mass of sample increases as the voids gets filled up due to their formation. During the later stages of study the magnesium sulphate solution causes a significantly damaging effect on the hydration products in concrete. As the Ca+ and Mg+ ions have same near similar valence and ionic radii, magnesium sulphate and calcium silicate hydrate (CSH) react with each other to form brucite and silicate hydrate. The decomposition of polymeric CSH into simpler compounds leads to decrease in mass.

For concrete samples containing FBA, the raw aggregate has a rough and angular texture which resulted in higher voids in concrete samples. The higher voids in concrete matrix causes delay in decomposition of hydration products by accommodating the formation of ettrengite. Another possible reason is the stable and durable nature of FBA. The resilient form of raw aggregate creates a hindrance in movement of sulphate solution into concrete matrix thus delaying the mass loss (Nyunin 1984).

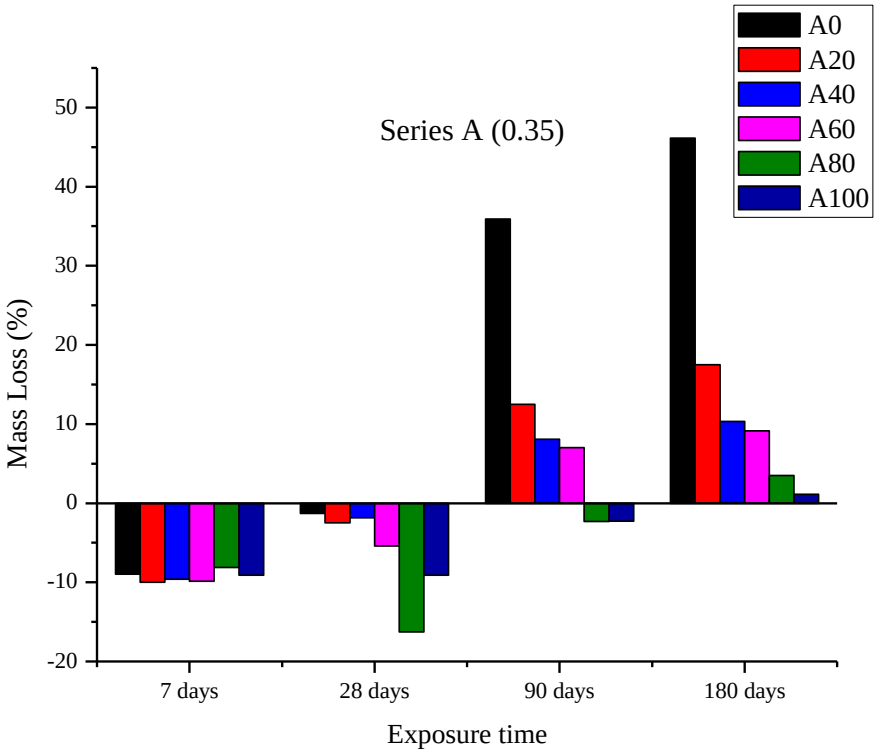

Fig. 8.15 Change in mass due to sulphate attack on FBA concrete mixes (Series A)

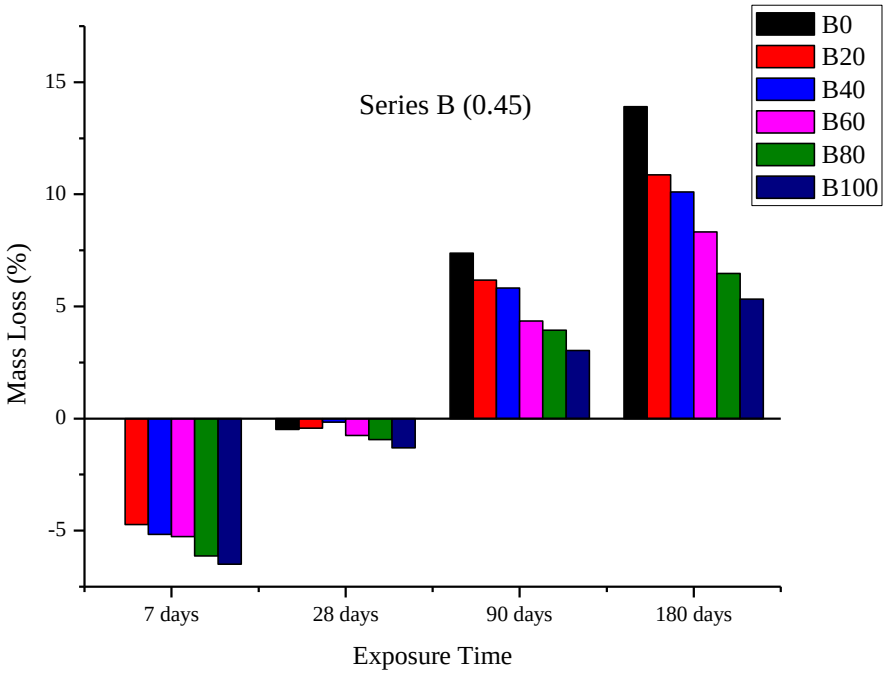

Fig. 8.16 Change in mass due to sulphate attack on FBA concrete mixes (Series B)

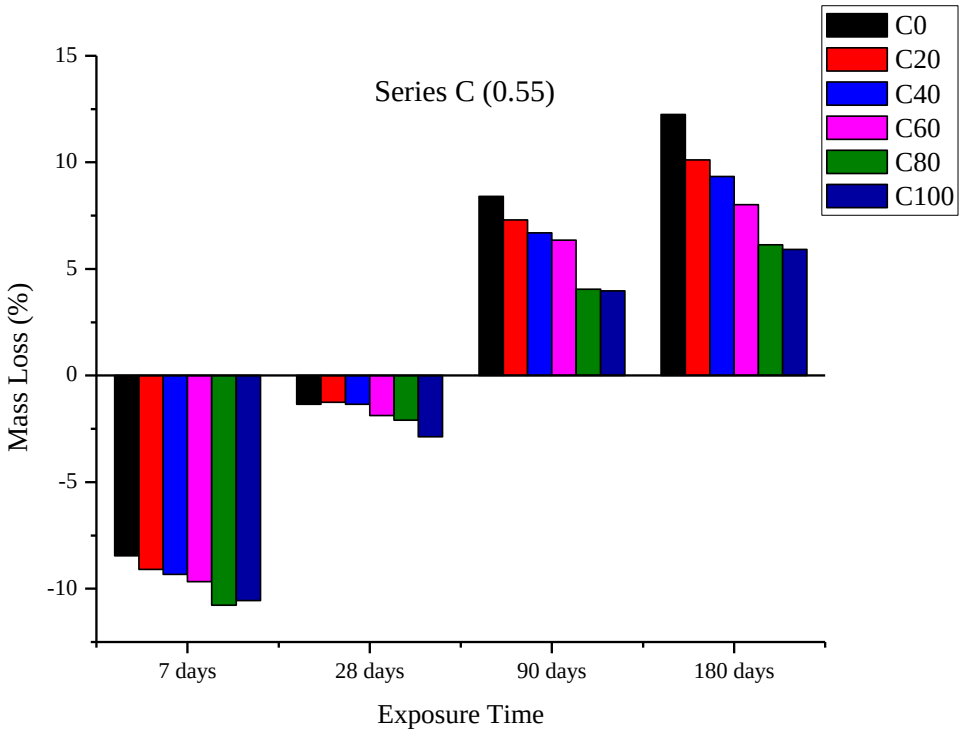

Fig. 8.17 Change in mass due to sulphate attack on FBA concrete mixes (Series C)

8.3.2.2 Change in compressive strength

Percentage change in compressive strength for samples of series A, B and C is shown in Figs. 8.18-8.20. Highest reduction in compressive strength was observed for control concrete of all three series. Concrete samples with FBA fared much better for resistance to sulphate attack. As discussed in previous section that sulphate solution reacts with CSH to form brucite and silicate hydrate. The brucite formed then further reacts with silicate hydrate to form magnesium silicate hydrate which have little to no cohesive property leading to lack of inter-particle bonding in the concrete matrix.

The initial growth in compressive strength can be attributed to the hydration effect and development of ettringite in voids and pores in the concrete matrix, both of which tend to increase the volume and reduce the porosity. For longer duration of exposure the voluminous

expansion due to ettringite results in internal stresses compromising the microstructure of concrete.

The dual attack of sulphate (formation of ettringite and magnesium silicate hydrate) forms a weak and compromised structure of concrete. The reduced binding agent and increased internal stresses leads to loss in compressive strength.

Concrete containing FBA have higher resistance against sulphate attack. The dense CSH gel along with the tortuosity of the raw aggregate create a barrier in the ingress of sulphate solution. The higher ratio of Ca+ ions to Mg+ ions delay the breakdown of CSH gel into magnesium silicate hydrate. Since the formation of magnesium silicate hydrate is considerably slowed, another product of the reaction ettringite is also reduced to great extent.

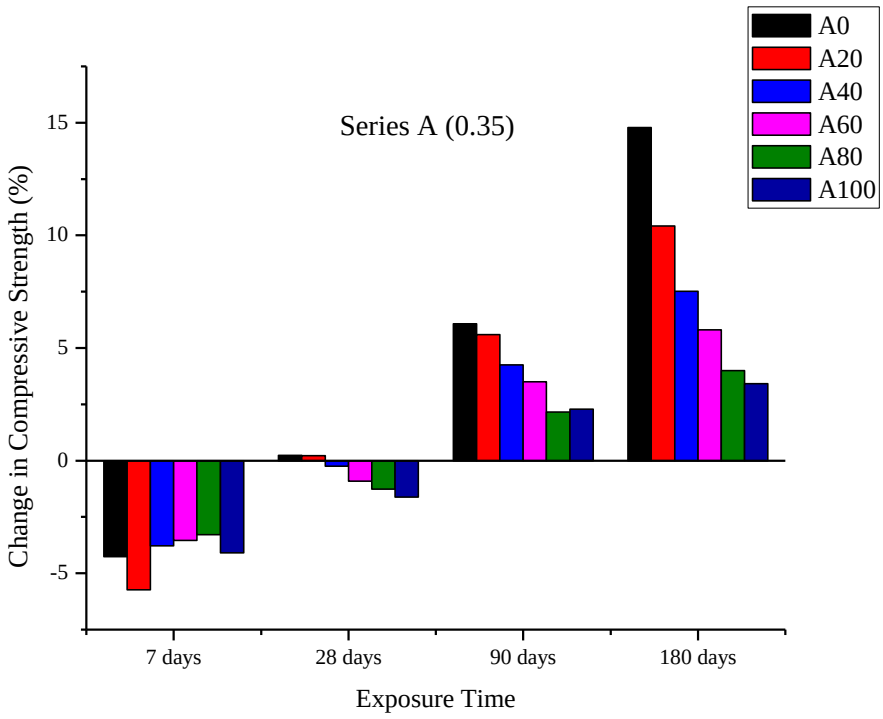

Fig. 8.18 Change in compressive strength due to sulphate attack on FBA concrete mixes (Series A)

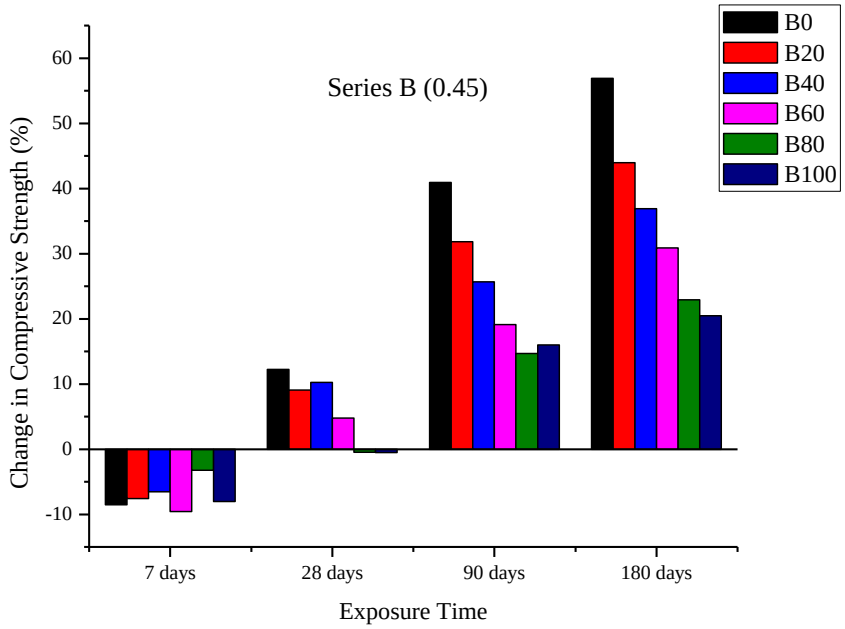

Fig. 8.19 Change in compressive strength due to sulphate attack on FBA concrete mixes (Series B)

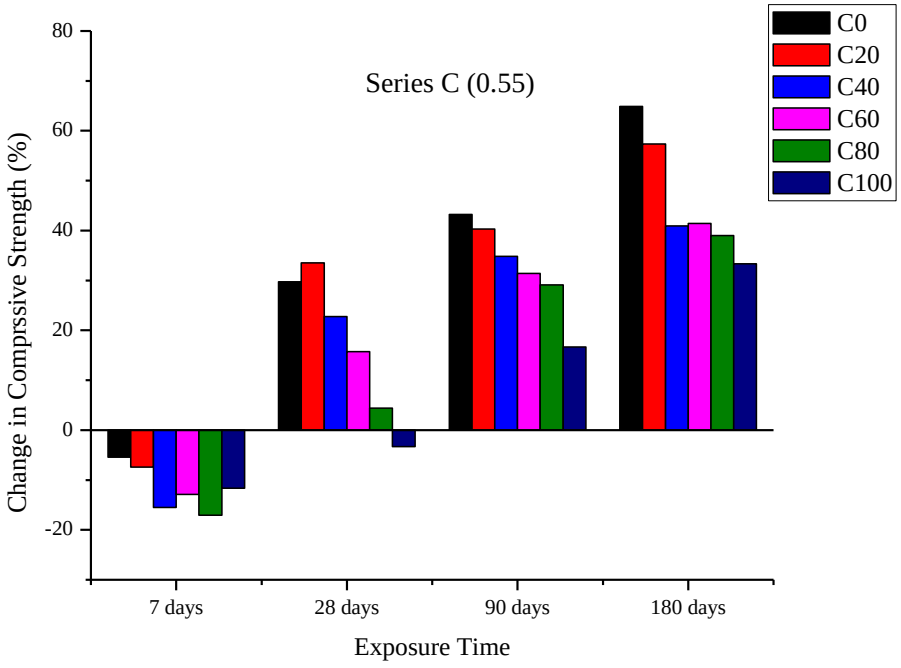

Fig. 8.20 Change in compressive strength due to sulphate attack on FBA concrete mixes (Series C)

8.3.2.3 Chemical Properties

8.3.2.3.1 FT-IR measurements

Figs. 8.21-26 shows the FT-IR spectra of 180 days sulphate exposed sample and normal condition concrete sample. Few common observations present in all sulphate exposed samples is the lower intensity of various bond bands of hydration products. The decomposition of $Ca(OH)_2$ results in weaker bond band for all concrete samples on exposure to sulphate solution.

For control concrete sample A0 the CSH bond band was observed at 992.40 cm^{-1} in normal condition whereas on exposure to sulphate solution the peaks shifted to 1108.61 cm^{-1} (SO_4) wave number representing formation of ettrengite. For sulphate exposed sample CSH bond band was also observed at 989.32 cm-1. The shifting of CSH to lower band and presence of ettrengite bond bands leads to severely compromised chemical characteristics of concrete. Bond band of brucite ($Mg(OH)_2$) is observed at 2926.32 cm-1 for samples exposed to sulphate solution. For sulphate exposed sample two bond bands of CaCO3 is observed at 1434.53 cm-1 and 1738.25 cm-1. The carbonation of $Ca(OH)_2$ due to atmospheric carbon dioxide causes an increase in the formation of $CaCO_3$ leading to a positive shifting of bond by 18.38 cm^{-1}. The second bond band of CaCO3 (1738.25 cm^{-1}) is formed during the disintegration of $Ca(OH)_2$ to gypsum.

For sulphate exposed concrete samples containing FBA brucite bond band were observed only in A20 and A40 mix. A20 sample also recorded a bond band for ettrengite at wave number 1102.05 cm^{-1}. For concrete samples containing 60%, 80% and 100% FBA no bonds of ettrengite and brucite were observed.

The CSH bond band for A20, A40, A60, A80 and A100 sulphate exposed sample was observed at 985.66 cm^{-1}, 995.19 cm^{-1}, 987.25 cm^{-1}, 989.97 cm^{-1} and 984.55 cm^{-1} respectively. Since the CSH bond bands of sulphate exposed samples are more or less at the same wave number as

that of normal condition samples it can be stated that the loss in compressive strength is due to the lower intensity of these bond bands. Another observation that can be drawn is the lower intensity of $CaCO_3$ bond bands for sulphate exposed sample of A40, A60, A80 and A100 mix. The lowered pH of sulphate solution attacks the $CaCO_3$ formed at the surface of samples. The lattice ions of Ca+ and CO_3^{-2} dissolve in the solution thus leaching out the $CaCO_3$ from concrete (Teir et al. 2006). This phenomenon is exhibited only in select concrete samples as the FBA concrete limits the ingress of sulphate solution into the concrete matrix. Thus leaving the exposed outer surface to dissolution of $CaCO_3$.

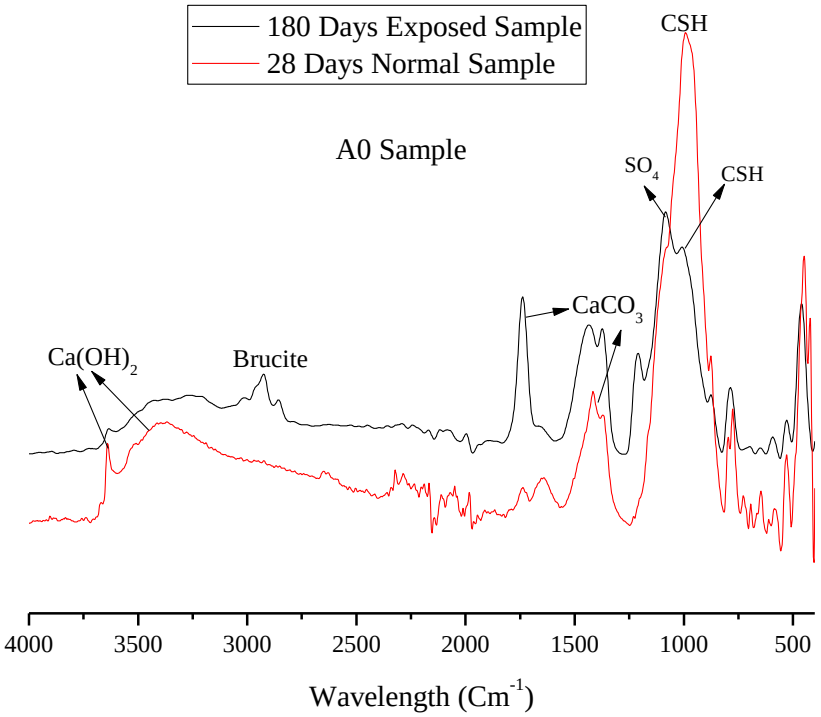

Fig. 8.21 FT-IR spectra of A0 concrete sample before and after 180 days exposure to sulphate attack

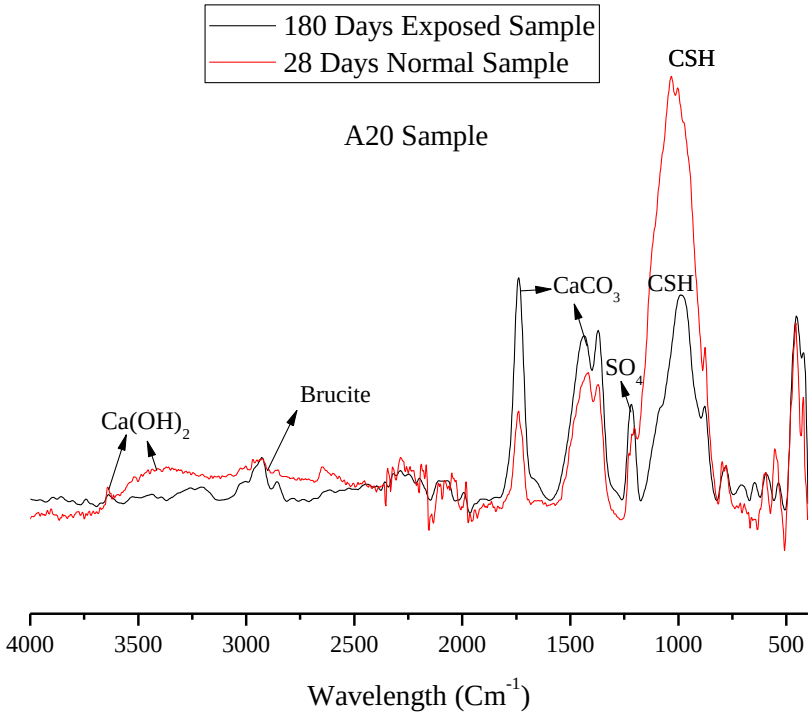

Fig. 8.22 FT-IR spectra of A20 concrete sample before and after 180 days exposure to sulphate attack

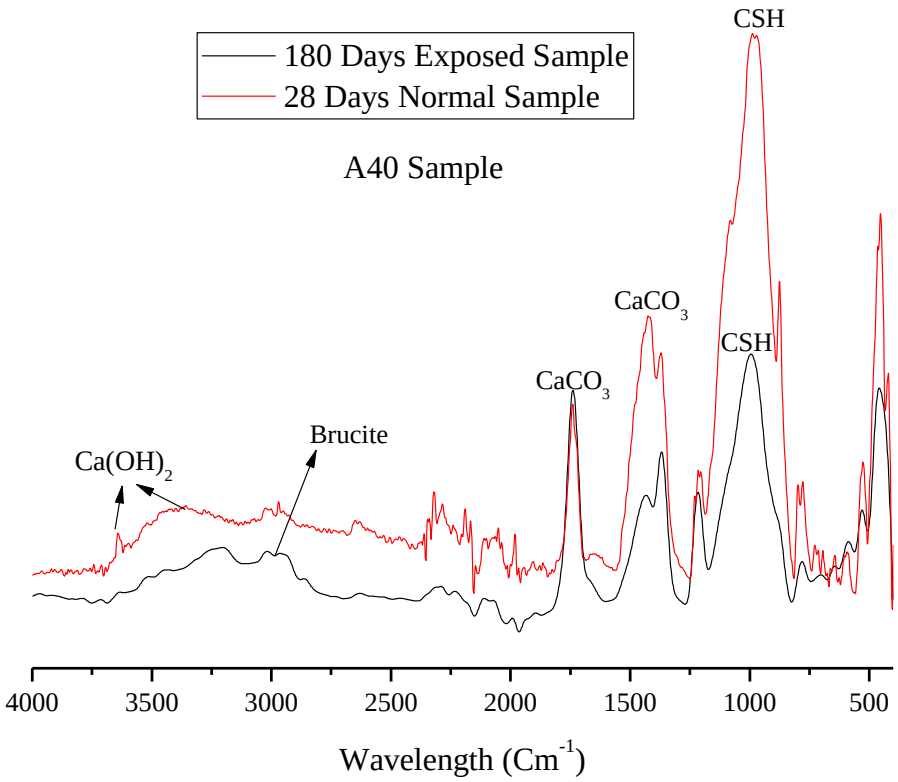

Fig. 8.23 FT-IR spectra of A40 concrete sample before and after 180 days exposure to sulphate attack

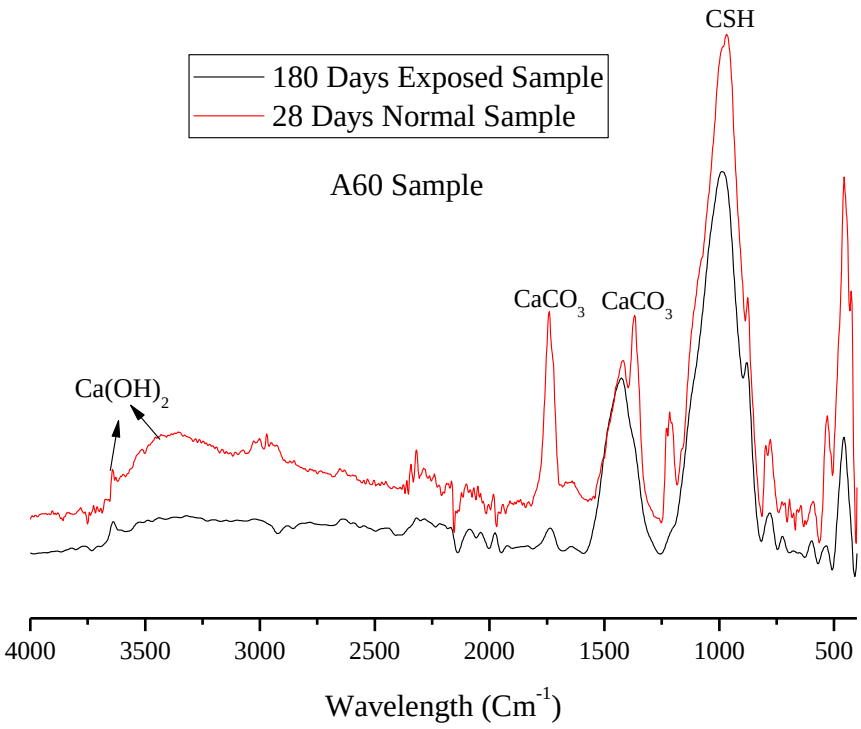

Fig. 8.24 FT-IR spectra of A60 concrete sample before and after 180 days exposure to sulphate attack

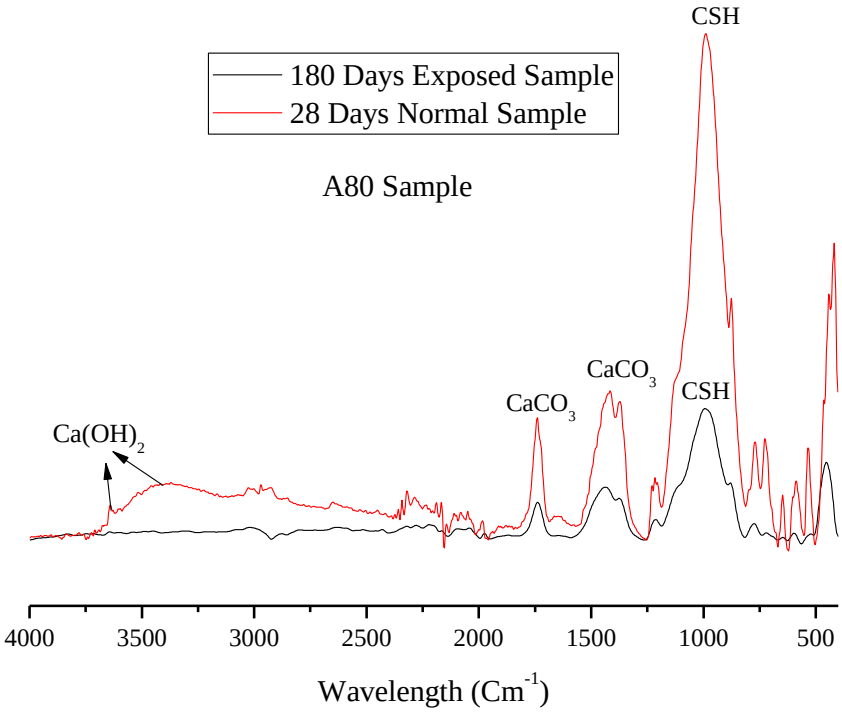

Fig. 8.25 FT-IR spectra of A80 concrete sample before and after 180 days exposure to sulphate attack

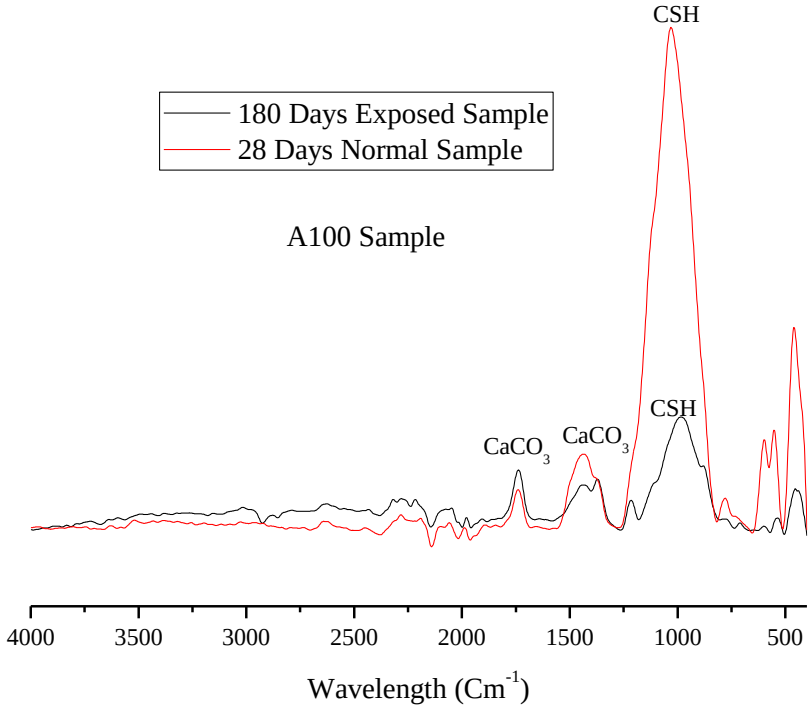

Fig. 8.26 FT-IR spectra of A100 concrete sample before and after 180 days exposure to sulphate attack

8.3.2.3.2 XPS measurements

The XPS measurements for 180 days sulphate exposed FBA concrete samples are shown in Fig. 8.27. The atomic percentage of elements, C/S (Ca/Si) and O/S (O/Si) ratios observed in XPS spectra are presented in Table 8.4.

Sulphate attack on concrete creates magnesium silicate hydrate by replacing calcium silicate hydrate which is evident by lowered atomic percentage and intensity of calcium (Ca2p, Ca2s and Ca2p1/2) element. For FBA concrete samples the values are higher than control concrete (A0) indicating better durability characteristics. The slightly lowered value of Ca2p for A40 mix may be due to some impurity during the sample making process. The higher atomic percentage of silica (Si2s and Si2p) in FBA concrete can be due to the much more durable nature of CSH due to incorporation of FBA. The higher atomic percentage of carbon (C1s) observed for A0 sample is due to formation of $CaCO_3$. Another important observation is the lowered atomic percentage of C1s for A60, A80 and A100 concrete mix. The lowered values provide support the observation in FT-IR measurements. The breakdown of $CaCO_3$ into simpler elements can lead to lower values of C1s. Thus safeguarding concrete mixes from carbonation and subsequent corrosion.

The values of O/S ratio observed is highest for A0 mix. The transformation of calcium silicate hydrate into magnesium silicate hydrate can cause release of Si2s and Si2p which can later on form Si-O-Si with bridging oxygen atoms. Thus, increasing the O/S ratio in concrete mixes. Since the influence of sulphate attack is highest on A0 control concrete it records highest value of O/S ratio showing durable nature of FBA concrete.

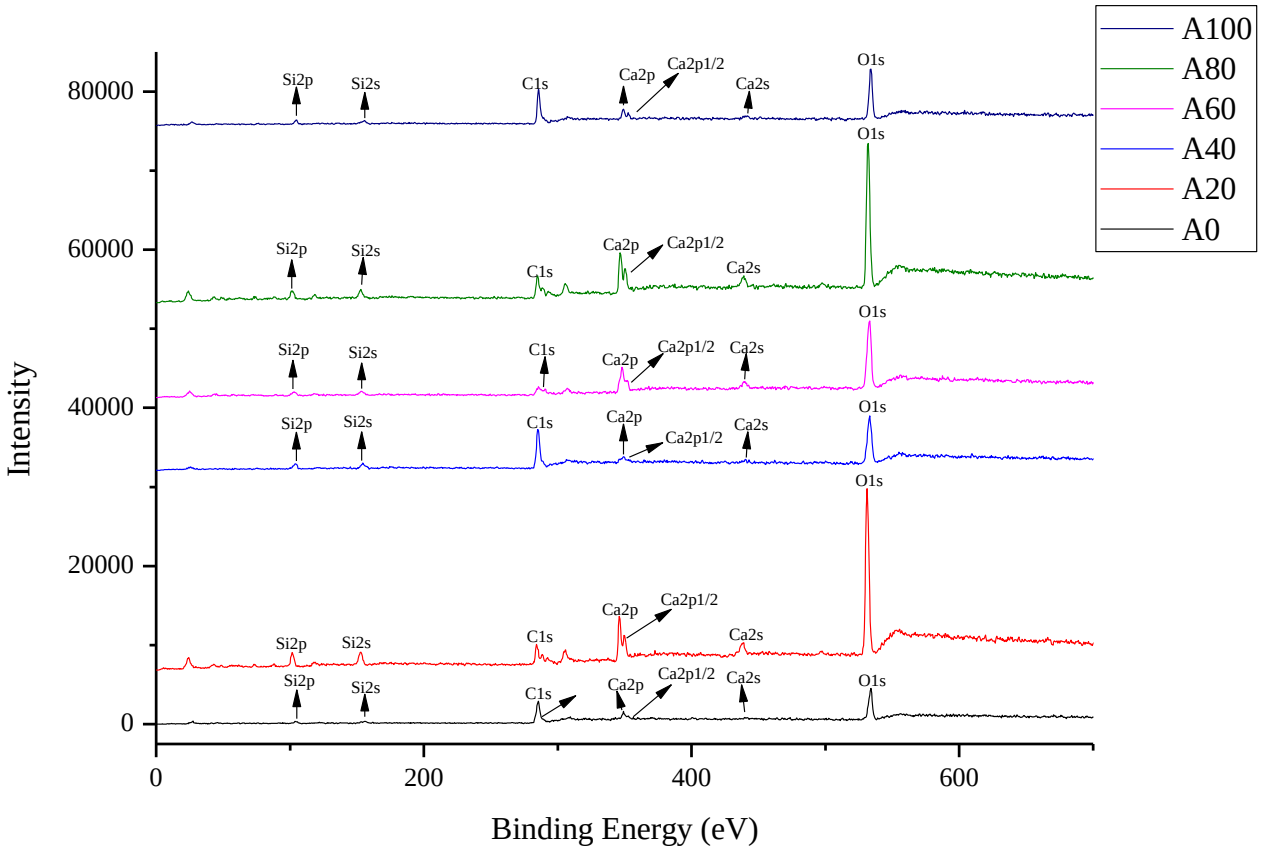

Fig. 8.27 XPS spectra of FBA concrete mixes exposed to 180 days of sulphate attack

Table 8.4 XPS observations obtained for different elements in FBA concrete mixes exposed to 180 days of sulphate attack

Mix	Ca2p	Ca2s	Ca2p1/2	Si2p	Si2s	C1s	O1s	O/S
	Atomic percent							
A0	2.90	1.48	2.10	6.10	3.94	56.10	27.35	1.55
A20	6.42	3.24	6.38	13.04	10.82	13.52	46.56	1.11
A40	0.81	1.74	2.02	9.02	8.43	55.37	24.62	0.80
A60	7.36	4.88	5.51	11.37	7.70	12.07	51.07	1.52
A80	7.10	3.60	7.89	10.28	7.71	16.75	46.63	1.47
A100	2.50	1.07	4.50	6.96	3.77	54.13	27.05	1.43

8.4 CONCLUSIONS

Figs. 8.28-8.30 presents the resistance to chemical attack durability indices for concrete series A, B and C respectively. The nomenclature followed in indices are such that values higher than 1 indicate better performance for respective FBA concrete. The indices for acid and sulphate attack are for final testing value observed, i.e. 180 days.

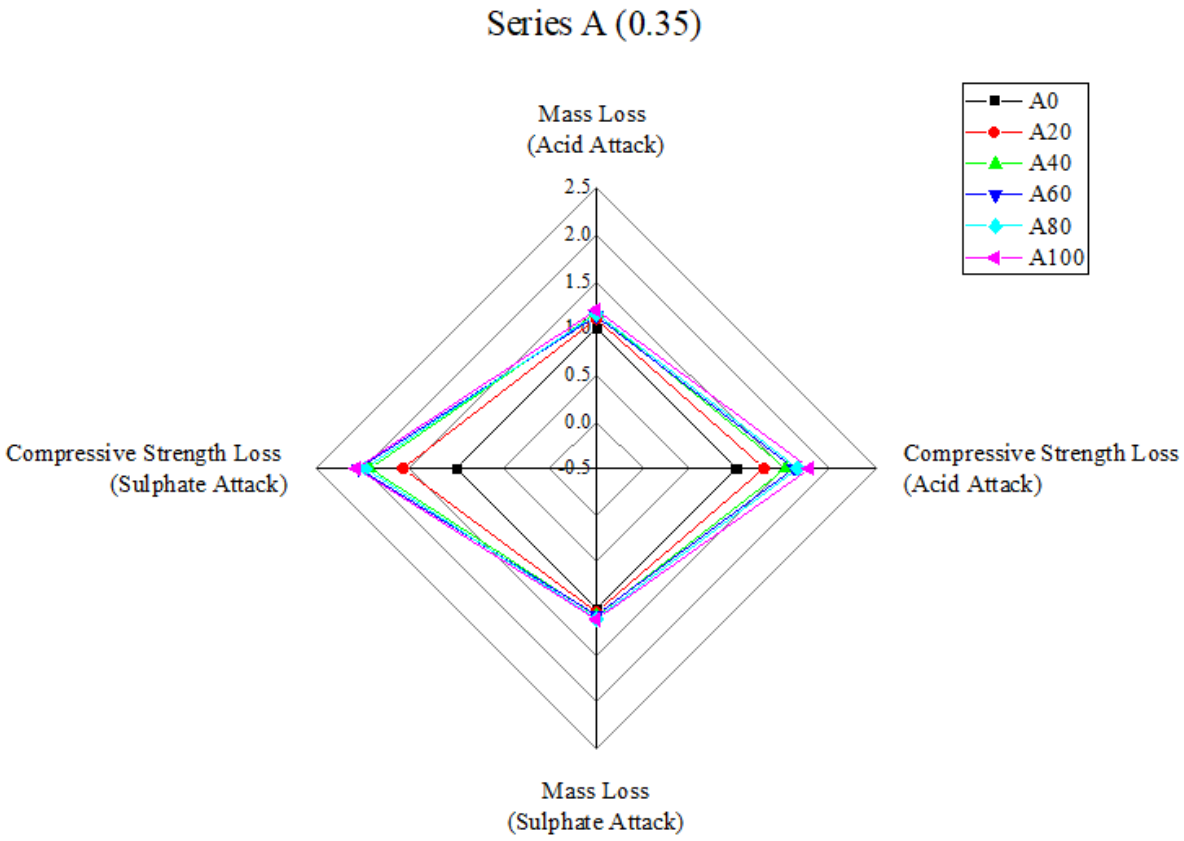

Fig. 8.28 Resistance to chemical attack durability properties indices of FBA concrete (Series A)

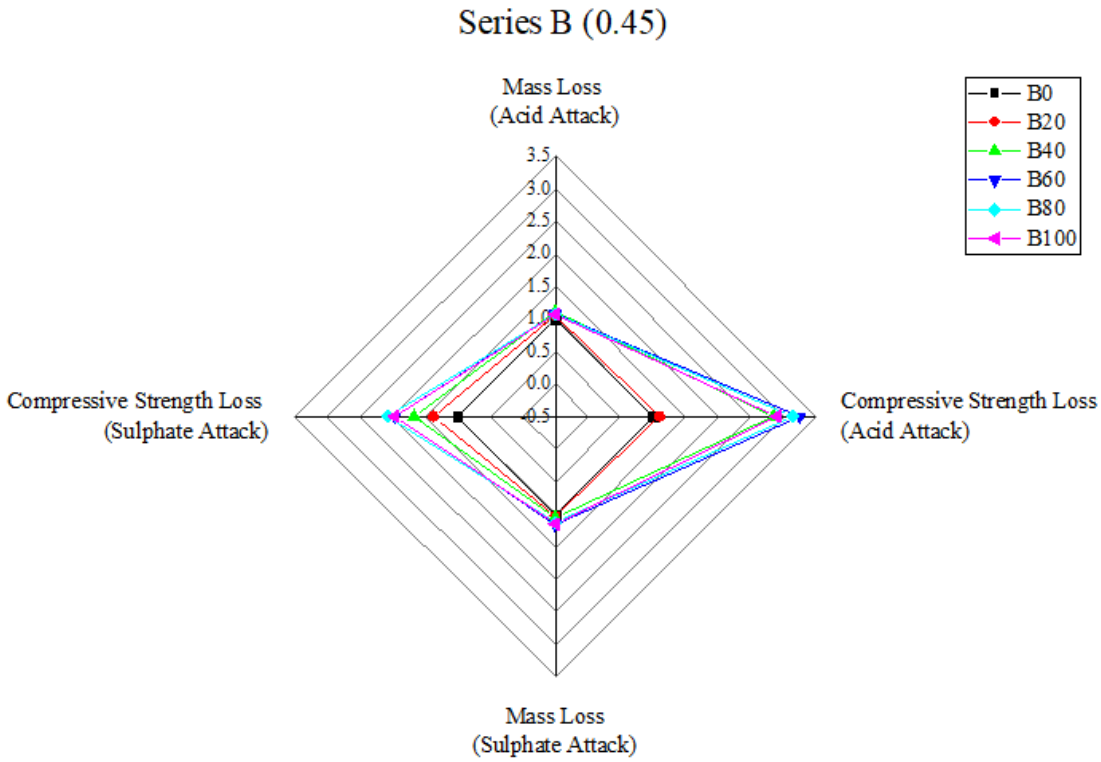

Fig. 8.29 Resistance to chemical attack durability properties indices of FBA concrete (Series B)

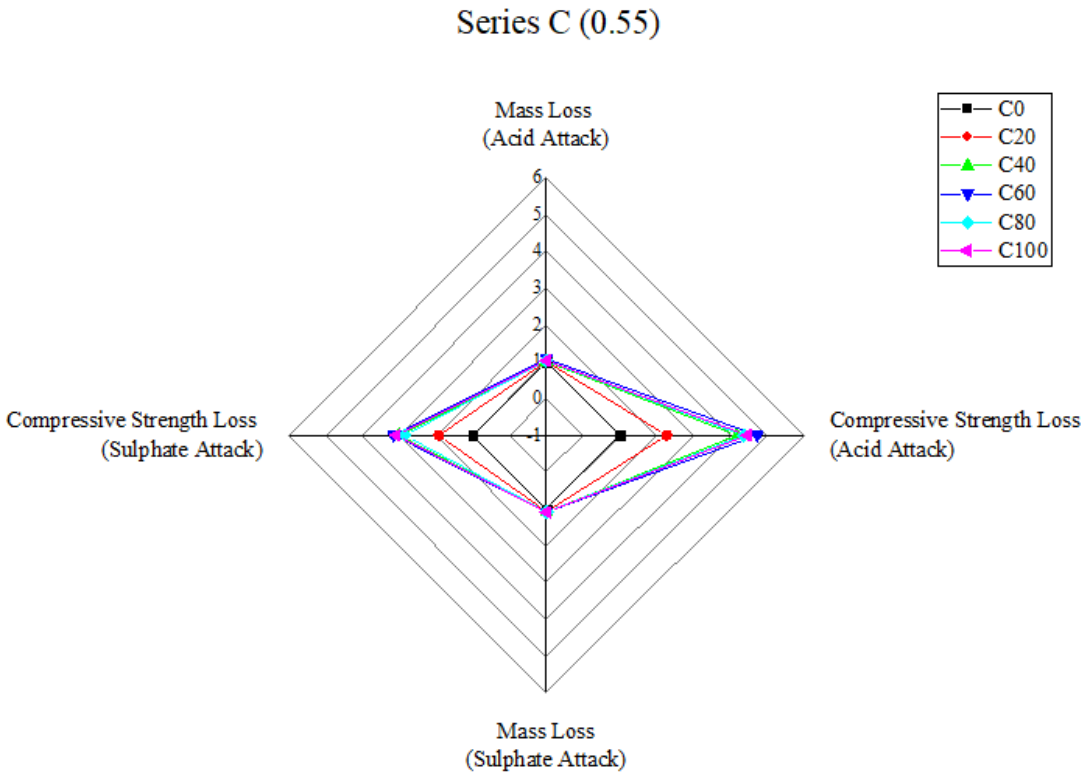

Fig. 8.30 Resistance to chemical attack durability properties indices of FBA concrete (Series C)

As seen from different experimental programme that FBA concrete exhibits superior durability characteristics than control concrete when exposed to chemical attack. Following conclusions are drawn:

1. High visual deterioration was observed for control concrete samples at 180 days of acid attack. The formation of gypsum and calcium sulfoaluminate was pinpointed as potential causes for such extent of damage.
2. Deterioration in terms of mass loss was also higher for samples of control concrete for both acid and sulphate attack. The dissolution and disintegration of hydration products along with corrosive nature of acid resulted in mass loss across all three concrete series. The stable, durable and high amount of hydration products in FBA concrete make it resilient against such chemical attack.
3. Loss in compressive strength due to formation of non-cohesive chemical compounds and the dissolution of hydration products was higher in control concrete than FBA concrete.
4. Chemical changes due to 180 days acid attack indicate disintegration of CSH in control concrete sample due to the formation of calcium sulfoaluminate. Use of FBA in concrete resulted in higher atomic percent of hydration elements even after chemical attack.

The observations and conclusions drawn from the experimental programme indicate that FBA as fine aggregate provides suitable resistance against chemical attack. Replacement of NFA by FBA (40%-100%) can be recommended for areas near industrial units, food processing plants, mining zones and sewage processing units.

CHAPTER 9

OPTIMUM REPLACEMENT: IMPACT, ELEVATED TEMPERATURE AND ENVIRONMENTAL PROPERTIES

9.1 INTRODUCTION

The multi-functional operation of concrete as a building material provides a wide scope of application in many specific situations. Similarly, any alternative concrete making material is also expected to maintain the multi-functional aspect of concrete. Concrete incorporating waste/recycled materials should be evaluated for impact loading, residual properties after exposure to elevated temperature, photocatalytic action and economic aspect.

In the previous chapters it was observed that FBA concrete mixes provide substantial strength and durability property regarding adverse conditions and chemical attack. The only weak link is the higher depth of water penetration and water absorption characteristics of FBA concrete. Therefore, an optimum replacement of NFA by 40% FBA is proposed and further investigated.

9.1.1 Objectives

The general objectives of this chapter are to observe and analyse the properties of FBA concrete mixes under impact loading, elevated temperature, photocatalytic and anti-bacterial properties.

The specific objectives being covered from previously defined are:

1. To adopt suitable experimental programme investigating impact loading, elevated temperature, photocatalytic and anti-bacterial properties of the concrete mixes.
2. To observe and analyse the obtained data for each concrete mix and provide suitable comparisons within and among different concrete mixes.

3. To provide specific discussions regarding the observed findings for different concrete mixes.
4. To investigate chemical changes in concrete mixes on exposure to elevated temperature by FT-IR and TGA measurements.
5. To observe and analyse the obtained cost for each concrete mix and provide suitable comparisons among different concrete mixes.

9.1.2 Program of the study

The aforementioned objectives will be addressed by describing the experimental protocol and its results. In first step the methodology adopted for the investigation will be presented, highlighting the provisions followed. Afterwards, each result of the experimental programme will be presented by specific property. In the end the conclusions arising from the chapter will be drawn.

9.2 EXPERIMENTAL PROGRAMME

9.2.1 Drop weight impact test

Impact resistance under drop weight test was carried as per the guidelines of ACI committee 544 (ACI544.2R-89 1999). Three cylindrical samples of 150 mm diameter and 75 mm height were cast for drop weight test. The experiment consisted of falling a ball of 4.5 kg weight from a height of 450 mm on a hardened steel ball of 65 mm diameter which rested on the concrete sample (Fig. 2). The total number of blows till first crack (N1) and failure (N2) of the sample were observed. The impact energy of samples were calculated as follows:

$$E = Nmgh \qquad (9.1)$$

where,

E is the impact energy, N is the number of blows till failure of sample, m is mass of drop ball (4.5 kg), g is gravity based acceleration (9.8 m/s^2) and h is height of the ball drop (450 mm).

9.2.2 Rebound impact test

Impact resistance under rebound test was carried out on 150 mm cubic samples. A steel ball of weight 130 g was dropped from a fixed height of 1m. The rebound height of ball was recorded on a sensitive camera. The energy imparted to the concrete sample is the difference between initial and final potential energy. Drag resistance due to air was considered to be negligible. The initial and final potential energy were calculated as follows:

$$E_i = mgh_i \quad (9.2)$$

$$E_f = mgh_f \quad (9.3)$$

where,

E_i and E_f are the initial and final potential energy, m is the mass of steel ball (130 g), g is the acceleration due to gravity, h_i is the initial height of drop (1 m), h_f is the observed rebound height.

The energy absorbance capacity of the sample (E) is calculated as the difference between the initial and final potential energy, E_i and E_f respectively.

9.2.3 Resistance to elevated temperature

The resistance to elevated temperature was observed on 100 mm cubic samples. The samples were exposed to 800 °C for 3 hours to ensure proper distribution of heat into samples. After the exposure period, the samples were kept for 24 hours in open laboratory environment for air cooling. The loss in mass, compressive strength was measured and average of 3 samples was reported.

9.2.3.1 FT-IR measurements

Fourier transformation infrared (FT-IR) spectroscopy of samples exposed to elevated temperature was carried out to observe the chemical changes. The spectra was obtained at a wavelength of 400 cm^{-1} to 4000 cm^{-1} with spectral resolution of 4 cm^{-1}. Table 9.1 presents the wavenumber corresponding to the particular bond.

9.2.3.2 TGA measurements

Thermo-gravimetric analysis was carried out to observe the changes in mass when concrete is exposed to progressively elevated temperatures at a fixed rate of increment. The range of temperature observed was 30°C to 900°C for a heating rate of 10°C/minute.

Table 9.1 Assigned peaks in FT-IR spectra

Wave number (cm^{-1})	**Functional Bond**	**Assinged to**	**Reference**
1641, 3000–3750	O–H	$Ca(OH)_2$	(Lavat et al. 2009; Lodeiro et al. 2009; Rubio et al. 1997; Villain et al. 2007)
1324–1576, 1640-1800, 2501-2550	CO	$CaCO_3$	(Hughes et al. 1995; Lodeiro et al. 2009; Ylmén et al. 2009)
852, 890–1079	Si–O	CSH	(Rubio et al. 1997; Villain et al. 2007)

450–650, 796	Si–O–Si	SiO_2	(Lodeiro et al. 2009; Rubio et al. 1997)
1100–1150, 2330-2370	S–O	SO_4	(Mollah et al. 2000; Nasrazadani et al. 2016)
2850-2925	CH_2/CH_3	Methyl and Methylene	(Chollet and Horgnies 2011)

9.2.4 Photocatalytic property

For investigation for photocatalytic property TiO_2 powder (anatase phase) was added (5% of cement weight) in concrete mixes. The samples were cast and were kept for 28 days of curing.

In order to observe photocatalytic properties of concrete mixes, the degradation of methylene blue (MB) solution under ultraviolet (UV) radiation was investigated. Concrete samples of 100 mm×100 mm ×10 mm were immersed in 300 ml MB solution (10 mg/L) under the condition that TiO_2 surface was placed at a distance of 500 mm away from the UV light. The samples of solutions were collected every 30 minutes upto 150 minutes and were then studied for ultraviolet and visible light spectrometry to obtain the absorbency at the wavelength of 665 nm. The degradation ratio, A_t, of photocatalytic properties of concrete surface was obtained from

$$A_t = \frac{I_a}{I_0} = \frac{I_0 - I_t}{I_0} \qquad (9.4)$$

where,

A_t is the degradation ratio, the I_0 is the base absorbency, I_t is the absorbency after time t.

9.2.5 Cost economics and environmental benefits

The FBA being a waste material is dumped in yards and is freely available except for crushing and transportation cost. The cost of $1m^3$ of concrete having 40% FBA was compared to that NFA concrete.

9.3 RESULTS AND DISCUSSIONS

9.3.1 Impact resistance under drop weight

The impact resistance of concrete was calculated by observing the number of blows to initial (N1) cracking and failure (N2) of sample. The difference between the failure blows and first crack blows and their ratio are given in Table 9.2.

The number of blows for initial crack and failure were found to be more for concrete samples containing FBA. The number of blows for initial crack increased by 8.91%, 1.31% and 31.52% for series A, series B and series C respectively. The inclusion of FBA also increased the number of blows till failure of the sample (N2) as shown in Table 4.

The results indicate that inclusion of FBA enhances the energy absorption capacity of concrete. Such behaviour can be due to the increased strength characteristics of FBA concrete. As discussed in chapter 5, CSH gel is the dominating factor in providing the strength and bonding properties of concrete. For impact resistance under drop weight the contact point between the CSH gel and aggregate matters the most to resist crack propagation. The inclusion of rough FBA improves the contact area between mortar paste and aggregate and the pozzolanic behaviour develop higher amount of hydration product increasing the bond area between aggregate and mortar paste. The dual beneficial role of fine bone china aggregate, roughness

coupled with higher strength characteristics of concrete provide enhanced resistance to drop weight impact.

The fracture pattern observed for concrete samples is shown in Fig. 9.1. The inclusion of FBA changed the failure pattern from a single large crack to a group of cracks. Another observation that can be drawn is the propagation of crack in 40% FBA concrete. The cracks move around the aggregate and sample to propagate through the weakest portion. This conglomeration of cracks movement delays the failure of the sample.

Table 9.2 Impact resistance of FBA concrete mixes at initial crack and failure

Mix	**Impact resistance (Number of blows)**		**N2-N1**	**N2/N1**	**Impact Energy (J)**	
	Initial Crack (N1)	**Failure (N2)**			**Initial**	**Failure**
A0	393	400	7	1.02	7807.04	7946.10
A40	428	439	11	1.03	8502.33	8720.84
B0	305	311	6	1.02	6058.90	6178.09
B40	309	327	18	1.06	6138.36	6495.94
C0	92	105	13	1.14	1827.60	2085.85
C40	142	155	13	1.09	2403.70	2820.87

Fig. 9.1 Fracture pattern of concrete sample due to drop weight impact

9.3.2 Impact resistance under rebound test

The energy absorbed due to impact under rebound is shown in Fig. 9.2. It can be observed that the inclusion of FBA leads to enhanced impact resistant performance. On 40% replacement of natural sand with FBA concrete, the absorbed impact energy rises from 0.94 J to 0.99 J, 0.89 J to 0.92 J and 0.86 J to 0.89 J for series A, series B and series C respectively.

The rebound test is dependent upon the surface and its hardness. For concrete sample containing FBA the ITZ layer is superior to that of control concrete (As observed in LFM imaging). The improved ITZ layer enhances the hardness of concrete samples leading to higher energy absorption capacity (Wang et al. 2012). The hydration products such as CSH gel provide a sound and compact microstructure structure along with cohesive binding between aggregate. The quality and amount of CSH gel also provide a minor influence on the hardness of concrete (Li et al. 2014; Taha et al. 2010). As discussed earlier the quality and amount of

CSH gel in FBA concrete is superior to that of control concrete. These two factors can be the contributing influence towards higher impact energy absorption of FBA concrete.

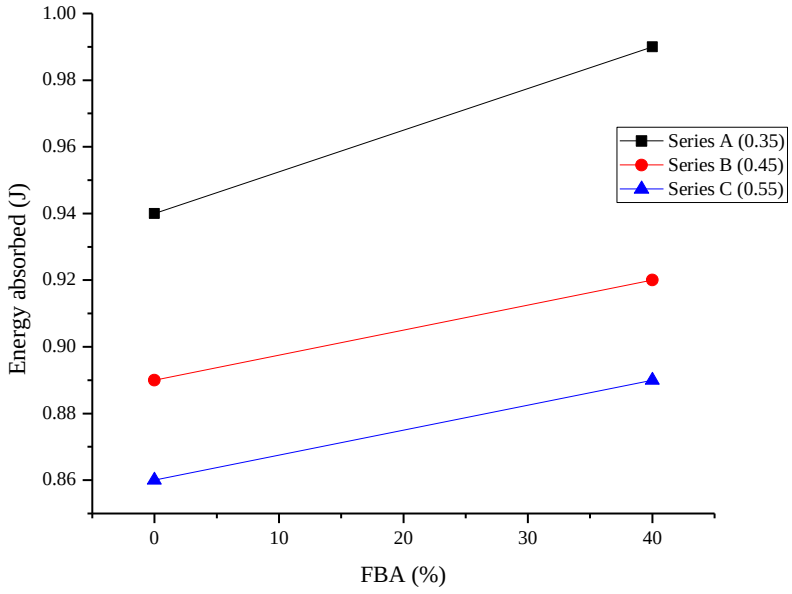

Fig. 9.2 Impact energy absorbed by FBA concrete samples

9.3.3 Resistance to elevated temperature

The loss in mass and compressive strength due to exposure to elevated temperature are shown in Figs. 9.3-9.4. The mass loss observed in sample is due to dissipation of chemically bound water and disintegration of hydration products. The loss in compressive strength is due to the weakened state of hydration products and development of thermal stress cracks. The presence of voids due to loss of water also allows for faster crack propagation resulting in loss of strength. In this study the FBA concrete exhibited better resistance to elevated temperature than control concrete.

To understand the influence of elevated temperature on the microstructure of concrete, FT-IR analysis (Figs. 9.5-9.6) was carried out for both A0 and A40 sample and compared to the spectra at normal temperature (30°C). For elevated temperature exposed control concrete

specimen, the peak for CSH gel is observed at 959 cm^{-1} and for concrete specimen at normal temperature at 992 cm^{-1} wave number. Another peak is observed at 874 cm^{-1} which shows the bond wavelength of disintegrated CSH gel. The shift of 33 cm^{-1} and presence of disintegrated CSH gel shows the damage extent of elevated temperature on concrete. The lower wavelength number signifies a weaker bond with longer length. For A40 concrete sample at normal temperature CSH bond is observed at 988.08 cm^{-1} and 1213.66 cm^{-1} wave number. For sample exposed to elevated temperature, the CSH bond is observed at 987.13 cm^{-1} and 1084.83 cm^{-1}. Although the peak at 1213.66 cm^{-1} shifted by 128 cm^{-1} due to elevated temperature, it still provides stronger bond characteristics than control concrete. Another possible reason for such a huge peak shift can be the thermal property of raw aggregate as it is known that ceramic material goes through different chemical phases at different temperatures. It is possible that the CSH gel of mortar paste containing majority of ceramic aggregate may also undergo some chemical transformation.

TGA analysis was also carried out to calculate the mass loss between 50 °C to 600 °C (Fig. 9.7). The mass loss in this particular range depicts dehydration of chemically bound water and disintegration of hydration products. For sample A0 and A40, the mass loss observed is 7.81% and 6.03% respectively. The lower mass loss observed for A40 sample can be due to the resistant nature of ceramic waste against elevated temperature (Halicka et al. 2013). The mortar paste containing FBA have superior hydration products which also provides additional resistance to mass loss on exposure to elevated temperature.

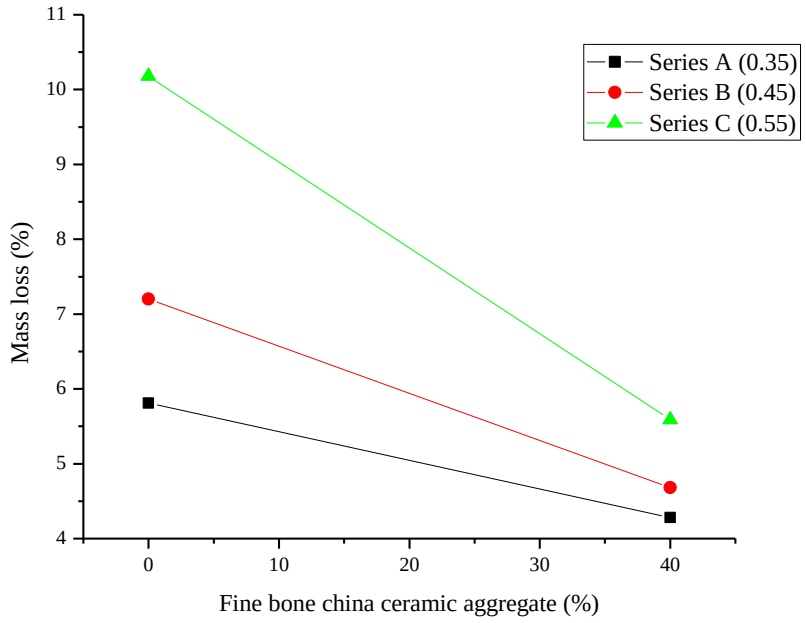

Fig. 9.3 Mass loss in FBA concrete mixes exposed to 800 °C

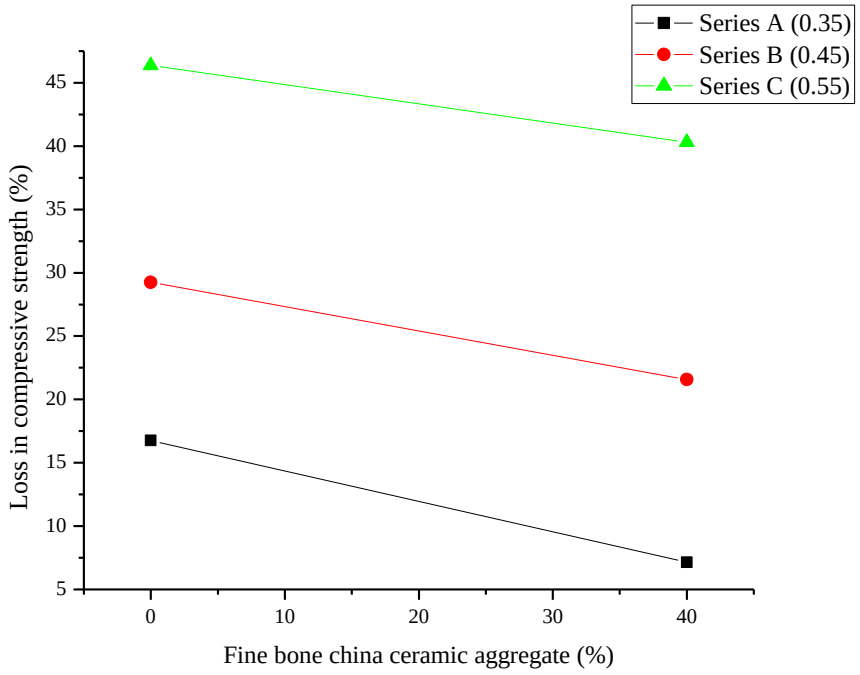

Fig. 9.4 Loss in compressive strength of FBA concrete mixes exposed to 800 °C

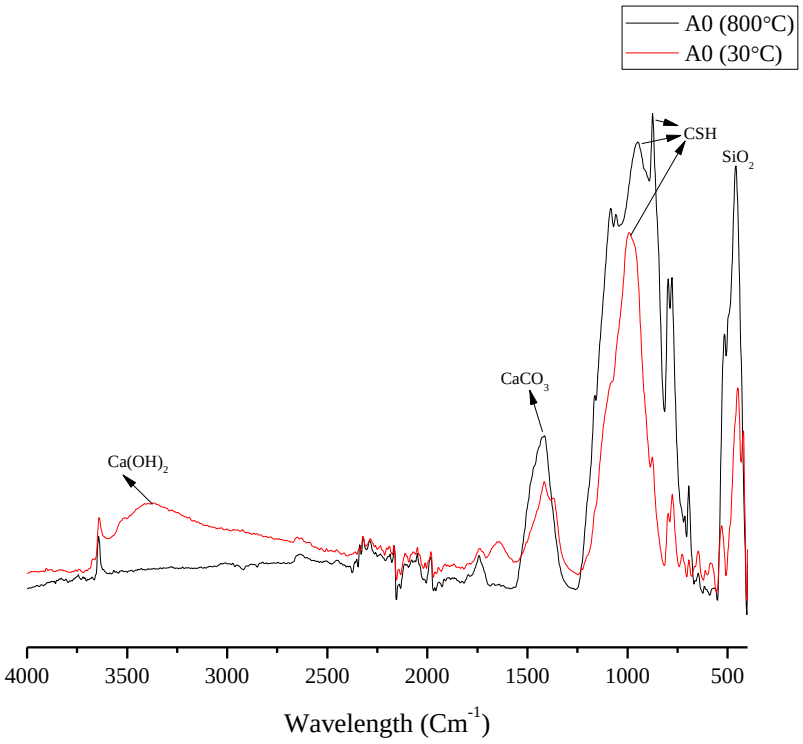

Fig. 9.5 FT-IR spectra of A0 concrete mix exposed to 800 °C

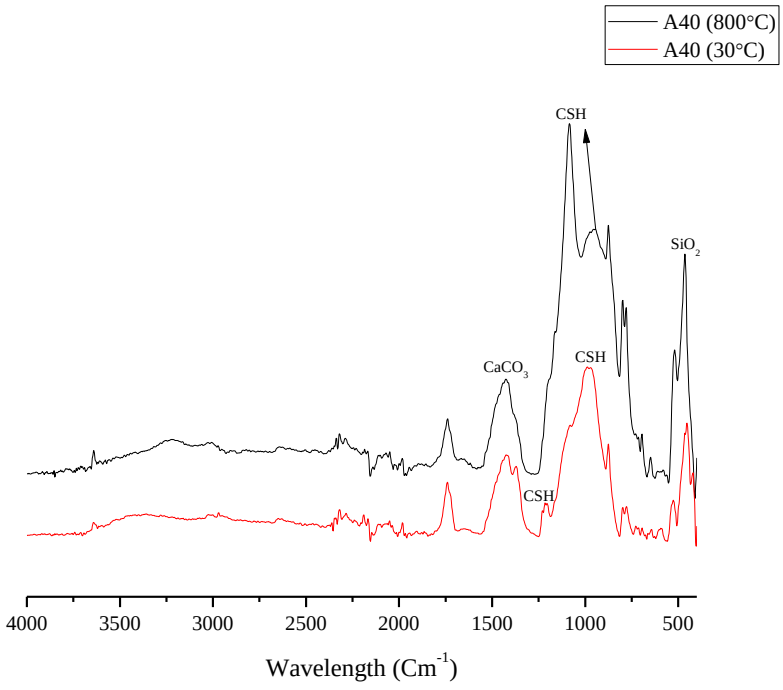

Fig. 9.6 FT-IR spectra of A40 concrete mix exposed to 800 °C

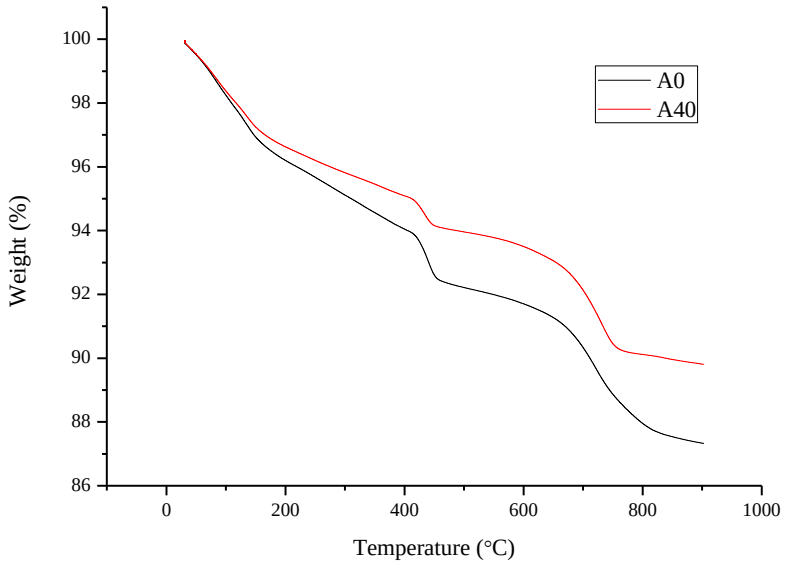

Fig. 9.7 TGA curves of A0 and A40 FBA concrete mixes

9.3.4 Photocatalytic property

The combination of cementitious materials with nano TiO_2 provide suitable development of functional photocatalytic products. The surface area covered by concrete and the adhesive properties provided by it make it an ideal matrices to incorporate photocatalyst material. Another advantage is the porous structure of concrete which allows for maximum degradation of target pollutants, thus facilitating the photocatalytic behaviour.

The photocatalysis (degradation of MB) of mixing based samples is shown in Fig. 9.3. The degradation of MB keeps on increasing with the exposure time. Initially, control concrete has higher degradation percentage than 40% FBA concrete. After 120 minutes of exposure, the degradation percentage of FBA concrete surpasses that of control concrete. The initial slower rate of photocatalytic degradation may be due to the white colour of FBA aggregate. The lighter coloured materials are strong in scattering of the light than absorption thus delaying photoctalysis. Similar observations were drawn by Guo and Poon (2013) on using different coloured pigments in photocatalytic concrete.

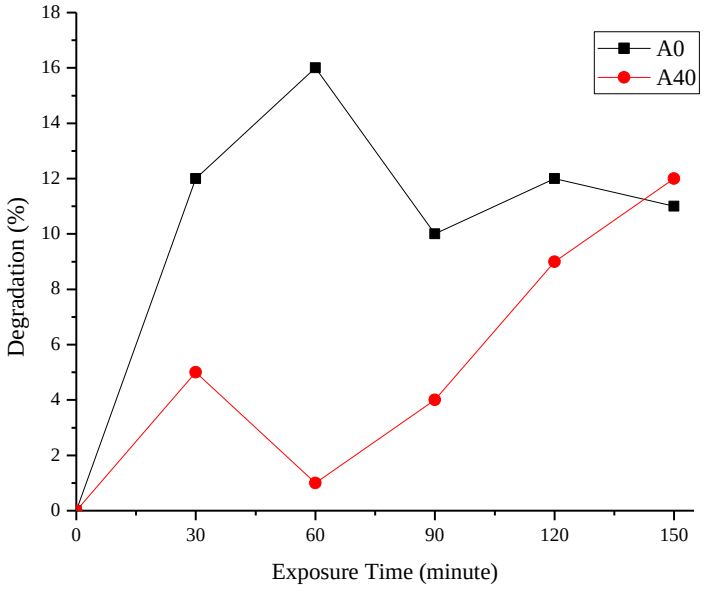

Fig. 9.8 Photocatalytic property of FBA concrete

9.3.5 Cost economics and environmental benefit

The cost for 1m^3 concrete A0 with 100% NFA and A40 with 40% FBA are given in Table 9.3. The cost calculations considers the prices of raw materials supplied in Jaipur for the year of 2016. The cost of 1 m^3 of A0 concrete with 100% NFA is Rs. 4038.7 (63.63 US$). The rate of 1 m^3 of A40 concrete with 40% partial replacement of NFA with FBA is Rs. 3763.5 (59.29 US$). The fine aggregate replacement indicates a benefit of 6.82%.

Although, the virgin raw material has superior quality advantages over alternative waste materials, the economic benefits of utilising waste materials will increase, as the tighter restrictions of government and judiciary for conservation of environment is leading to reduced mining and higher disposal cost of waste materials. The use of FBA in any form has multiple advantages, such as saving in disposal cost and preservation of environment from the negative effects of landfilling with FBA. It has been established from this study that FBA can safely be used as partial replacement of natural sand in concrete without affecting strength and durability aspects. Utilization of FBA will help in three ways (i) by reducing the cost of concrete

production; (ii) saving in carbon dioxide (CO_2) emissions to the atmosphere though it may be small and (iii) protection of environment from bad effect of disposal on open land.

Annual concrete production worldwide is nearly 25 billion Tonnes (World Business Council for Sustainable Development, 2009). Natural aggregate, cement and water are the main constituent resources used for production of concrete. Nearly 0.05-0.13 Tonnes CO_2 is released into the atmosphere on production of 1 Tonnes of concrete. (Obla, 2009). Accordingly, worldwide, 1.25 to 3.25 billion Tonnes of CO_2 is released to the atmosphere annually. The studies carried out so far for sustainable aspect of concrete focussed on the partial replacement of cement with supplementary cementing material in concrete but the impact of natural aggregate in terms of CO_2 emissions from concrete has not been considered significant. The use of virgin aggregate contributes only 1% of all greenhouse gas emissions from concrete (Obla, 2009). As such, the use of waste materials in place of natural aggregate did not attract the attentions of researchers. Till now, small efforts has been made in this direction. The use of waste materials such as stone dust, foundry sand, FBA etc. as replacement of fine aggregate in concrete not only prevents landfilling, but also provide environmental preservation, saving in concrete cost and disposal cost of these waste materials. Though it is considered that contribution of natural aggregate in concrete towards CO_2 emissions is small, but if quantity of concrete produced worldwide is considered, the total CO_2 emissions to the atmosphere annually vary from 12.5 to 32.5 million Tonnes. Considering 43:57 ratio of fine and coarse aggregate in concrete in this study, CO_2 emissions to the atmosphere range from 5.37 to 13.98 million Tonnes, annually from use of natural fine aggregate. In India, about 1500 million Tonnes of concrete is produced annually. Thereby 75 to 195 million Tonnes of CO_2 is released to the atmosphere annually. These emissions can be reduced by using FBA as partial replacement of NFA in concrete.

Table 9.3 Cost economics of FBA concrete mixes

Constituent material	Rate (per kg)	A0		A40	
		Quantity (kg)	Amount (Rs.)	Quantity (kg)	Amount (Rs.)
Cement	6.4	383	2451.2	383	2451.2
NFA	1	821	821	492.6	492.6
FBA	0.18	0	0	295.56	53.2008
Coarse aggregate	0.7	1095	766.5	1095	766.5
Total		**4038.7 (63.63 US$)**		**3763.5 (59.29 US$)**	

1 US$ = Rs. 63.48 (Indian)

9.4 CONCLUSIONS

As seen from different experimental programme that FBA concrete exhibits superior performance under impact loading and elevated temperature exposure and have higher photocatalytic characteristics than control concrete. Following conclusions are drawn:

1. The number of blows for failure and initial crack under drop weight test increases on incorporation of FBA.
2. The inclusion of FBA imparts higher energy absorption capacity in concrete specimens. The better ITZ characteristics of FBA concrete leads to higher energy absorbance.
3. FBA concrete displayed superior resistance to elevated temperature as compared to control concrete. Lower disintegration of CSH gel and better bond characteristics of hydration products can be the suitable parameters for such better resistance to elevated temperature.
4. The photocatalytic behaviour of FBA concrete is nearly equivalent to that of NFA concrete upto 90 minutes. For longer duration of exposure the FBA concrete displayed higher photocatalytic property than NFA.

5. FBA is a potential material to be used as partial replacement of NFA in concrete for achieving the sustainable construction. On recycling of FBA in concrete, reduction in CO_2 emissions as well as saving in disposal cost can be achieved.

CHAPTER 10

CONCLUSIONS

10.1 SUMMARY

In this study, the scope of ceramic waste specifically fine bone china ceramic waste for the elaboration of ceramic concrete has been studied and analysed from both mechanical and durability properties point of view. Different concrete mixes, compromising of varying percentage of FBA have been assessed for their fresh, mechanical, microstructural, chemical and durability performance. With this, the present investigation offers new solutions and contributions along with new information regarding the use of FBA in concrete mixes.

The obtained results of this thesis provide an insight that use of FBA not only lessen the use of natural resources, but also maintains the mechanical and durability characteristics as that of control concrete mixes containing NFA.

The specific and important conclusions of this investigation are listed below:

1. From the physical characteristics of FBA, it can be stated that FBA is a feasible material having shape and texture near similar to fine aggregates while having slightly higher water absorption. In addition, its adaptation also enhances the pozzolanic potential of concrete mix.
2. Concerning the workability of concrete mixes, it was observed that concrete mixes containing FBA required higher doses of superplasticiser to maintain the range of compaction factor.
3. The fresh density and air content of fresh FBA concrete reduced due to lower specific gravity of raw FBA. The higher amount of mixing water coupled with superplasticiser lowered the fresh state air content.

4. The use of FBA resulted in higher bleed out of mixing water which resulted in a network of capillaries after hardening.
5. The assessment of mechanical properties of concrete resulted in similar, and in some cases better performance when designed with FBA and compared to control concrete mix. The compressive strength observed at 180 days of curing showed higher values even for 100% FBA concrete mixes.
6. The split tensile strength, flexure strength and resistance to abrasion was higher for FBA concrete mixes due to better ITZ characteristics between aggregate and FBA mortar paste.
7. The microstructural images showed better hydration products along with lowered roughness values of ITZ in FBA concrete mixes than control concrete mix.
8. From the chemical assessment it can be concluded that incorporation of FBA in concrete mixes results in higher, better, denser and stable phases of hydration products.
9. The water based durability properties obtained from the investigation, it was observed that concrete mixes containing FBA recorded higher values of total voids, water absorption and depth of water penetration. Meanwhile, better microstructural characteristics of FBA concrete mixes restricted the ingress of chloride ions and maintained the dimensional stability of samples.
10. The presence of higher total voids in FBA concrete resulted in better resistance against freeze thaw conditions. The superior microstructure of FBA concrete yielded in better resistance against drying and wetting cycles as well as chloride penetration.
11. The better resistance against chloride ingress resulted in reduced probability for initiation of corrosion.

12. For chemical attack, FBA concrete displayed much higher resistance against corrosive action. The influence of aggressive compounds and lowered pH of concrete on chemical transformations of hydration products is also fairly restricted in FBA concrete mixes..
13. From the impact loading based properties obtained in this investigation, it is observed that FBA concrete exhibited slightly better performance when compared to control concrete in terms of energy absorption capacity.
14. The residual properties of FBA concrete after exposure to elevated temperature are better than that of control concrete. The better thermal durability of raw FBA aggregate may be one of the central factors for such properties.
15. The photocatalytic behaviour of FBA concrete is higher than that of control concrete on longer duration of exposure.
16. Sustainable concrete produced with FBA makes positive impact on environment by reducing CO_2 emissions. Sustainable concrete made with FBA as NFA replacement is economical when compared to conventional concrete.

Considering the performance of FBA concrete mixes under various conditions and environments, the applicability of such concrete mix is an important part of this investigation. For structural use, upto 40% FBA can be used to replace NFA to obtain superior strength based property and near similar water durability properties. For underwater construction such as piers, bridges etc. upto 100% FBA can be used in concrete mixes to be durable against chemical ingress. For non-structural applications, such as pavement blocks, tiles and refractory lining upto 40% FBA can be suitably utilised in concrete mixes.

CHAPTER 11

FUTURE SCOPE

The present study has elucidated some of the knowledge gaps regarding utilisation of fine bone china ceramic waste as fine aggregate, specifically regarding its influence on microstructure and durability properties of concrete. However, there are many potential aspects of the ceramic waste and the issues associated to be solved and investigated, some of which are summarized below.

To the best knowledge of author, no study is available on the utilisation of fine bone china ceramic waste as cement waste. A small pilot study was done by the author to highlight the potential of such study. Fine bone china ceramic waste was crushed into cement form (90 micron sieve passing) and was used to replace cement upto 30%. The mix composition details are presented in Table 11.1 and results of few concrete properties investigated are presented in Tables 11.2-11.3.

Table 11.1 Mix composition

Mix	**Cement (kg/m^3)**	**Fine bone china powder (kg/m^3)**	**Sand (kg/m^3)**	**Coarse Aggregate (kg/m^3)**	**Water (kg/m^3)**	**Admixture (%)**
CC	383	0 (0%)	813	1095	134.05	0.5
CC5	363.85	19.15 (5%)	813	1095	134.05	0.5
CC10	344.7	38.3 (10%)	813	1095	134.05	0.5
CC15	325.55	57.45 (15%)	813	1095	134.05	0.5
CC20	306.4	76.6 (20%)	813	1095	134.05	0.5
CC25	287.25	95.75 (25%)	813	1095	134.05	0.6
CC30	268.1	114.9 (30%)	813	1095	134.05	0.6

Table 11.2 Results of investigated properties

Mix	28 day Compressive strength (MPa)	Apparent density (Mg/m^3)	Bulk density (Mg/m^3)	Voids (%)	Water absorption (%)
CC	42.33	2.581	2.467	7.22	3.01
CC5	43.33	2.588	2.464	6.17	2.59
CC10	41	2.513	2.431	5.45	2.29
CC15	43.33	2.587	2.461	5.51	2.29
CC20	40	2.641	2.522	5.21	2.24
CC25	42	2.609	2.505	5.27	2.66
CC30	40	2.556	2.476	5.19	2.14

Table 11.3 Hydration of OPC and ceramic cement

CC			
Phases	**Total amount [mol.]**	**Volume [cm^3]**	**Mass [g]**
CSHQ	0.425	29.685	66.905
SO4_OH_AFm	0.0089	2.777	5.595
Portlandite	0.398	13.176	29.529
CC30			
Phases	**Total amount [mol.]**	**Volume [cm^3]**	**Mass [g]**
CSHQ	0.500	34.47	77.437
SO4_OH_AFm	0.017	12.27	21.786
Portlandite	0.16	5.29	11.86

Apart from the properties investigated above the detailed mechanical properties, durability characteristics and the environmental properties along with the economic concerns for cement replacement can be studied.

The curvature and thinness of fine bone china ceramic waste can be a weak point as utilisation in 18 mm or 20 mm coarse aggregate. For self-compacting concrete, the shape and size of 8-10 mm coarse aggregate can be achieved for fine bone china ceramic waste. The fresh state, mechanical, durability and microstructural properties of such self-compacting concrete can be investigated.

For fine aggregate replacement the issue of high water permeability can be tackled by utilising various fillers to counter the roughness and angularity of FBA.

The scope of utilising fine bone china ceramic waste as supplementary cementitious material or fine aggregate in recycled aggregate concrete.

The behaviour of FBA with various types of cement such as fly ash Portland cement, slag Portland cement, sulfo aluminate cement, magnesium oxysulphate cement, magnesium phosphate cement, high alumina cement, polymer cement and nano cement can be studied and investigated to provide a comprehensive study on the ceramic waste aggregate.

REFERENCES

Acharya, P. K., and Patro, S. K. (2016). "Strength, sorption and abrasion characteristics of concrete using ferrochrome ash (FCA) and lime as partial replacement of cement." *Cement and Concrete Composites*, 74, 16-25.

ACI 544.2R-89 (1999). "Measurement of properties of fiber reinforced concrete." ACI, West Conshohocken, PA.

Adak, D., Sarkar, M., and Mandal, S. (2017). "Structural performance of nano-silica modified fly-ash based geopolymer concrete." *Construction and Building Materials*, 135, 430-439.

Adamson, M., Razmjoo, A., and Poursaee, A. (2015). "Durability of concrete incorporating crushed brick as coarse aggregate." *Construction and Building Materials*, 94(Supplement C), 426-432.

AIGMF (2011). "OVERVIEW ON CERAMIC & GLASS TABLEWARE." The All India Glass Manufacturers' Federation, New Delhi, India.

Alderete, N., Villagrán, Y., Mignon, A., Snoeck, D., and De Belie, N. (2017). "Pore structure description of mortars containing ground granulated blast-furnace slag by mercury intrusion porosimetry and dynamic vapour sorption." *Construction and Building Materials*, 145(Supplement C), 157-165.

Alves, A. V., Vieira, T. F., de Brito, J., and Correia, J. R. (2014). "Mechanical properties of structural concrete with fine recycled ceramic aggregates." *Construction and Building Materials*, 64, 103-113.

Andrade, C. (1993). "Calculation of chloride diffusion coefficients in concrete from ionic migration measurements." *Cement and Concrete Research*, 23(3), 724-742.

Ardalan, R. B., Jamshidi, N., Arabameri, H., Joshaghani, A., Mehrinejad, M., and Sharafi, P. (2017). "Enhancing the permeability and abrasion resistance of concrete using

colloidal nano-SiO2 oxide and spraying nanosilicon practices." *Construction and Building Materials*, 146, 128-135.

Ariffin, M. A. M., Bhutta, M. A. R., Hussin, M. W., Mohd Tahir, M., and Aziah, N. (2013). "Sulfuric acid resistance of blended ash geopolymer concrete." *Construction and Building Materials*, 43, 80-86.

ASTM C157 (2017). "Standard Test Method for Length Change of Hardened Hydraulic-Cement Mortar and Concrete." ASTM International, West Conshohocken, PA.

ASTM C232 (2014). "Standard Test Method for Bleeding of Concrete." ASTM International, West Conshohocken, PA.

ASTM C267 (2012). "Standard Test Methods for Chemical Resistance of Mortars, Grouts, and Monolithic Surfacings and Polymer Concretes." ASTM International, West Conshohocken, PA.

ASTM C311 (2016). "Standard Test Methods for Sampling and Testing Fly Ash or Natural Pozzolans for Use in Portland-Cement Concrete." ASTM International, West Conshohocken, PA.

ASTM C469 (2014). "Standard Test Method for Static Modulus of Elasticity and Poisson's Ratio of Concrete in Compression." ASTM International, West Conshohocken, PA.

ASTM C642 (2013). "Standard Test Method for Density, Absorption, and Voids in Hardened Concrete." ASTM International, West Conshohocken, PA.

ASTM C666 (2015). "Standard Test Method for Resistance of Concrete to Rapid Freezing and Thawing ", ASTM International,, West Conshohocken, PA.

ASTM C672 (2012). "Standard Test Method for Scaling Resistance of Concrete Surfaces Exposed to Deicing Chemicals." ASTM International, West Conshohocken, PA.

ASTM C876 (2015). "Standard Test Method for Corrosion Potentials of Uncoated Reinforcing Steel in Concrete ", ASTM International, West Conshohocken, PA.

ASTM C1585 (2013). "Standard Test Method for Measurement of Rate of Absorption of Water by Hydraulic-Cement Concretes." ASTM International, West Conshohocken, PA.

ASTM G109 (2013). "Standard Test Method for Determining Effects of Chemical Admixtures on Corrosion of Embedded Steel Reinforcement in Concrete Exposed to Chloride Environments." ASTM International, West Conshohocken, PA.

Azdarpour, A., Asadullah, M., Junin, R., Manan, M., Hamidi, H., and Mohammadian, E. (2014). "Direct carbonation of red gypsum to produce solid carbonates." *Fuel Processing Technology*, 126, 429-434.

Barbhuiya, S., Chow, P., and Memon, S. (2015). "Microstructure, hydration and nanomechanical properties of concrete containing metakaolin." *Construction and Building Materials*, 95(Supplement C), 696-702.

Binici, H. (2007). "Effect of crushed ceramic and basaltic pumice as fine aggregates on concrete mortars properties." *Construction and Building Materials*, 21(6), 1191-1197.

BIS 383 (2016). "Coarse and Fine Aggregate for Concrete - Specification." Bureau of Indian Standards, New Delhi, India.

BIS 516 (1959) [Reaffirmed 2013]. "Methods of tests for strength of concrete." Bureau of Indian Standards, New Delhi, India.

BIS 1199 (1959). "Methods of sampling and analysis of concrete." Bureau of Indian Standards, New Delhi, India.

BIS 1237 (2012). "Specification for Cement Concrete Flooring Tiles ", Bureau of Indian Standards, New Delhi, India.

BIS 2386-3 (1963) [Reaffirmed 2016]. "Methods of test for aggregates for concrete, Part 3: Specific gravity, density, voids, absorption and bulking." Bureau of Indian Standards, New Delhi, India.

BIS 5816 (1999). [Reaffirmed 2004] "Splitting tensile strength of concrete - method of test." Bureau of Indian Standards, New Delhi, India.

BIS 10262 (2009). "Concrete mix proportioning- Guidelines." Bureau of Indian Standards, New Delhi.

BIS 8112 (2013). "Ordinary Portland cement, 43 Grade-Specification." Bureau of Indian Standards, New Delhi.

BS-EN 196-5 (2011). "Methods of testing cement. Part 5: pozzolanicity test for pozzolanic cement."

Bulatović, V., Melešev, M., Radeka, M., Radonjanin, V., and Lukić, I. (2017). "Evaluation of sulfate resistance of concrete with recycled and natural aggregates." *Construction and Building Materials*, 152, 614-631.

Cachim, P. B. (2009). "Mechanical properties of brick aggregate concrete." *Construction and Building Materials*, 23(3), 1292-1297.

CGCRI (2012). "Annual Report 2011-12." Central Glass and Ceramic Research Institute, Kolkata, India.

Chollet, M., and Horgnies, M. (2011). "Analyses of the surfaces of concrete by Raman and FT-IR spectroscopies: comparative study of hardened samples after demoulding and after organic post-treatment." *Surface and Interface Analysis*, 43(3), 714-725.

CII (2009). "Ceramics Industry in India: A Trade Perspective." Confederation of Indian Industry, New Delhi, India.

Cook, R. L., and Andrews, A. I. (1945). "Chemical Durability of Porcelain Enamels." *Journal of the American Ceramic Society*, 28(9), 229-256.

Correia, J. R., de Brito, J., and Pereira, A. S. (2006). "Effects on concrete durability of using recycled ceramic aggregates." *Materials and Structures*, 39(2), 169-177.

DIN1048 (1991). "Testing Concrete: Testing of Hardened Concrete Specimens Prepared in Mould, Part 5."Deutsches Institut fur Normung,Germany.

DIPP (2011). "Annual report 2010-11 ", Department of Industrial policy and promotion, New Delhi, India.

Etxeberria, M., and Vegas, I. (2015). "Effect of fine ceramic recycled aggregate (RA) and mixed fine RA on hardened properties of concrete." *Magazine of Concrete Research*, 67(12), 645-655.

Florea, M. V. A., and Brouwers, H. J. H. (2012). "Chloride binding related to hydration products." *Cement and Concrete Research*, 42(2), 282-290.

Ganjian, E., Khorami, M., and Maghsoudi, A. A. (2009). "Scrap-tyre-rubber replacement for aggregate and filler in concrete." *Construction and Building Materials*, 23(5), 1828-1836.

Gomes, M., and de Brito, J. (2009). "Structural concrete with incorporation of coarse recycled concrete and ceramic aggregates: durability performance." *Materials and Structures*, 42(5), 663-675.

Gonzalez-Corominas, A., and Etxeberria, M. (2014). "Properties of high performance concrete made with recycled fine ceramic and coarse mixed aggregates." *Construction and Building Materials*, 68, 618-626.

González, J. S., Gayarre, F. L., Pérez, C. L.-C., Ros, P. S., and López, M. A. S. (2017). "Influence of recycled brick aggregates on properties of structural concrete for manufacturing precast prestressed beams." *Construction and Building Materials*, 149(Supplement C), 507-514.

Guo, M.-Z., and Poon, C.-S. (2013). "Photocatalytic NO removal of concrete surface layers intermixed with TiO2." *Building and Environment*, 70(Supplement C), 102-109.

Halicka, A., Ogrodnik, P., and Zegardlo, B. (2013). "Using ceramic sanitary ware waste as concrete aggregate." *Construction and Building Materials*, 48, 295-305.

Higashiyama, H., Sappakittipakorn, M., Mizukoshi, M., and Takahashi, O. (2014). "Efficiency of ground granulated blast-furnace slag replacement in ceramic waste aggregate mortar." *Cement and Concrete Composites*, 49, 43-49.

Higashiyama, H., Yagishita, F., Sano, M., and Takahashi, O. (2012). "Compressive strength and resistance to chloride penetration of mortars using ceramic waste as fine aggregate." *Construction and Building Materials*, 26(1), 96-101.

Johansen, V., Thaulow, N., and Skalny, J. (1993). "Simultaneous presence of alkali — silica gel and ettringite in concrete." *Advances in Cement Research*, 5(17), 23-29.

Kannan, D. M., Aboubakr, S. H., El-Dieb, A. S., and Reda Taha, M. M. (2017). "High performance concrete incorporating ceramic waste powder as large partial replacement of Portland cement." *Construction and Building Materials*, 144, 35-41.

Kotoh, K., Miura, K., Nishikawa, M., Irube, M., and Muta, M. (1990). "Measurement of Tritiated Moisture in Gas Stream by Collection Method Using P2O5 Desiccant." *Journal of Nuclear Science and Technology*, 27(10), 944-949.

Lavat, A. E., Trezza, M. A., and Poggi, M. (2009). "Characterization of ceramic roof tile wastes as pozzolanic admixture." *Waste management*, 29(5), 1666-1674.

Li, W., Xiao, J., Kawashima, S., Shekhawat, G. S., and Shah, S. P. (2015). "Experimental Investigation on Quantitative Nanomechanical Properties of Cement Paste." *ACI Materials Journal*, 112(2).

Li, W. G., Xiao, J. Z., Shi, C. J., and Shah, S. P. (2014). "Nanomechanical Properties of Cement Paste: Nanoindentation, Modulus Mapping and Peak-Force Qnm." *Design, Performance and Use of Self-Consolidating Concrete (Scc 2014)*, 93, 235-242.

Lodeiro, I. G., Macphee, D., Palomo, A., and Fernández-Jiménez, A. (2009). "Effect of alkalis on fresh C–S–H gels. FTIR analysis." *Cement and Concrete Research*, 39(3), 147-153.

Medina, C., de Rojas, M. I. S., and Frias, M. (2012). "Reuse of sanitary ceramic wastes as coarse aggregate in eco-efficient concretes." *Cement & Concrete Composites*, 34(1), 48-54.

Medina, C., Frias, M., de Rojas, M. I. S., Thomas, C., and Polanco, J. A. (2012). "Gas permeability in concrete containing recycled ceramic sanitary ware aggregate." *Construction and Building Materials*, 37, 597-605.

Medina, C., Sánchez de Rojas, M. I., and Frías, M. (2013). "Properties of recycled ceramic aggregate concretes: Water resistance." *Cement and Concrete Composites*, 40, 21-29.

Medina, C., Sánchez de Rojas, M. I., Thomas, C., Polanco, J. A., and Frías, M. (2016). "Durability of recycled concrete made with recycled ceramic sanitary ware aggregate. Inter-indicator relationships." *Construction and Building Materials*, 105, 480-486.

Mollah, M., Yu, W., Schennach, R., and Cocke, D. L. (2000). "A Fourier transform infrared spectroscopic investigation of the early hydration of Portland cement and the influence of sodium lignosulfonate." *Cement and concrete research*, 30(2), 267-273.

Muller, A. C. A., Scrivener, K. L., Skibsted, J., Gajewicz, A. M., and McDonald, P. J. (2015). "Influence of silica fume on the microstructure of cement pastes: New insights from 1H NMR relaxometry." *Cement and Concrete Research*, 74(Supplement C), 116-125.

Nyunin, G. I. (1984). "Means of increasing the acid resistance of porcelain and earthenware." *Glass and Ceramics*, 41(5), 209-211.

Obla, K. H. (2009). "What is Green Concrete?" *The Indian Concrete Journal*, 24, 26-28.

Oltulu, M., and Şahin, R. (2014). "Pore structure analysis of hardened cement mortars containing silica fume and different nano-powders." *Construction and Building Materials*, 53(Supplement C), 658-664.

Pacheco-Torgal, F., and Jalali, S. (2010). "Reusing ceramic wastes in concrete." *Construction and Building Materials*, 24(5), 832-838.

Papadakis, V. G., Pedersen, E. J., and Lindgreen, H. (1999). "An AFM-SEM investigation of the effect of silica fume and fly ash on cement paste microstructure." *Journal of Materials Science*, 34(4), 683-690.

Peled, A., Castro, J., and Weiss, W. J. (2013). "Atomic force and lateral force microscopy (AFM and LFM) examinations of cement and cement hydration products." *Cement & Concrete Composites*, 36, 48-55.

Pérez-Moreno, S. M., Gázquez, M. J., and Bolívar, J. P. (2015). "CO2 sequestration by indirect carbonation of artificial gypsum generated in the manufacture of titanium dioxide pigments." *Chemical Engineering Journal*, 262, 737-746.

Rashad, A. M. (2013). "A preliminary study on the effect of fine aggregate replacement with metakaolin on strength and abrasion resistance of concrete." *Construction and Building Materials*, 44, 487-495.

Rashid, K., Razzaq, A., Ahmad, M., Rashid, T., and Tariq, S. (2017). "Experimental and analytical selection of sustainable recycled concrete with ceramic waste aggregate." *Construction and Building Materials*, 154(Supplement C), 829-840.

Rubio, F., Rubio, J., and Oteo, J. (1997). "A DSC study of the drying process of TEOS derived wet silica gels." *Thermochimica acta*, 307(1), 51-56.

Senthamarai, R., and Manoharan, P. D. (2005). "Concrete with ceramic waste aggregate." *Cement & Concrete Composites*, 27(9-10), 910-913.

Senthamarai, R. M., Manoharan, P. D., and Gobinath, D. (2011). "Concrete made from ceramic industry waste: Durability properties." *Construction and Building Materials*, 25(5), 2413-2419.

Subaşı, S., Öztürk, H., and Emiroğlu, M. (2017). "Utilizing of waste ceramic powders as filler material in self-consolidating concrete." *Construction and Building Materials*, 149(Supplement C), 567-574.

Suryavanshi, A. K., Scantlebury, J. D., and Lyon, S. B. (1996). "Mechanism of Friedel's salt formation in cements rich in tri-calcium aluminate." *Cement and Concrete Research*, 26(5), 717-727.

Szyszka, A., Wośko, M., Szymański, T., and Paszkiewicz, R. (2016). "Surface topography analysis with application of roughness area dependence method." *Ultramicroscopy*, 170, 77-85.

Powers T.C., Hayes J.C. and Mann H.M. (1954). "Permeability of Portland Cement Paste." Portland Cement Association, Skokie, Illinois.

Taha, M. R., Soliman, E., Sheyka, M., Reinhardt, A., and Al-Haik, M. (2010). "Fracture toughness of hydrated cement paste using nanoindentation." *Fracture Mechanics of Concrete and Concrete Structures-Recent Advances in Fracture Mechanics of Concrete*.

Teir, S., Eloneva, S., Fogelholm, C.-J., and Zevenhoven, R. (2006). "Stability of calcium carbonate and magnesium carbonate in rainwater and nitric acid solutions." *Energy Conversion and Management*, 47(18), 3059-3068.

Thomas, J. J., Jennings, H. M., and Allen, A. J. (1999). "The surface area of hardened cement paste as measured by various techniques." *Concrete Science and Engineering*, 1(1), 45-64.

Thomas, M., Folliard, K., Drimalas, T., and Ramlochan, T. (2008). "Diagnosing delayed ettringite formation in concrete structures." *Cement and concrete research*, 38(6), 841-847.

Vieira, T., Alves, A., de Brito, J., Correia, J. R., and Silva, R. V. (2016). "Durability-related performance of concrete containing fine recycled aggregates from crushed bricks and sanitary ware." *Materials & Design*, 90, 767-776.

Villain, G., Thiery, M., and Platret, G. (2007). "Measurement methods of carbonation profiles in concrete: thermogravimetry, chemical analysis and gammadensimetry." *Cement and Concrete Research*, 37(8), 1182-1192.

Wang, L., He, Z., and Dong, Y. "Investigation of the Pozzolanic Reaction in Silica Fume-Cement Paste by 29Si MAS NMR." *Proc., Advanced Materials Research*, Trans Tech Publ, 2774-2777.

Wang, X.-Y., and Park, K.-B. (2015). "Analysis of compressive strength development of concrete containing high volume fly ash." *Construction and Building Materials*, 98(Supplement C), 810-819.

Wang, Z.-j., Wang, Q., and Wei, Y.-f. (2012). "Effects of mineral admixtures and superplasticizers on micro hardness of aggregate-paste interface in cement concrete." *Journal of Shanghai Jiaotong University (Science)*, 17(5), 629-634.

World Business Council for Sustainable Development, 2009. Cement Industry Energy and CO2 Performance: Getting the Numbers Right, p. 43. http://www.wbcsd.org/DocRoot/02fH0Bj3tZNV1RvmG2mb/CSIGNRReportfinal.pdf

Xiao, J. Z., Li, W. G., Sun, Z. H., Lange, D. A., and Shah, S. P. (2013). "Properties of interfacial transition zones in recycled aggregate concrete tested by nanoindentation." *Cement & Concrete Composites*, 37, 276-292.

Zanni, H., Cheyrezy, M., Maret, V., Philippot, S., and Nieto, P. (1996). "Investigation of hydration and pozzolanic reaction in Reactive Powder Concrete (RPC) using 29Si NMR." *Cement and Concrete Research*, 26(1), 93-100.

Zegardło, B., Szeląg, M., and Ogrodnik, P. (2016). "Ultra-high strength concrete made with recycled aggregate from sanitary ceramic wastes–The method of production and the interfacial transition zone." *Construction and Building Materials*, 122, 736-742.

Appendix A

OPC Cement Technical Data Sheet

BINANI CEMENT LIMITED

(AN ISO 9001, 14001 & OHSAS 18001 CERTIFIED CO.)

BINANIGRAM, PINDWARA

R/15-21

TEST CERTIFICATE

Ordinary Portland Cement "43 GRADE"

IS : 8112

CM/L-8214190

PARTICULARS	TEST RESULTS	REQUIREMENTS AS PER IS-8112: 2013
Chemical Requirements :		
1.Lime Saturation Factor $\frac{CaO-0.7SO_3}{(2.8SiO_2+1.2Al_2O_3+0.65Fe_2O_3)}$	0.97	0.66 to 1.02
2. Ratio of % of Alumina to that of Iron Oxide $(\%Al_2O_3/\%Fe_2O_3)$	1.76	0.66 min
3. Insoluble Residue (% by Mass)	2.62	4.00 max
4. Magnesia (% by Mass)	1.84	6.00 max
5. Sulphuric Anhydride (% by Mass)	2.06	3.5 max
6. Total Loss on Ignition(%)	2.47	5.00 max
7. Total Chlorides (%)	0.020	0.10 max
Physical Requirements		
1. Consistency (%)	28.25	
2. Fineness (m^2/ Kg)	298	225 min.
3. Setting Time (Minutes)		
(a) Initial	125	30 min
(b) Final	175	600 max.
4. Soundness		
(a) Le Chatelier (mm)	1.0	10.0 max
(b) Autoclave (%)	0.11	0.8 max
5. Compressive Strength (MPa)		
(a) 72 ± 1 h (3 days)	37	23 min
(b) 168 ± 2 h (7 days)	48	33 min
(c) 672 ± 4 h (28 days)	57	43 min 58 max

ABOVE CEMENT COMPLIES WITH THE REQUIREMENTS OF IS-8112 : 2013 FOR ORDINARY PORTLAND CEMENT "43 GRADE"

DATE OF DESPATCH : 01/04/2008

WEEK NO. : 14

CHECKED BY : .....

BINANI CEMENT LIMITED

Authorised Signatory

43

Appendix B

Admixture Technical Data Sheet

Auramix 400

constructive solutions

Advanced Low Viscosity High Performance Superplasticiser, based on Polycarboxylic technology

Uses

Auramix 400 is a high performance superplasticiser intended for applications where high water reduction and long workability retention are required, and it has been developed for use in:

- Self-compacting concrete,
- Pumped concrete,
- Concrete requiring long workability retention,
- High performance concrete.

Standard Compliance

Auramix 400 complies with IS:9103-1999(2007). It also complies with ASTM C494 Type G depending on the dosage used.

Advantages

- Low viscosity suitable for pumping of different grades of concrete to higher floors
- Higher E modulus
- Improved adhesion to reinforcing and prestressing steel
- Better resistance to carbonation
- Lower permeability
- Better resistance to aggressive atmospheric conditions
- Reduced shrinkage and creep
- Increased durability

Description

Auramix 400 is a unique combination of the latest generation superplasticisers, based on a polycarboxylic ether polymer with long lateral chains. This greatly improves cement dispersion. At the start of the mixing process an electrostatic dispersion occurs but the cement particle's capacity to separate and disperse. This mechanism considerably reduces the water demand in flowable concrete.

Auramix 400 combines the properties of water reduction and workability retention. It allows the production of high performance concrete and/or concrete with high workability.

Technical support

Fosroc provides a technical advisory service for on-site assistance and advice on mix design, admixture selection, evaluation trials and dispensing equipment.

Properties

Appearance	:	Light yellow coloured liquid
pH	:	Minimum 6.0 *
Volumetric mass @ 20° C	:	1.09 kg/litre
Chloride content	:	Nil to IS:456 *
Alkali content	:	Typically less than 1.5 g Na_2O equivalent / litre of admixture.

* The uniformity parameters like specific gravity, pH, chloride content etc. will vary for specific customer requirements and mix design. Please refer our MTC issued for specific product configuration for measuring our product parameters that will be constantly and consistently administered.

Dosage

The optimum dosage of Auramix 400 to meet specific requirements should always be determined by trials using the materials and conditions that will be experienced in use. The normal dosage range is between 0.5 to 3.0 ltrs/100 kg of cementitious material.

Use at other dosages

Dosage outside the normal range quoted above can be used to meet particular mix requirements. Contact Fosroc for advice in these cases

Effects of overdosing

Overdosage may cause delay in the setting time and segregation.

Estimating

Packaging

Auramix 400 is available in 200kg and 250kg drums and bulk tanker.

Appendix C

Set of LFM images taken for the study

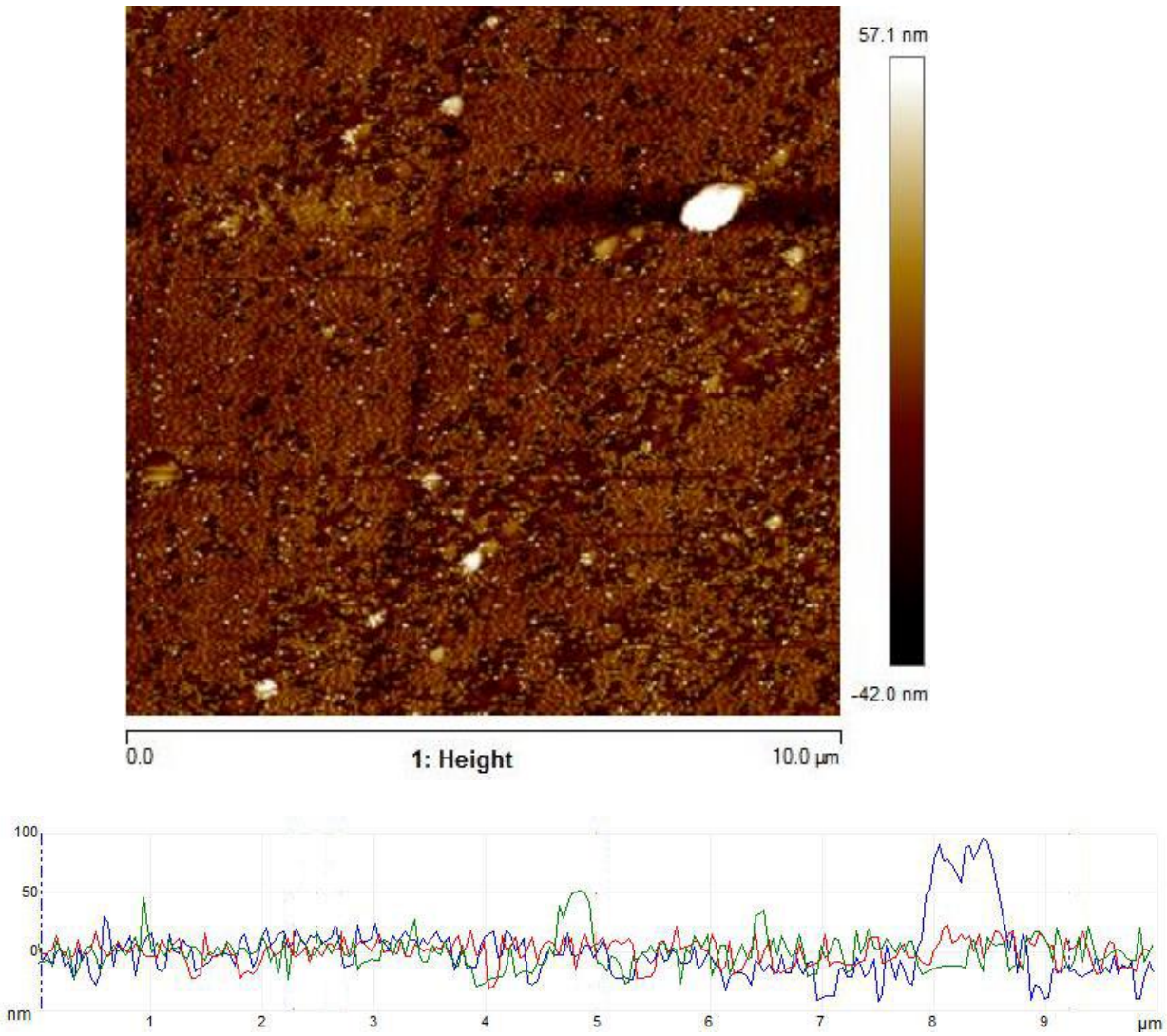

Fig. C1. Surface topography with roughness distribution of A0 sample ITZ at 10 µm scan range

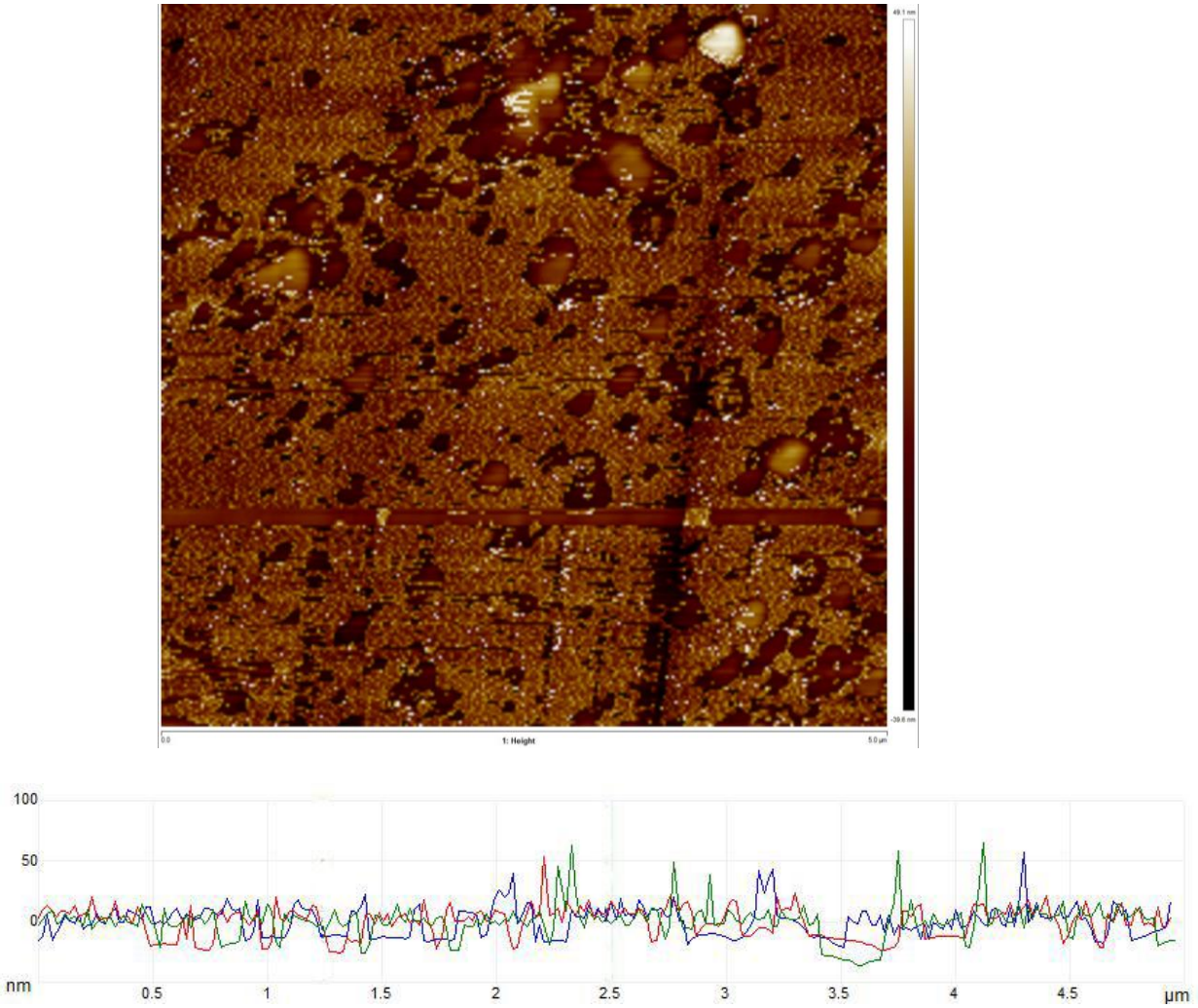

Fig. C2. Surface topography with roughness distribution of A0 sample ITZ at 5 µm scan range

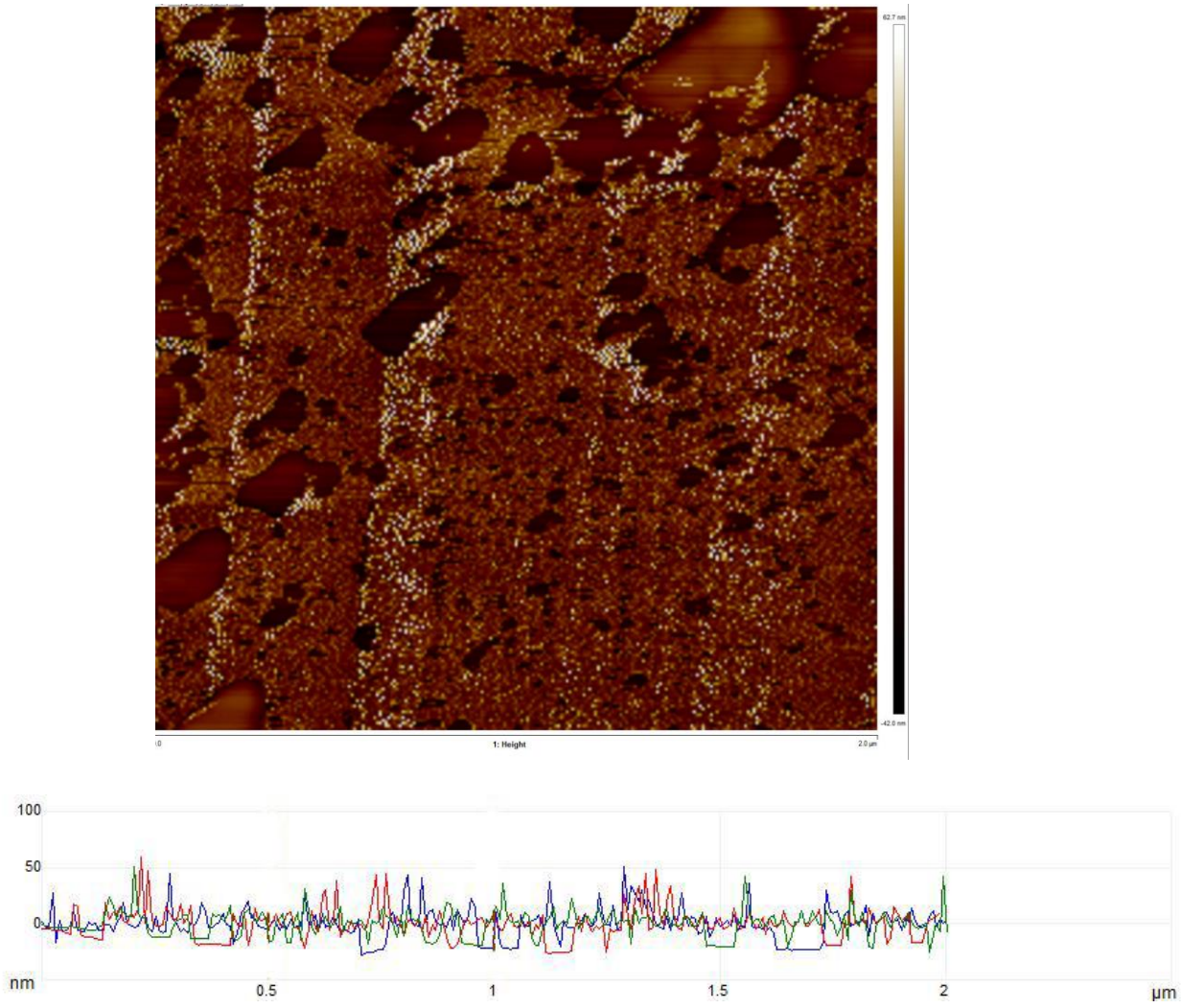

Fig. C3. Surface topography with roughness distribution of A0 sample ITZ at 2 µm scan range

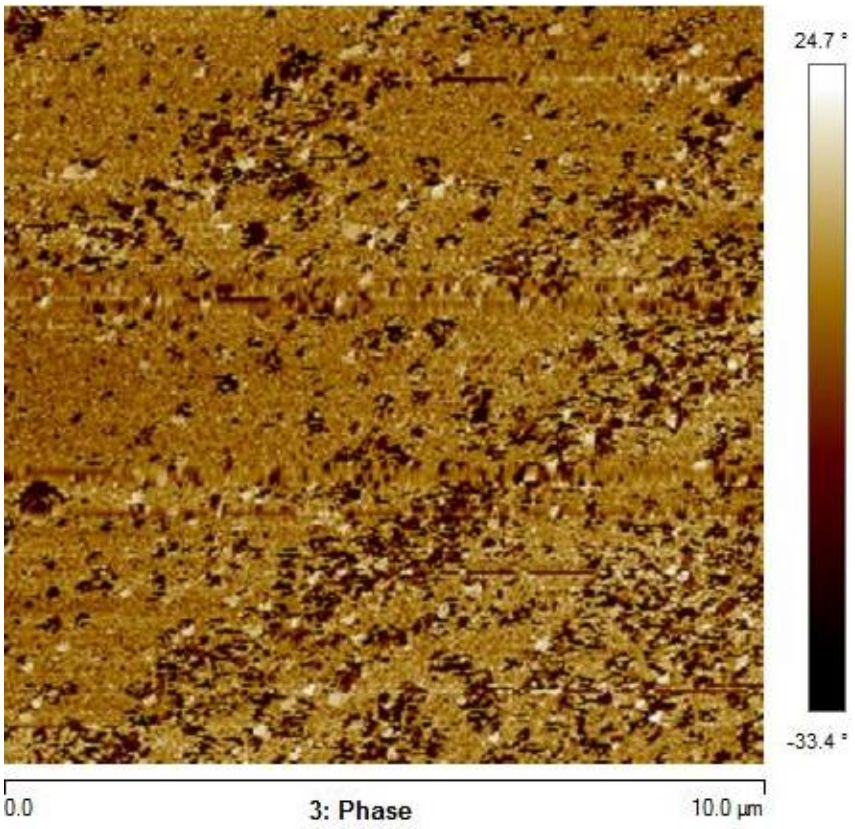

Fig. C4. Phase characteristics with grain distribution of A0 sample ITZ at 10 µm scan range

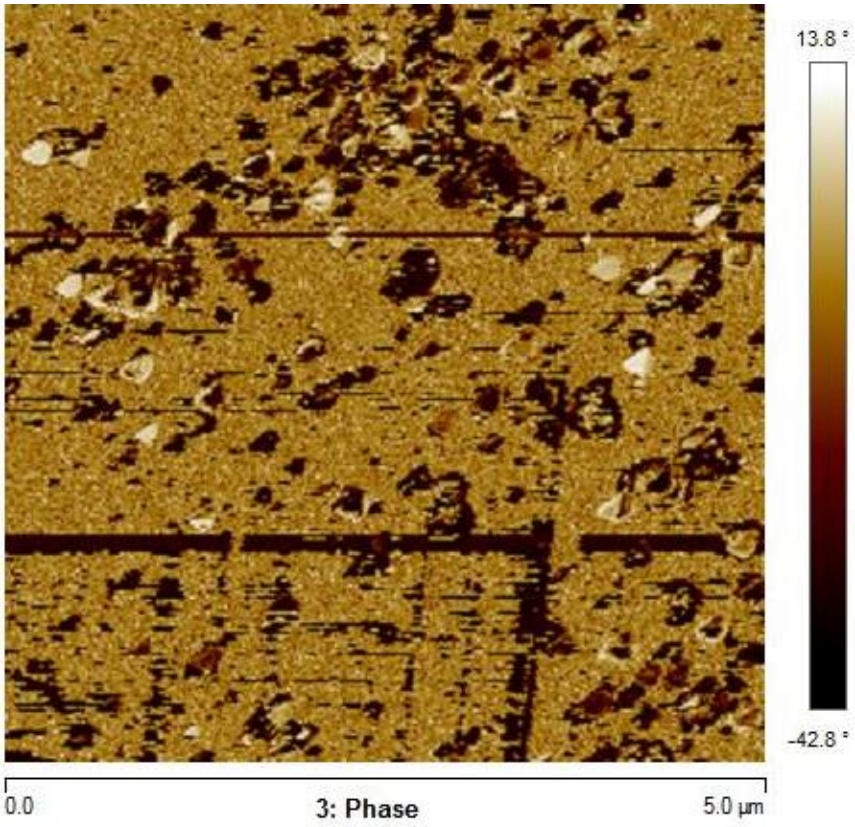

Fig. C5. Phase characteristics with grain distribution of A0 sample ITZ at 5 µm scan range

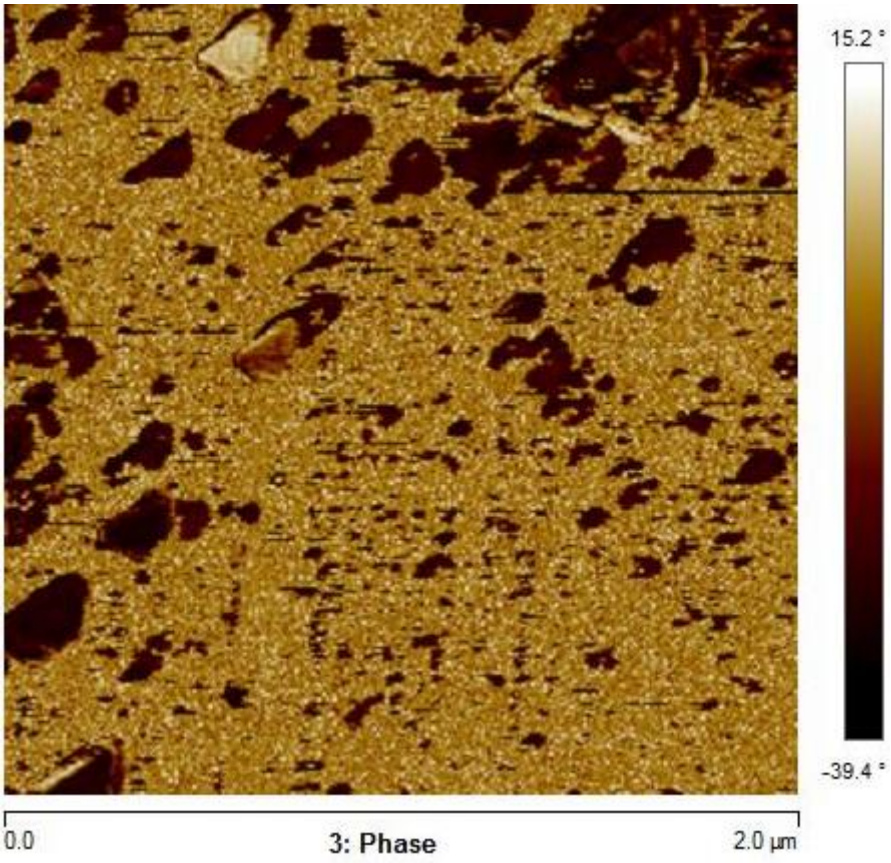

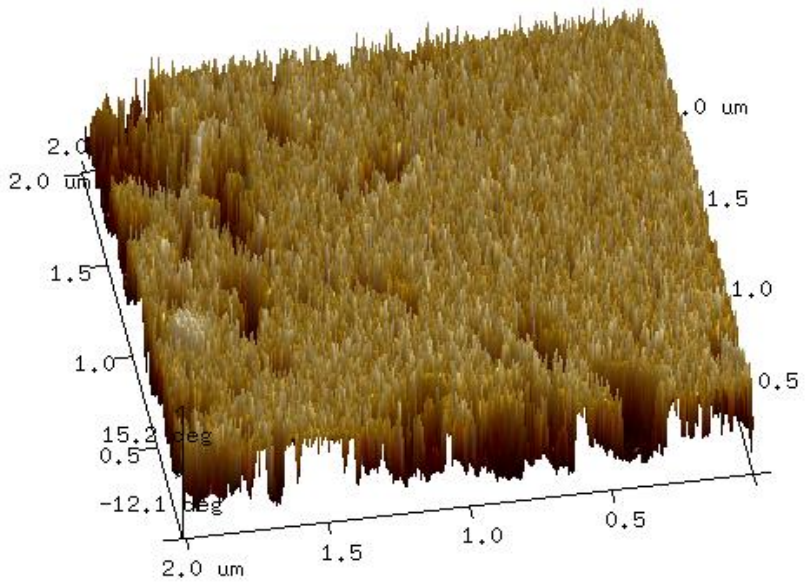

Fig. C6. Phase characteristics with grain distribution of A0 sample ITZ at 2 µm scan range

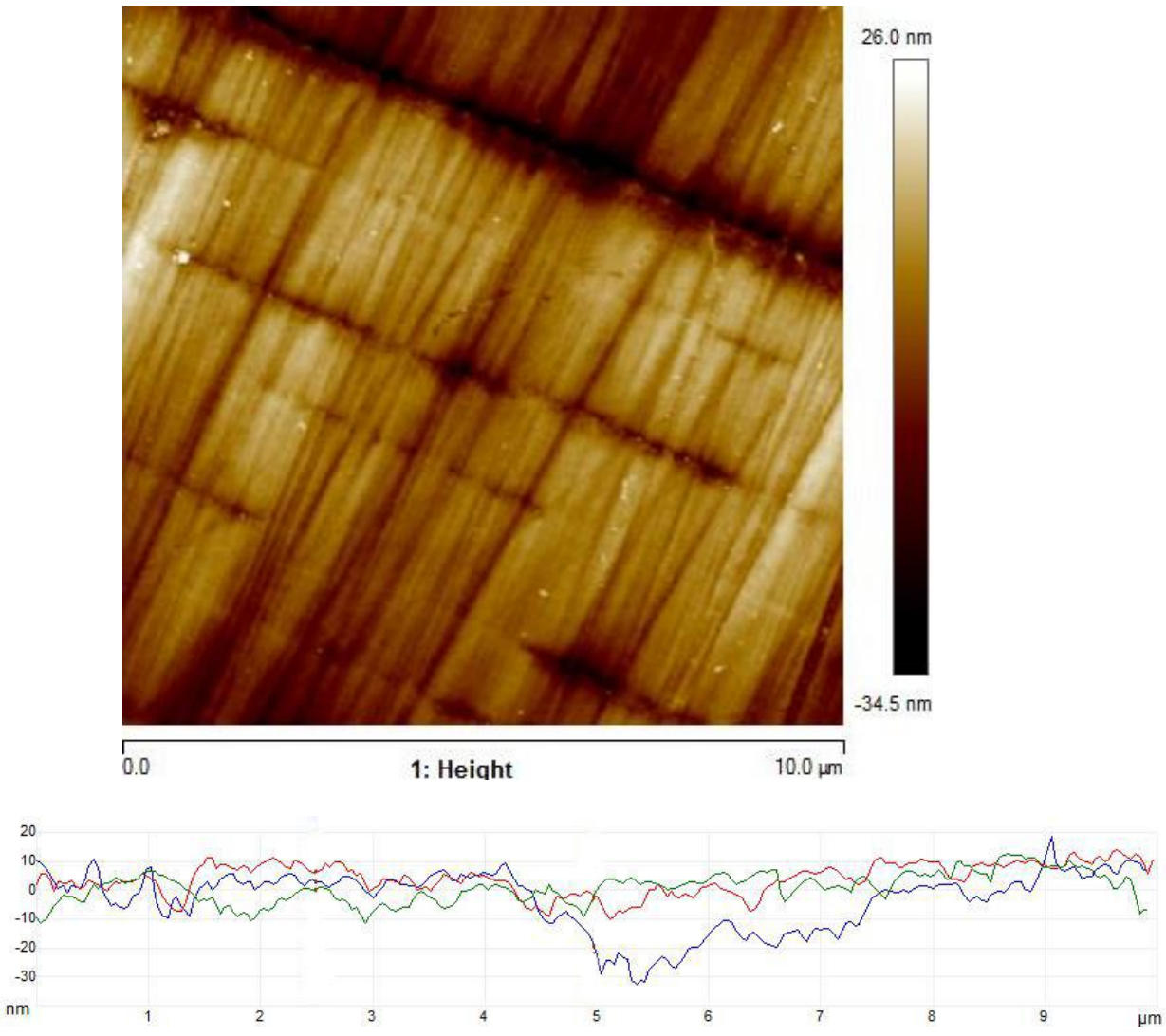

Fig. C7. Surface topography with roughness distribution of A20 sample ITZ at 10 µm scan range

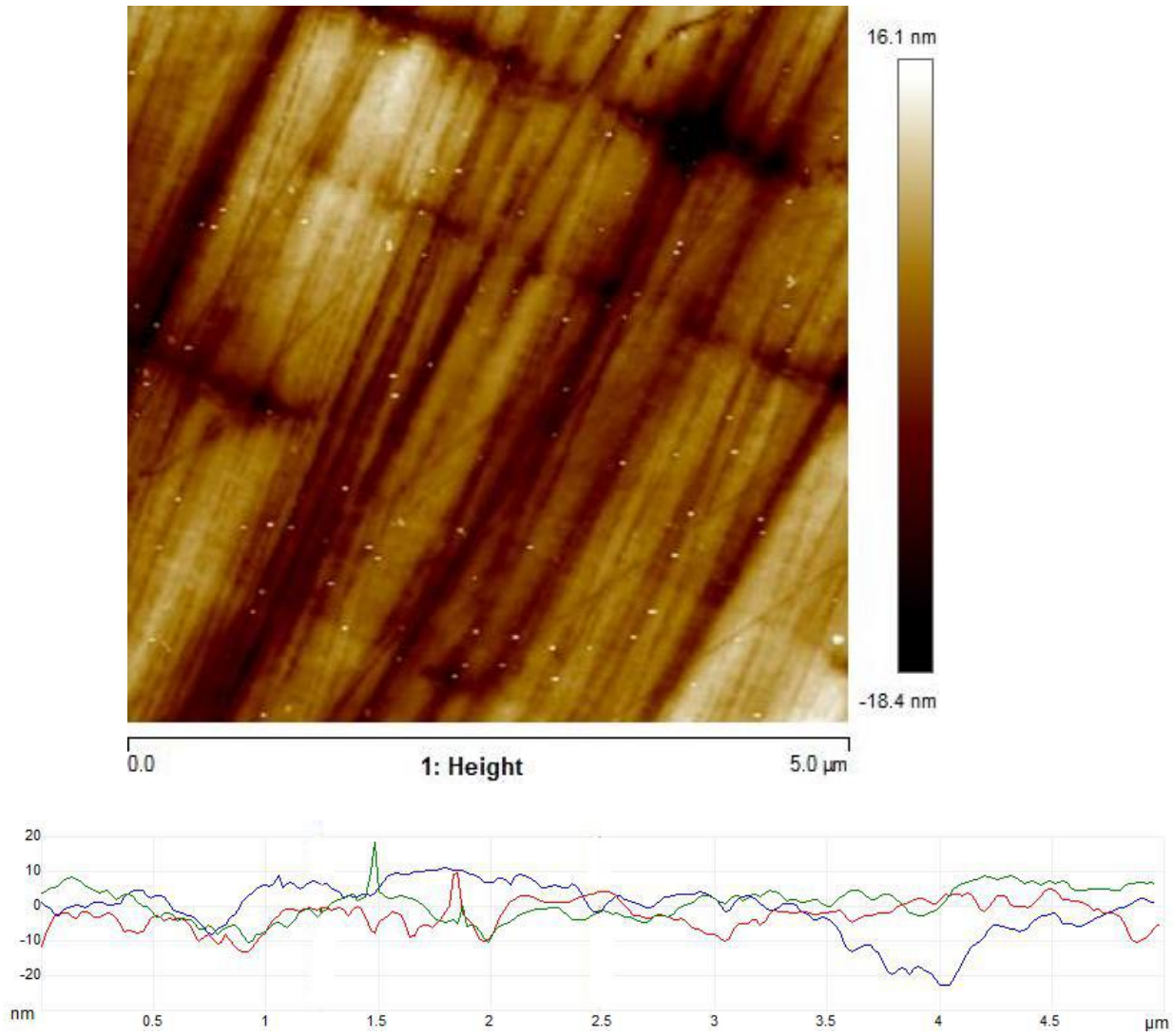

Fig. C8. Surface topography with roughness distribution of A20 sample ITZ at 5 µm scan range

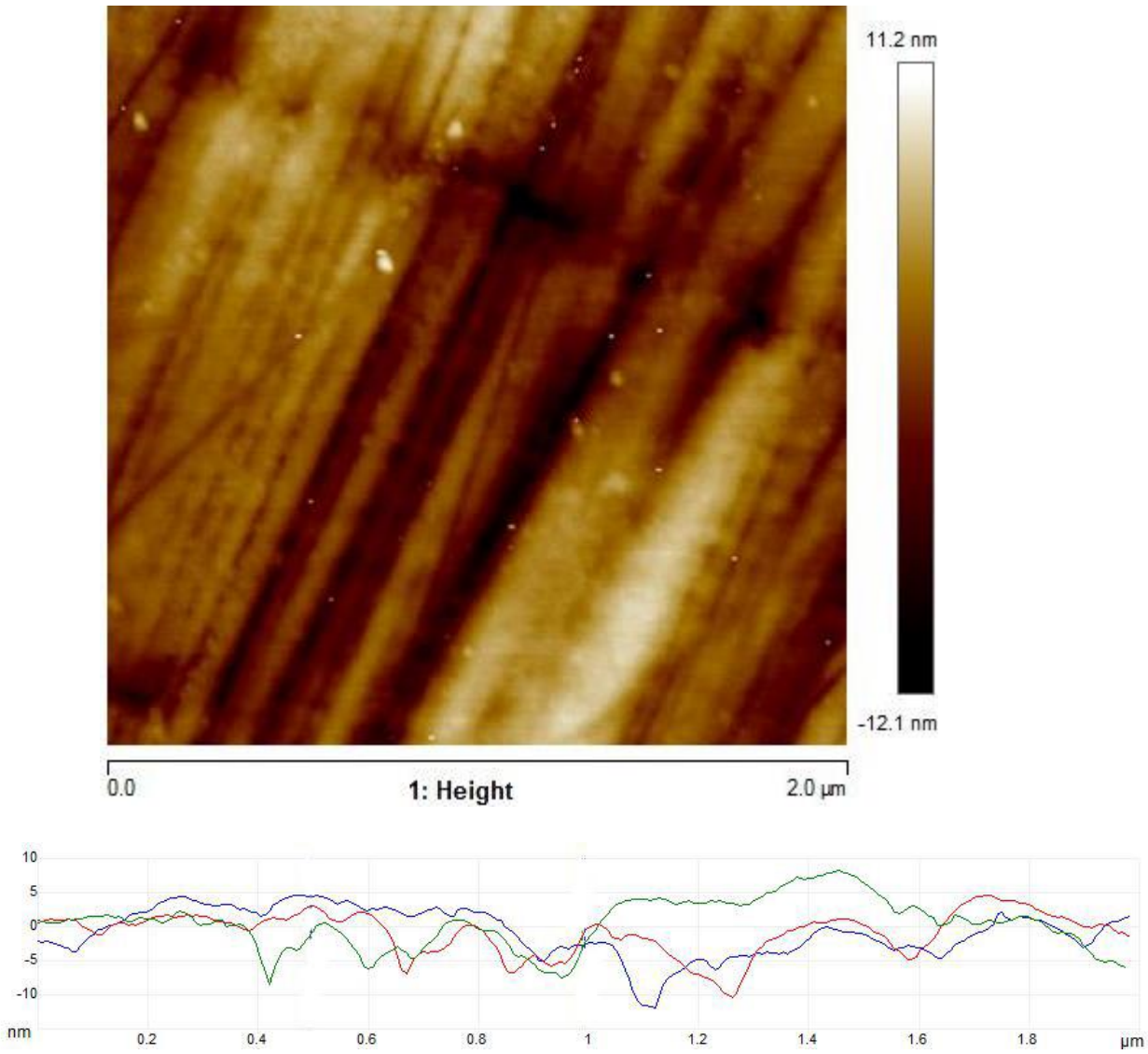

Fig. C9. Surface topography with roughness distribution of A20 sample ITZ at 2 µm scan range

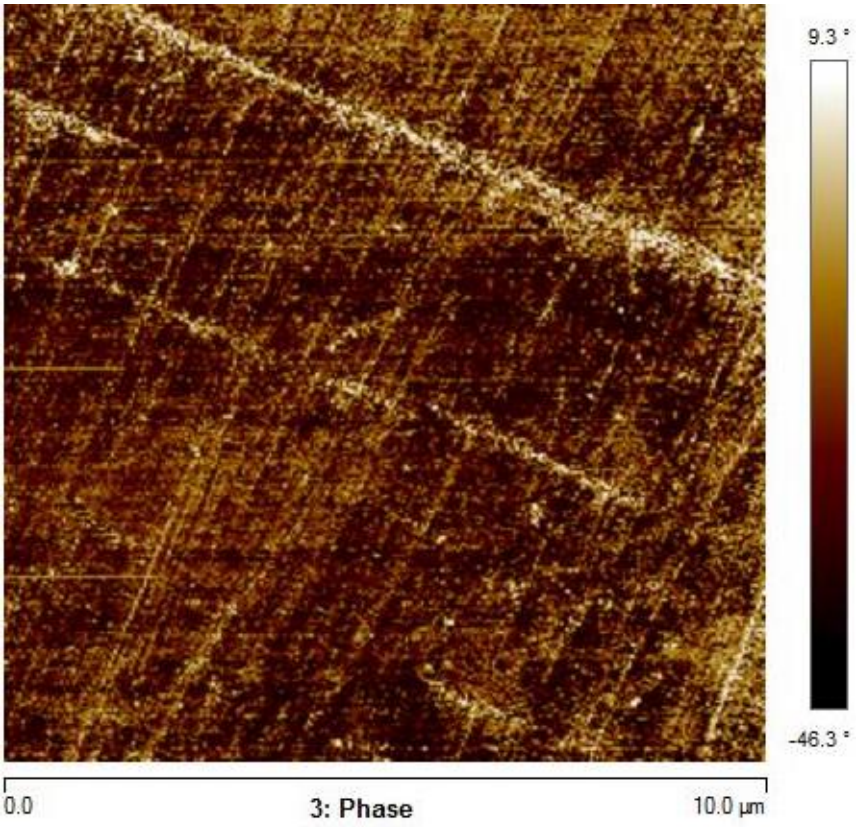

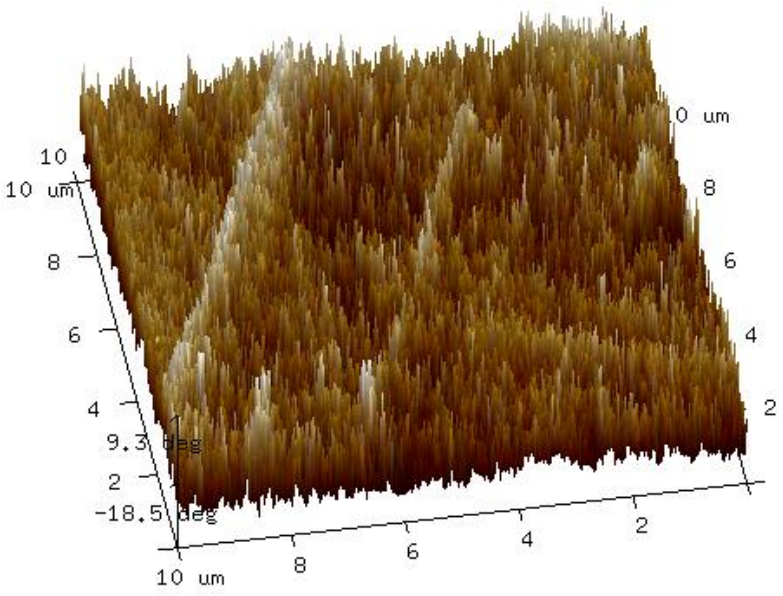

Fig. C10. Phase characteristics with grain distribution of A20 sample ITZ at 10 µm scan range

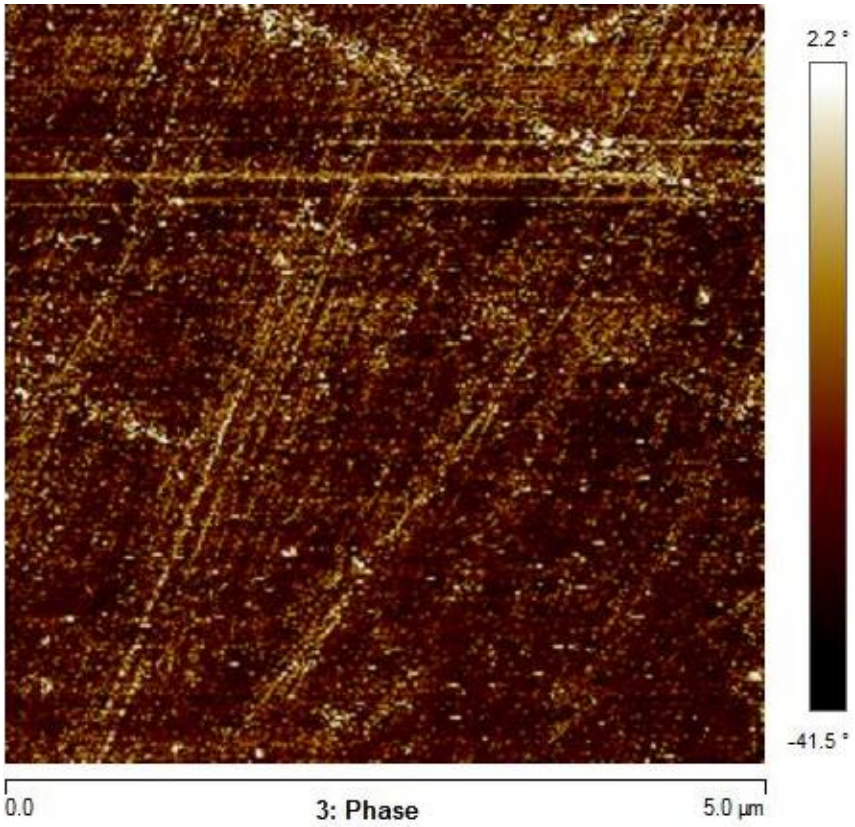

Fig. C11. Phase characteristics with grain distribution of A20 sample ITZ at 5 µm scan range

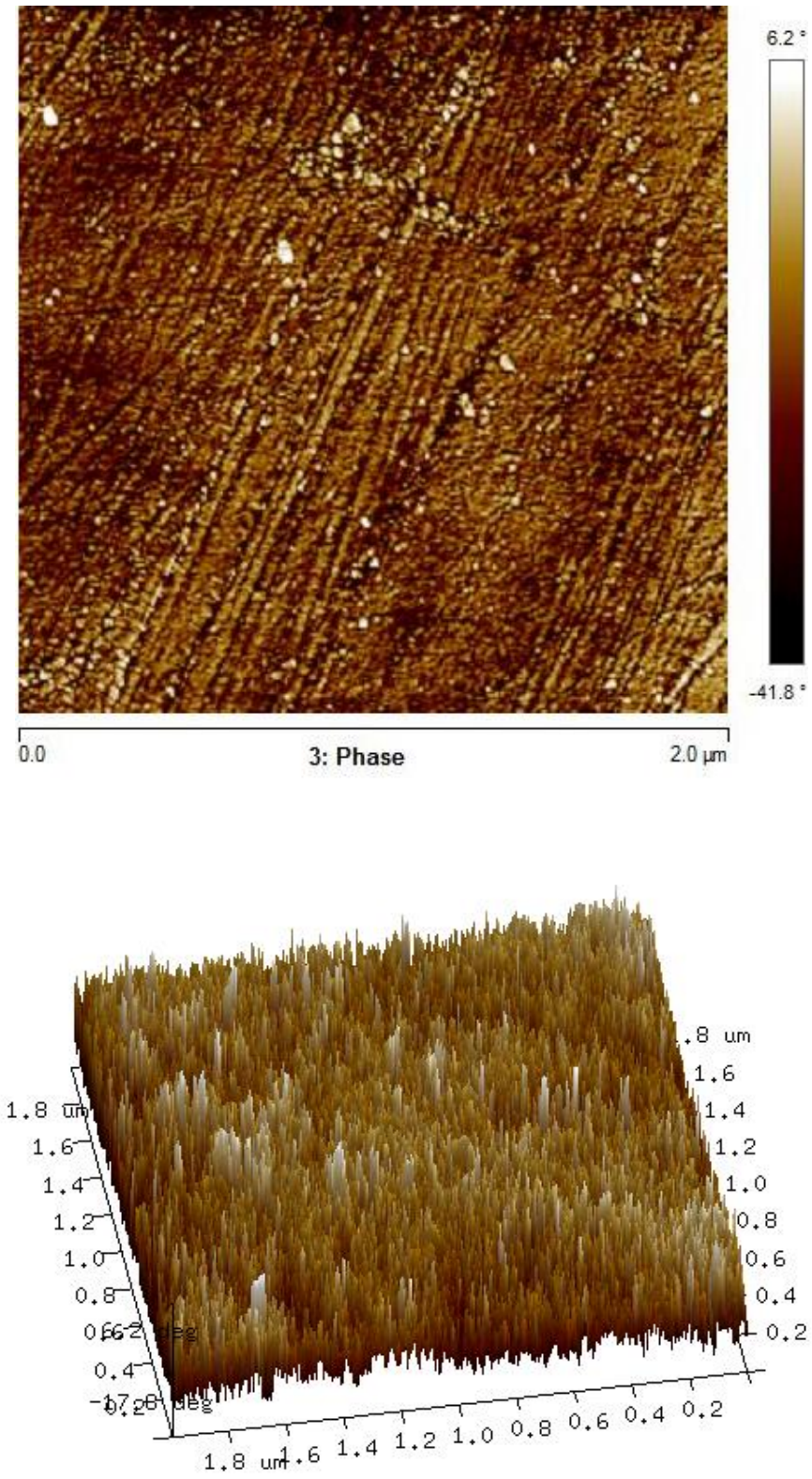

Fig. C12. Phase characteristics with grain distribution of A20 sample ITZ at 2 µm scan range

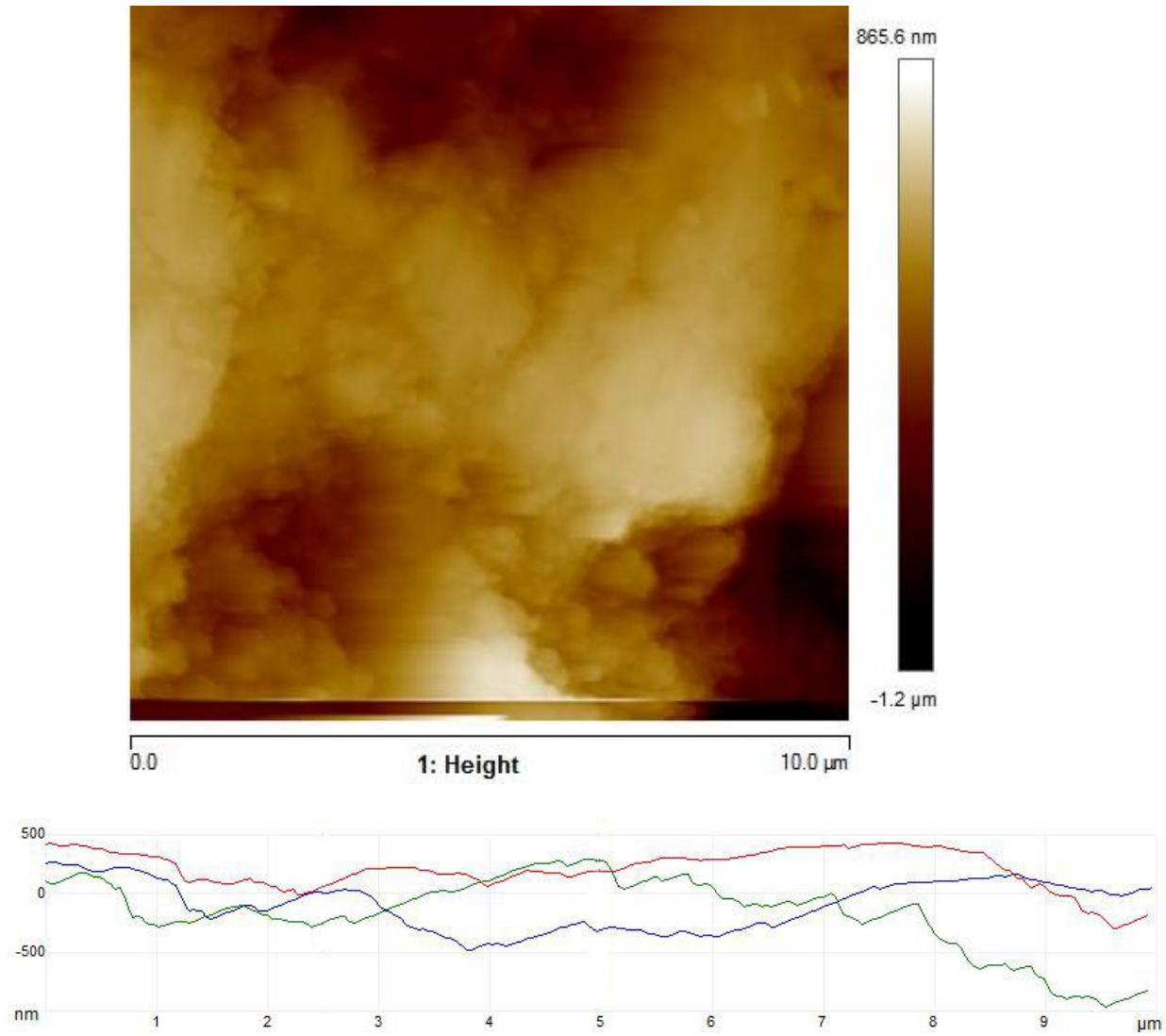

Fig. C13. Surface topography with roughness distribution of A40 sample ITZ at 10 µm scan range

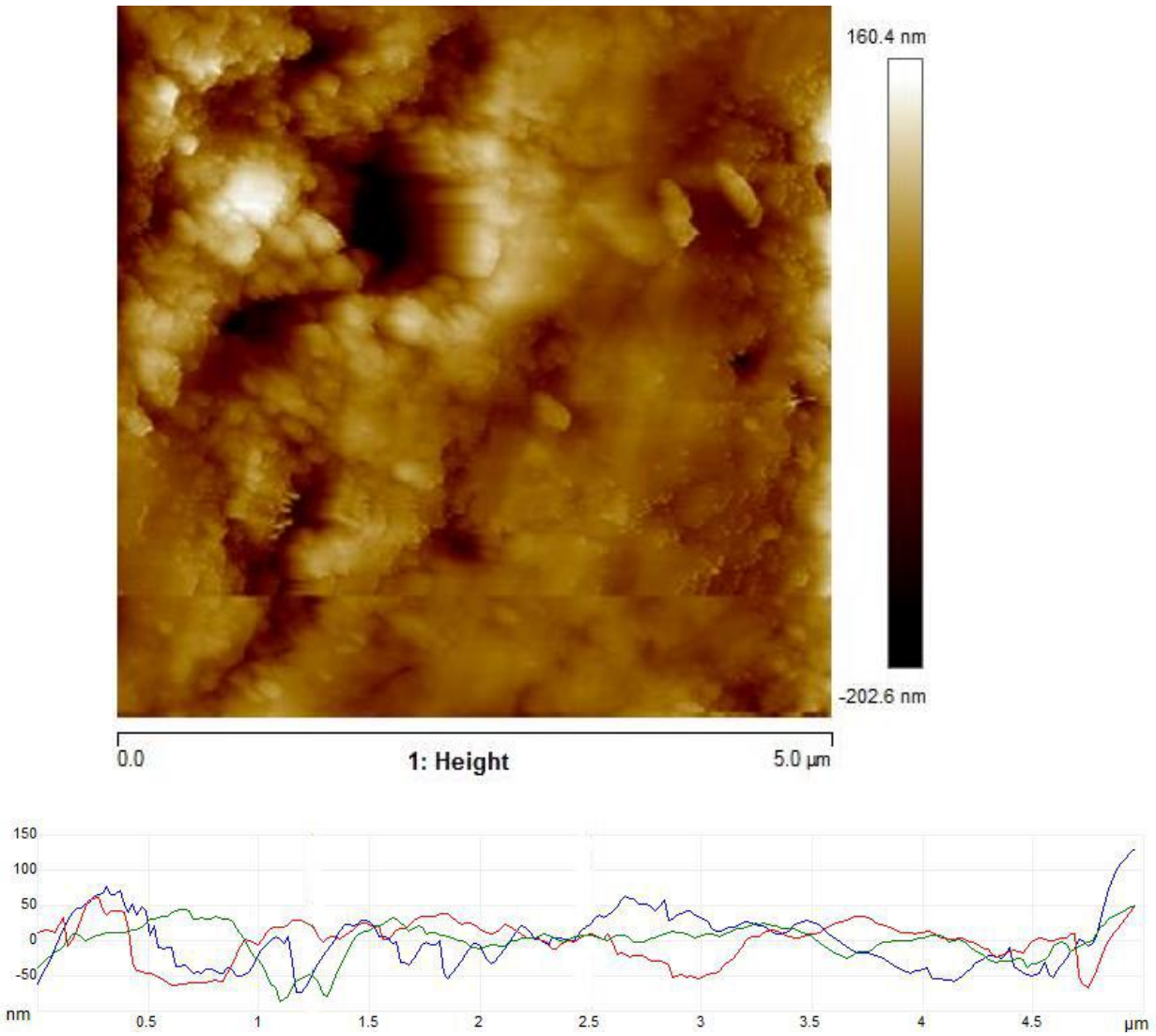

Fig. C14. Surface topography with roughness distribution of A40 sample ITZ at 5 µm scan range

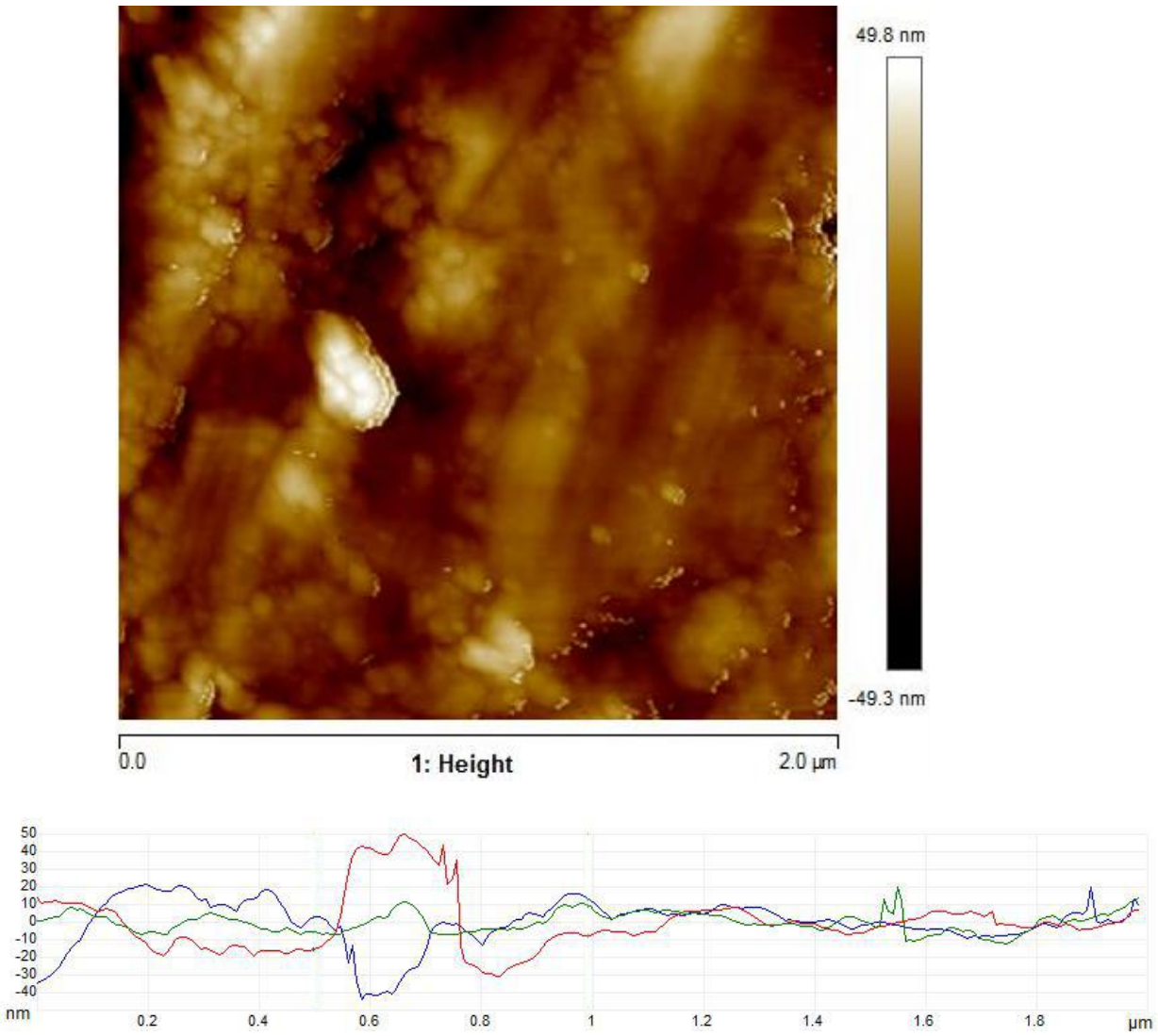

Fig. C15. Surface topography with roughness distribution of A40 sample ITZ at 2 µm scan range

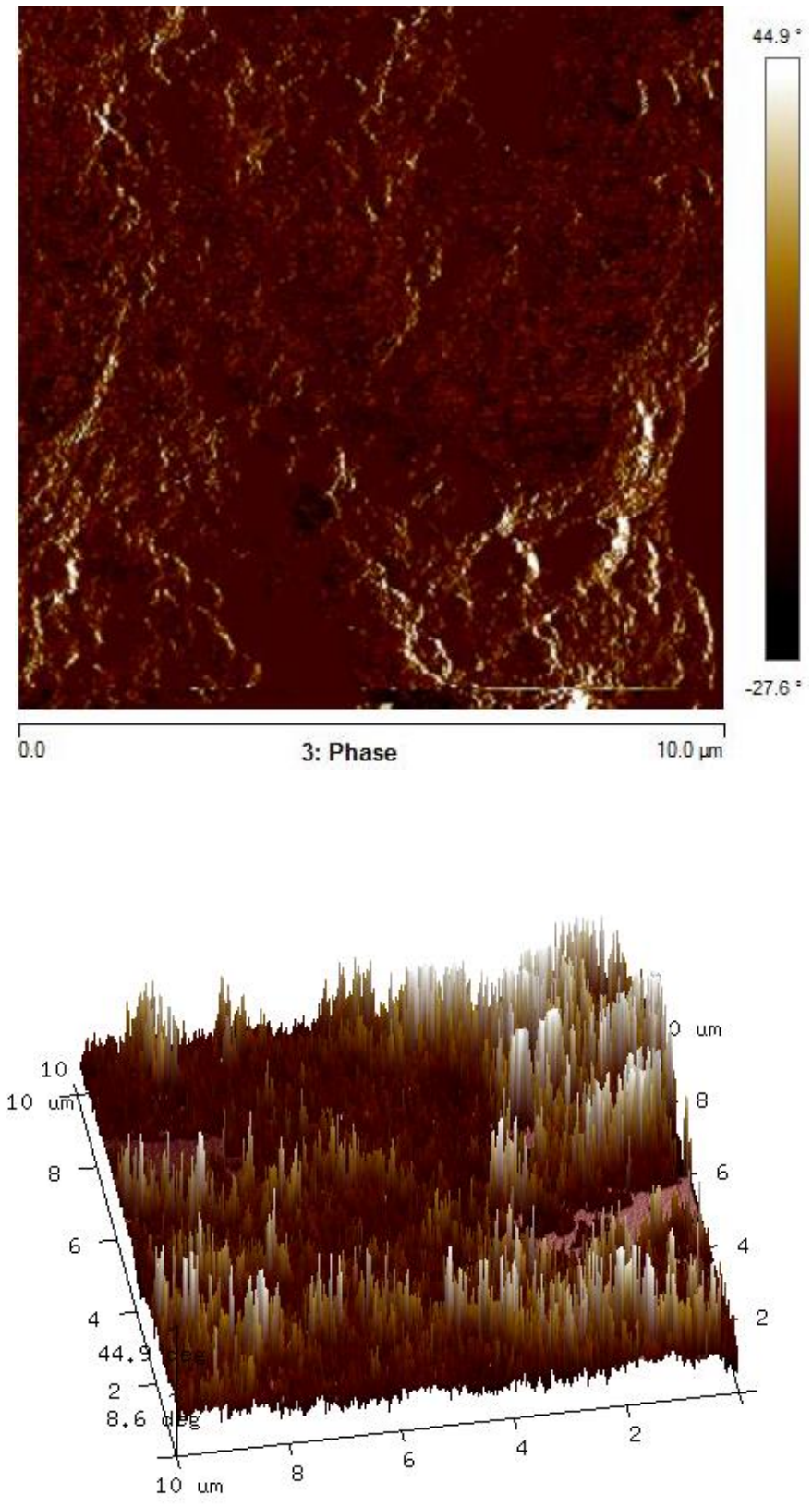

Fig. C16. Phase characteristics with grain distribution of A40 sample ITZ at 10 µm scan range

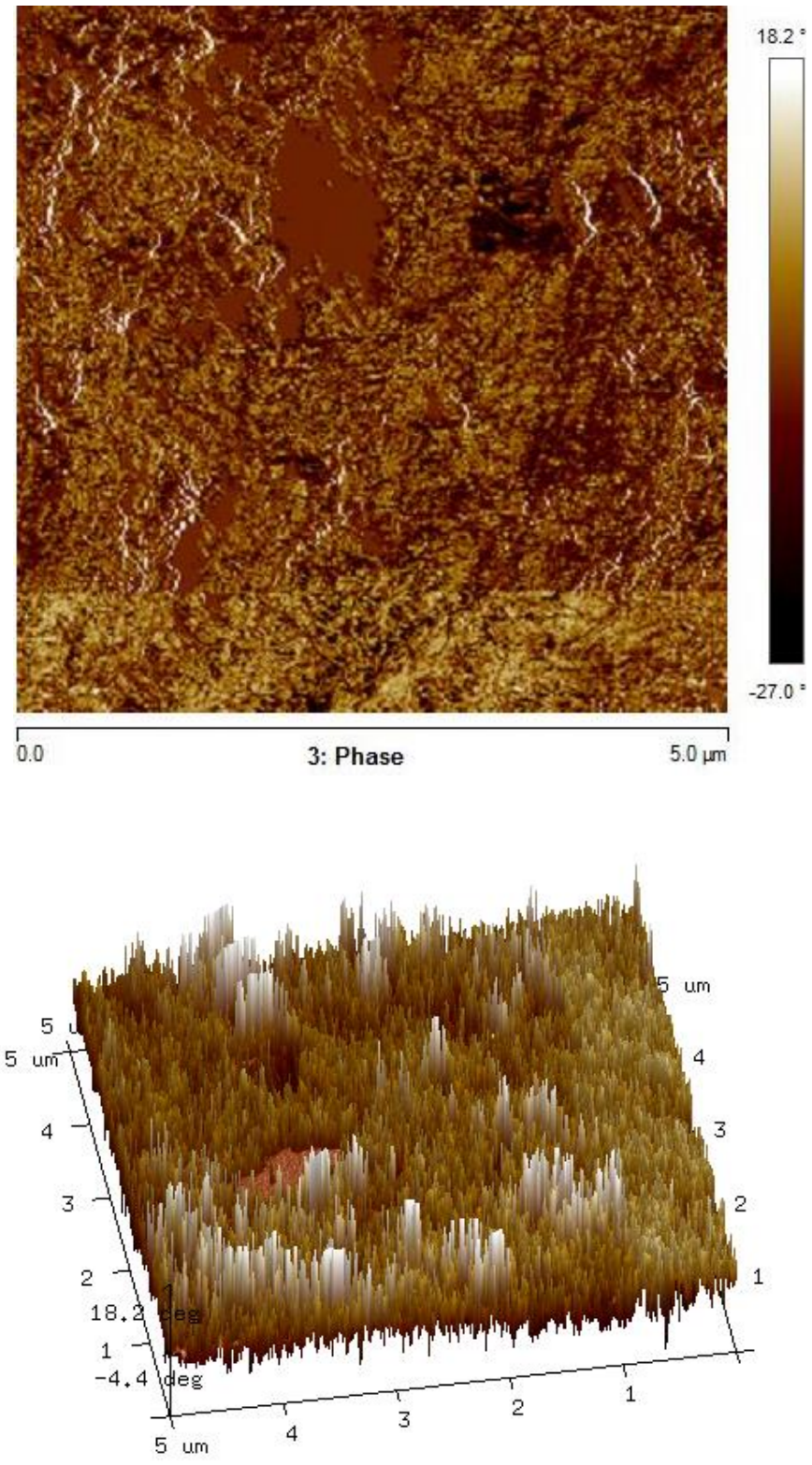

Fig. C17. Phase characteristics with grain distribution of A40 sample ITZ at 5 µm scan range

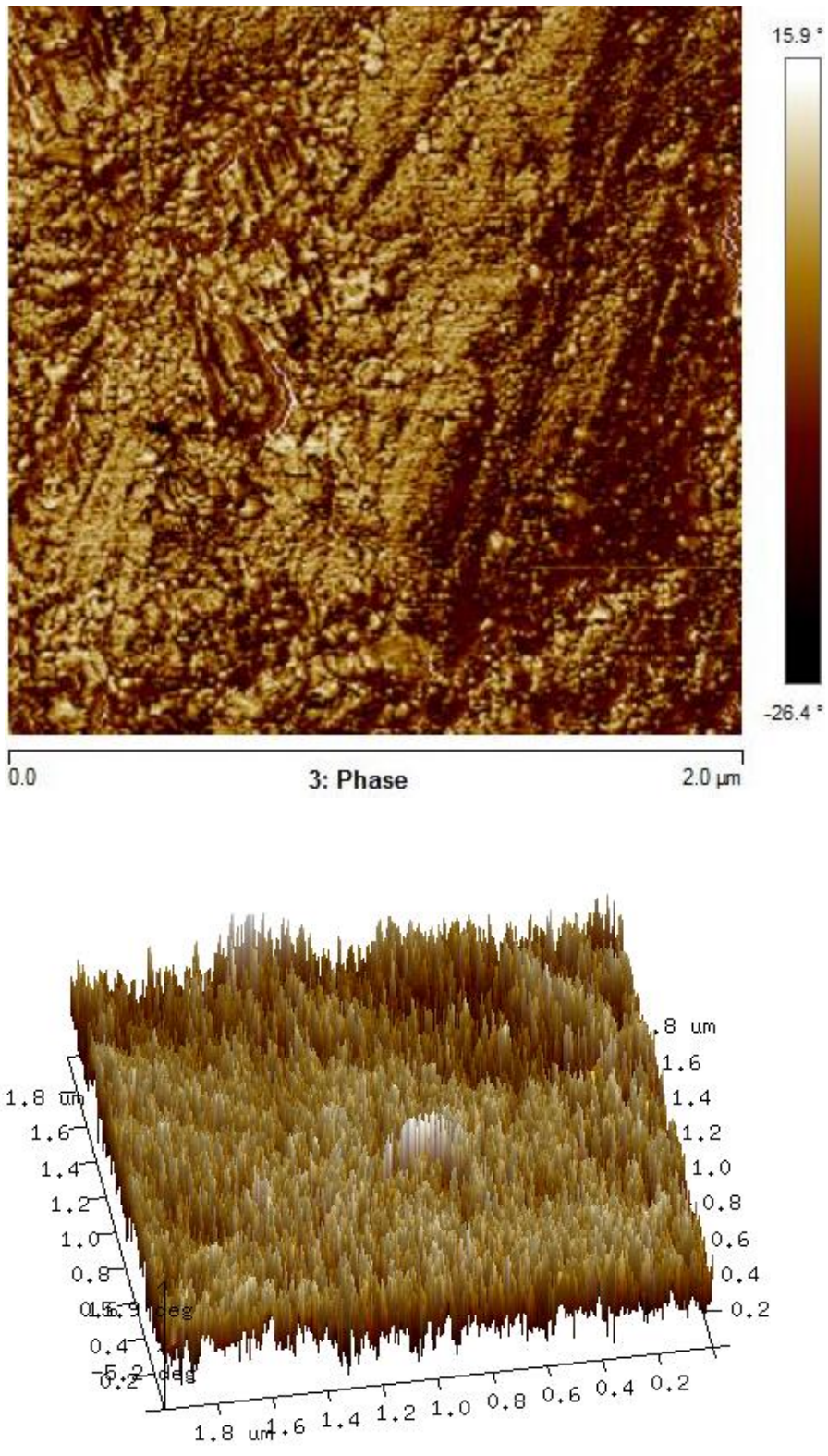

Fig. C18. Phase characteristics with grain distribution of A40 sample ITZ at 2 µm scan range

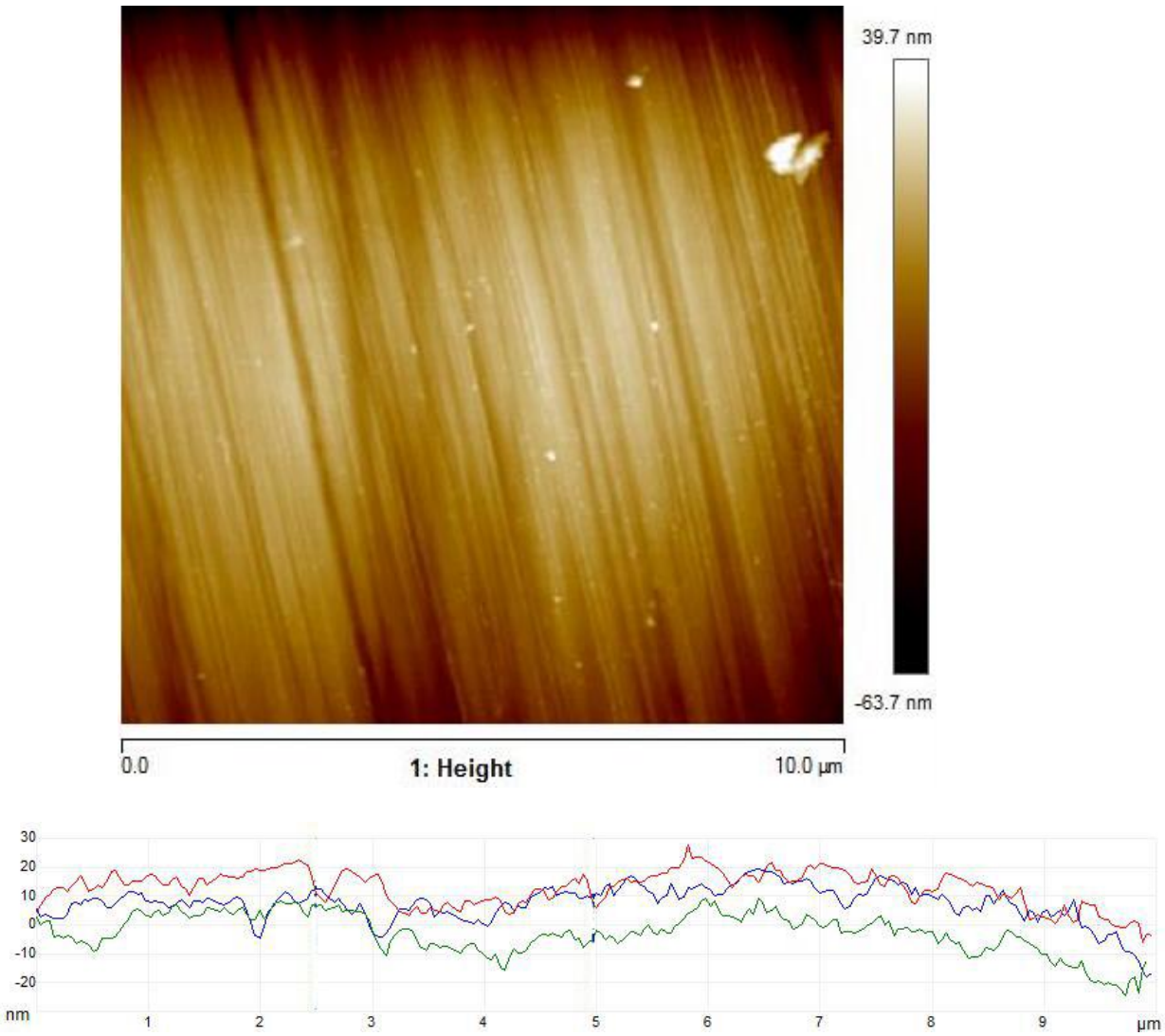

Fig. C19. Surface topography with roughness distribution of A60 sample ITZ at 10 µm scan range

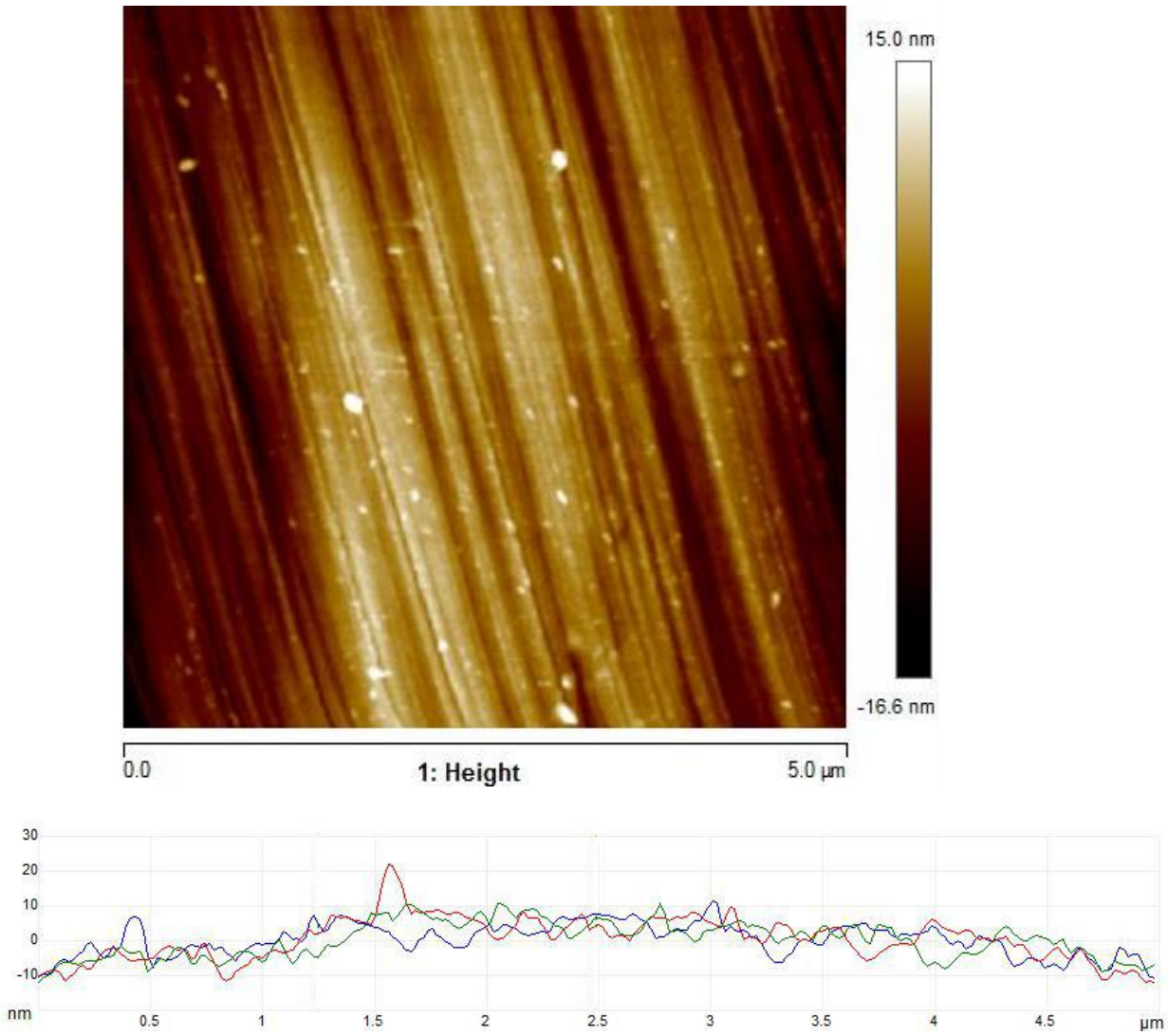

Fig. C20. Surface topography with roughness distribution of A60 sample ITZ at 5 µm scan range

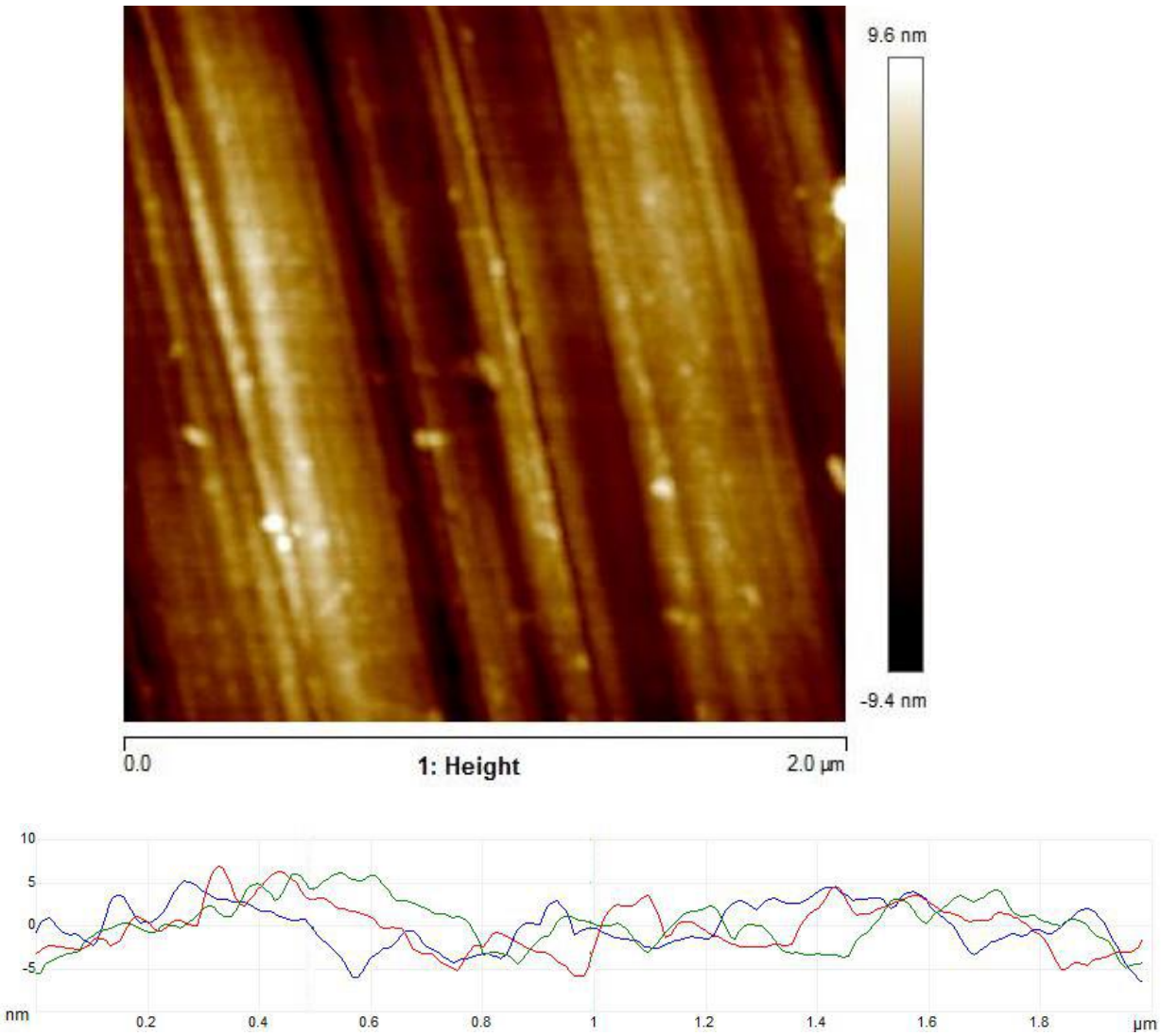

Fig. C21. Surface topography with roughness distribution of A60 sample ITZ at 2 µm scan range

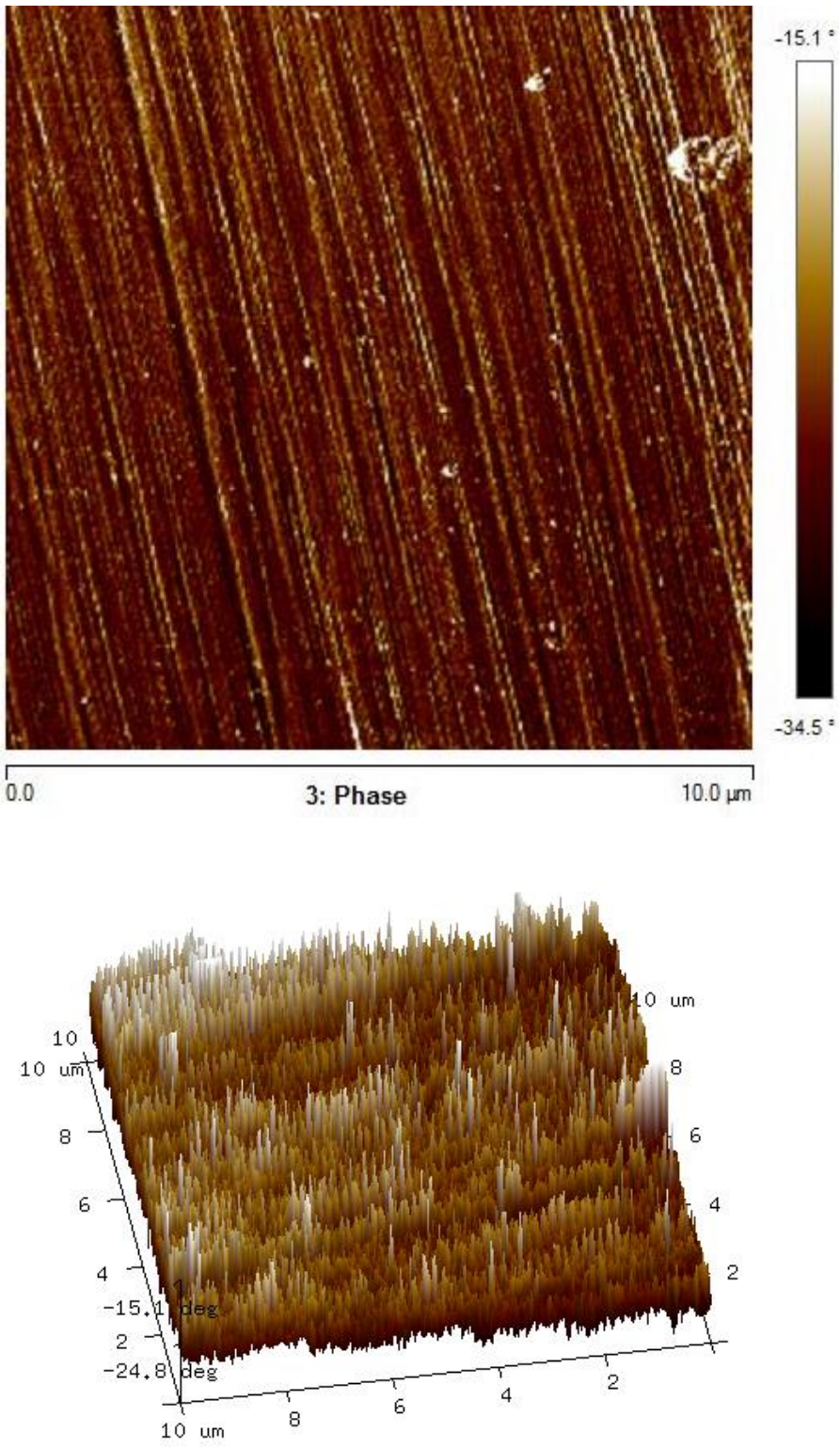

Fig. C22. Phase characteristics with grain distribution of A60 sample ITZ at 10 µm scan range

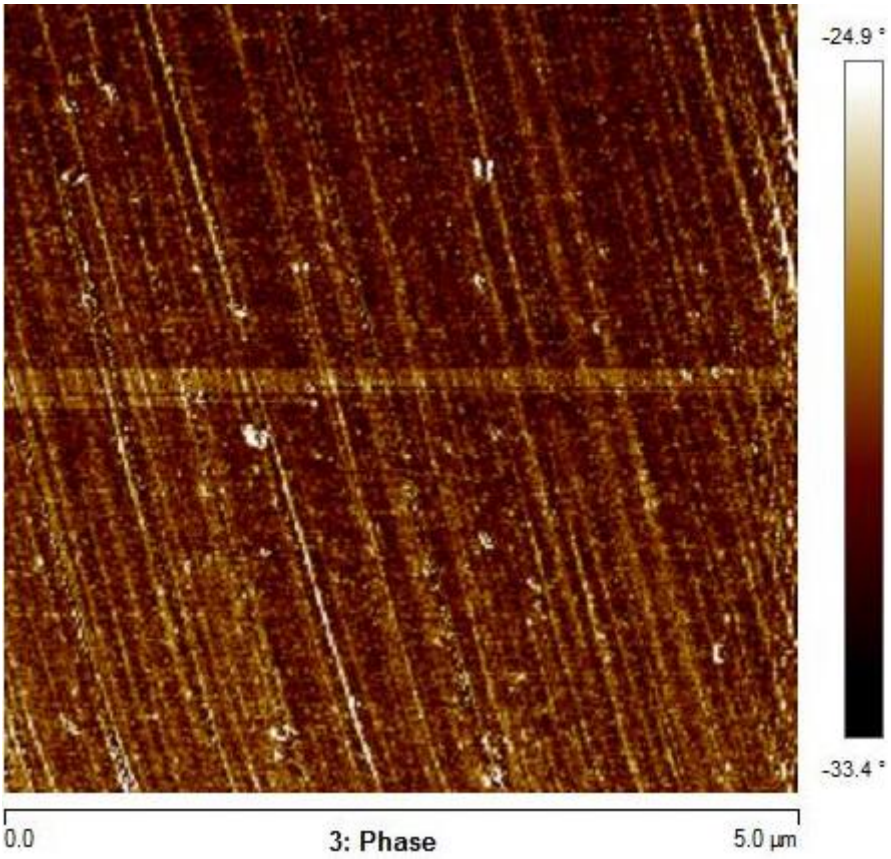

Fig. C23. Phase characteristics with grain distribution of A60 sample ITZ at 2 µm scan range

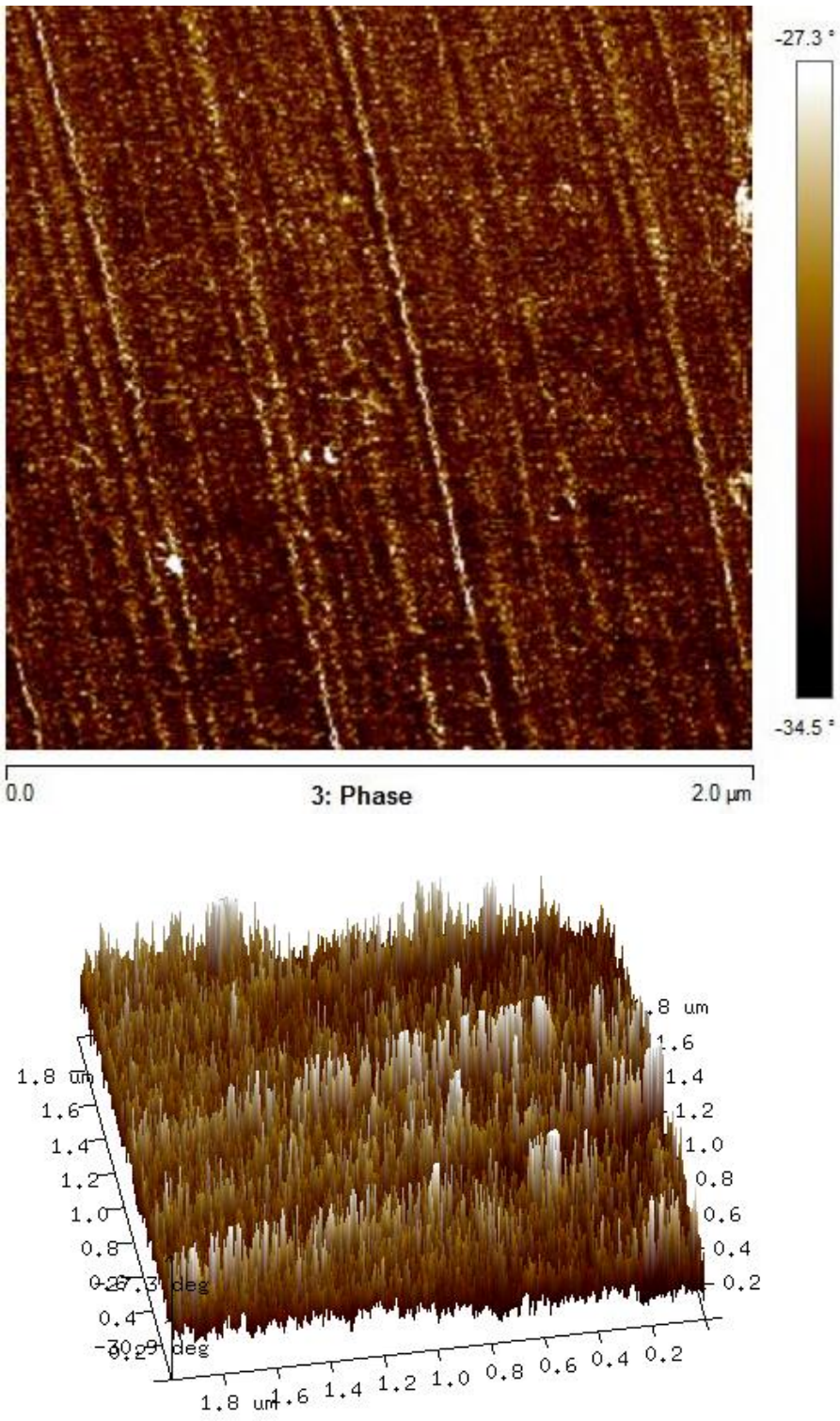

Fig. C24. Phase characteristics with grain distribution of A60 sample ITZ at 2 µm scan range

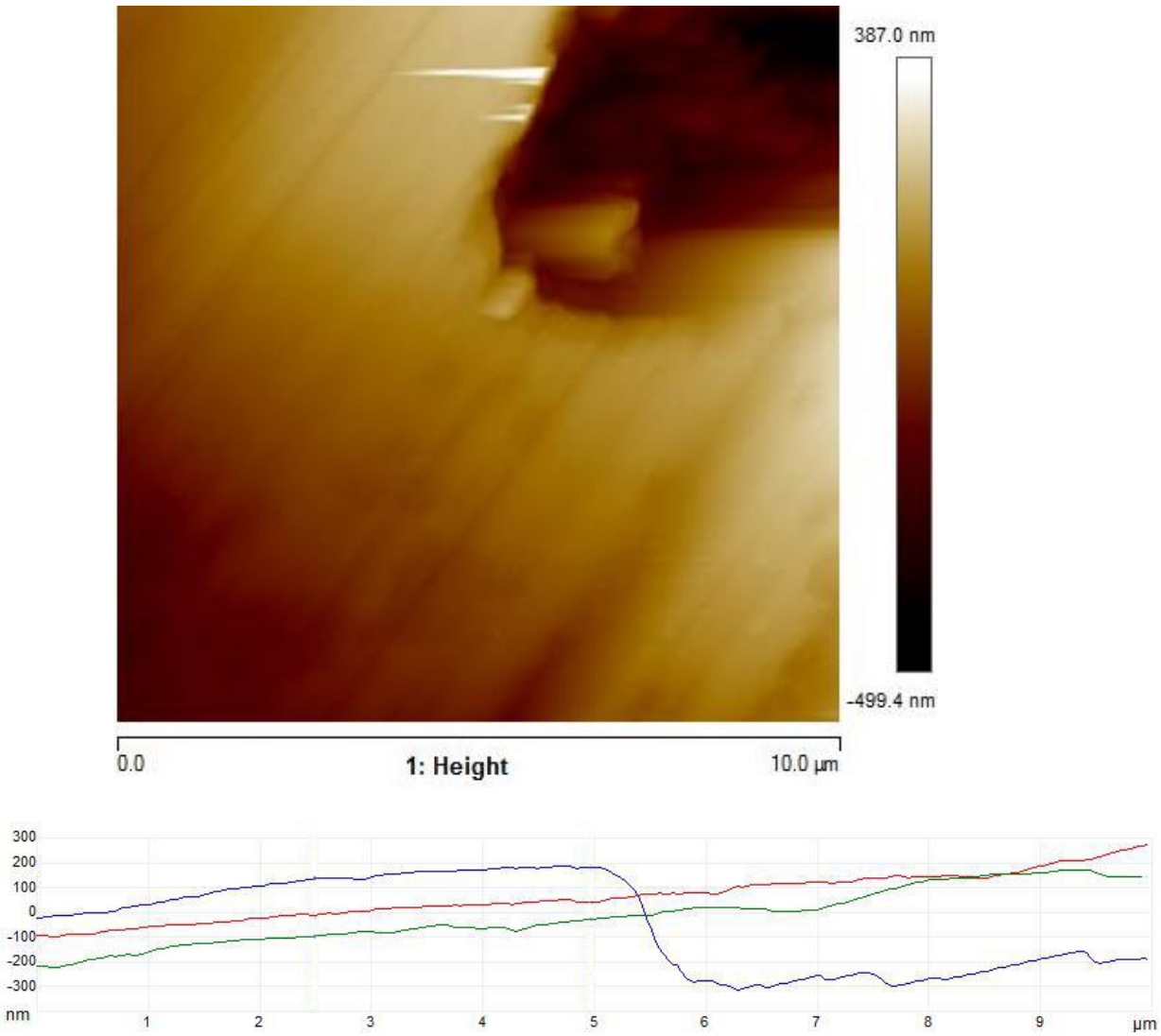

Fig. C25. Surface topography with roughness distribution of A80 sample ITZ at 10 µm scan range

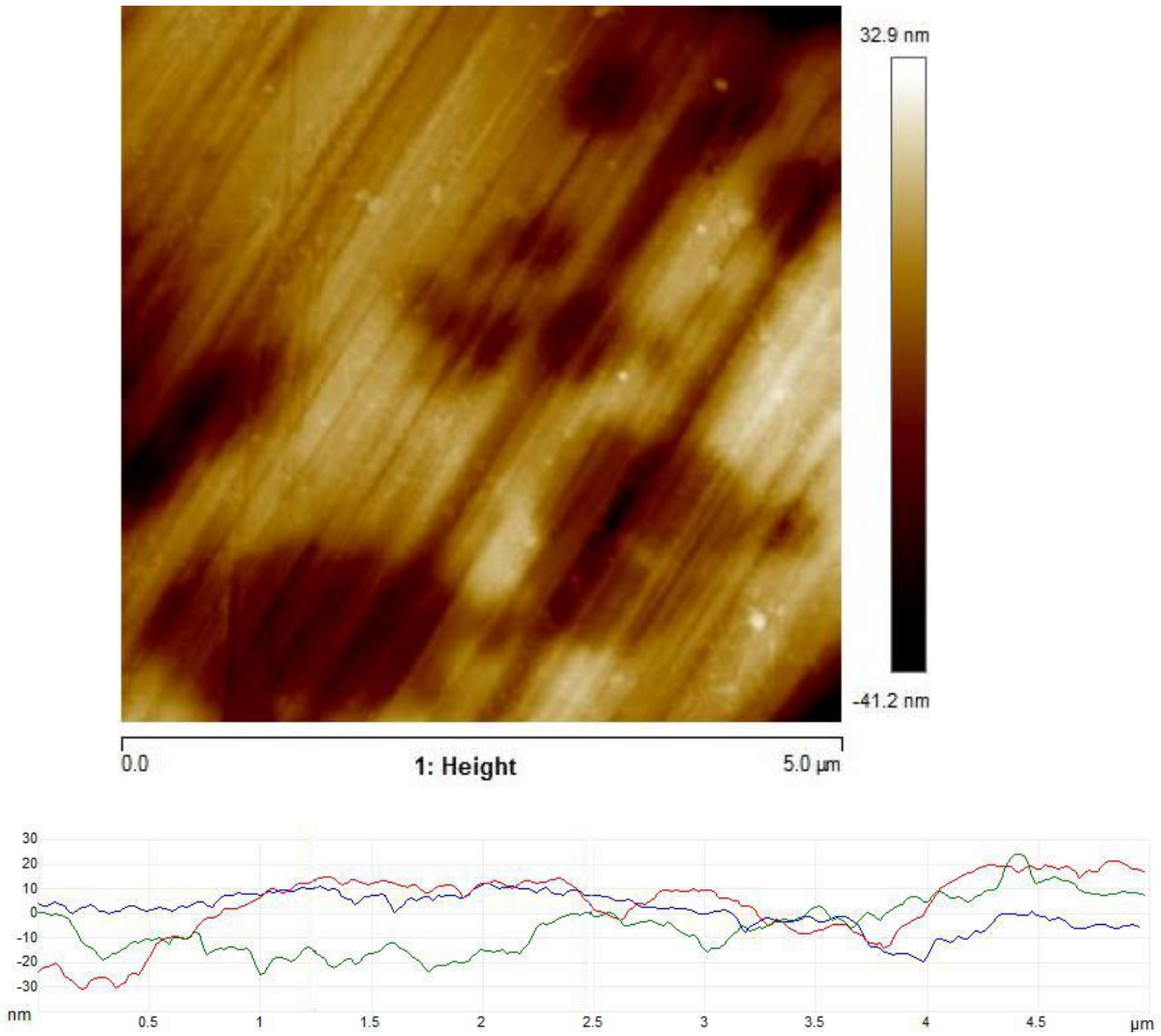

Fig. C26. Surface topography with roughness distribution of A80 sample ITZ at 5 µm scan range

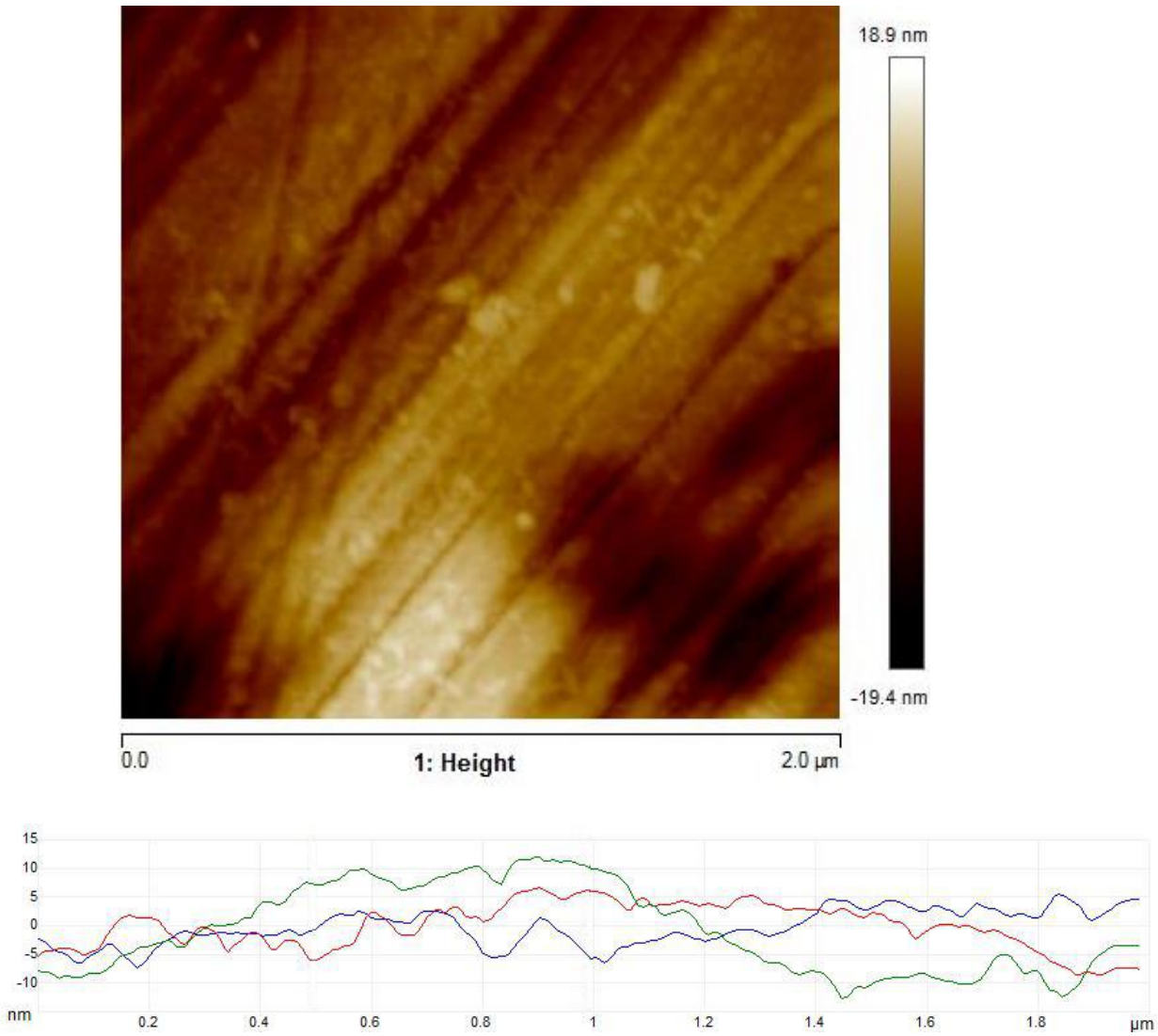

Fig. C27. Surface topography with roughness distribution of A80 sample ITZ at 2 µm scan range

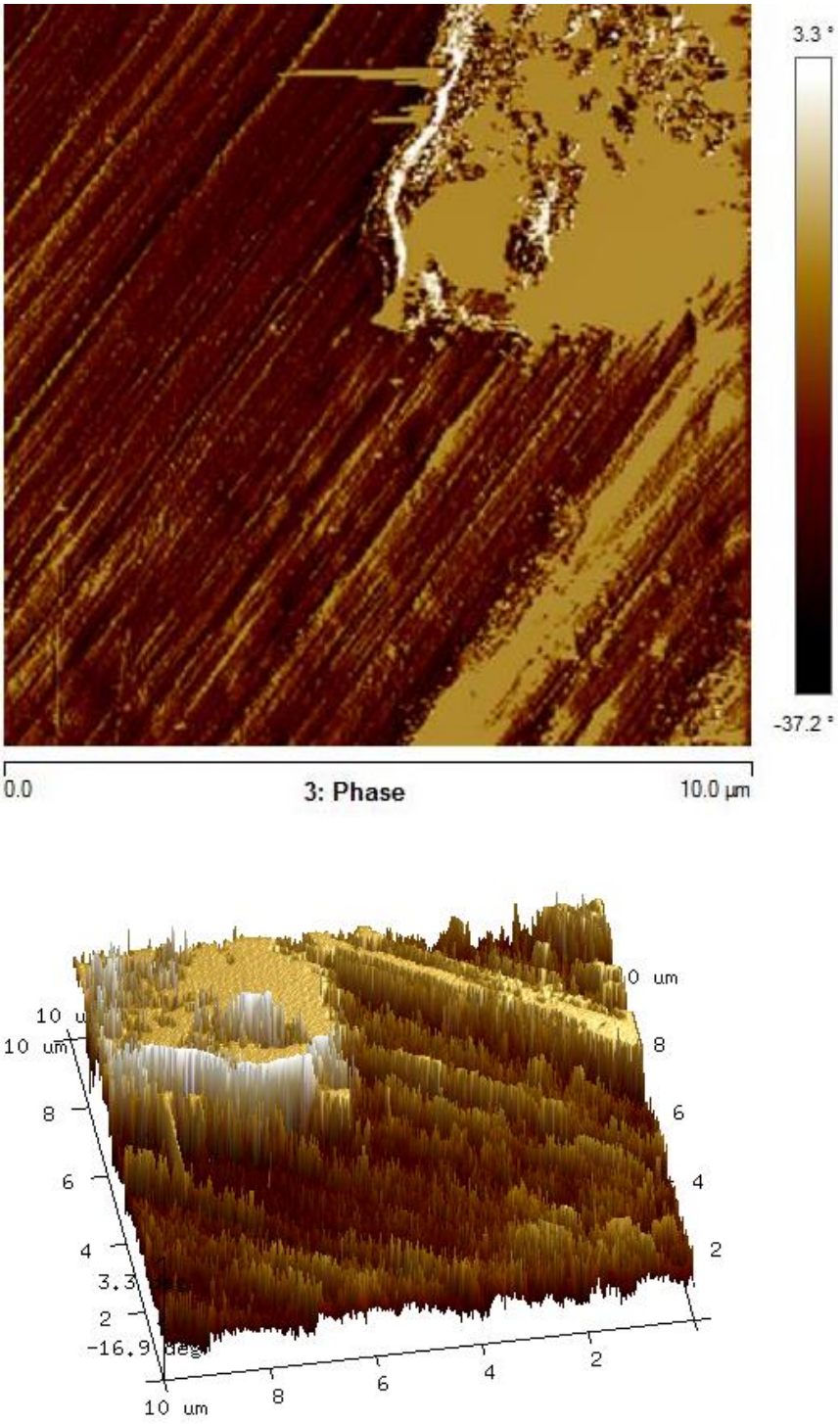

Fig. C28. Phase characteristics with grain distribution of A80 sample ITZ at 10 µm scan range

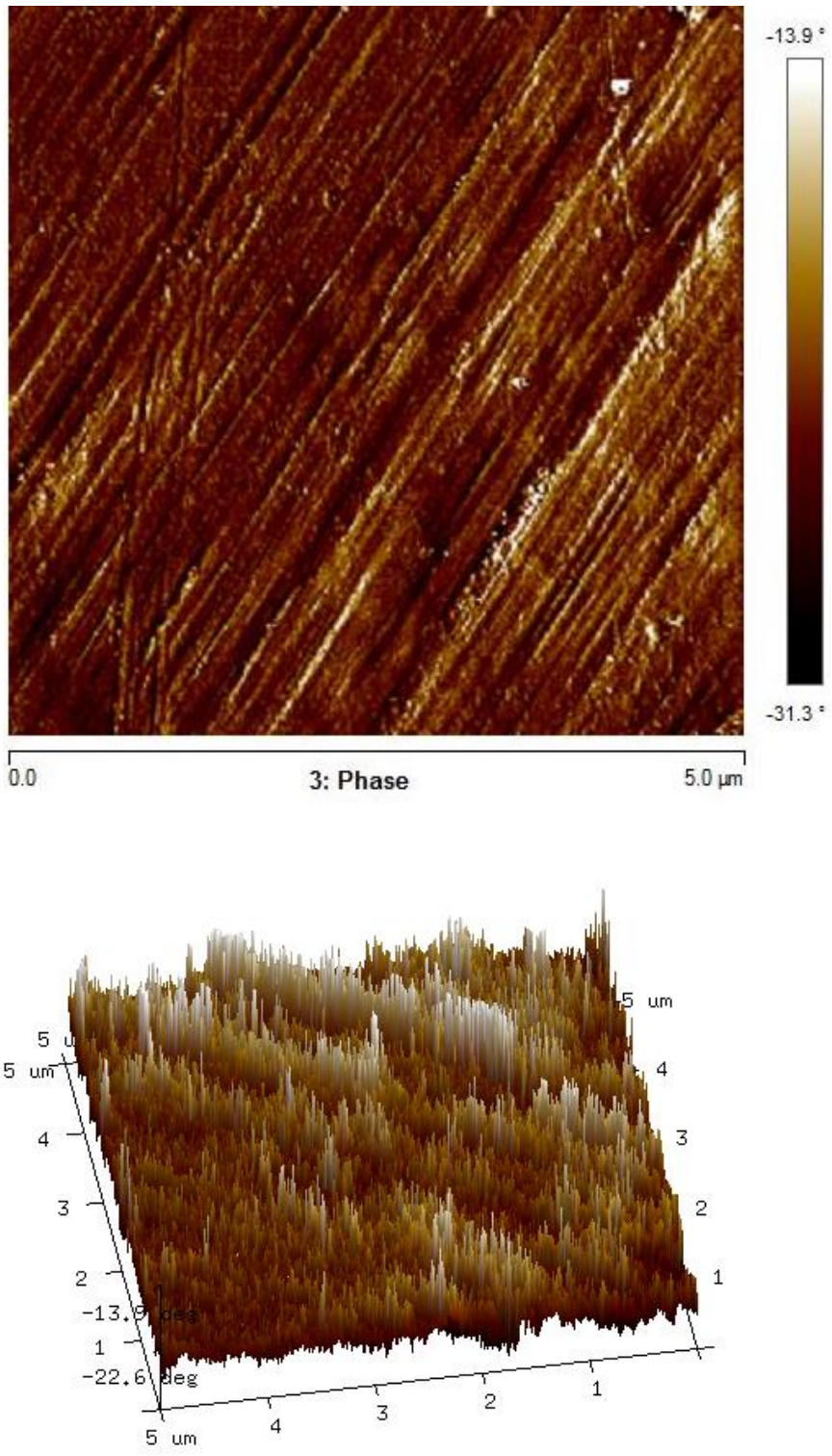

Fig. C29. Phase characteristics with grain distribution of A80 sample ITZ at 5 µm scan range

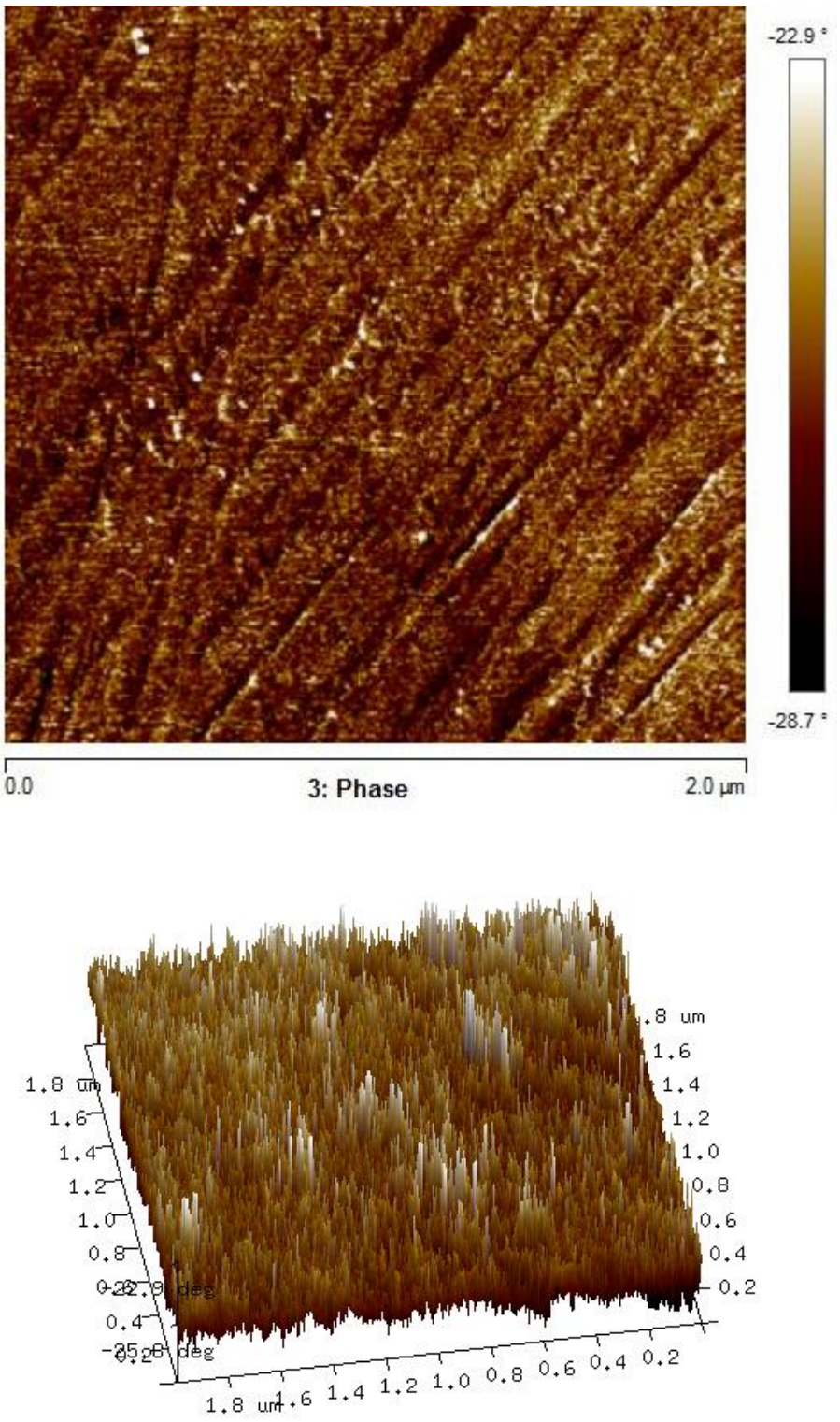

Fig. C30. Phase characteristics with grain distribution of A80 sample ITZ at 2 µm scan range

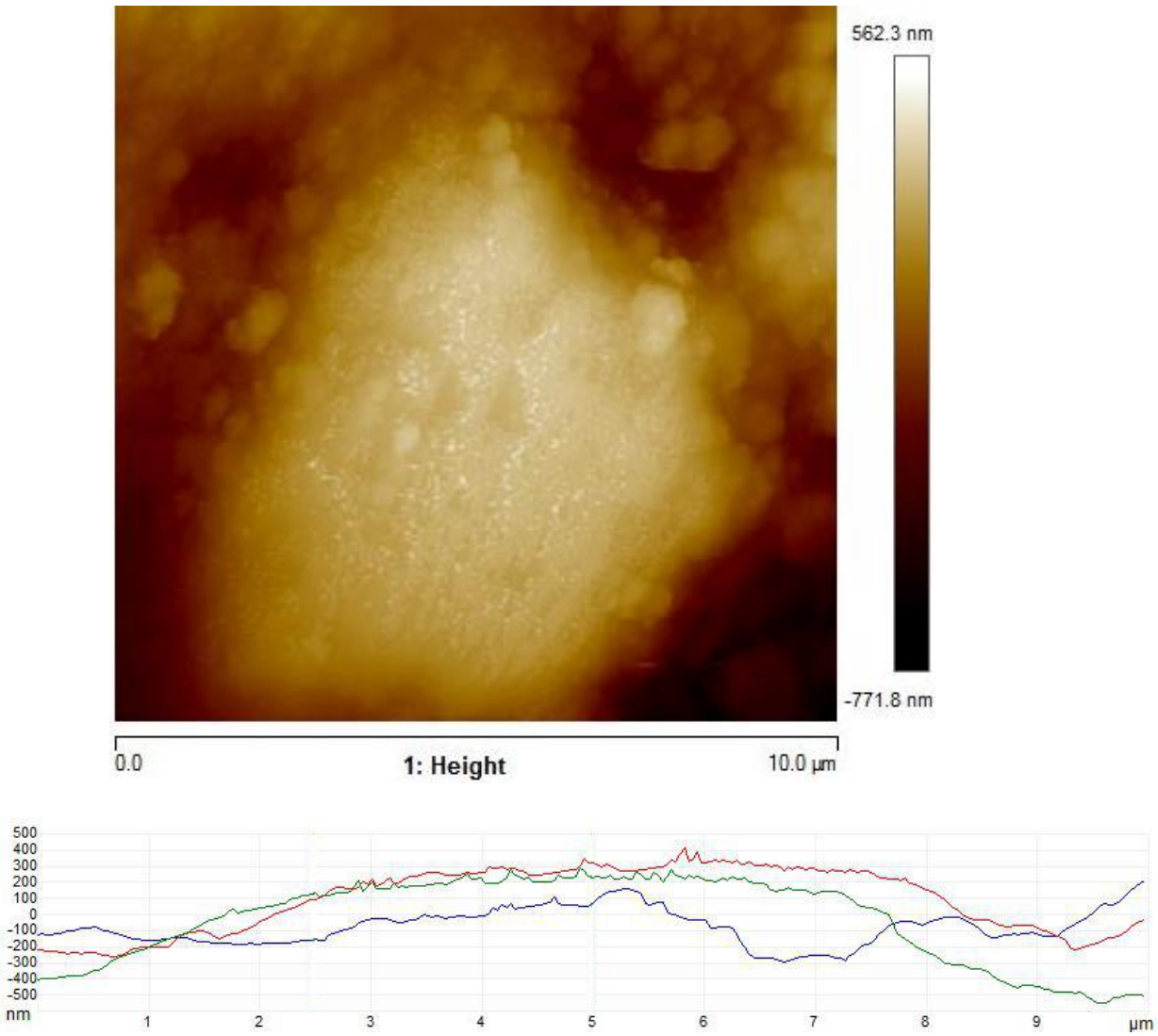

Fig. C31. Surface topography with roughness distribution of A100 sample ITZ at 10 µm scan range

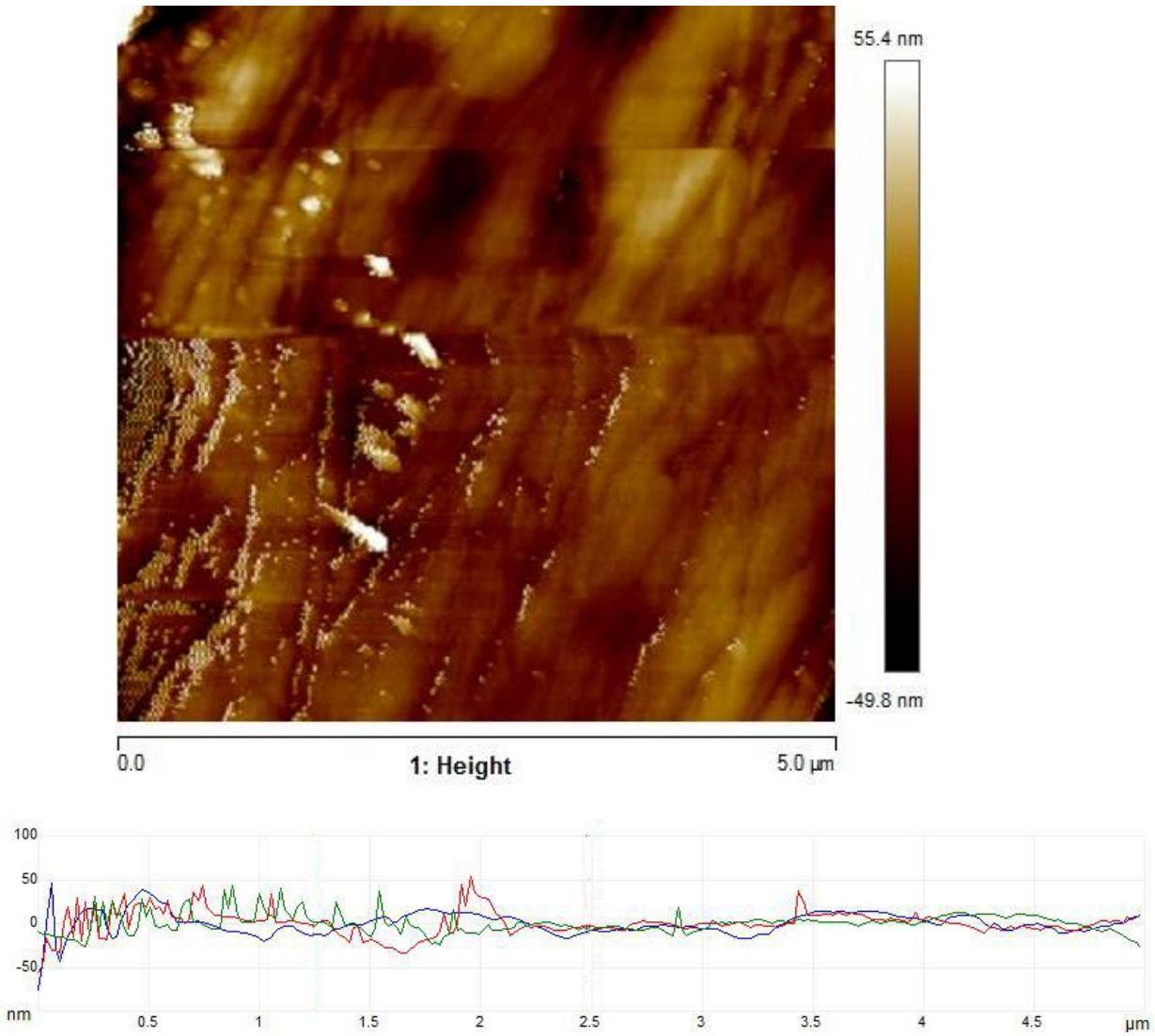

Fig. C32. Surface topography with roughness distribution of A100 sample ITZ at 5 µm scan range

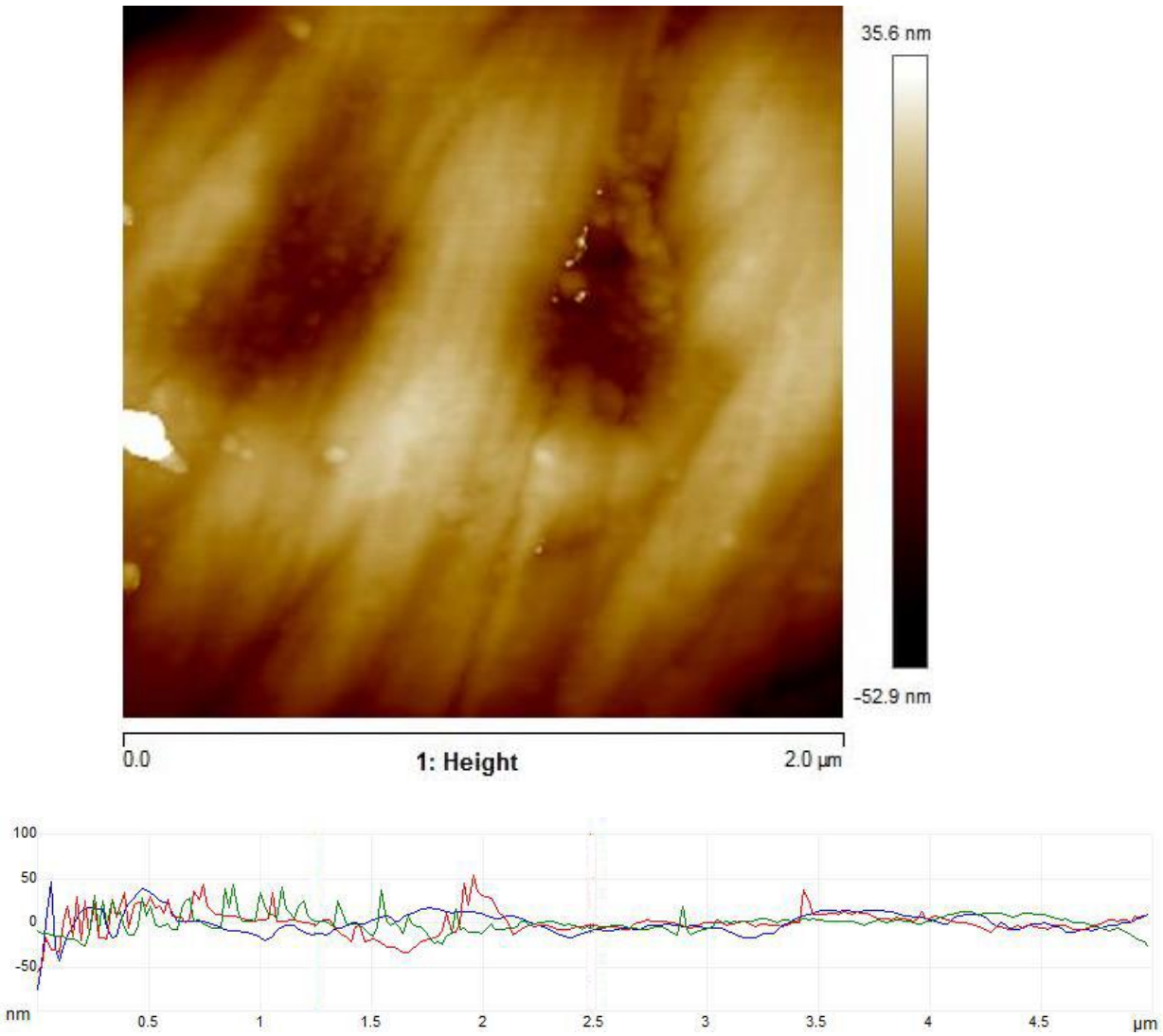

Fig. C33. Surface topography with roughness distribution of A100 sample ITZ at 2 µm scan range

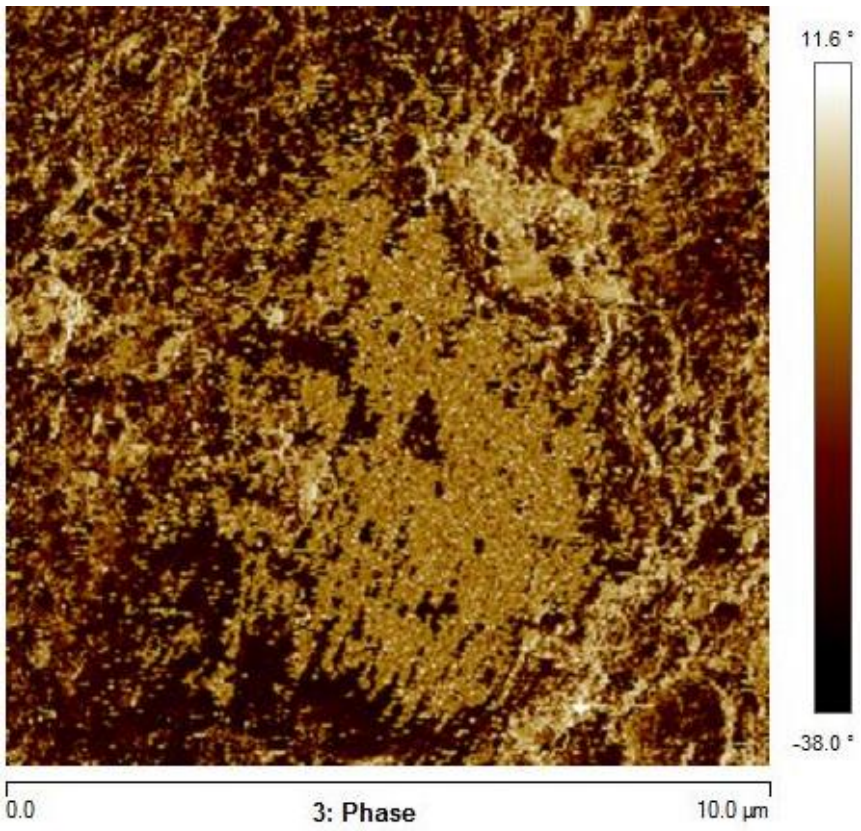

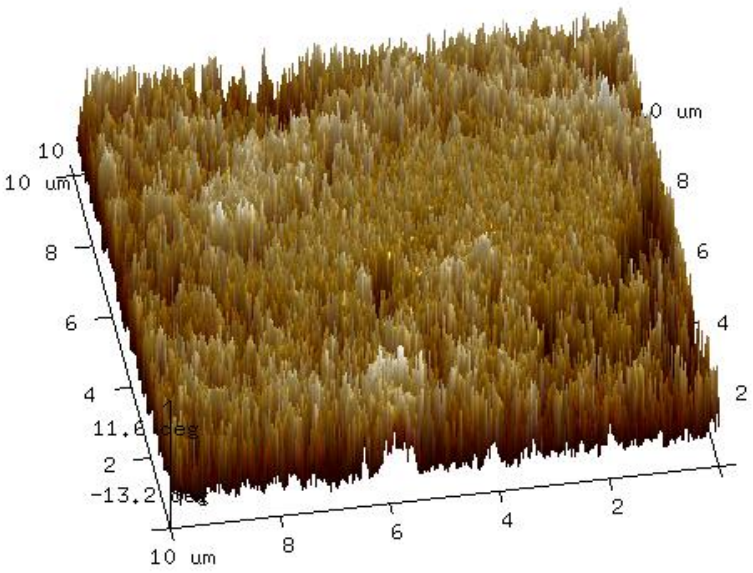

Fig. C34. Phase characteristics with grain distribution of A100 sample ITZ at 10 µm scan range

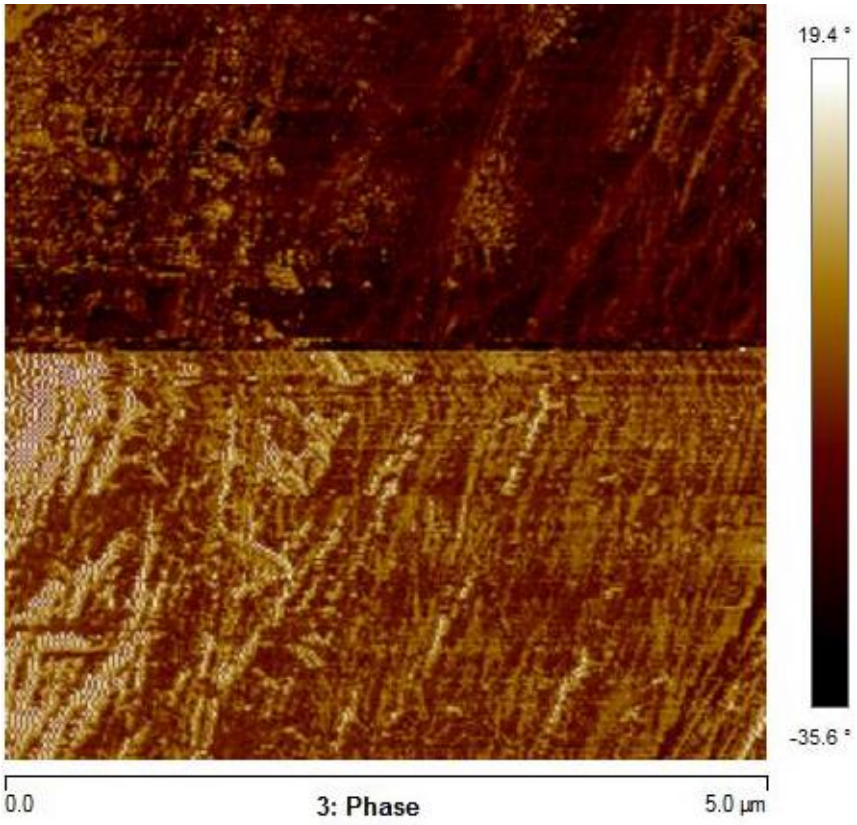

Fig. C35. Phase characteristics with grain distribution of A100 sample ITZ at 5 µm scan range

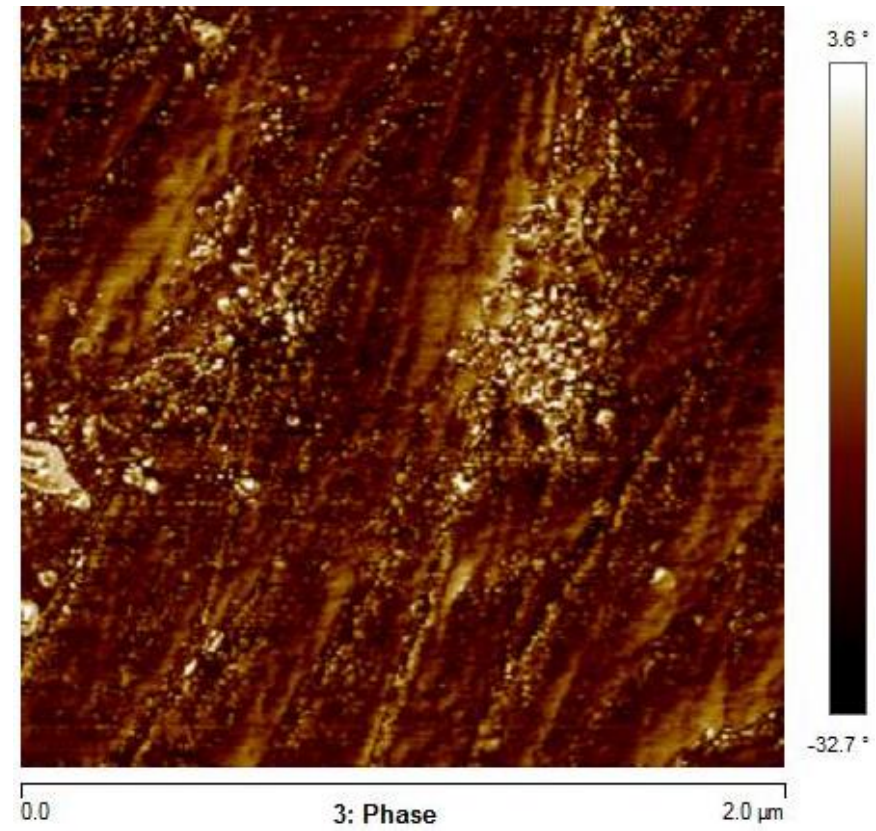

Fig. C36. Phase characteristics with grain distribution of A100 sample ITZ at 2 µm scan range

LIST OF PUBLICATIONS AND PATENT

PUBLICATIONS

1. Salman Siddique, Sandeep Shrivastava, Sandeep Chaudhary and Trilok Gupta. (2018) "Sustainable utilisation of ceramic waste in concrete: Exposure to adverse conditions." *Journal of Cleaner Production,* DOI: 10.1016/j.jclepro.2018.10.231.

2. Salman Siddique, Sandeep Shrivastava and Sandeep Chaudhary. (2018) "Evaluating resistance of fine bone china ceramic aggregate concrete to sulphate attack." *Construction and Building Materials,* 186, 826-832.

3. Deepak Rajawat**,** Salman Siddique, Sandeep Shrivastava Sandeep Chaudhary and Trilok Gupta. (2018) "Influence of fine ceramic aggregates on the residual properties of concrete subjected to elevated temperature" *Fire and Materials,* 42(7), 834-842.

4. Salman Siddique, Sandeep Shrivastava and Sandeep Chaudhary. (2018) "Durability properties of bone china ceramic fine aggregate concrete" *Construction and Building Materials,* 173, 323-331.

5. Salman Siddique**,** Sandeep Shrivastava and Sandeep Chaudhary. (2018) "Influence of ceramic waste as fine aggregate in concrete: Pozzolanic, XRD, FT-IR and NMR investigations." *Journal of Materials in Civil Engineering,* 30(9), 04018227.

6. Salman Siddique, Sandeep Shrivastava, Sandeep Chaudhary and Trilok Gupta. (2018) "Strength and Impact Resistance Properties of Concrete Containing Fine Bone China Ceramic Aggregate." *Construction and Building Materials,* 169, 289-298.

7. Salman Siddique, Sandeep Shrivastava and Sandeep Chaudhary (2017). "Lateral force microscopic examination of interfacial transition zone in ceramic concrete." *Construction and Building Materials*, 155, 688–725.

8. Salman Siddique, Sandeep Shrivastava and Sandeep Chaudhary (2017). "Influence of ceramic waste on the fresh properties and compressive strength of concrete" *European Journal of Civil and Environmental Engineering*, 1-14.

PATENT

1. Filed a patent titled “Recycling fine bone china product waste as supplementary cementitious material/ pozzolana” (Application No. 201811028533)